Biogeochemical Changes during the Cenomanian-Turonian Oceanic Anoxic Event (OAE 2)

Thesis presented by

Haydon Mort

in November 2006 for a
'Doctorate in Science'

at the University of Neuchâtel, Switzerland

Jury Commitee

Prof. Thierry Adatte (Neuchâtel)	***Supervisor***
Prof. Karl Föllmi (Neuchâtel)	*Examiner*
Dr. Philipp Steinmann (Lausanne)	*Examiner*
Prof. Hugh Jenkyns (Oxford, UK)	*Examiner*
Prof. Thomas Wagner (Newcastle, UK)	*Examiner*

Swiss National Science Foundation: Project Numbers 21-67702.02/1 and FN 200020-105261/1

Keywords

Palaeoceanography, palaeoclimatology, geochemistry, biogeochemistry, phosphorus, nutrients, recycling, feedbacks, cyclicity, organic matter, productivity, preservation, modeling, dysoxia, anoxia, oxygen minimum zone, partial pressure, oxidation, reduction, authigenesis, iron cycle, mineralogy, biostratigraphy, Cenomanian-Turonian boundary, OAE 2.

Mots Clés

Paléocéanographie, paléoclimatologie, géochimie, biogéochimie, phosphore, nutriments, recyclage, rétroactions, cyclicité, matière organique, productivité, préservation, modélisation, dysoxie, anoxie, zone à oxygène minimum, pression partielle, oxydation, réduction, authigenèse, cycle du fer, minéralogie, biostratigraphie, limite Cenomanien-Turonien, OAE 2.

Abstract

Understanding how nutrients behave during sub-oxic environments is crucial in predicting future changes in the ocean-climate system. This study focuses on the role of phosphorus, in its different sedimentary reservoirs, during the Cenomanian-Turonian anoxic event (OAE 2), which occurred during the late Cretaceous (~93.5 Ma). In the geological record this period in the Earth's history is represented by the widespread occurrence of sediments containing elevated organic matter content and a large positive $\delta^{13}C$ excursion. Within these lithologies are biological and geochemical signatures that indicate a significant depletion in the amount of oxygen present in the water column.

Phosphorus is a macronutrient, used during primary productivity. After the life cycle of the organism, the subsequent destruction of its organic matter on the sea floor releases phosphate at the sediment-water interface. The phosphate can then follow a number of possible biogeochemical pathways, including its mineralization and sorption into authigenic minerals and oxyhydroxides. The path it follows is largely dependent on the concentration of oxygen in the surrounding water. During periods of oxygen deficiency the oxygen required for the degradation of organic matter is derived by oxidants (e.g. MnO_2, $Fe(OH)_3$ and SO_4^{2-}), which are also binding sites for the phosphorus in the water. The reduction in the number of binding sites causes the sediments retention ability for phosphorus to decrease resulting a net increase in the concentration of phosphate in the water column. This phosphate is then available again for primary producers, should it be recycled into the photic zone.

By studying the behaviour of phosphorus we attempt to infer switches in the mode of sediment accumulation and to consequently reconstruct the oxidation history of OAE 2. To do this, a sequential extraction technique (SEDEX) is used to identify the various types (or phases) of phosphorus found in five exposures distributed across the Tethyan Realm (Europe and North Africa) and the Western Interior Seaway (North America). Other proxies are used to consider of regional influences in our data (e.g. $\delta^{13}C$, mineralogy, hydrogen and oxygen indices, planktonic foraminiferal biostratigraphy).

Phosphorus mass accumulation rates (P MARs) show a distinct trend, similar in each of the five sections. A generalised observation is as follows; (1) a peak in P MARs at the *start* of the increase in $\delta^{13}C$ values; (2) a sharp decrease in inorganic-P phases *during* the isotope excursion itself and a smaller reduction in organic-P. Two sections actually see an enrichment of organic-P during this time. The C_{org}/

$P_{reactive}$ molar ratios (Redfield ratio) begin to increase at this point as does the quantity of organic matter in the sections; (3) A return to 'background' values at or just after the start of the isotope plateau.

This is interpreted in the following way; (1) an environmental perturbation caused a rapid increase in the amount of phosphate in the ocean, which resulted in the initial increase in P MARs. At present, the most plausible explanation is that increase was caused by a maximum flooding event that caused the rapid reworking of nutrients stored on previously dry land allowing them to settle on the bottom of the ocean but also to become bioavailable. (2) The decrease in inorganic-P was caused by the desorption of phosphate from oxyhydroxides and the reduction in phosphorus authigenesis. We suggest that this phosphate became recycled into the upper water column to further stimulate productivity which, in-turn, consumed more O_2 on the sea floor. Organic-P either increased later (as is seen in sections with a deep paleodepth) or did not decrease very much because of decelerated bacterial degradation of organic matter due to oxygen deficient conditions. The increase in organic matter content *after* P MARs start to decrease is seen as evidence to support this hypothesis (3) Pre-excursion MAR values are low considering how much phosphate was in the water column, suggesting that phosphorus recycling was sustaining the $\delta^{13}C$ plateau.

Intense and sustained primary productivity consumed bottom water oxygen but simultaneously increased atmospheric O_2 concentrations. It is possible that atmospheric O_2 eventually acted as a negative feedback when the partial pressure of free O_2 in the atmosphere became greater than in the mixing layer of the ocean, starting the oxidation of nutrients in the ocean. We present tentative evidence for this with a P curve from an Egyptian section. The preservation of organic matter in black shales would have dramatically reduced the concentration of CO_2 in the atmosphere, cooling the climate leading to a reduction in humidity, precipitation, and continent-ocean nutrient fluxes.

Table of Contents

Acknowledgements

Several times during the first two years of this Ph.D I came close to giving it up entirely. Dispite numerous personal difficulties over the past four years, I have somehow managed to find it within myself to carry on with something that I believed in. The fact that I am now writing acknowledgements is a tribute to all those who have helped in my academic and personal life.

I would like to thank my supervisors, each of whom has brought to my thesis strengths that have helped make this a successful project. Their guidance in their field of expertise has been invaluable. Their support and understanding in difficult personal situations has been touching. It is for these reasons I would like to thank very much Thierry Adatte, Karl Föllmi and Gerta Keller. They were not only my great colleagues, but also good friends.

I would like to thank Philippe Steinman for helping me in numerous way, but most notably in the laboratory on and off for the first three years of my Ph.D, Virgine Matera for essentially doing all of the ICP-MS work for the Furlo, Manilva and Pueblo sections, with minimal input from me. I would especially like to thank Federica Tamburini for helping us organise the phosphorus speciation equipment and always being on hand to help with any follow-up questions. She was very patient and professional! Zsolt Berner of the University of Karlsruhe, Germany, for carrying out much of our stable isotope analysis. The other members of the geology department who have also provided help and basically been nice, smiley, chatty people! I would like to thank two Masters students at the University of Neuchâtel who have now moved on. Olivier Jaquat and Pascal Ducommon. They carried out much of the work on the Furlo and Manilva sections. Also thanks to Brian Gertsch for collaborating with me in the last years on two of the manuscripts, his insightful comments and discussion were always stimulating. André Villard, the technician in our department was a constant source of humour and was very tolerant with my 'difficult-to- prepare' thin sections from Mexico and Morocco.

All the scientists who I have met in workshops and conferences, who have taken an interest in my work and given me new ideas and encouragement. Jens and Ines Wendler, Ian Jarvis, Hugh Jenkyns, Thomas Wagner, Paul Wignal, Karen Bice and Rob Scott to name a few. I would especially like to that Hugh Jenkyns and Thomas Wagner for accepting to be on my thesis jury and giving me a good grilling. I'm sincerely looking forward to it!

I would like to thank my friends at the University of Neuchâtel. Those I have come to know best are Alexis Godet, Stephane Bodin and Pascal Linder. I thank them for their occasional assistance in the lab, their frequent calls for help using the English language (making me feel useful) and their understanding and thoughtfulness during difficult times. I especially want to emphasis my thanks to Alexis Godet and Stephane Bodin, my office colleagues for the follow things. 1. Putting up with someone who gives up speaking French half way through a sentence, even after 4 years of living in Neuchâtel. 2. For instructing in the subtleties of the French language and teaching me words and expressions that I might not otherwise have learnt! Raul Quezada has also become a good friend since his short time in Neuchâtel.

Acknowledgements

I would like to thank the University of Neuchâtel, the Swiss National Science Foundation and the National Science Fund of the USA, for giving me money to pay my salary, do my fieldwork and, most importantly, for helping me find my gorgeous girlfriend who I met on a fieldtrip to Brazil, in September 2005. Not matter what comes out of this Ph.D both these organisation will be delighted to know that they have united two people who now love each other very much!

Following on from this, I would like to thank my girlfriend herself, Carlinha, for being so encouraging and supportive. Você me ajudou a encontrar o meu foco outra vez, depois de um período longo e difícil. Embora você não seja fluente em inglês, teu conselho teve uma grande significação pra mim, maior que um nativo da língua inglesa poderia tê-lo. Você me tornou mais forte e mais feliz. Tenho a certeza que algumas pessoas pensaram que ter uma namorada Brasileira poderia ser uma distração pra mim. Na realidade você tem sido a motivação principal, a força por trás do meu Ph.D. no ultimo ano. (For those not fluent with Portuguese, I basically that said she is a wonderful girl who was, despite what people may have thought, the motivating force behind my Ph.D. in the final year). Thanks to Marco Silva, of La Chaux-de-Fonds, for providing me with this translation!

The biggest thanks go to my parents. There are no words that I know in my own tongue that are enough to say 'thank you'. So I will just thank you for supporting me emotionally and financially in this endeavour and for rather large role you have both played in making me who I am, which has, in turn, allowed me to start and finish this Ph.D.

Finally I would like to thank a special man. It is possible that I would have never even started on my academic career if he had not taught me GCSE and A'level physical geography at Liskeard School and Community College in Cornwall, UK. His name is Mr McGreal and I am sure that he would be very perplexed to know that he was receiving the last word in these acknowledgements. His lessons didn't exactly shatter my view of the word, but he was able impart an understated enthusiasm for his fascination of the natural world. It was a style that I found difficult to resist and made my mind up to study a Bachelors in Earth Sciences.

Thank you all...

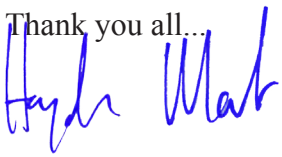

Haydon Mort

What I know now, that I didn't know then, is that I don't know much!

Source unknown

For Mum and Dad...

- A -

Introduction

This section is a synthesis of current ideas about oceanic anoxic events, introduced in a way that guides the reader into the central ideas of this project (redox conditions, phosphorus recycling, productivity and preservation).

A.1. Understanding the ocean

The ocean and atmosphere are two systems, which are increasingly considered as one. The exchange of gases between these two types of fluid is occurring on a constant basis and climate models of the modern ocean increasingly see the air and the water entities as merely two facets of one system (e.g. Nuttle et al., 1991; Wanninkhof, 1992; Roche et al., 2004; Seidov et al., 2005). Despite decades of research the complexities involved in gaining even a basic understanding of this system have caused geoscientists to time-and-again revise their views.

If study of the various fluid mechanical properties within the zone of atmosphere-ocean exchange (**mixing layer**) were not complex enough by themselves there is a raft of other variables to consider. How do the gigatonnes of material of continental origin impact on chemical changes in the ocean water column and what causes variations in the flux of this 'terrigenous' material anyway? What are the biogeochemical impacts to the sensitive ocean-atmosphere system if vast areas of dry land are flooded by rising sea-level? After massive amounts of research, the answers have not been forthcoming. Finding the answers to these types of questions are important today as humans continue to fertilize the ocean with carbon dioxide and nutrients (e.g. phosphates and nitrates), global (**eustatic**) sea-level rise threatens to flood many of the worlds low lying regions (Chen-Tung and Chen, 1993; Xu et al., 2000; Matear, 2001; Mackenzie et al., 2002; Gehrels et al., 2005; Gehrels et al., 2006). Understanding the processes in the ocean is important as we attempt to predict the consequences of global warming, when certain thresholds maybe crossed and how we may mitigate against the effects of these changes.

An important way we may understand the causes and consequences of the interactions between the ocean, the atmosphere and continents is to look into the Earth's past, a notion first realised in the 1800s (Lyell, 1837, 1872). The various kinds of strata that record shifts in how the geosphere operates can give us valuable clues into the causal mechanisms of global change. The geological record is an archive of possible scenarios that humans may one day live through.

A.2. The Cretaceous ocean

The Cretaceous period was a time of increased global temperatures, large sea-level variations and high oceanic crust production (Schlanger and Jenkyns, 1976; Hart, 1980; Jenkyns, 1980; Schlanger et al., 1981; Caron, 1983; Schlanger et al., 1983; Kaiho and Saito, 1994; Kerr, 1998). Leckie et al., (2002) presented an overview of the sea-level fluctuations and major volcanic episodes from the Lower to Upper Cretaceous (Fig. 1). Strontium isotopes are used as an indicator (a **proxy**) for changes in crustal production. There is a good coincidence between lower $^{87}Sr/^{87}Sr$ (increased volcanism, hence crustal production) and lower sea-levels. Since new crust is derived from mid-ocean ridge activity, the obvious conclusion is that high sea-floor spreading rates changed the area of the ocean basins, decreasing or increasing the eustatic sea-level. Superimposed on this long-term sea-level undulation are shorter-term variations as well as climatic changes not visible on the timeframe in Fig. 1.

This project focuses on an event in the upper epoch of the Cretaceous period, close to the boundary of two geological stages called the Cenomanian and the Turonian. In Fig. 1 it is represented as the fifth of a series episodes labelled OAEs (**Oceanic Anoxic Events**). These events are thought to represent major disturbances in the global carbon cycle. This cycle is arguably the most important of all biogeochemical cycles on Earth. In studying OAEs it is important to consider the sources and fate of carbon in both it's inorganic (e.g. carbon dioxide, carbonate) and organic (life) states. The Cenomanian-Turonian event (OAE 2), like many other OAEs, is typically characterised by the occurrence of globally distributed black shale. These shales have been recognised as far back as the 18th Century (Woodward, 1864; Veith, 1895; Suess, 1904; China, 1922; Sorgenfrei, 1960) although their spatial extent and the complexities that went into forming them were not considered until the 1970s and early 1980s (Schlanger and Jenkyns, 1976; Ryan and Cita, 1977; Jenkyns, 1980; Arthur and Premoli-Silva, 1982). Typical

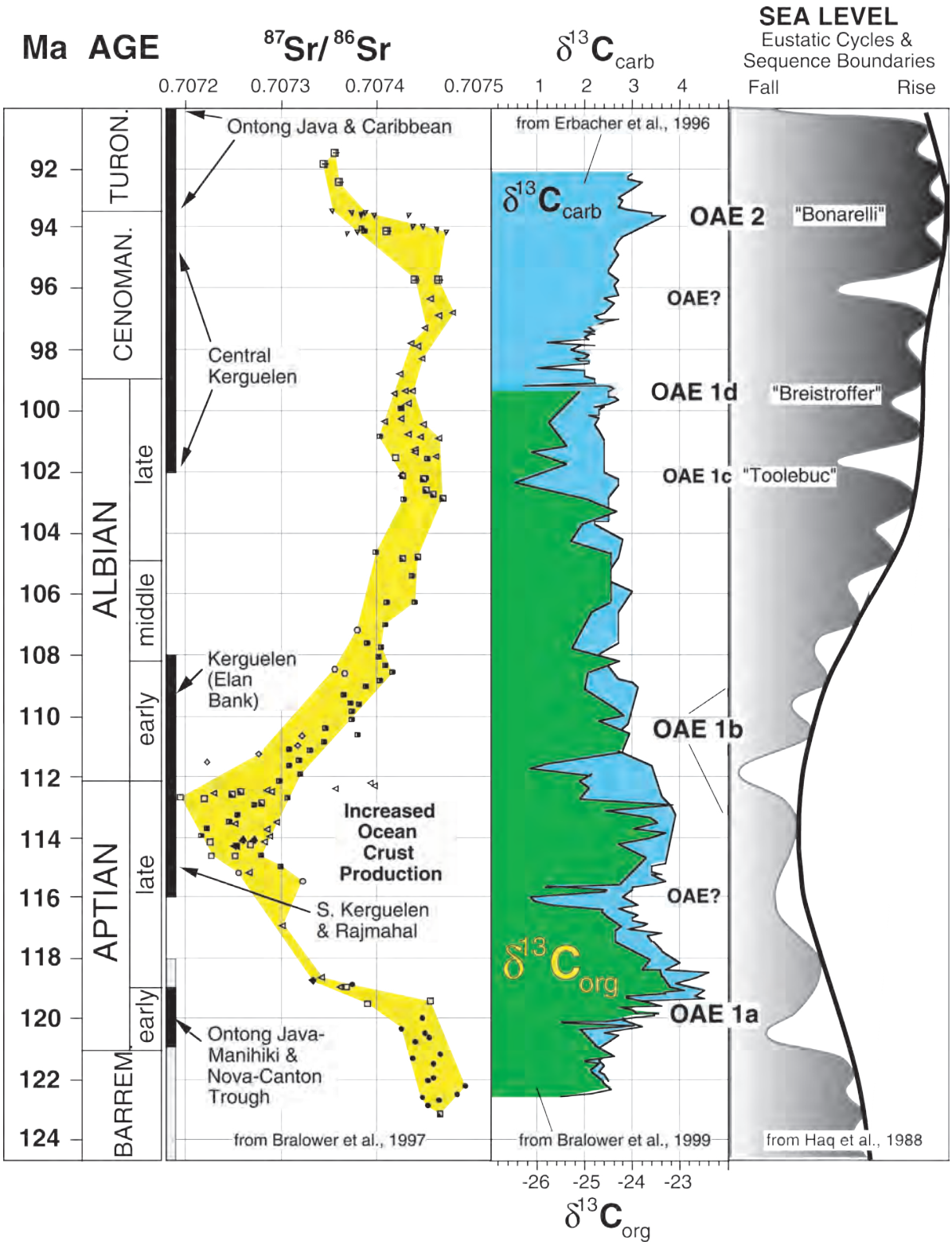

Figure 1. Adapted from Leckie et al., (2002). The authors correlate changes in $\delta^{13}C$ with eustatic sea-level flucuations and $^{87}Sr/^{86}Sr$ (proxy for hydrothermal activity/crustal production). A positive correlation is seen between long-term sea-level change and volcanism, whereby increase volcanism amounts to low sea-level.

black shale deposits are usually organic rich; typically containing over 10 % total organic carbon (**TOC**). The most striking examples are found in sediments that were deposited in deeper water settings where organic matter accumulation has been the most effective. Fig. 2 is a photograph from the Furlo section (featured in Section E of this thesis) and shows a dramatic series of black

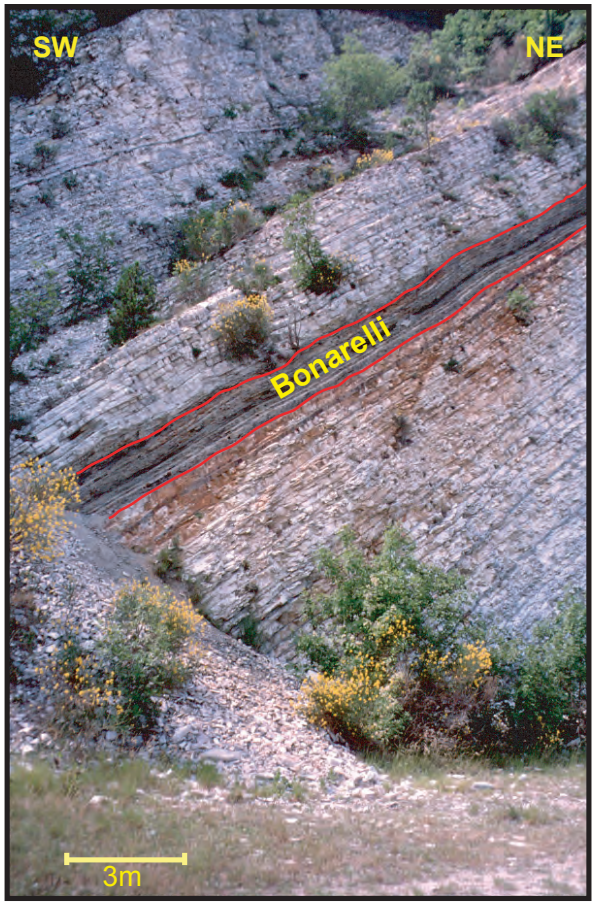

Figure 2. A typical representation of OAE 2 in the Italian Apennines. This is the Furlo section. The 'so-called' Bonarelli Level is seen as a 1 - 1.5 meter think unit comprised of black shales and radiolarian rich mudstones.

shale horizons interpreting a bedded limestone succession in the Umbria-Marche northern Italian Apennines. Such dramatic changes in lithologies are not often seen. However, even in sections containing no organic matter or significant change in lithology there exists other proxies, which draw geologists from different sub-disciplines to the same conclusion: that the oceans, atmosphere and continents underwent substantial changes in the way they interacted with one another.

A.2.2. Biological Changes

OAE 2 is the fifth largest extinction event in the past 600 million years (**Ma**) with the changes occurring in both the planktonic and benthic realms of the ocean (e.g. Hart, 1980; Leckie, 1985; Hart and Ball, 1986; Jenkyns, 1991; Mermighis et al., 1991; Philip and Airaudcrumiere, 1991; Grosheny and Tronchetti, 1993; Gusic and Jelaska, 1993; Kaiho et al., 1993; Kaiho and Hasegawa, 1994; Grosheny and Malartre, 1997; Leckie et al., 1998; Premoli-Silva et al., 1999b; Keller et al., 2001; Leckie et al., 2002). Decreases in the thermal stratification in the water column are suggested when measuring the $\delta^{18}O$ (**paleotemperature** proxy) variations in deep water planktic foraminiferal. Bathyal waters are thought to have warmed from ~15 to ~19°C, the warmest temperatures in the past 145 Ma (Huber et al., 1999; Huber et al., 2002). With the extinction of *Rotaliporids* and *Globigerinelloides* (deeper water taxa) this suggests breakdown in the vertical structure of the water column, which would have led to decreased convection and bottom water ventilation (e.g. Bralower and Thierstein, 1984; Leckie et al., 2002). Blooms in primary productivity in the sea-surface caused eutrophication and a preference in the production of siliceous organisms over carbonate which can be dissolved rapidly via dissolution (Bak, 1996; Erbacher et al., 1996; Erbacher and Thurow, 1997; Racki, 1999). The absence of carbonate and abundance of radiolarian rich shales is commonly seen in many European sections during OAE 2 (Luciani and Cobianchi, 1999). The environmental stress is seen as marked changes in planktonic foraminifera morphology. For example unstable shell structure, dwarfism (Coccioni and Luciani, 2004) and drops in diversity (e.g. Hradecka and Svabenicka, 1995; Kauffman, 1995; Gale et al., 2000; Keller et al., 2001; Keller and Pardo, 2004).

The eutrophication of the ocean water column leadds to the increased delivery of organic matter to the sea-floor during heightend productivity. Organic matter decomposition consumes O_2 and produces CO_2 (Demaison and Moore, 1980). Thus an environmental perturbation that causes a dramatic increase in productivity has the potential to generated a significant reduction in O_2 beneath areas of high productivity, at around the sediment-water interface. This can occur especially within the oxygen minimum zone (**OMZ**) that extends from the lower continental shelf onto the upper slope. In regaions of high primary productivity this zone can intensify and expand (see below for more details). This can have a significant impact

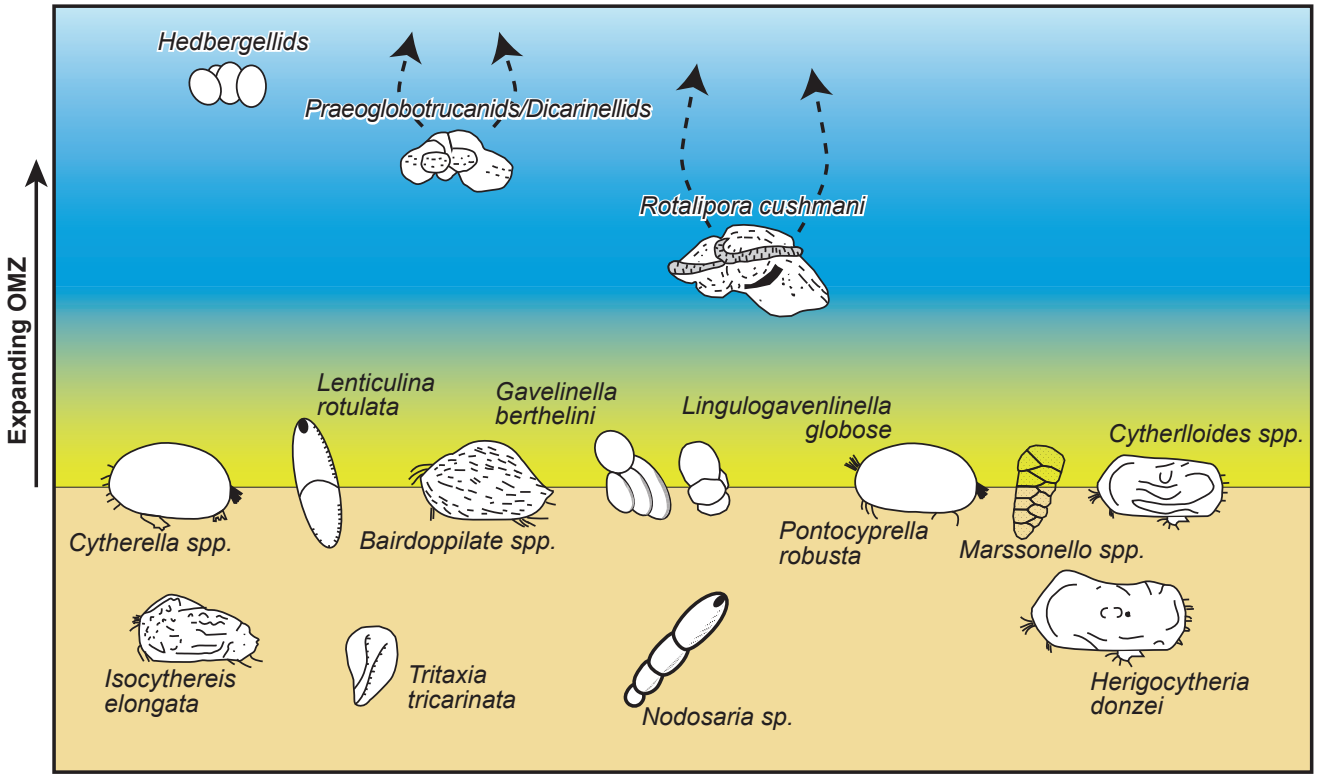

Figure 3. Redrawn from Jarvis et al., (1988). This diagram demonstrates the responce of planktonic foraminifera to the intensification and expansion of the oxygen minimum zone (yellow/green shading). The expansion was not thought to be very rapid, producing the stepwise extinction of species with a higher depth tolerance first (e.g. Rotalipora Cushmani). See text for details.

on the flora and fauna in the region. The pattern of planktonic foraminifera extinction during OAE 2, is thought to reflect a gradual expansion in the OMZ (Jarvis et al., 1988; Ulicny et al., 1997; Keller and Pardo, 2004). The extinction occurs in a stepwise fashion with high depth tolerant species becoming extinct first, circuming the encroaching sub-oxic waters (Fig. 3).

A.2.3. Stable Isotopes

The increase in productivity at the start of OAE 2 is registered in the fractionation of carbon and the consequent enrichment of the ocean in ^{13}C. The enrichment is seen as a + 2 - 2.5 ‰ shift in $\delta^{13}C_{carb}$ values, which, when viewed through a window spanning the Upper Cretaceous, is seen as a large, abrupt shift (see Fig. 4. Jarvis et al., 2006). The detail of this shift is classically seen as a large initial positive increase. A subsequent trough in values creates a **first peak**. Values increase again and culminate in a plateau, the start of which maybe termed a *second peak*. The plateau of values continues until the Cenomanian-Turonian boundary (approximately 93.5 Ma) where they begin to decrease reaching pre-excursion values in the late Early Turonian.

$\delta^{18}O$ isotopes measurements have generally be used to construct paleotemperature records in the ocean water column by analyzing individual species of planktonic foraminifera (see biotic changes) but have also been used to infer the diagenetic alteration of sediments and changes in fresh water input (Valladares et al., 1996; Keller et al., 2004). Whereas $\delta^{18}O$ can be used to construct temperatures in the water column, bulk rock measurements are considerably scattered. This problem is considerable in the Cretaceous with the large number of shallow seas and basins (Jenkyns, 1980) ensuring a *relatively* high amount of fresh water input.

A.3. The formation of black shales: Productivity vs. Preservation

A.3.1. Productivity

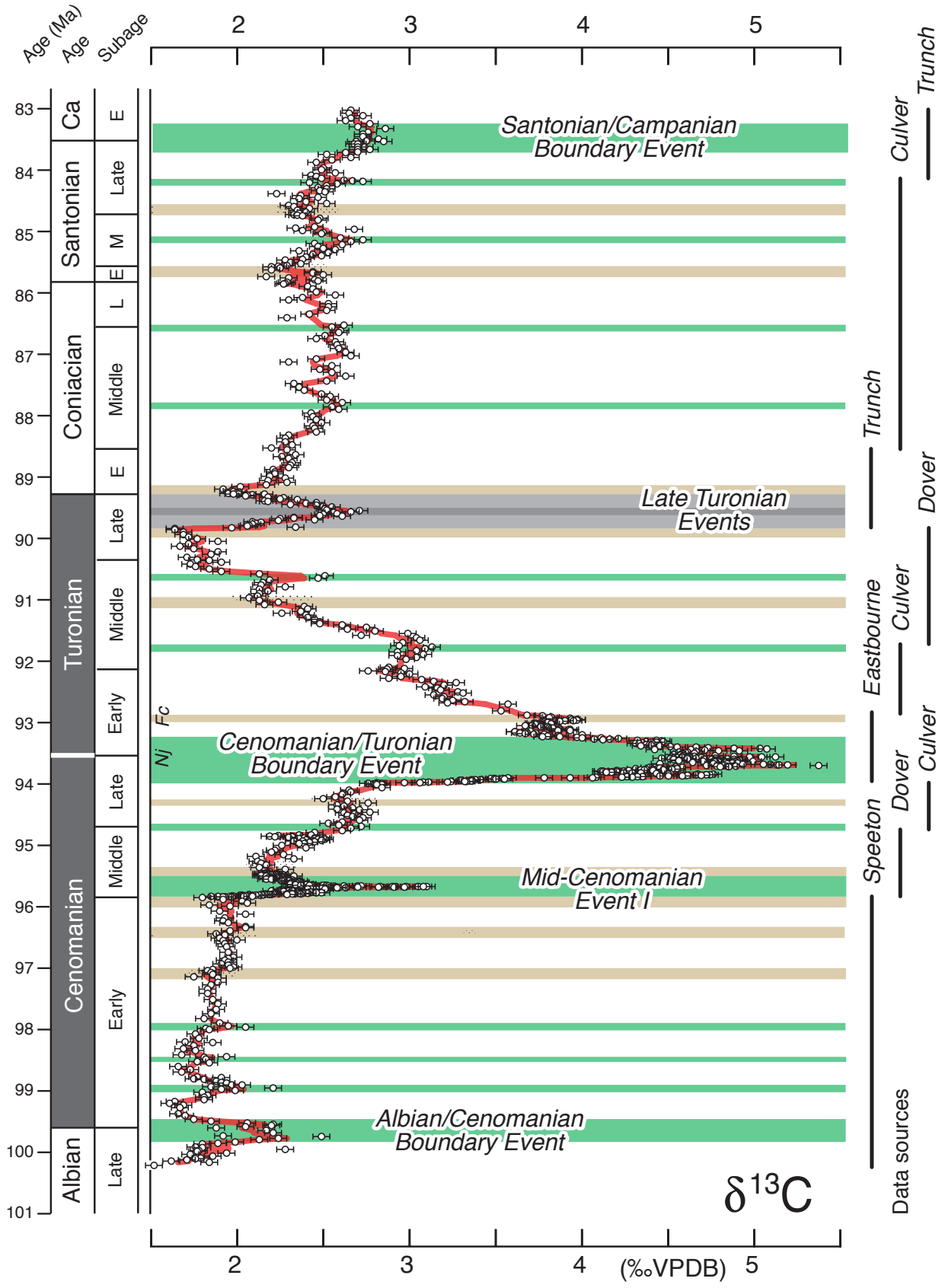

Figure 4. Adapted from Jarvis et al., (2006). A composite plot of $\delta^{13}C$ values from ten sections across the south and northeast of England. The curve highlights many of the major oceanographic and climatological events in the late Cretaceous, most notably oceanic anoxic event 2 (OAE 2), otherwise known as the 'Cenomanian-Turonian Boundary Event' (CTBE)

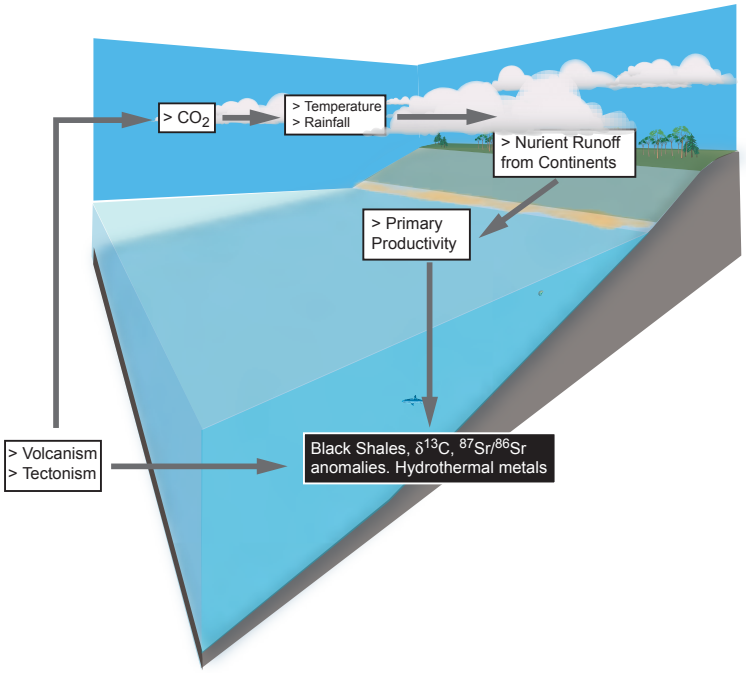

Figure 5. An adaptation of the model put forward to explain OAE 1b by Larson and Erba (1999). It is a commonly cited mechanisms used to explain increases in productivity. Volcanism (or anything else that might warm the planet) increases global temperatures and consequently humidity, precipitation and global weathering rates, supplying the ocean with nutrients leeched from the continents.

Certain elements are enriched in the absence of oxygen (e.g. Bi, Cd, Co, Cr, Cu, Mo, Ni, Re, Sb, Tl, U, V). Their differing redox sensitivities make them useful when constructing the oxygenation history of fresh water and marine environments (see Morford and Emerson, 1999; Yarinkcik et al., 2000). Redox-sensitive metals have been successfully applied to several anoxic episodes throughout the Mesozoic (Mostafa, 1999; Nijenhuis et al., 1999; Algeo, 2004; Bodin et al., 2006; Brumsack, 2006). Enrichments are observed during OAE 2 although not at all paleodepths. For example Kuypers et al., (2002) infers, from green sulfur reducing bacteria, that dysoxic conditions periodically occurred at very shallow water depths of 15 m or less. In the same study, redox sensitive metals, do not record any enrichment on the sea-floor. Therefore, the authors conclude that organic rich deposits during OAE 2 were (at least in their study area, the North Atlantic) formed predominantly as a result of increased primary productivity. This opinion is shared by many others in the Cretaceous geoscience community (Kuhnt et al., 1990; Pedersen and Calvert, 1990; Premoli-silva et al., 1999a). In a productivity-driven model Cretaceous black shales are as a result of high primary productivity in the photic zone of the ocean. The increase in organic matter production may have occurred as a result of a variety of factors. These include a greater flux of nutrients from the continents into the ocean, volcanic CO_2 forcing of the climate, increased humidity and precipitation (Fig. 5: see Larson, 1991; Larson and Erba, 1999; Hasegawa, 2003) causing an intensified hydrological cycles, delivery nutrients in greater quantities to the ocean. Alternatively, these nutrients could have been derived from the flooding and subsequent erosion of previously dry coastal regions (Hilbrecht et al., 1996; Voigt and Hilbrecht, 1997; Jarvis et al., 2006; Voigt et al., 2006).

A.3.2. Preservation

Although OAE 2 led to a large extinction in the oceans, there is a large amount of evidence to support the conclusion that productivity actually increased (see above). However, there is a growing understanding that whilst productivity did increase, it was probably not the only factor involved in forming black shales (see Sageman

et al., 2003 for a review of the mechanisms affecting black shale formation). Organic matter is sensitive towards oxidative destruction both biologically and chemically (see Rullkötter, 2000 and references therein). As a result, it is thought that the concentration of free oxygen at the sediment-water interface is the most important factor in determining the amount of organic matter that becomes perminently stored in sediments (Demaison and Moore, 1980). There exist bacteria and other microorganisms that degrade organic matter both under oxic and anoxic conditions. Under anoxic conditions, anaerobic bacteria find the oxygen required to oxidize organic matter in various electron donors (oxygen providers) that exist in the water column (e.g. NO_3^-, MNO_2, $Fe(OH)_3$, SO_4^{3-}). The order in which these ions are processed is largely dependent on how much energy is needed to reduce each one (either bacterially or inorganically; see Table 1). The energy required is expressed as kilojoules per mol of reactant (kJ mol^{-1}). ΔG^o represents free energy and therefore if $\Delta G^o = 0$ there is neither a gain nor a loss in energy but it is unlikely to take place without the aid of bacteria. If ΔG^o is negative then there is a net gain in energy meaning that the destruction of organic matter can take place spontaneously, with or without the involvement of bacteria. If ΔG^o is positive then energy is required to drive the reactions that will supply the oxygen. In short, the higher the ΔG^o value, the slower it is to produce the oxygen needed to oxidize organic matter (for an overview of these processes see Jorgensen, 2000, and references therein). Therefore, in theory, it is entirely possible to accumulate organic matter without productivity being particularly intense, so long as conditions are dysoxic enough.

A.3.3. Summary

In reality, both productivity and preservation have a crucial role in forming black shale deposits. The former is essential in order to provide the organic matter in the first place. The latter makes it much easier to accumulate the organic matter by slowing down the rate at which it is destroyed. Understanding and studying both of these

Pathways of Organic Matter Oxidation	ΔG^o (kJ mol^{-1})
Oxic Respiration:	
$CH_2O + O_2 \longrightarrow CO_2 + H_2O$	-479
Denitrification:	
$5CH_2 + 4NO_3^- \longrightarrow 2N_2 + 4HCO_3^- + CO_2 + 3H_2O$	-453
Mn(IV) reduction:	
$CH_2O + 3CO_2 + H_2O + 2MnO_2 \longrightarrow 2Mn^{2+} + 4HCO_3^-$	-349
Fe(III) reduction:	
$CH_2O + 7CO_2 + 4Fe(OH)_3 \longrightarrow 4Fe^{2+} + 8HCO_3^- + H_2O$	-114
Sulphate reduction:	
$2CH_2O + SO_4^{2-} \longrightarrow H_2S + 2HCO_3^-$	-77
$4H_2 + SO_4^{2-} + H^+ \longrightarrow HS^- + 4H_2O$	-152
$CH_3COO^- + SO_4^{2-} + 2H^+ \longrightarrow 2CO_2 + HS^- + 2H_2O$	-41
Methane production:	
$4H_2 + HCO_3^- + H^+ \longrightarrow CH_4 + H_2O$	-136
$CH_3COO^- + CO_3^- + H^+ \longrightarrow CH_4 + CO_2$	-28
Fermentation:	
$CH_3CH_2OH + H_2O \longrightarrow CH_3COO^- + 2H^2 + H^+$	10
$CH_3CH_2COO^- + 3H_2O \longrightarrow CH_3COO^- + CH_3COO^- + HCO_3^- + 3H_2 + H^+$	77

processes, is important because they directly affect the oceanic nutrient cycles (see below), which, in turn, affect models for predicting climate change.

A.4. The behaviour of nutrients under anoxic conditions

Nitrogen (N) and Phosphorus (P) are important productivity limiting nutrients. Both are directly involved in photosynthesis:

A.4.1. Equation 1: photosynthesis $\longrightarrow$

$$106CO_2 + 16NO_3^- + 122HPO_4^{2-} + H_2O + 18H^+ + C_{106}H_{263}O_{110}N_{16}P + 138O_2$$

The ratio of C:N:P, as shown in the equation, is 106:16:1. This is called the Redfield ratio (Redfield, 1958). Once dead, the organic matter sinks to the sea floor where it is oxidized:

A.4.2. Equation 2: Oxidation of organic matter using oxygen $\longrightarrow$

$$(CH_2O)_{106}(NH_3)_{16}(H_3PO_4) + 138O_2 \quad 106HCO_3^- + 16NO_3^- + HPO_4^{-2} + 124H^+ + 16H_2O + O_2$$

Phosphates (HPO_4^{2-}) are released into sediment pore waters where they have two possible fates. If there is an abundance of free oxygen then they may be oxidized in the sediment, forming authigenic minerals (**mineralization/authigensis**). This happen to phosphate only. Nitrates have a ΔG^o very low (close to O_2) and is quickly used by bacteria provide O_2 to oxidize organic matter (see Table 1 and Equation 3).

A.4.3. Equation 3: Reduction of organic matter using nitrate $\longrightarrow$

$$(CH_2O)_{106}(NH_3)_{16}(H_3PO_4) + 94.4NO_3^- \quad 13.6CO_2 + 92.4HCO_3^- + 55.2N_2 + HPO_4^{-2} + 84.8H_2O \quad \Delta G^o = \mathbf{-453}$$

The resulting N_2 becomes released into the water column and is again bioavailable for primary producers. If productivity in the ocean becomes intense, then the delivery of organic matter to the sea-floor will increase, as will the demand for O_2 to processes this organic matter. Once conditions become dysoxic enough, the mineralization of phosphates into authigenic minerals may be prevented (Ingall et al., 1993) causing P to be recycled back into the water column where it can, again, be a nutrient.

This has significant consequences. Although N is the most abundant nutrient incorporated into organic matter during photosynthesis, its residence time on the sea-floor is relatively short before it is reduced and therefore reused (**recycled**). It is also the most abundant element in atmosphere (~ 68 %). Therefore it limits productivity only on short timescales. Because of its involvement in authigenesis, P has a longer residence time, but is equally as important in primary production. Therefore when its reduction threshold it crossed it may, too, be recycled becoming the dominant biolimiting nutrient.

A.4.4. Control of P accumulation by Fe and Mn

Many studies suggest that the abundance of Fe and Mn oxides control phosphate pore water concentrations (Sundby et al., 1992; Jensen and Thamdrup, 1993; Slomp et al., 1996; Slomp et al., 2002; Slomp et al., 2004). The destruction of organic matter will release phosphate, which are frequently incorporated into in Fe and Mn oxydroxides (a process called **sorption**) Fig. 6). Reduction of these oxyhydroxides, in the redox cascade, (Table 1) will cause the **desorption** of the phosphate molecule (Fig. 6) allowing it to be recycled.

A.5. Phosphorus: the state of research in the Cretaceous

These mechanisms of nutrient recycling have been modeled and investigated extensively in the modern and ancient oceans (Gächter et al., 1988; Ingall and Van Cappellen, 1990; Ingall et al., 1993;

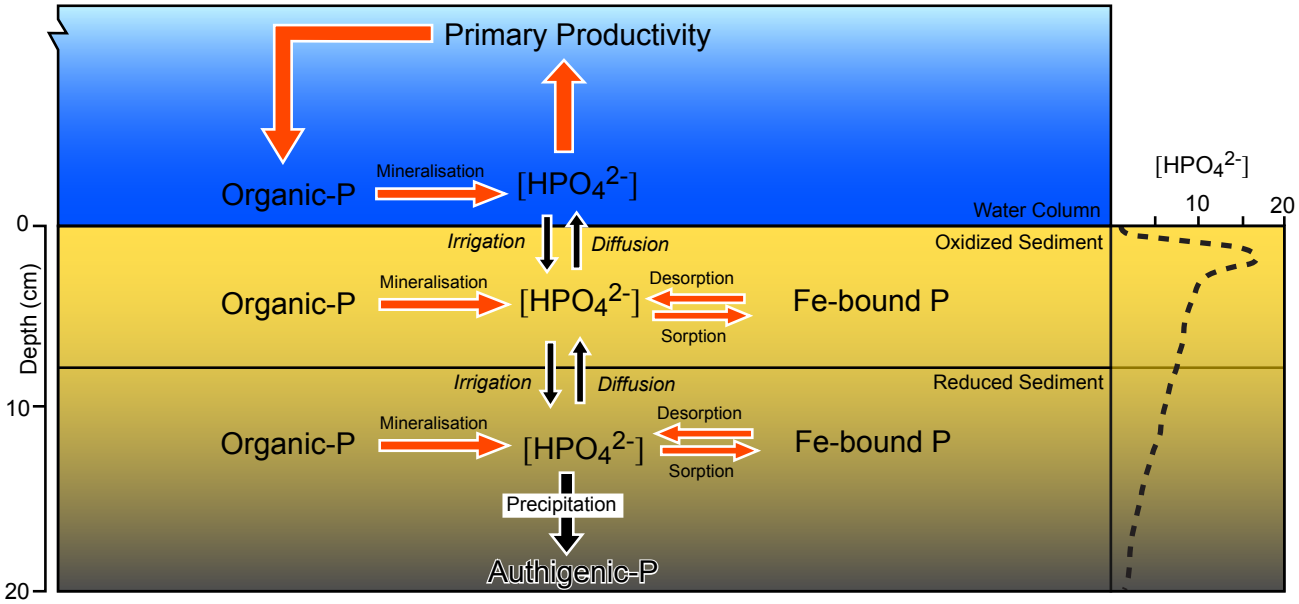

Figure 6: Redrawn for Slomp et al., (1996). The phosphate molecule (the most abundant of which, in the ocean, is HPO_4^{2-}) progresses through a series of redox states which largely depend on abundance of oxygen in thet water. The sorption/desorption (incorporation/release) of phosphate into Fe oxyhydroxides can be inferred using the the sequential extraction first developed by Ruttenburg (1992).

Van Cappellen and Ingall, 1994; Calvert et al., 1996; Filippelli and Ruttenberg, 1997; Clark et al., 1998; Filippelli, 2001; Kolowith et al., 2001; Slomp et al., 2002; Handoh and Lenton, 2003; Payton et al., 2003; Nederbragt et al., 2004; Slomp et al., 2004; Schenau et al., 2005). Several studies mentioned in this list have modeled the behaviour of P during Cretaceous OAEs. However, with the exception of a general study (Föllmi., 1995) very few actual measurements of P have been made in the Cretaceous.

Two studies (Nederbragt et al., 2004; Bodin et al., 2006) have presented total-P measurements, each of which has shown a decrease in P accumulation at the onset of supposed dysoxic conditions (OAE 2 and the Hauterivian-Barremian Faraoni Level (130 Ma) respectively). P is a major productivity-limiting nutrient but it is intimately linked to redox processes on the sea-floor. It is therefore ideally suited to advance our understanding into the roles of productivity and preservation during Cretaceous OAEs.

In the past two decades techniques have been developed to not only measure the amount of P contained in sediments, but also using a sequential extraction technique (known as SEDEX), measure the different types of P (i.e. organic-P, Fe-P, authigenic-P, detrital-P and, more recently, opal-P) (Ruttenberg, 1992; Eijsink et al., 1997; Anderson and Delaney, 2000; Latimer et al., 2006). The advantage of distinguishing between the different types of P is that is allows us to infer changes in the mode of deposition. For example, our comprehensive understanding of P in modern oceans and lakes allow us to draw conclusions about the fluctuation in abundance of authigenic-P in the geological record. If we see a period of increased authigenic-P accumulation we can say, with some degree of confidence, that sediment pore waters were relative oxic at the time of deposition. Alternatively a rise in the amount of $P_{organic}$ may be explained in two ways: extremely high productivity and organic matter burial, not allowing time for organic matter oxidation; or the reduction of oxygen content at the sediment-water interface, reducing the rate at which organic matter is oxidized and its phosphate liberated. By studying the behavior of the other types (*species* or *phases*) or P we can be more confident about which processes were taking place.

A.6. Implications and importance of studying nutrient recycling

Why are these biogeochemical processes important to us today? Inherent in the mechanisms described above is the possibility that a positive feedback may result. This possibility has been conceptually and numerically modeled by Ingall and Jahnke, (1997); Handoh and Lenton, (2003) and Wallmann, (2003). Normally, primary producers in the ocean derive the nutrients required for photosynthesis from the flux of material constantly arriving from rivers and aeolian sources (see Broeker and Peng, 1982). However, this *steady state* could change given a larger enough environmental perturbation. Humans are currently fertilizing the ocean with over 2.4 gigatonnes of CO_2 entering the mixing layer, annually (Chen-Tung and Chen, 1993; Matear and Hirst, 1999; Matear, 2001). This appears to increase the rate of primary productivity, in turn creates more organic matter on the sea-floor. As this is oxidized, oxygen is consumed and conditions will become more dysoxic. As this develops authigenesis maybe be prevented and Fe/Mn-oxyhydroxides would switch from being a sink of phosphate into being a source. This will furnish the ocean with an addition source of a major productivity limiting nutrient, stimulating productivity still further, increasing oxidation of the sea-floor, consuming O_2, desorping more phosphate and so-on in a nutrient recycling-productivity feedback.

If a greater proportion of the water column was sub-oxic then this could decrease the calcite compensation depth (CCD), increasing dissolution of calcium carbonate ($CaCO_3$) producing carbon dioxide. Because the partial pressure of CO_2 (pCO_2) is currently higher in the atmosphere than in the mixing layer of the ocean, the oceans are currently a sink for over half of our fossil fuel emissions (see above references). However, if the pCO_2 in the oceans became greater that pCO_2 in the atmosphere then the ocean would become a source of CO_2, rather than a sink. The consequences of this for humans would be undesirable, quickly warming the planet, thermally expanding the ocean, dramatically changing weather patterns in potentially catastrophic ways. For marine life, the decrease in oxygen availability would cause a dramatic reorganization of habitats and extinctions both in the affected benthic zones and within the water column.

This scenario would not be directly caused by humans, but by the inevitable processes caused by the first *new* source of nutrients; the benthos of the ocean via nutrient recycling. One way we can assess the plausibility of this it to study a period in time where a large amount of organic matter deposition occurred. Cenomanian-Turonian successions are some of the largest source rocks of oil in the world (see Roden and Edmonds, 1997; Akande et al., 1998; Khaled, 1999; Katz et al., 2000; Kolonic et al., 2002; Nzoussi-Mbassani et al., 2003). Understanding the processes involved in their formation will help us appreciate the limits, thresholds and reactions the modern ocean has.

A.7. Introduction to thesis

Understanding the complex biogeochemical processes in the water column and at the sea-floor provides geology with new insights into what can drive the biological, chemical and sedimentological features observed in geological record. Observing these changes in the past helps us to more effectively predict the future of the ocean-atmosphere system.

This project will be the first time geologists have specifically studied the behavior of a productivity-limiting nutrient during a Cretaceous anoxic event. Using the SEDEX protocol for distinguising between the different phases of phosphorus it will test ideas about nutrient recycling during Cretaceous OAEs that have so far only been modeled (Ingall et al., 1993; Van Cappellen and Ingall, 1994, 1996; Handoh and Lenton, 2003; Nederbragt et al., 2004). The project will draw on a variety of proxies to independently assess changes in productivity, preservation, continental delivery of nutrients and sea-level change.

This thesis is presented in seven parts:

A. This introduction

B. The presentation, discussion and implications of the speciation of P during the initial stages

of OAE 2

C. A more in-depth investigation and discussion of the behavior of P. We present a speciation from an additional section in Morocco and present a model that explains the evolution and termination of OAE 2, linking the P and Fe cycles.

D. A site-specific investigation of a coastal section in Morocco using a variety of geochemical, biostratigraphic and sedimentological techniques. This section is unique in this project as it is believed that during the late Cretaceous it was an active upwelling zone.

E. The numerical modelling of organic matter accumulation in two sections, from Italy and Spain. The Italian section is extensively investigated using geochemical, biostratigraphic, and sedimentological techniques.

F. Conclusions

A.P.'s Affiliated paper (not first author)

G. Annexes (Raw data, conference abstracts etc)

References

Akande, S.O., Ojo, O.J., Erdtmann, B.D., Hetenyi, M., 1998. Paleoenvironments, source rock potential and thermal maturity of the Upper Benue rift basins, Nigeria: Implications for hydrocarbon exploration. Organic Geochemistry 29, 531-542.

Algeo, T.J., 2004. Can marine anoxic events draw down the trace element inventory of seawater? Geology 32, 1057-1060.

Anderson, D.L., Delaney, M.L., 2000. Sequential extraction and analysis of phosphorus in marine sediments: streamlining of the SEDEX procedure. Limnology and Oceanography 45, 509-515.

Arthur, M., Premoli-Silva, I., 1982, Development of widespread organic rich strata in Mediterranean Tethys. In: Schlanger, A., and Cita, M.B., (Eds.), Nature and Orgin of Cretaceous Carbon-rich Facies. Academic Press, London/New York/Paris, 7-54.

Bak, M., 1996. Cretaceous radiolaria from Niedzica succession of the Pieniny Klippen Belt in Polish Carpathians. Acta Palaeontologica Polonica 41, 91-110.

Bodin, S., Alexis, G., Matera, V., Steinmann, P., Vergmeulen, J., Gardin, S., Adatte, T., Coccioni, R., Föllmi, K.B., 2006. Enrichment of redox-sensative trace metals (U. V, Mo, As) associated with the late Hautervian Faraoni oceanic anoxic event. International Journal of Earth Sciences DOI 10.1007/s00531-006-0091-9, 1-15.

Bralower, T.J., Thierstein, H., R., 1984. Low productivity and slow deep-water circulation in Mid-Cretaceous oceans. Geology 12, 614-618.

Brumsack, H.J., 2006. The trace metal content of recent organic-rich sediments: Implications for Cretaceous black shale formation. Palaeogeography Palaeoclimatology Palaeoecology 232, 344-361.

Calvert, S.E., Bustin, R.M., Ingall, E.D., 1996. Influence of water column anoxia and sediment supply on the burial and preservation of organic carbon in marine shales. Geochimica Et Cosmochimica Acta 60, 1577-1593.

Caron, M., 1983. La spéciation chez les foraminifères planctiques: une réponse adaptée au contrainte de l'environnement. Zitteliana 10, 671-676.

Chen-Tung, Chen, A., 1993. The oceanic anthropogenic CO2 sink. Chemosphere 27, 1041-1064.

China, G.S.o., 1922. Bulletin of the Geological Society of China.

Clark, L.L., Ingall, E.D., Benner, R., 1998. Marine phosphorus is selectively remineralized. Nature 393, 426-426.

Coccioni, R., Luciani, V., 2004. Planktonic formainifera and environmental changes across the Bonarelli Event (OAE 2, latest Cenomanian) in it type area. A high resolution study from the Tethyan reference Bottaccione Section (Gubbio, Central Italy). Journal of Foraminiferal Research 34, 109-129.

Demaison, G.T., Moore, G.T., 1980. Anoxic environments and oil source bed genesis. Organic Geochemistry 2, 9-31.

Eijsink, L.M., Krom, M.D., de Lange, G.J., 1997. The use of sequential extraction techniques for sedimentary phosphorus in eastern Mediterranean sediments. Marine Geology 139, 147-155.

Erbacher, J., Thurow, J., 1997. Influence of oceanic anoxic events on the evolution of mid-Cretaceous radiolaria in the North Atlantic and western Tethys. Marine Micropaleontology 30, 139-158.

Erbacher, J., Thurow, J., Littke, R., 1996. Evolution patterns of radiolaria and organic matter variations: A new approach to identify sea-level changes in mid-Cretaceous pelagic environments. Geology 24, 499-502.

Filippelli, G.M., 2001. Carbon and phosphorus cycling in anoxic sediments of the Saanich Inlet, British Columbia. Marine Geology 174, 307-321.

Filippelli, G.M., Ruttenberg, K.C., 1997. Preface - Phosphorus cycling and sedimentation in marine and freshwater systems. Marine Geology 139, 1-4.

Gale, A.S., Smith, A.B., Monks, N.E.A., Young, J.A., Howard, A., Wray, D.S., Huggett, J.M., 2000. Marine biodiversity through the Late Cenomanian-Early Turonian: palaeoceanographic controls and sequence stratigraphic biases. Journal of the Geological Society 157, 745-757.

Gehrels, R., Kirby, J.R., Prokoph, A., Newnham, R.M., Achterberg, E.P., Evans, H., Black, S., Scott, D.B., 2005. Onset of recent rapid sea-level rise in the western Atlantic Ocean. Quaternary Science Reviews 24.

Gehrels, R.W., Szkorbik, K., Bartholody, J., Kirby, J.R., Bradley, S.L., Marshall, W.A., Heinemeier, J.,

Pedersen, J., B. T., 2006. Late Holocene sea-level changes and isostacy in western Denmark. Quaternary Research 66, 288-302.

Grosheny, D., Malartre, F., 1997. Adaptive strategies of planktonic foraminifera and sedimentary systems tract: the Cenomanian-Turonian deposits of southeastern France. Comptes Rendus De L Academie Des Sciences Serie Ii Fascicule a-Sciences De La Terre Et Des Planetes 324, 491-497.

Grosheny, D., Tronchetti, G., 1993. Cenomanian-Turonian Crisis - Comparative Responses of Benthic Foraminifera Assemblages of the Carbonate Platform and the Basin in Southeastern France. Cretaceous Research 14, 397-408.

Gusic, I., Jelaska, V., 1993. Upper Cenomanian Lower Turonian Sea-Level Rise and Its Consequences on the Adriatic Dinaric Carbonate Platform. Geologische Rundschau 82, 676-686.

Gächter, R., Meyer, J.S., Mares, A., 1988. Contribution of bacteria to release and fixation of phosphorus from marine sediments. Limnology and Oceanography 33, 1542-1558.

Handoh, I.C., Lenton, T.M., 2003. Periodic mid-Cretaceous oceanic anoxic events linked by oscillations of the phosphorus and oxygen biogeochemical cycles. Global Biogeochemical Cycles 17, doi:10.1029/2003GB002039.

Hart, M.B., 1980. The recognition of Mid-Cretaceous sea-level changes by means of foraminifera. Cretaceous Research 1, 289-297.

Hart, M.B., Ball, K.C., 1986, Late Cretaceous anoxic events, sea-level changes and the evolution of planktonic formainfera. In: Summerhayes, C.P., and Shackleton, N.J., (Eds.), North Atlantic Paleogeography. Geological Society of America, Boulder, Colorado, 67-78.

Hasegawa, T., 2003. Cretaceous terrestrial paleoenvironments of northeastern Asia suggested from carbon isotope stratigraphy: Increased atmospheric pCO(2)-induced climate. Journal of Asian Earth Sciences 21, 849-859.

Hilbrecht, H., Frieg, C., Troger, K.A., Voigt, S., Voigt, T., 1996. Shallow water facies during the Cenomanian-Turonian anoxic event: Bio-events, isotopes, and sea level in southern Germany. Cretaceous Research 17, 229-253.

Hradecka, L., Svabenicka, L., 1995. Foraminifera and calcareous nannoplankton assemblages from the Cenomania-Turonian boundary interval of the Knoviz section, Bohemian Cretaceous Basin. Geologica Carpathica 46, 267-276.

Huber, B.T., Leckie, R.M., Norris, R.D., Bralower, T.J., CoBabe, E., 1999. Foraminiferal assemblage and stable isotopic change across the Cenomanian-Turonian boundary in the subtropical North Atlantic. Journal of Foraminiferal Research 29, 392-417.

Huber, B.T., Norris, R.D., Macleod, K.H., 2002. Deep-sea paleotemperature record of extreme warmth during the Cretaceous. Geology 30, 123-126.

Ingall, E., Jahnke, R., 1997. Influence of water-column anoxia on the elemental fractionation of carbon and phosphorus during sediment diagenesis. Marine Geology 139, 219-229.

Ingall, E.D., Bustin, R.M., Vancappellen, P., 1993. Influence of Water Column Anoxia on the Burial and Preservation of Carbon and Phosphorus in Marine Shales. Geochimica Et Cosmochimica Acta 57, 303-316.

Ingall, E.D., Van Cappellen, P., 1990. Relation between Sedimentation-Rate and Burial of Organic Phosphorus and Organic-Carbon in Marine-Sediments. Geochimica Et Cosmochimica Acta 54, 373-386.

Jarvis, I., Carson, G.A., Cooper, M.K.E., Hart, M.B., Leary, P.N., Tocher, B.A., Horne, D.J., Rosenfeld, A., 1988. Microfossil assemblages and the Cenomanian-Turonian (late Cretaceous) oceanic anoxic event. Cretaceous Research 9, 3-103.

Jarvis, I., Gale, A.S., Jenkyns, H.C., Pearce, M.A., 2006. Secular variation in late Cretaceous carbon isotopes: a new d13C carbonate reference curve for the Cenomanian-Campanian (99.6-70.6 Ma). Geological Magazine 143, 561-608.

Jenkyns, H.C., 1980. Cretaceous anoxic events, from continents to oceans. Journal of the Geological Society of London 137, 171-188.

---. 1991. Impact of Cretaceous Sea-Level Rise and Anoxic Events on the Mesozoic Carbonate Platform of Yugoslavia. Aapg Bulletin-American Association of Petroleum Geologists 75, 1007-1017.

Jensen, H.S., Thamdrup, B., 1993. Iron-bound phosphorus in marine-sediments as measured by bicarbonate-dithionite extraction. Hydrobiology.

Jorgensen, B.B., 2000, Bacteria and marine Biogeochemistry. In: Schulz, H.D., and Zabel, M., (Eds.), Marine Geochemistry. Springer, 173-207.

Kaiho, K., Fujiwara, O., Motoyama, I., 1993. Midcretaceous Faunal Turnover of Intermediate-Water Benthic Foraminifera in the Northwestern Pacific-Ocean Margin. Marine Micropaleontology 23, 13-49.

Kaiho, K., Hasegawa, T., 1994. End-Cenomanian Benthic Foraminiferal Extinctions and Oceanic Dysoxic Events in the Northwestern Pacific-Ocean. Palaeogeography Palaeoclimatology Palaeoecology 111, 29-43.

Kaiho, K., Saito, S., 1994. Ocean crust production and climate durin the last 100 Myr. Terra Nova 6, 376-384.

Katz, B.J., Dittmar, E.I., Ehret, G.E., 2000. A geochemical review of carbonate source rocks in Italy. Journal of Petroleum Geology 23, 399-424.

Kauffman, E.G., 1995, Global Change Leading to Biodiversity Crisis in a Greenhouse World: The Cenomanian-Turonian (Cretaceous) Mass Extinction, Effects of Global Change on Life. Panel on Effects of Past Global Change on Life, National Research Council, 47-71.

Keller, G., Han, Q., Adatte, T., Burns, S.J., 2001. Palaeoenvironment of the Cenomanian-Turonian transition at Eastbourne, England. Cretaceous Research 22, 391-422.

Keller, G., Pardo, A., 2004. Age and paleoenvironment of the Cenomanian-Turonian global stratotype section and point at Pueblo, Colorado. Marine Micropalaeontology 51, 95-128.

Keller, G., Stueben, D., Berner, Z., Adatte, T., 2004. Cenomanian - Turonian d13C, d18O, Sea level and salinity variations at Pueblo, Colorado. Palaeogeography, Palaeoclimatology, Palaeoecology 211, 19-43.

Kerr, A.C., 1998. Oceanic plateau formation: a cause of mass extinction and black shale deposition around the Cenomanian-Turonian boundary? Journal of the Geological Society London 155, 619-626.

Khaled, K.A., 1999. Cretaceous source rocks at the Abu Gharadig oil- and gasfield, northern Western Desert, Egypt. Journal of Petroleum Geology 22, 377-395.

Kolonic, S., Damste, J.S.S., Bottcher, M.E., Kuypers, M.M.M., Kuhnt, W., Beckmann, B., Scheeder, G.,

Wagner, T., 2002. Geochemical characterization of Cenomanian/Turonian black shales from the Tarfaya Basin (SW Morocco) - Relationships between palaeoenvironmental conditions and early sulphurization of sedimentary organic matter. Journal of Petroleum Geology 25, 325-350.

Kolowith, L.C., Ingall, E.D., Benner, R., 2001. Composition and cycling of marine organic phosphorus. Limnology and Oceanography 46, 309-320.

Kuhnt, W., Herbin, J.P., Thurow, J., Wiedmann, J., 1990, Distribution of Cenomanian-Turonian Oragnic Facies in the Western Mediterranean and Along the Adjacent Atlantic Margin. In: Huc, A.Y., ed., Deposition of Organic Facies. AAPG Studies in Geology, 133-160.

Kuypers, M.M.M., Pancost, R.D., Nijenhuis, I.A., Damste, J.S.S., 2002. Enhanced productivity led to increased organic carbon burial in the euxinic North Atlantic basin during the late Cenomanian oceanic anoxic event. Paleoceanography 17, art. no.-1051.

Larson, R.L., 1991. Geoogical consequences of superplumes. Geology 19, 963-966.

Larson, R.L., Erba, E., 1999. Onset of the mid-Cretaceous greenhouse in the Barremian-Aptian: Igneous events and the biological, sedimentary, and geochemical responses. Paleoceanography 14, 663-678.

Latimer, J.C., Filippelli, G.M., Hendy, I., Newkirk, D.R., 2006. Opal-associated particulate phosphorus: Implications for the marine P cycle. Geochimica et Cosmochimica Acta 70, 3843-3854.

Leckie, M.R., Bralower, T.J., Cashman, R., 2002. Oceanic anoxic events and plankton evolution: Biotic response to tectonic forcing during the mid-Cretaceous. Paleoceanography 17, 1-29.

Leckie, R.M., 1985. Foraminifera of the Cenomanian-Turonian Boundary Interval, Greenhorn Formation, Rock Canyon Anticline, Pueblo, Colorado. Fine-Grained Deposits and Biofacies of the Cretaceous Western Interior Seaway: Evidence of Cyclic Sedimentary Processes., 4, SEPM Bulletin, 139-149 pp.

Leckie, R.M., Yuretich, R.F., West, L.O.L., Finkelstein, D., Schmidt, M., 1998, Paleooceanography of the south west Interior Sea during the time of the Cenomanian-Turonian boundary (late Cretaceous). In: Dean, W.E., and Arthur, M.A., (Eds.), Concepts in Sedimentology and Paleontology. SEPM, 101-126.

Luciani, V., Cobianchi, M., 1999. The Bonarelli Level and other black shales in the Cenomanian-Turonian of the northeastern Dolomites (Italy): calcareous nannofossil and foraminiferal data. Cretaceous Research 20, 135-167.

Lyell, C., 1837. Principles of geology: being an enquiry how far the former changes of the Earth's surface are referable to causes now in operation, Philadelphia, 546 pp.

---. 1872. Principles of geology of the modern changes of the Earth and its inhabitants considered as illustrative of geology., D. Appleton, New York.

Mackenzie, F.T., Ver, L.M., Lerman, A., 2002. Century-scale nitrogen and phosphorus controls of the carbon cycle. Chemical Geology 190, 13-32.

Matear, R.J., 2001. Effects of numerical advection schemes and eddy parameterizations on ocean ventilation and oceanic anthropogenic CO2 uptake. Ocean modelling 3, 217-248.

Matear, R.J., Hirst, A.C., 1999. Climate Change feedback on the future oceanic CO2 uptake. Tellus 51, 722-733.

Mermighis, A., Philip, J., Tronchetti, G., 1991. Carbonate Platform Sequences and System Tracts at the Cenomanian-Turonian Boundary, Internal Hellenids (Peloponnesus, Greece). Bulletin de la Société Géologique de France 162, 547-552.

Morford, J.L., Emerson, S., 1999. The geochemistry of redox sensative trace metals in sediments. Geochimica Et Cosmochimica Acta 63, 1735-1750.

Mostafa, A.R., 1999. Organic geochemistry of the Cenomanian-Turonian sequence in the Bakr area, Gulf of Suez, Egypt. Petroleum Geoscience 5, 43-50.

Nederbragt, A.J., Thurow, J., Vonhof, H., Brumsack, H.J., 2004. Modelling oceanic carbon and phosphorus fluxes: implications for the cause of the late Cenomanian Oceanic Anoxic Event (OAE 2). Journal of the Geological Society, London 141, 721-728.

Nijenhuis, I.A., Bosch, H.J., Damste, J.S.S., Brumsack, H.J., De Lange, G.J., 1999. Organic matter and trace element rich sapropels and black shales: a geochemical comparison. Earth and Planetary Science Letters 169, 277-290.

Nuttle, W.K., Wrobleski, J.S., Sarmiento, J.L., 1991. Advances in modeling ocean primary production and its role in the global carbon cycle. Advances in Space Research 11, 67-76.

Nzoussi-Mbassani, P., Disnar, J.R., Laggoun-Defarge, F., 2003. Organic matter characteristics of Cenomanian-Turonian source rocks: implications for petroleum and gas exploration onshore Senegal. Marine and Petroleum Geology 20, 411-427.

Payton, A., Cade-Menun, B.J., MacLaughlin, K., Faul, K.L., 2003. Phosphorus regeneration of sinking marine particles: evidence from 31P-NMR. Marine Chemistry 82, 55-70.

Pedersen, T.F., Calvert, S.E., 1990. Anoxia vs. Productivity: what controls the formation of organic carbon-rich sediments and sedimentary rocks? Bulletin of the American Association of Petroleum Geologists 74, 454-466.

Philip, J.M., Airaudcrumiere, C., 1991. The Demise of the Rudist-Bearing Carbonate Platforms at the Cenomanian Turonian Boundary - a Global Control. Coral Reefs 10, 115-125.

Premoli-silva, I., Erba, E., Salvini, G., Locatelli, C., Verga, D., 1999a. Biotic changes in Cretaceous oceanic anoxic events of the tethys. Journal of Foraminiferal Research 29, 352-370.

Premoli-Silva, I., Erba, E., Salvini, G., Locatelli, C., Verga, D., 1999b. Biotic changes in Cretcaeous oceanic anoxic events of the Tethys. Journal of Foraminiferal Research 29, 352.

Racki, G., 1999. Silica-secreting biota and mass extinctions: survival patterns and processes. Palaeogeography Palaeoclimatology Palaeoecology 154, 107-132.

Redfield, A.C., 1958. The biological control of chemical factors in the environment. American Scientist 46.

Roche, D., Paillard, D., Ganopolski, A., Hoffmann, G., 2004. Oceanic oxygen-18 at the preent day and LGM: equilibrium soimulations with a coulpled climate model of intermeadiate complexity. Earth and Planetary Science Letters 218, 317-330.

Roden, E.E., Edmonds, J.W., 1997. Phosphate mobilization in iron-rich anaerobic sediments: Microbial Fe(III) oxide reduction versus iron-sulfide formation. Archiv Fur Hydrobiologie 139, 347-378.

Rullkötter, R., 2000, Organic matter: The driving force for early diagensis. In: Schulz, H.D., and Zabel, M.,

(Eds.), Marine Geochemistry. Springer, 129-172.
Ruttenberg, K.C., 1992. Development of a sequential extraction method for different forms of phosphorus in marine sediments. Limnology and Oceanography 37, 1460-1482.
Ryan, W.B.F., Cita, M.B., 1977. Ignorance concerning episodes of ocean-wide stagnation. Marine Geology 23, 197-215.
Sageman, B.B., Murphy, A.E., Werne, J.P., Straeten, C.A.V., Hollander, D.J., Lyons, T.W., 2003. A tale of shales: the relative roles of production, decomposition and dilution in the accumulation of organic-rich strata, Middle-Upper Devonian, Appalachian Basin. Chemical Geology 195, 229-273.
Schenau, S.J., Reichart, G.J., Lange, G.J., 2005. Phosphorus burial as a function of paleoproductivity and redox conditions in Arabian Sea sediments. Geochimica et Cosmochimica Acta 69, 919-931.
Schlanger, S.O., Arthur, M.A., Jenkyns, H.C., Scholle, P.A., 1983. Stratigraphic and Paleo-oceanographic setting of organic carbon-rich strata deposited during Cenomanian-Turonian Oceanic Anoxic Event. AAPG Bulletin-American Association of Petroleum Geologists 67, 545-545.
Schlanger, S.O., Jenkyns, H.C., 1976. Cretaceous oceanic anoxic events: Causes and consequences. Geol. Mijnbouw 55, 179-184.
Schlanger, S.O., Jenkyns, H.C., Premoli-silva, I., 1981. Volcanism and Vertical Tectonics in the Pacific Basin Related to Global Cretaceous trangressions. Earth and Planetary Science Letters 52, 435-449.
Seidov, D., Stouffer, R.J., Haupt, R.J., 2005. Is there a simple bi-polar seesaw? Global and Planetary Change 49, 19-27.
Slomp, C.P., Epping, E.H.G., Helder, W., Van Raaphort, W., 1996. A key role for iron-bound phosphorus in authigenic apatite formation in North Atlantic continental platform sediments. Journal of Marine Research 54, 1179-1205.
Slomp, C.P., Thompson, J.A., de Lange, G.J., 2002. Enhanced regeneration of phosphorus during formation of the most recent eastern Mediterranean sapropel (S1). Geochimica Et Cosmochimica Acta 66, 1 April 2002.
Slomp, C.P., Thomson, J., de Lange, G.J., 2004. Controls on phosphorus regeneration and burial during formation of eastern Mediterranean sapropels. Marine Geology 203, 141-159.
Sorgenfrei, T., 1960. Report of the twenty-first session, Norden, Det Berlingske Bogtrkkeri, 252 pp.
Suess, E., 1904. The Face of the Earth (Das Antiltz Der Erde), 3, Clarendon Press.
Sundby, B., Gobeil, C., Silcerberg, N., Mucci, A., 1992. The phosphorus cycles in coastal marine sediments. Limnology and Oceanography 37, 1129-1145.
Ulicny, D., Hladikova, J., Attrep, M.J., Cech, S., Hradecka, L., Svobodova, M., 1997. Sea-level changes and geochemical anomalies across the Cenomanian-Turonian boundary: Pecinov quarry, Bohemia. Palaeogeography Palaeoclimatology Palaeoecology 132, 265-285.
Valladares, I., Recio, C., Lendinez, A., 1996. Sequence stratigraphy and stable isotopes (delta C-13,delta O-18) of the late Cretaceous carbonate ramp of the western margin of the Iberian chain (Soria, Spain). Sedimentary Geology 105, 11-28.
Van Cappellen, P., Ingall, E.D., 1994. Benthic Phosphorus Regeneration, Net Primary Production, and Ocean Anoxia - a Model of the Coupled Marine Biogeochemical Cycles of Carbon and Phosphorus. Paleoceanography 9, 677-692.
---. 1996. Redox stabilization of the atmosphere and oceans by phosphorus-limited marine productivity. Science 271, 493-496.
Veith, A., 1895. Petroleum, H. C. Baird & Co., 715 pp.
Voigt, S., Gale, A.S., Voigt, T., 2006. Sea-level chane, carbon cycling and palaeoclimate during the Late Cenomanian of northwest Europe; an integrated palaeoenvironmental analysis. Cretaceous Research doi:10.1016/j.cretres.2006.04.005.
Voigt, S., Hilbrecht, H., 1997. Late Cretaceous carbon isotope stratigraphy in Europe: Correlation and relations with sea level and sediment stability. Palaeogeography Palaeoclimatology Palaeoecology 134, 39-59.
Wallmann, K., 2003. Feedbacks between oceanic oceanic redox states and marine productivity: A model perspective focused on benthic phosphorus cycling. Global Biogeochemical Cycles 17, 10-1 - 10-18.
Wanninkhof, R., 1992. Relationship bewteen wind speek and gas exchange over the ocean. Journal of Geophysical Research 97, 7373-7382.
Woodward, H., 1864. Geological Magazine, Columbia University Press.
Xu, Y., Watanabe, Y.W., Aoki, S., Harada, K., 2000. Simulations of storage of anthropogenic carbon dioxide in the North Pacific using an ocean general circulation model. Marine Chemistry 72, 221-238.
Yarinkcik, K.M., Murray, R.W., Lyons, T.W., Peterson, L.C., Haug, G.H., 2000. Oxydation history of bottom waters in the Cariaco Basin Venezuela, over the past 578,000 years: Results from redox-sensative metals (Mo, V, Mn, and Fe). Paleoceanography 15.

- B -

Phosphorus and the roles of productivity and nutrient recycling during Oceanic Anoxic Event 2

Accepted in November 2006, for publication in GEOLOGY
Revised version accepted in January 2007

The following short paper introduces the speciation of phosphorus in four sections containing a Cretaceous Oceanic Anoxic Event. It contains an abridged discussion into the implications of the data.

Common sense is the collection of prejudices acquired by age eighteen.

Albert Einstein

Phosphorus and the roles of productivity and nutrient recycling during OAE 2

Haydon P. Mort[1], Thierry Adatte[1], Karl B. Föllmi[1], Gerta Keller[2], Philipp Steinmann[1]
Virginie Matera[1], Zsolt Berner[3], Doris Stüben[3]

[1] *Rue Emile Argand 11, Institute of Geology, University of Neuchatel, Case postale 158, CH-2009 Neuchatel, Switzerland*
[2] *Department of Geosciences, Princeton University, Guyot Hall, Princeton, NJ 08544-1003, USA*
[3] *Institut für Mineralogie und Geochemie, Universität Karlsruhe, 76128 Karlsruhe, Germany*
**haydon.mort@unine.ch*

Abstract

Four representative sections documenting the impact of the late Cenomanian oceanic anoxic event, OAE 2, have been studied in different basins with different paleobathymetric regimes. Accumulation rates of phosphorus bound to iron, organic matter and authigenic phosphate are shown to rise and arrive at a distinct maximum at the onset of OAE 2, with an associated increase in $\delta^{13}C$ values. Phosphorus accumulation rates return to pre-excursion values in the interval where the $\delta^{13}C$ record reaches its first maximum. A positive correlation is observed between increases in organic matter contents, hydrogen indices, and Corg/Preact molar ratios, and the evolution of the $\delta^{13}C$ record. The offset in time between the maximum in P accumulation, and the peaks in organic carbon burial, hydrogen indices, Corg/Preact molar ratios, and the $\delta^{13}C$ record, are explained by the evolution of OAE 2 in the following steps: (1) An increase in productivity increased the flux of organic matter and P into the sediments; the initial preservation potential for organic matter was low and most of the organic matter decomposed, releasing P which was transferred into an authigenic phase; (2) Continuing enhanced productivity created dysaerobic conditions in bottom waters; the preservation potential for organic matter increased, whereas the sediments retention ability for phosphorus decreased; the latter effect sustained high productivity rates through the benthic regeneration of phosphorus; (3) Primary productivity led to an increase in the abundance of free oxygen in the ocean and atmosphere system. After the sequestration of CO2 in the form of black shales, this oxygen aided in pushing the ocean back into equilibrium, terminating black shale deposition and removing bioavailable P from the water column.

Keywords: **Phosphorus, recycling, feedbacks, marine geochemistry, productivity, preservation.**

B.1. Introduction

Periods during which oceanic bottom waters became oxygen depleted are well documented for the Cretaceous, and their study has led to an improved understanding of the global carbon cycle and climate change in a greenhouse world (Jenkyns, 1980; Schlanger et al., 1983; Arthur et al., 1988; Tyson et al., 1991). The late Cenomanian oceanic anoxic event (OAE 2) is one of the most prominent anoxic episodes of the Mesozoic, characterized by the widespread accumulation of organic-carbon rich sediment and diagnostic redox-sensitive metals (Orth et al., 1993; Lipinski et al., 2003; Kolonic et al., 2005; Meyers et al., 2005; Snow et al., 2005). OAE 2 is accompanied by a 2‰ positive $\delta^{13}C$ excursion in marine carbonates and organic matter with a plateau of high $\delta^{13}C$ values that persisted during the anoxic episode (see above refs). Major biotic effects resulting in the extinction as well as the evolution of new species have been observed during OAE 2 (Leckie, 1985; Jarvis et al., 1988; Elder, 1989; Keller and Pardo, 2004).

Various OAE triggering mechanisms have been proposed ranging from increased oceanic

CO2 derived from large igneous province (LIP) activity (Kerr, 1998), through increased nutrient delivery into surface waters from continental sources (Hilbrecht et al., 1996; Larson and Erba, 1999), to the automated flipping between oxic and anoxic states driven by an interplay between atmospheric and oceanic biogeochemical positive and negative feedbacks, which existed against the background of the Cretaceous climate regime (Handoh and Lenton, 2003).

The ancient greenhouse world and its environmental and biotic interactions can provide an analogue for evaluating the potential consequences of the climate warming we face today. However, large gaps still exist in our understanding of these events, particularly with respect to the rate of primary productivity, its interactions with the carbon and nutrient cycles, and feedback mechanisms related to low-oxygen bottom waters. Here, we present a detailed study on the behaviour of phosphorus (P) during OAE 2, in order to evaluate the roles of primary productivity and nutrient cycling and to test the outcome of a numerical model by (Van Cappellen and Ingall, 1994, 1996), in which a relationship is postulated between anoxic conditions, P regeneration, and sustained primary productivity (further discussed by (Nederbragt et al., 2004)

The behaviour of the carbon and phosphorus cycles during OAE 2 are reconstructed in four geographic localities representative of differing paleobathymetric and paleoceanographic regimes, based on whole-rock stable carbon isotopes, quantities and types of organic matter, and phosphorus mass accumulation rates (P MARs) for iron bound (PFe), authigenic (Pauthigenic), organic phosphorus (Porganic), and detrital phosphorus (Pdetrital). The sections studied are at Pueblo (Colorado, USA), Eastbourne (UK), Furlo (Italy) and Manilva (Spain). The Pueblo section is located in the relatively shallow US Western Interior Seaway (WIS) and, as the Cenomanian-Turonian (C-T) stratotype section and point, forms an ideal reference point for dating other sections based on high-resolution planktic foraminiferal biostratigraphy and the typical □13C record for OAE 2 (Fig. 1, Site 1) (Keller and Pardo, 2004;

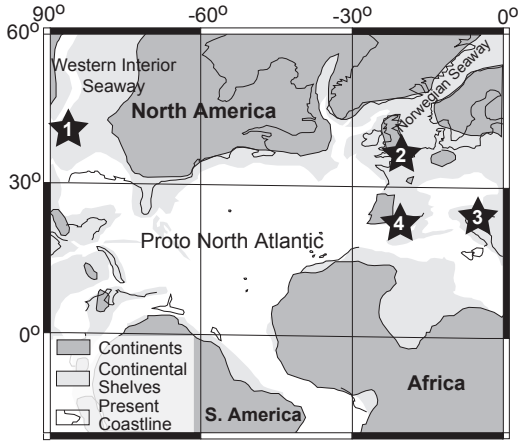

Figure 1. Palaeogeography of the western northern hemisphere at the Cenomanian-Turonian boundary (93.5 Ma). Adapted from (Kuypers et al., 2002). Study locations: (1) Pueblo, (2) Eastbourne, (3) Furlo, (4) Manilva.

Keller et al., 2004; Caron et al., 2006). Recently a new chronostratigraphic framework was applied to the Pueblo section (Sageman et al., 2006) using high-resolution bulk $\delta^{13}C$ determination and relative ages based on orbital frequencies identified above Bed 63 (see Pueblo bed number in fig. 2). The section at Eastbourne (Site 2) was deposited in a continental shelf setting and has also been studied extensively (Gale et al., 1993; Paul et al., 1999; Keller et al., 2001; Tsikos et al., 2004; Gale et al., 2005). The sections at Furlo (Site 3), located in the Umbria-Marche Basin, Italy, and Manilva (Site 4), located in Andalusia, southern Spain (Reicherter et al., 1994; Mort et al., in press), were deposited in deep pelagic environments marked by organic-rich sediment deposition (i.e. the Bonarelli level; Luciani and Cobianchi, (1999)) and coeval carbonate dissolution that limits age control based on calcareous microfossils.

B.2. Methods

The SEDEX sequential extraction and analysis method (Ruttenberg, 1992; Anderson and Delaney, 2000) was used to obtain P contents for phases associated with iron and manganese oxyhydroxides and P contained within authigenic francolite, detrital apatite, and organic remains. Instrumental accuracy (as determined by an internal standard and 2 replicates) was < 5 % using a Perkin Elmer Lambda 10 spectrophometer

(see appendix 2 for additional information). The P MAR was calculated in mg/cm2/ka. Rock densities were taken as 2.3, 2.4 and 2.5 g/cm3 for marl, shale and limestone, respectively (Attewell and Farmer, 1976). These densities were also verified in the laboratory by measuring the displacement of water by a sample of known mass. For the Pueblo section, the accumulation rates used were based on dating from Hardenbol et al., (1998); Keller and Pardo, (2004) as well as the new cyclostratigraphic framework from (Sageman et al., 2006). Additional online material (Appendix 1) contains the raw concentrations of P to enable other timescales to be used to construct MARs (Gradstein et al., 2004). Total reactive P (Preactive) was calculated by an addition of all the measured phases, under the assumption that most "detrital" P represents authigenic P. This assumption is well justified for all

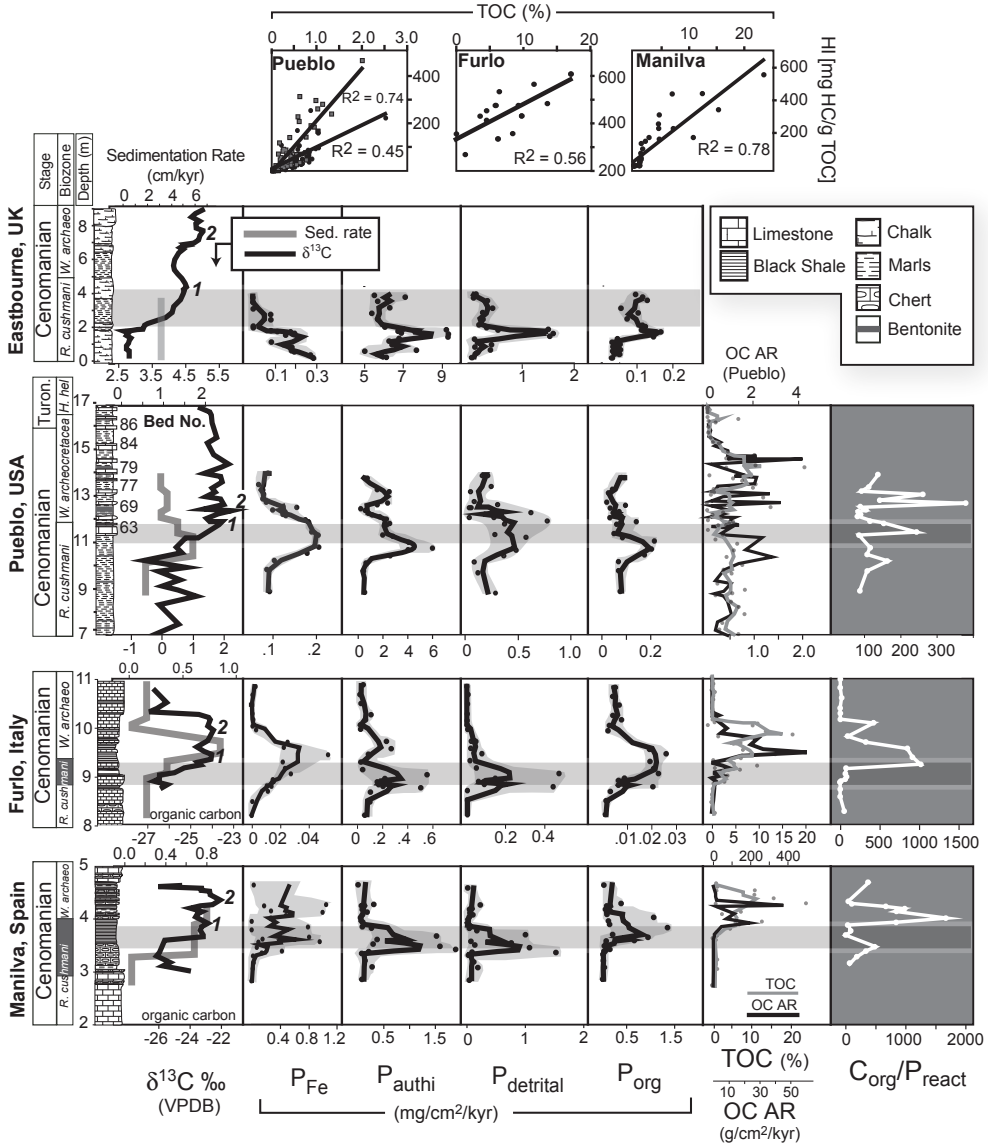

Figure 2. Phosphorus speciation with accumulation rates (mg/cm2/k.y.) in the four sections, plotted against their corresponding $\delta^{13}C$ curves. Total Preactive can be found in appendix 1 in addition to all the raw P-speciation data used to in this figure. The grey shaded area highlights the interval in time between the peak in P MARs and the 1st peak in $\delta^{13}C$ values. The percentages for total organic carbon, the hydrogen indices and the Corg/Preactive molar ratios are also shown. Smoothed lines are 3 point moving averages. The scatter-plot is a correlation between TOC and Hydrogen Index. Two correlations are made for Pueblo. The black circles correlations based on predominantly terrestrial, largely organic matter (pre-OAE). The grey squares are derived from predominantly marine organic matter (above Bed 63). The Rotalipora cushmani biozones in Furlo and Manilva are extended with grey bars, which represent the probable extinction level. Thin section analyses see R. cushmani disappearing at the top of the white bar, an artifact of dissolution. The extinction of R. cushmani is not used to construct MARs in these sections.

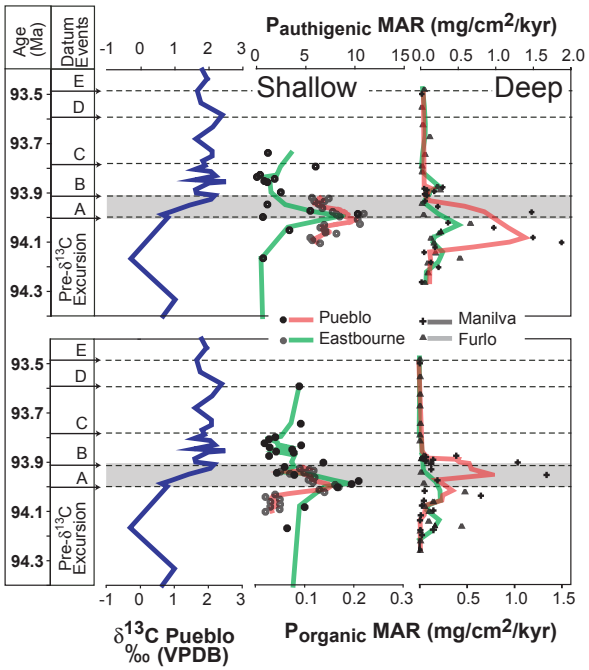

Figure 3. Isotopic and biostratigraphic datum points allow ages to be assigned to each sample for the four sections and plotted against time. Organic and authigenic phosphorus as determined from the SEDEX sequential extractions are shown. Shallow (Pueblo, Eastbourne) and deeper sections (Manilva, Furlo) are separated. This also allows us to observe differences in the P MAR relating to paleodepth. The d^{13}C isotope curve from Pueblo is presented for correlation (Keller et al., 2004). A series of dates that are used to construct this age model are presented A-E. A = d^{13}C excursion onset (94 Ma ± 0.2); B = 1st peak in d^{13}C values (93.91 Ma ± 0.2); C = Heterohelix shift (93.78 Ma ± 0.2); D = LAD Neocardioceras juddi (93.59 Ma ± 0.2); E = FAD Watinoceras devonense (93.49 Ma ± 0.2). Dates A, B, and C were taken from Keller et al. (2004). Dates for D and E are taken from Hardenbol et al. (1998). Error bars for first and last appearances result from the extrapolation of these events from paleomagnetic dates and radiometric dates of Hardenbol et al. (1998).

sections with the exception of Pueblo, where some truly detrital-P may occur. Given that detrital-P is low in this section, in comparison to the authigenic P, and that both phases behave similarly, we assume that, here also, most detrital P represents crystallized authigenic P. The occurrence of this type of recrystalization has been documented in younger sediments (Filippelli and Delaney, 1995; Föllmi et al., 2005). The authigenic P phase may locally include biogenic P, such as fish debris, but a systematic analysis of thin sections showed that fish debris is only a minor source of P limited to local levels in the sections at Furlo and Manilva. Total organic carbon (TOC) and hydrogen indices were measured by Rock-Eval, with precisions of < 1%. Molecular Corg/Preactive ratios were calculated to assess the relative importance of the vertical flux of P to and from the sediment. Age control and correlation between sites were based on well-dated sequences at Pueblo and Eastbourne, and correlation with Furlo and Manilva was based on microfossil biostratigraphy and the δ^{13}C curves derived from organic carbon.

B.3. Results

In all four sections, concentrations and MARs of all measured P species (except for PFe in Eastbourne or Porg in Furlo and Manilva) generally reach maximum values within or close to the sediment interval in which the onset of the δ^{13}C positive excursion is registered. They return to pre-excursion values in intervals close to those where the first peak in δ^{13}C has been detected (Fig. 2). The reductions in P MARs are synchronous with increases in hydrogen indices and Corg/Preactive ratios (Fig. 2). Rock-Eval data for the Eastbourne section are not available, due to very low organic carbon contents (<0.1 %). In all other sections, there is a positive correlation between organic carbon contents and their associated hydrogen indexes. The three scatter plots in Figure 2 demonstrate this, with R2 values of 0.78, 0.56 and 0.74 for Manilva, Furlo and Pueblo, respectively. There is a noticeable improvement in the correlation at the Pueblo section above Bed 63, where the origin of organic matter becomes more marine (Keller et al., 2004). At Pueblo, the organic matter content begins to increase well after the first δ^{13}C peak. This is not the case at Furlo and Manilva, where increasing TOC begins at the onset of the δ^{13}C excursion.

The section at Pueblo reveals relatively low Corg/Preactive molar ratios, with a poorly constrained peak just above the maximum in P MARs (Fig. 2). The background Corg/Preactive molar ratios in sediments below and above the organic-rich interval at Furlo are close to 1, implying a significant enrichment of P relative to TOC. The section at Manilva, however, contains higher Corg/Preactive molar ratio background values (~70). In both sections, a well-defined peak

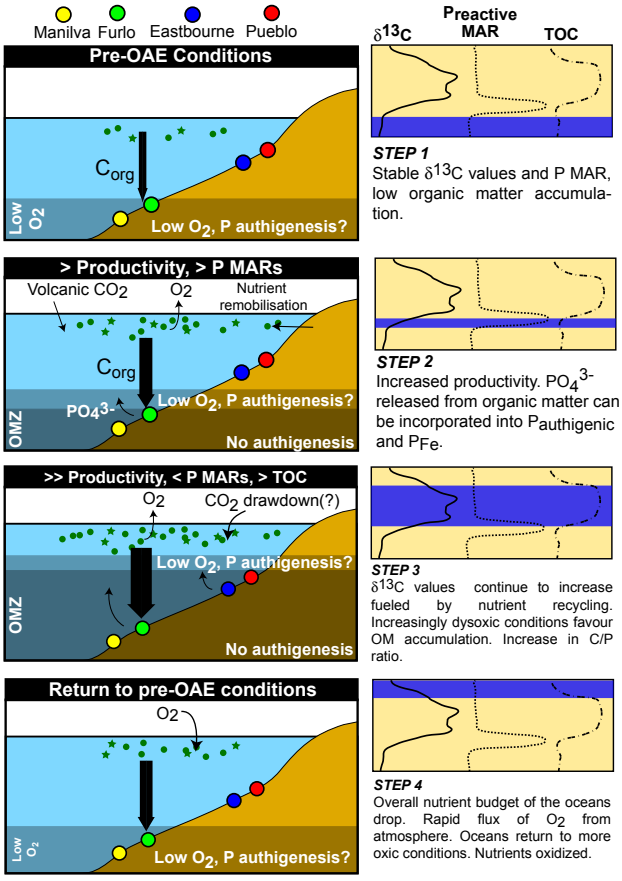

Figure 4: Schematic model of events that may have took place during OAE 2 that could explain our data. See figure and main text body for details.

in Corg/Preactive molar ratios of 1000 and 1600, respectively, is observed immediately above the interval in which P MARs decrease. A temporal comparison between Pauthigenic and Porganic MARs for shallow and deep-water sections is shown in Fig. 3.

B.4. Discussion

The coeval nature of the rises in P MAR during the $\delta^{13}C$ excursion at all four sections is strong evidence for the primary nature of the P signal, rather than being a computational artifact related, for instance, to changing sediment accumulation rates. We therefore consider this signal to be genuine, and the expression of an important change in the marine P cycle during the onset of OAE 2. The so-called '2nd peak' in the $\delta^{13}C$ record is difficult to identify in the Furlo and Manilva sections, as in many other more pelagic environments (Tsikos et al., 2004). This difficulty means that sedimentation rates above the isotope excursion are likely to be wrong. However, we do not consider this important to the present study, which focuses on events during the onset of the isotope excursion and immediately after the first isotope peak.

Previous empirical and modelling studies have observed a decrease in phosphorus burial efficiency (PBE) during periods of increased productivity (Ingall and Jahnke, 1994; Van Cappellen and Ingall, 1994; Schenau et al., 2005). In the model proposed here, we follow up on these studies and take into account the initial increase in P burial efficiency, which is observed for the first time here (Fig. 4). We assume that an initial increase in productivity would have started to reduce the amount of available O2 in deeper waters but not sufficiently to directly augment the accumulation of TOC, which was probably subjected to early diagenetic re-oxidation (indicated by the low background Corg/Preactive molar ratios in the sections of Manilva and especially Furlo). The deeper water conditions at this stage did not impede the increase in precipitation of Pauthigenic derived from the lateral transfer of PO43- from the re-oxidation of organic matter (step 2, Fig. 4) either. The coeval increase in Porganic MARs is not reflected in an increase in TOC contents. This is an indication that sedimentation rate was an important control in Porganic accumulation. Increases and decreases in hydrogen index (HI) have a positive relationship between changes in the preservation and maturity of organic matter (Demaison and Moore, 1980; Espitalié et al., 1985; Akande et al., 1998). Low hydrogen index values indicate that organic matter preservation was poor during the onset of the $\delta^{13}C$ excursion and peak in Preactive MARs.

Increasing dysoxic bottom-water conditions related to the progressive decomposition of organic matter would have gradually inhibited the formation of Pauthigenic, which makes up the bulk of the Preactive (step 4 in Fig. 4). Once this threshold was passed, Preactive MARs appears to have decreased. The fact that $\delta^{13}C$ continues to increase, suggests that surface productivity continued without interruption, possibly sustained by the recycling of bottom-water phosphate and other redox sensitive nutrients (e.g. nitrates from the breakdown of organic matter) back into surface waters. With

this came the introduction of a flux in P from the sediment into the water column, which is indicated by an increase in the Corg/Preactive ratio at the decrease in P MARs in Furlo and Manilva (step 3 in figure 4). This is not observed in Eastbourne, due to insufficient quantities of organic matter, and is highly ambiguous in Pueblo. Nevertheless, Pueblo, like Furlo and Manilva shows a switch from a productivity- to preservation-driven depositional system with the increase in organic matter content occurring after P began to reflux into the water column. This is good evidence that the reduction in P MAR and increases in TOC content are linked to the diminished availability of free oxygen. Furthermore, the hydrogen indices show a good positive correlation with the TOC contents indicating that preservation, not productivity, was the primary factor responsible for the accumulation of organic matter (Erlich et al., 1999; Kolonic et al., 2002). It is plausible that P regeneration would generate new surface productivity in a 'productivity- dysoxia - nutrient regeneration' positive feedback loop.

The accumulation rate of Porganic, however, also decreases with Pauthigenic. The drop is less pronounced than the inorganic P phases. This indicates that sink switching from inorganic to organic matrices occurred but on a limited basis. The fact that Porganic MAR does decrease suggests that the oxidative degradation of organic matter was decelerated under slower bacterial respiration, typical in dysoxic environments (see Jorgensen, 2000 for review).

A significant difference between the shallow and deeper sections is that Pauthigenic MARs in Pueblo and Eastbourne are consistently an order of magnitude higher than at Manilva and Furlo. This is likely because the last two sections record deep-water environments with lower abundances of free O2, thus predisposing Pauthigenic production to be less efficient (Van Cappellen and Ingall, 1996; Filippelli, 1997; Schenau et al., 2005). The phosphorus speciation data do not extend high enough into each lithology to be sure of how OAE 2 was terminated. However, we may speculate on events that would logically play out as a result of our data.

The majority of recent studies propose that a humid climate and higher/rising sea-levels may have reworked nutrients on previously dry land, thus stimulating the initial increase in productivity during OAE 2 (Hilbrecht et al., 1996; Caron et al., 1999; Jarvis et al., 2006). A more arid environment during the $\delta^{13}C$ plateau may have reduced productivity by restricting delivery of phosphate to the sea surface. The decrease in productivity would be accompanied by the gradual introduction of more oxic bottom waters.

In addition, enhanced primary productivity may have had two effects: (1) increase in the concentration of atmospheric O2; (2) sequestration of atmospheric CO2, which may have been partly responsible for creating the conditions necessary for the formation of OAE 2. This CO2 may have become incorporated into organic matter or carbonate or, indeed may have directly enhanced nutrient recycling by contributing to bottom-water dysoxia. The build-up of atmospheric O2, produced during the enhanced primary productivity, may have triggered a negative feedback, flipping the ocean into an oxic state, once a critical threshold in atmospheric O2 concentration had been reached (Arthur et al., 1988; Handoh and Lenton, 2003). We would therefore expect to see Pauthigenic MAR values to increase close to, or just above the Cenomanian-Turonian boundary, as oxygenated waters became reintroduced into the water column. The above factors would have worked against the productivity – anoxia – recycling – productivity feedback, returning the ocean to the pre-OAE state (step 4, Fig. 4).

B.5. Conclusions

In the investigated sections, covering the initial stages of OAE 2 at Pueblo, Eastbourne, Manilva and Furlo, P MARs reach a distinct maximum, which predates the start of the $\delta^{13}C$ positive plateau by some 10's of ka. Together with our observations on the quality and quantity of preserved TOC and on calculated Corg/Preactive molar ratios, we propose the following model for the evolution of the late Cenomanian OAE 2 (Fig. 4):

1. At the start of OAE 2, productivity rates increased, but initial preservation conditions remained poor for organic matter. Phosphorus was liberated from organic matter during early diagenesis, and simultaneously precipitated as Pauthigenic within the sediment.

2. Environmental conditions gradually became too dysoxic for inorganic-P to form effectively. The timing of this appears to depend on the paleodepth of a given section and/or local oxygen availability although we are unable to rule the possibility that errors in sedimentation rates, derived from $\delta^{13}C$ correlations for the more condensed, deeper sections, may effect the apparent timing we see in our data (cf. (Gale et al., 2005). At the same time, preservation conditions for TOC improved, raising TOC contents.

3. Bottom waters sediments?? switched from being a P sink to a P source (indicated by an increase in Corg/Preactive ratio), sustaining the productivity-driven $\delta^{13}C$ peak and plateau in a positive feedback loop.

4. The accumulation of organic matter was strongly linked to preservation (indicated by a positive correlation with hydrogen indices), and increased during the fall in phosphate accumulation rates.

5. A combination of increased aridity, increased atmospheric O2 content, and a reduction in nutrient availability (nutrient burial flux exceeding regeneration flux in deeper sections) may have all been factors that worked against the anoxic event, bringing about a return to more oxic waters column. This idea is fully testable. In this paper, we argue that inorganic-P accumulation is inhibited by bottom-water oxygen depletion. If oxygenated condition returned, via a negative feedback, we would predict that Pauthigenic would start to accumulate more rapidly during this time (possible close to the Cenomanian/Turonian boundary).

Acknowledgements

This manuscript has greatly benefited from constructive reviews from Ian Jarvis, Brad Sageman, Michael Arthur, Philippe Van Cappellen, Harilaos Tsikos and two anonymous reviewers. We also thank Olivier Jaquat and Pascal Ducommun at the University of Neuchâtel, Switzerland for collecting samples from Furlo and Manilva respectively. This project was supported by the Swiss National Fund, No. FN21-67702.02 and US National Science Foundation Grant No. 0115357 (GK).

References

Akande, S.O., Ojo, O.J., Erdtmann, B.D., and Hetenyi, M., 1998, Paleoenvironments, source rock potential and thermal maturity of the Upper Benue rift basins, Nigeria: Implications for hydrocarbon exploration: Organic Geochemistry, v. 29, p. 531-542.

Anderson, D.L., and Delaney, M.L., 2000, Sequential extraction and analysis of phosphorus in marine sediments: streamlining of the SEDEX procedure: Limnology and Oceanography, v. 45, p. 509-515.

Arthur, M.A., Dean, W.E., and Pratt, L.M., 1988, Geochemical and climatic effects of increased marine organic-carbon burial at the Cenomanian Turonian boundary.: Nature, v. 335, p. 714-717.

Attewell, P.B., and Farmer, I.W., 1976, Principles of engineering geology: London, Chapman and Hall.

Caron, M., Dall'Agnono, S., Accarie, H., Barrera, E., Kauffman, E.G., Amédro, F., and Robaszynski, F., 2006, High-resolution stratigraphy of the Cenomanian–Turonian boundary interval at Pueblo (USA) and Wadi Bahloul (Tunisia): stable isotope and bio-events correlation: Geobios, v. 39, p. 171-200.

Caron, M., Robaszynski, F., Amedro, F., Baudin, F., Deconinck, J.F., Hochuli, P., Nielsen, K.V., and Tribovillard, N., 1999, Duration of the oceanic anoxic event at the Cenomanian/Turonian boundary. Cyclostratigraphic interpretation of the Bahloul Formation in Central Tunisia: Bulletin de la Société Géologique de France, v. 170, p. 145-160.

Demaison, G.T., and Moore, G.T., 1980, Anoxic environments and oil source bed genesis: Organic Geochemistry, v. 2, p. 9-31.

Elder, W.P., 1989, Molluscan extinction patterns across the Cenomanian-Turonian stage boundary in the Western Interior of the United-States: Paleobiology, v. 15, p. 299-320.

Erlich, R.N., Palmer-Koleman, S.E., and Lorente, M.A., 1999, Geochemical characterization of oceanographic and climatic changes recorded in upper Albian to lower Maastrichtian strata, western Venezuela: Cretaceous Research, v. 20, p. 547-581.

Espitalié, J., Deroo, G., and Marquis, F., 1985, La pyrolyse Rock-Eval et ses applications: Revue de l'Institut Français du Pétrole, v. 40, p. 563-579.

Filippelli, G.M., 1997, Controls on phosphorus concentration and accumulation in oceanic sediments: Marine Geology, v. 139, p. 231-240.

Filippelli, G.M., and Delaney, M.L., 1995, Phosphorus geochemistry, diagenesis and mass balances of

the Miocene Monterey Formation at Shell Beach California, in Keller, M.A., ed., Evolution of sedimentary basins/onshore oil and gas investigations - Santa Maria Province, U.S. Geological Survey Bulletin, p. G1-G11.

Föllmi, K.B., Badertsher, C., Kaenel, E.d., Stille, P., Cédric, J.M., Adatte, T., and Steinmann, P., 2005, Phosphogenesis and organic-carbon preservation in the Miocene Monterey Formation at Naples Beach, California - The Monterey hyphothesis revisited.: GSA Bulletin, v. 117, p. 589-619.

Gale, A.S., Jenkyns, H.C., Kennedy, W.J., and Corfield, R.M., 1993, Chemostratigraphy versus biostratigraphy - data from around the Cenomanian-Turonian boundary: Journal of the Geological Society, v. 150, p. 29-32.

Gale, A.S., Kennedy, W.J., Voigt, S., and Walaszczyk, I., 2005, Stratigraphy of the Upper Cenomanian-Lower Turonian Chalk succession at Eastbourne, Sussex, UK: ammonites, inoceramid bivalves and stable carbon isotopes.: Cretaceous Research, v. 26, p. 460-487.

Gradstein, F.M., Ogg, J.G., and Smith, A.M., 2004, A Geological Time Scale 2004, Cambridge University Press, 600 p.

Handoh, I.C., and Lenton, T.M., 2003, Periodic mid-Cretaceous oceanic anoxic events linked by oscillations of the phosphorus and oxygen biogeochemical cycles: Global Biogeochemical Cycles, v. 17, p. doi:10.1029/2003GB002039.

Hardenbol, J., Thierry, J., Farley, M.B., Jacquin, T., De Graciansky, P.-C., and Vail, P.R., 1998, Mesozoic and Cenozoic sequence chronostrigraphic framework of European Basins., in Graciansky, J., and Hardenbol, T., eds., Mesozoic and Cenozoic Sequence Stratigraphy of European Basins, Volume 60, SEPM Special Publication, p. 3-13.

Hilbrecht, H., Frieg, C., Troger, K.A., Voigt, S., and Voigt, T., 1996, Shallow water facies during the Cenomanian-Turonian anoxic event: Bio-events, isotopes, and sea level in southern Germany: Cretaceous Research, v. 17, p. 229-253.

Ingall, E., and Jahnke, R., 1994, Evidence for enhanced phosphorus regeneration from marine-sediments overlain by oxygen depleted waters: Geochimica et Cosmochimica Acta, v. 58, p. 2571-2575.

Jarvis, I., Carson, G.A., Cooper, M.K.E., Hart, M.B., Leary, P.N., Tocher, B.A., Horne, D.J., and Rosenfeld, A., 1988, Microfossil assemblages and the Cenomanian-Turonian (late Cretaceous) oceanic anoxic event.: Cretaceous Research, v. 9, p. 3-103.

Jarvis, I., Gale, A.S., Jenkyns, H.C., and Pearce, M.A., 2006, Secular variation in late Cretaceous carbon isotopes: a new d13C carbonate reference curve for the Cenomanian-Campanian (99.6-70.6 Ma): Geological Magazine, v. 143, p. 561-608.

Jenkyns, H.C., 1980, Cretaceous anoxic events, from continents to oceans: Journal of the Geological Society of London, v. 137, p. 171-188.

Jorgensen, B.B., 2000, Bacteria and marine Biogeochemistry, in Schulz, H.D., and Zabel, M., eds., Marine Geochemistry, Springer, p. 173-207.

Keller, G., Han, Q., Adatte, T., and Burns, S.J., 2001, Palaeoenvironment of the Cenomanian-Turonian transition at Eastbourne, England: Cretaceous Research, v. 22, p. 391-422.

Keller, G., and Pardo, A., 2004, Age and paleoenvironment of the Cenomanian-Turonian global stratotype section and point at Pueblo, Colorado: Marine Micropalaeontology, v. 51, p. 95-128.

Keller, G., Stueben, D., Berner, Z., and Adatte, T., 2004, Cenomanian - Turonian d13C, d18O, Sea level and salinity variations at Pueblo, Colorado: Palaeogeography, Palaeoclimatology, Palaeoecology, v. 211, p. 19-43.

Kerr, A.C., 1998, Oceanic plateau formation: a cause of mass extinction and black shale deposition around the Cenomanian-Turonian boundary? Journal of the Geological Society London, v. 155, p. 619-626.

Kolonic, S., Damste, J.S.S., Bottcher, M.E., Kuypers, M.M.M., Kuhnt, W., Beckmann, B., Scheeder, G., and Wagner, T., 2002, Geochemical characterization of Cenomanian/Turonian black shales from the Tarfaya Basin (SW Morocco) - Relationships between palaeoenvironmental conditions and early sulphurization of sedimentary organic matter: Journal of Petroleum Geology, v. 25, p. 325-350.

Kolonic, S., Wagner, T., Forster, A., Damste, J.S.S., Walsworth-Bell, B., Erba, E., Turgeon, S., Brumsack, H.J., Chellia, E.H., Tsikos, H., Kuhnt, W., and Kuypers, M.M.M., 2005, Black shale deposition on the northwest African shelf during the Cenomanian/Turonian oceanic anoxic event: Climate coupling and global organic carbon burial.: Paleoceanography, v. 20.

Kuypers, M.M.M., Pancost, R.D., Nijenhuis, I.A., and Damste, J.S.S., 2002, Enhanced productivity led to increased organic carbon burial in the euxinic North Atlantic basin during the late Cenomanian oceanic anoxic event: Paleoceanography, v. 17, p. art. no.-1051.

Larson, R.L., and Erba, E., 1999, Onset of the mid-Cretaceous greenhouse in the Barremian-Aptian: Igneous events and the biological, sedimentary, and geochemical responses: Paleoceanography, v. 14, p. 663-678.

Leckie, R.M., 1985, Foraminifera of the Cenomanian-Turonian Boundary Interval, Greenhorn Formation, Rock Canyon Anticline, Pueblo, Colorado., SEPM Bulletin, 139-149 p.

Lipinski, M., Warning, B., and Brumsack, H.J., 2003, Trace metal signatures of Jurassic/Cretaceous black shales from the Norwegian Shelf and the Barents Sea: Palaeogeography Palaeoclimatology Palaeoecology, v. 190, p. 459-475.

Luciani, V., and Cobianchi, M., 1999, The Bonarelli Level and other black shales in the Cenomanian-Turonian of the northeastern Dolomites (Italy): calcareous nannofossil and foraminiferal data: Cretaceous Research, v. 20, p. 135-167.

Meyers, S., Sageman, B.B., and Lyons, T., 2005, Organic carbon burial rate and the molybdenum proxy: Theoretical framework and application to Cenomanian-Turonian OAE II: Paleoceanography, v. PA2002, 10.1029/2004PA001068.

Mort, H.P., Jaquat, O., Adatte, T., Steinmann, P., Follmi, K., Matera, V., Berner, Z., and Stuben, D., in press, The Cenomanian-Turonian anoxic event in Italy and Spain: enhanced productivity and/or better preservation: Cretaceous Research.

Nederbragt, A.J., Thurow, J., Vonhof, H., and Brumsack, H.J., 2004, Modelling oceanic carbon and phosphorus fluxes: implications for the cause of the late Cenomanian Oceanic Anoxic Event (OAE 2): Journal of the Geological Society, London, v. 141, p. 721-728.

Orth, C.J., Attrep, M., Quintana, L.R., Elder, W.P., Kauffman, E.G., Diner, R., and Villamil, T., 1993, Elemental

abundance anomalies in the Late Cenomanian extinction interval - a search for the source(s): Earth and Planetary Science Letters, v. 117, p. 189-204.

Paul, C.R.C., Larnolda, M.A., Mitchell, S.F., Vaziri, M.R., Gorostidi, A., and J.D, M., 1999, The Cenomanian–Turonian boundary at Eastbourne (Sussex, UK): a proposed European reference section: Palaeogeography, Palaeoclimatology, Palaeoecology, v. 150, p. 83-121.

Reicherter, K., Pletsch, T., Kuhnt, W., Manthey, J., Homeier, G., Wiedmann, J., and Thurow, J., 1994, Mid-Cretaceous paleogeography and paleoceanography of the Betic Seaway (Betic Cordillera, Spain): Palaeogeography Palaeoclimatology Palaeoecology, v. 107, p. 1-33.

Ruttenberg, K.C., 1992, Development of a sequential extraction method for different forms of phosphorus in marine sediments.: Limnology and Oceanography, v. 37, p. 1460-1482.

Sageman, B.B., Meyers, S.R., and Arthur, M.A., 2006, Orbital time scale and new C-isotope record for the Cenomanian-Turonion boundary stratotype: Geology, v. 34(2), p. 125-128.

Schenau, S.J., Reichart, G.J., and Lange, G.J., 2005, Phosphorus burial as a function of paleoproductivity and redox conditions in Arabian Sea sediments: Geochimica et Cosmochimica Acta, v. 69, p. 919-931.

Schlanger, S.O., Arthur, M.A., Jenkyns, H.C., and Scholle, P.A., 1983, Stratigraphic and Paleo-oceanographic setting of organic carbon-rich strata deposited during Cenomanian-Turonian Oceanic Anoxic Event: AAPG Bulletin-American Association of Petroleum Geologists, v. 67, p. 545-545.

Snow, L.J., Duncan, R.A., and Bralower, T.J., 2005, Trace element abundance in the Rock Canyon Anticline, Pueblo, Colorado, marine sedimentary section and their relationship to Caribbean plateau construction and Oceanic Anoxic Event 2: Paleoceanography, v. 20, p. doi: 10.1029/2004PA001093.

Tsikos, H., Jenkyns, H.C., Walsworth-Bell, B., Petrizzo, M.R., Forster, A., Kolonic, S., Erba, E., Premoli-silva, I., Baas, M., Wagner, T., and Sinninghe Damsité, J.S., 2004, Carbon-isotope stratigraphy recorded by the Cenomanian-Turonian Oceanic Anoxic Event: correlation and implications based on three key localities.: Journal of the Geological Society, v. 161, p. 711-719.

Tyson, R.V., Pearson, T.H., and Geological Society of London. Marine Studies Group. Meeting, 1991, Modern and ancient continental shelf anoxia: London, Geological Society, 470 p.

Van Cappellen, P., and Ingall, E.D., 1994, Benthic Phosphorus Regeneration, Net Primary Production, and Ocean Anoxia - a Model of the Coupled Marine Biogeochemical Cycles of Carbon and Phosphorus: Paleoceanography, v. 9, p. 677-692.

—, 1996, Redox stabilization of the atmosphere and oceans by phosphorus-limited marine productivity: Science, v. 271, p. 493-496.

VanCappellen, P., and Ingall, E.D., 1996, Redox stabilization of the atmosphere and oceans by phosphorus-limited marine productivity: Science, v. 271, p. 493-496.

- C -

The Role of Productivity and Nutrient Regeneration at the Cenomanian-Turonian Boundary (OAE 2)

To be submitted for publication in Paleoceanography

This paper is a more extensively look at the phosphorus cycle during OAE 2. It contains all the data presented in section A as well as a phosphorus speciation for a new section in Morocco, total phosphorus curves for Pueblo, Eastbourne, Furlo and Manilva and a detrital index as a proxy for changes in detrital input. The discussion contains an in-depth look at the implications of the data and considers various mechanisms that may explain the data. These mechanisms include sea-level change and auto-cyclic fluctuations that result from interactions between positive and negative biogeochemical feedbacks in the ocean. Drawing on the conclusions in the discussion, a testable model is put forward that links the iron and phosphorus cycles in a way that may provide a more satisfactory explanation for the formation of Cretaceous oceanic red beds (CORBs).

A facility for quotation covers the absence of original thought.

- Dorothy L. Sayers

C

The Role of Productivity and Nutrient Regeneration at the Cenomanian-Turonian Boundary (OAE 2)

H. P. Mort[1], T. Adatte[1], G. Keller[2], K. B. Föllmi[1], B. Gertsch[2], P. Steinmann[1], Z. Berner[3] and D. Stueben[3]

[1]*Institut de Geologie, 11 Rue Emile Argand, Case Postal 158, 2009 Neuchâtel, Switzerland, fax +41 (0) 32 718 26 01*

[2]*Department of Geoscience, Princeton University, Princeton NJ 08544, USA*

[3]*Institut für Mineralogie und Geochemie, Universität Karlsruhe, Germany*

Abstract

The availability of oxygen at the sediment-water interface is a dominant factor limiting the burial efficiency phosphorus (P). An increase in P mass accumulation rates (P MARs) is observed prior to the positive $\delta^{13}C$ excursion within the upper Rotalipora cushmani zone, in four sections with different palaeodepositional regimes covering the Cenomanian-Turonian anoxic event (OAE 2). This is followed by a sharp decrease in P MAR. P accumulation is affected by both P input from the continents, oxygen availability and productivity. We suggest that the initial increase in P is a result of elevated productivity or continental nutrient delivery, whereas the decrease is an artifact of benthic dysoxia and the associated decrease in P retention ability of the sediment. The transition from an oxidizing to reducing depositional system is indated by several lines of evidence. These include a good positive correlation between TOC content and Hydrogen Index and a decrease in the flux of nutrients from the continents into the ocean as indicated by a mineralogically constructed detrital index. The reducing conditions prevented inorganic-P from being permanently stored making it bioavailable by its reflux into the bottom water to stimulate further productivity. Sustained high rates of productivity increase the concentration of oxygen in the atmosphere. Concurrently CO_2 would have eventually been removed from the atmosphere and water column, as conditions become dysoxic enough to preserve and bury organic matter. The removal of CO_2 and production of O_2 in the atmosphere and ocean would have eventually led to an increase in P MARs, as high pO_2 oxidized nutrients making them unavailable in primary production. We show indications of this in the Whadi El Ghaib section, Egypt with an increase in P concentrations at the end of OAE 2, in the early Turonian. The scenario may have also occurred with iron (Fe); although its different redox sensitivity may cause these changes to be diachronous with P. The formation of Cretaceous Oceanic Red Beds (CORBs) is likely to been largely regulated by the abundance (or lack) of oxygen in the world's oceans. A gradual reintroduction of oxygenated bottom waters to the different basins of the world's oceans may cause the global budget of dissolved inorganic Fe (and P) budget to start fluxing back into sediments, creating the characteristic red pigmentation in many sediments in the Cretaceous. We present a testable model for the formation of CORBs by linking them to the formation of OAEs and changes in the P cycle.

Keywords: **Phosphorus, positive and negative feedbacks, OAE 2, Cretaceous Oceanic Reds**

C.1. Introduction

The Cretaceous Period was witness to a series of so-called oceanic anoxic events (OAEs), the sedimentary expressions of which represents major changes in the way organic carbon was stored in the ocean. The classical model used to explain these OAEs invokes a higher continent to marine nutrient flux and sea-level changes to enhance primary

productivity which in turn lead to the consumption of bottom water O_2 during bacterial respiration of significant quantities of organic matter [Jenkyns, 1980; Schlanger, et al., 1981; Jenkyns, 1991; Kuhnt, 1992; Davey and Jenkyns, 1999; Larson and Erba, 1999a]. During the Mid-Late Cretaceous it has been suggested that there was large igneous province (LIP) activity on the Central Kerguelen, Ontong Java and Caribbean plateaus. The resulting build-up of contributed CO_2 in the atmosphere caused global warming, increased continental temperatures, humidity and rainfall increasing weathering and nutrient transfer into the oceans, stimulating productivity [Sinton and Duncan, 1997; Kerr, 1998; Larson and Erba, 1999b; Racki and Wrzolek, 2001; Wignall, 2001; Leckie, et al., 2002; Snow, et al., 2005].

During OAE 2, close to the Cenomanian-Turonian boundary (~ 93.5 Ma), enhanced productivity and/or better preservation of organic matter under dysoxic-anoxic conditions are common explanations for the globally recognized positive 2-3‰ shift in $\partial^{13}C$ isotope values and the appearance of black shales, which are predominantly seen in pelagic environments [Bralower and Thierstein, 1984; Kuhnt, et al., 1990; Ingall, et al., 1993; Calvert, et al., 1996; Sageman, et al., 2003].

C.1.1. The Behaviour of Phosphorus Under Dysoxic Conditions

The role of nutrients in the evolution of OAEs is fundamental. Phosphorus is a critical macronutrient and significantly affects nitrogen fixation in the ocean [Karl, et al., 1997; Sanudo-Wilhelmy, et al., 2001]. Studying them is critical in understanding whether oxygen availability has wider implications for the way oceans evolve during these types of events. There have been considerable attempts to model and predict the behaviour of productivity limiting nutrients under differing degrees of oxygenation [Ingall, et al., 1993; Van Cappellen and Ingall, 1996; VanCappellen and Ingall, 1996; Filippelli, 2001; Handoh and Lenton, 2003]. Traditionally the fixation of P in sediments has been considered to be controlled by various abiotic processes (e.g. pH and redox processes) [Gächter, et al., 1988]. Once it has entered the oceanic $P_{reactive}$ (bioavailable) reservoir, continental P it can be incorporated into organic matter that will eventually fall to the sea floor as marine snow, pellets or organic matter in turbidity currents. P can then follow a series of biogeochemical pathways. This may involve its liberation from organic matter through bacterial respiration, a subsequent lateral transfer in authigenic minerals [Ingall, et al., 1990; Berner, et al., 1993; Compton, et al., 1993; Krajewski, et al., 1994] or vertical flux back into the water column as dissolved phosphate ions, a scenario which is typically seen in sediments overlain by dysoxic-anoxic waters [Coleman and Holland, 1994; Ingall and Jahnke, 1994; Coleman and Holland, 2000; Schenau, et al., 2005]. Likewise, P stored in authigenic minerals and sediment pore waters can be reduced by dysoxia creating an addition vertical flux of phosphate ions. This vertical component can be assessed by a comparison of the quantities of preserved organic and inorganic $P_{reactive}$ phases relative to total organic carbon. Appreciable deviations from the Redfield ratio (106/1/16), C/P/N [Redfield, 1958] in favour of organic carbon is an important indication for the preferential release of P from sediments back to the water column.

Despite these well-understood principles there is very little P data from the Cretaceous OAEs that allow us to tell which of these processes (if any) were occurring in benthic zones. In relation with an 'anoxic event' it is crucial to measure the extent to which bottom water O_2 deprivation influences the global nutrient cycles. Due to its associations with productivity and redox processes, P is ideally suited for this type of study.

C.1.2. Previous Geological Studies Involving Phosphorus

The study of P in the geological record has benefited from the creation and subsequent modifications of a sequential extraction method (SEDEX) for determining the abundance of phosphorus contained in its different sedimentary reservoirs (speciation) [Ruttenberg, 1992; Anderson and Delaney, 2000]. The SEDEX method has been used extensively in Quaternary-Recent studies and has been shown to be a reliable technique in a range of environmental settings

[Jensen and Thamdrup, 1993; Eijsink, et al., 1997; Kleeberg and Dudel, 1997; Rao and Berner, 1997; Rydin, 2000; Gonsiorczyk, et al., 2001; Kaiserli, et al., 2002; Tamburini, et al., 2003].

An overview of P mass accumulation rates (P MARs) for the last 160 Ma was carried out by Föllmi, [1995]. Fewer datasets were available in the Mesozoic and the temporal resolution was therefore not sufficient to significantly shed light on the processes involved during the Cretaceous OAEs.

Although there is a lack of data regarding P in the Cretaceous, geochemists studying younger sediments have not overlooked its importance, focusing their efforts predominately in the Neogene. Pliocene Mediterranean sapropels have been directly compared to the OAEs of the Cretaceous [Nijenhuis, et al., 1999] and have shown good evidence for P recycling under suboxic conditions [Slomp, et al., 2002; 2004; Meyers, 2006]. This conclusion was also reached by analyzing P_{total} in the Tarfaya Basin, Morocco during OAE 2 [Nederbragt, et al., 2004]. A decrease in P_{total} was observed at the onset of the $\delta^{13}C$ excursion in addition to an increase in the C_{org}:P_{total} molar ratio.

In contrast, vertical fluxes of P out of the sediment were not interpreted to have occurred when studied in the organic-rich Miocene Monterey Formation in California [Filippelli, et al., 1994; Filippelli and Delaney, 1995]. Here, C_{org}:$P_{reactive}$ ratios suggest that P regeneration from organic matter did not occur so readily during periods of enhanced organic carbon (OC) preservation [Föllmi, et al., 2005]. There was no evidence to show that a lateral transfer of phosphorus existed from organic carbon to authigenic minerals. Limnological studies, however, suggest that redox-dependent changes in bacterial physiology at the sediment-water interface may play a large role in P cycling / fixation [Gächter, et al., 1988].

In the Cretaceous, useful P-related studies have concentrated on modelling rather than measuring the behaviour of P during the OAEs [Handoh and Lenton, 2003; Wallmann, 2003]. The former consider a link between the P and oxygen (O_2) biogeochemical cycles. They discuss the possibility that the Cretaceous ocean, predisposed to dysoxia, may have generated a self-sustaining oxic-anoxic oscillating ocean through the long-term interaction between the positive feedback from dysoxic phosphorus regeneration and the negative feedback from a gradual increases in atmospheric O_2 concentrations. Meanwhile, Van Schootbrugge et al [2003] concluded, through measuring the accumulation of P_{total} that P recycling may have occurred along the northwest Tethyan margin near to the Valanginian-Hauterivian carbonate platform drowning event in the Early Cretaceous (~136.4 Ma). It was argued that this might have been the result of a more sluggish thermohaline circulation and poor benthic ventilation . Although many of the above-mentioned studies do not calculate the mass accumulation rate of P, what remains clear is that the sedimentary P content is very often linked to the availability of oxygen surrounding the sediment water interface. Minimums in Phosphorus mass accumulation rates were found at maximum flooding surfaces at the Hauterivian-Barremian boundary and higher in the Barremian, supporting the idea that it was the reworking of nutrients during flooding episodes, which caused the high productivity that ultimately caused the in sub-oxic conditions on the sea-floor [Bodin, et al., 2006].

C.1.3. Aims

Measurements of total-P in the Cretaceous have been rarely carried out. Furthermore, an attempt has never been made to discover which the relative quantities of the different types of P within any Cretaceous sediment. A decrease in sedimentary P fixation can cause nutrient recycling and directly impact the nature of the productivity during OAE 2, potentially forgoing the requirement of sustained continental nutrient input to generate the typical productivity driven isotope plateau. This study aims to chart the oxidation history of the initial phases of OAE 2, how these changes impacted productivity (if at all), and to cast light on the process of black shale formation. Given the redox sensitivity of the P cycle and the strong associate of P with Fe, we also aim to assess the implications our results on the formation of Cretaceous Oceanic Red Beds (CORBs), which are also hypothesized to have been caused by early diagenetic changes (oxidation

fluctuations) in sediment pore waters [Wang, et al., 2005; Hu, et al., 2006].

C.2. Study Sites and Previous Work

Sites were chosen according to their geographic dispersal and differing palaeoenvironmental situations (figure 1). This makes it easier to ascertain the global significance of the results obtained.

C.2.1. Pueblo GSSP, U.S.A.

The Rock-Canyon Anticline area of Lake Pueblo, Colorado was recently designated GSSP for the Cenomanian-Turonian boundary (site 1). It has the advantage of being a well-dated section with an abundance of well-preserved planktonic foraminiferal assemblages, ammonites, bentonites and high-resolution cyclostratigraphic framework. The Pueblo section is therefore important in providing a means of correlation with proxies (specifically $\delta^{13}C$) with those from other sections.

A broad separation can be made between the lower and upper part of this section. The lower part (Hartland Shale) consists of alternating shales and marls deposited during the mid-late Cenomanian. The lithologies change to marls and limestones (Bridge Creek Limestone) in the latest Cenomanian, reflecting a major sea level transgression that can be charted on regional and global basis [Jenkyns, 1991; Kennedy and Cobban, 1991; Curiale, 1994; Valladares, et al., 1996; Willems, et al., 1996; Abdallah, et al., 2000; Keller, et al., 2004]. Fluctuations in siliciclastic dilution due to Milankovitch forcing of precipitation and runoff patterns are thought to have developed the well-defined marl and limestone couplets [Barron, et al., 1985; Elder and Kirkland, 1985; Eicher and Diner, 1989, 1991; Ricken, 1991; Pratt, et al., 1993; Ricken, 1994; Sageman, et al., 1998; Meyers, et al., 2001; Sageman, et al., 2006]. The paleogeographical proximity of the Pueblo Section to land made for a consistently high terrigenous clastic flux throughout the Cenomanian-Turonian interval. This considerations are important as the dilution caused by such high terrigenous input

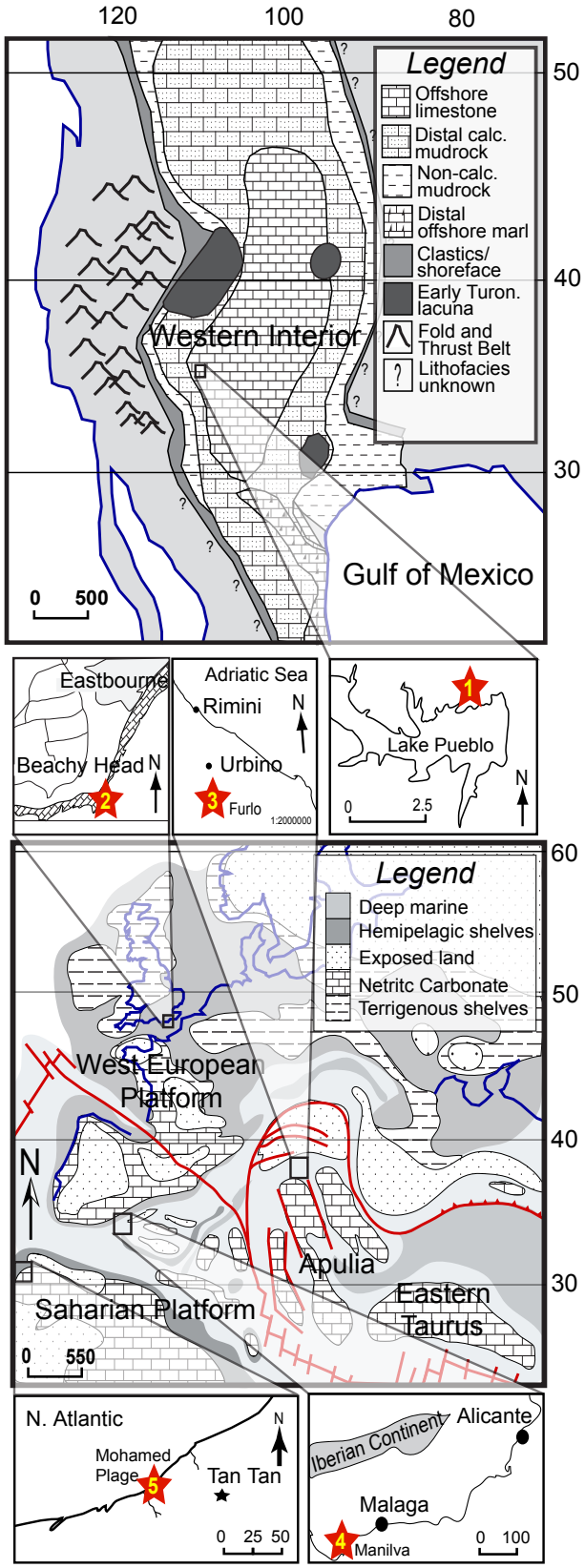

Figure 1. Paleogeographical reconstruction of the location of the sites analysed in this study. Paleomap of North America adapted from (Sageman et al., 1998)). Paleomap of Europe adapted from (Phillips et al., 2002). 1: Pueblo 2:Eastbourne 3: Furlo 4: Manilva 5: Mohammed Plage

would have been an important process in regulating the burial of organic carbon and the accumulation rate of P [Sageman, et al., 2003].

C.2.2. Eastbourne, U.K.

The Gun Gardens Section in Eastbourne (site 2) also possesses a well-defined $\delta^{13}C$ curve, which displays marked similarities, in terms of its $\delta^{13}C$ signature, with the Pueblo Section. Planktonic foraminiferal assemblage changes are consistent with the $\delta^{13}C$ data from Pueblo, with LAD and FAD of several species coinciding with similar trends in the positive $\delta^{13}C$ isotope excursion [Keller, et al., 2001; Keller, et al., 2004].

Despite these similarities, the chalk sea environment was considerably different to that of Pueblo. At approximately 13 m in thickness Eastbourne it is one of the most expanded C/T successions in the UK [Gale, et al., 1993; Paul, et al., 1999] consisting of a transition from chalk (Grey Chalk) to marly chalk and marls (Plenus Marls).

C.2.3. Furlo, Italy

The regional marker of OAE 2 in Italy is called the Bonarelli Level (BL) [Coccioni, et al., 1991; Coccioni and Galeotti, 2003; Coccioni and Luciani, 2004]. The Furlo section is located in the Umbria-Marche Apennines. In Furlo the BL itself is characterized by laterally continuous beds of alternating black mudstones and radiolarian rich cherts that occur within the uppermost part of the Scaglia Bianca Formation, consisting of pelagic limestones of mainly Cenomanian age [Bortolotti, et al., 1970; Arthur and Premoli-Silva, 1982; Cresta, et al., 1989; Coccioni, et al., 1991]. These sediments are deep pelagic with paleodepths of 1-2 kms, are very condensed and contain little or no carbonate across the OAE interval making direct dating using foraminifera impossible. An abrupt positive $\delta^{13}C$ isotope excursion and the synchronous development of a phosphatized hard ground suggest the presence of a hiatus. This type of isotope 'onset' is typical in sections with deep paleodepths, for examples other outcrops of the BL in the vicinity of Furlo [Tsikos, et al., 2004]. It therefore becomes important in these deeper sections to identify what is a rapid isotope shift as opposed a hiatus.

C.2.3. Manilva, Spain

Manilva's palaeogeography positions it on the outer shelf portion of the southern European tilted block [Kuhnt, et al., 1990] near to the margin of the open ocean. Sedimentologically, it is very similar to the Furlo section, with a 2 m intercalated organic rich radiolarian mudstone interrupting a large limestone succession. The tectonic history of the area is slightly complicated with a long-term subsidence history, which started in the early Cretaceous. Subsidence rates vary according to in which sub-basin in the Betic Seaway measurements where made [Schwenke and Kuhnt, 1992; Reicherter, et al., 1994]. Attempts at modelling the mode of organic matter accumulation (i.e. productivity versus preservation) were made comparing both the Furlo and Manilva sections [Mort, et al., in press]. Using a simple stock-flux numerical model a predicted output of organic carbon accumulation was generated by assuming that the $\delta^{13}C$ excursion was made through the fractionation of carbon isotopes via productivity alone. Comparing modelled organic carbon accumulation output with actual data it was seen that the measured values exceed the model values during the isotope excursion. This suggests that productivity alone was not enough to explain the observed increase in TOC values.

C.2.4. Mohammed Plage, Morocco

Mohammed Plage (site 5) is a coastal section located at the northern end of the Tarfaya Basin, Morocco. The Tarfaya Basin extends along the western coast of Morocco between 28°N and 24°N. The basin is situated at the stable western margin of the Saharan Platform, which is now tectonically stable. In the past it has been studied as part of regional examination of OAE 2 [Kuhnt, et al., 1997; Luderer and Kuhnt, 1997; El Albani, et al., 1999; Kolonic, et al., 2002; Kuhnt, et al., 2004; Kuhnt, et al., 2005]. The Tarfaya coast with the Mohammed Plage section are unique to this

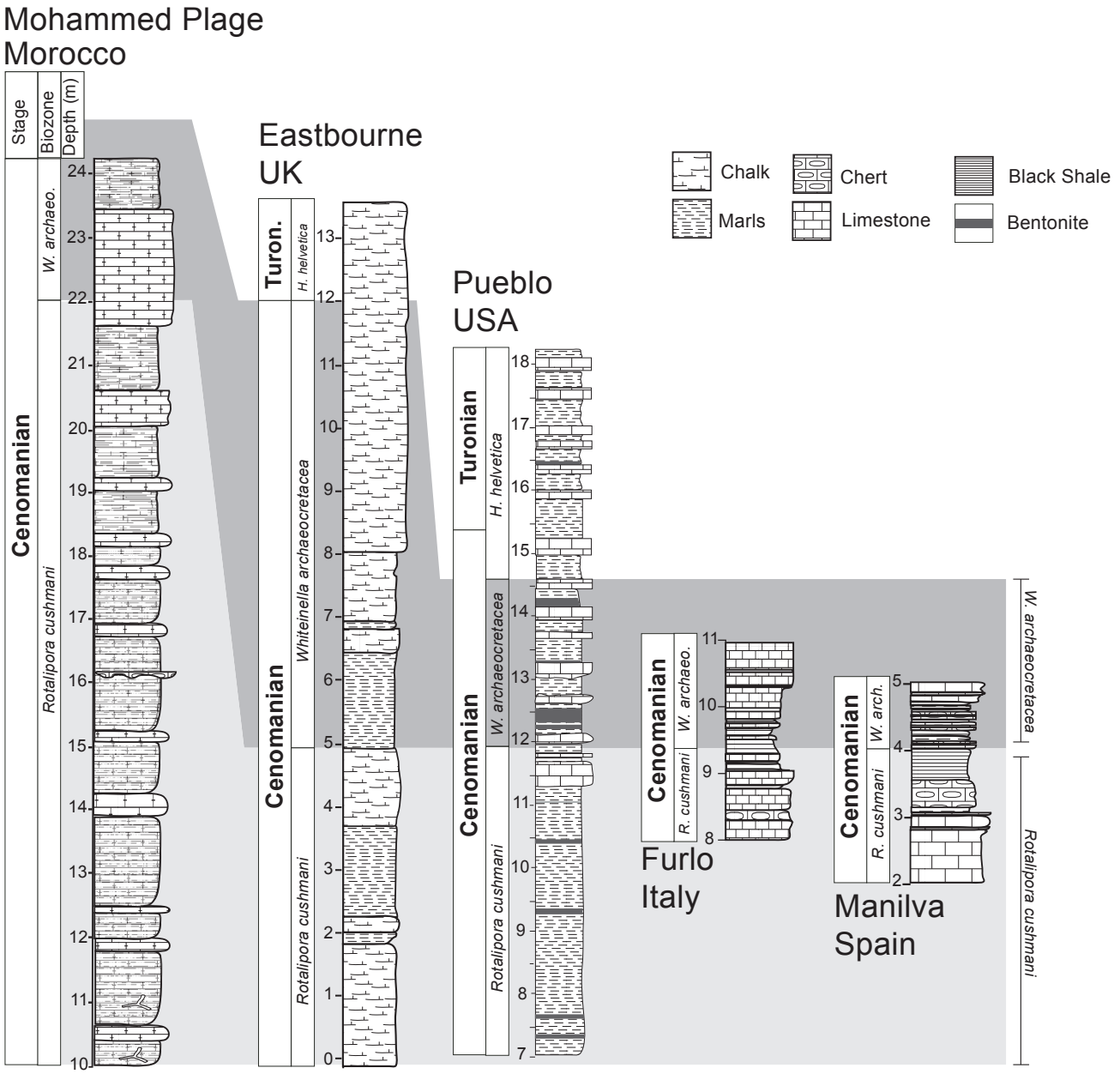

Figure 2. The lithologies of the Mohammed Plage, Eastbourne, Pueblo, Furlo and Manilva.

study as it is the only section which has a well documented history of late Cretaceous subsidence and upwelling activity [Bush and Philander, 1997; Luderer and Kuhnt, 1997; El Albani, et al., 1999; Gebhardt, et al., 2004]. Identifying trends in such a unique palaeoenvironmental setting, that are similar to those observed in other sections, would make the ramifications of the interpretations more significant.

C.3. Materials and Methods

Foraminifera were prepared for biostratigraphic analysis using standard methods at Princeton University, N.J, U.S.A. Samples were crushed to pea sized particles, placed in a beaker and soaked in dilute (3%) H_2O_2 for 24-48 hours. The residues were then washed through a 63μm screen, filtered and placed in the oven to dry at 50ºC. For faunal studies, the >63μm size fraction was analyzed quantitatively for biostratigraphic and environmental analyses based on representative splits of 250-350 specimens per sample. The identification of species and classification of genera follows previous work [Robaszynski and Caron, 1979; Caron, 1985; Caron, et al., 2006]. In Manilva, Furlo and Mohammed Plage high organic matter content made it difficult to separate foraminifera

Step	Supernatant	Phase Extracted	Processes Involved
I*	1 M MgCl2 (pH 8)	Exchangable or loosely sorbed P	Formation of $MgPO_4^-$ complex and/or mass action displacement by Cl^-
II	0.3 M Na3-citrate 1 M $NaHCO_3$ (pH 7.6) 1.125 g of Na-dithionite in 45 ml of citrate bicarbonate solution	Easily reducible or reactive ferris Fe-bound P (P_{Fe})	Reduction of Fe3+ by dithionite and subsequent chelation by citrate
III	1 M Na-acetate buffered to pH 4 with acetic acid	CFAP + biogenic hydroxyapatite + $CaCO_3$-bound P ($P_{authigenic}$)	Acid dissolution at moderately low pH and/or chelation of Ca^{2+} by acetate
IV	1 M HCl	Detrital-P (Pdetrital)	Acid dissolution
V	Ask at 550°C 1 M HCl	Organic-P (P_{org})	Dry oxidation at 550°C, 1 M HCl extraction of ashed residue

* Step 1 was repeated after steps 2 and 3 in order to wash samples of residual supernatant

Table 1. A summary of the reagents used in the SEDEX protocol and P-species drived from each

from the indurated bituminous that would thus prevent quantitative analysis of foraminifera. Thin sections were therefore made for biostratigraphic analyses. The resulting species ranges in this study are based on the presence or absence of species in thin section.

Total phosphorus (P_{total}) analysis was carried out on samples from the Eastbourne, Pueblo, Furlo and Manilva sections using techniques from Eaton, et al., [1995]. 100 mgs (± 5 mgs) of sediment crushed into powder were weighed into sterile glass bottles. Silver foil was placed over each bottle with a hole punched for ventilation. 1 ml of 1 M magnesium nitrate solution (reducing agent) was added to each bottle. Once dry, the bottles were ashed in a furnace at 550°C for two hours. 10 ml or 1 M HCl was added to the sediment in order to liberate the phosphorus from the sediment matrix. Samples were filtered and diluted by ten times before 90 μl of molybdate mixing reagent and ascorbic acid was added to 3 ml of solution. After being calibrated by internal standards analysis was made by a Perkin Elmer Lambda 10 spectrophotometer at the University of Neuchâtel with precision of better than 5 %.

The abundance of the different phosphorus phases was quantified following the sequential extraction (SEDEX) procedure [Ruttenberg, 1992; Eijsink, et al., 1997; Anderson and Delaney, 2000]. Measurements for authigenic-P, detrital-P and organic-P were conducted with a UV/Vis Perkin Elmer Lambda 10 spectrophotometer at the University of Neuchâtel. Precision was better that 5%. Due to the nature of the reagent matrix used to exact Fe-bound P, this phases was analysed via ICP-AES at government environmental laboratories in Neuchâtel, Switzerland. The reagents used to extract each phase are shown in table 1.

Phosphorus concentrations were converted into mass accumulation rates MAR as follows.

[P] (mg/g) x Sedimentation rate (cm/kyr) x Rock density = MAR ($mg/cm^2/kyr$)

Rock densities varied depending on the type of lithology analysed. Values were taken from [Attewell and Farmer, 1976]. These values were verified in the laboratory with simple water displacement measurements of representative samples of known mass placed into a measuring cylinder. Published

sedimentation rates based on cyclostratigraphy for the Mohammed Plage section were used [Kuhnt, et al., 1997; Kolonic, et al., 2005]. The sedimentation rates for the Pueblo Section are necessarily based on two age models. Prior to the bed 63 (isotope excursion, see figure 3) the rates are based on planktonic foraminifera datum levels [Hardenbol, et al., 1998; Keller and Pardo, 2004]. From bed 63 upwards, Sageman et al., [2006] provided a high resolution cyclostratigraphic framework which commences with sedimentation rates comparable to those calculated by [Mort, et al., submitted]. The planktonic foraminifera (Hedbergella) $\delta^{13}C$ curve of Keller, et al., [2003] was preferred over others [Pratt, 1985; Caron, et al., 2006; Sageman, et al., 2006] in making isotope stratigraphic correlations to other sections as the individual species measurements appeared to give a less scatter isotope curve. The latter isotope curves, although arguably made at higher resolutions were either based on organic carbon or bulk carbonate measurements both of which gave a more scattered and therefore less useful in making correlations. Furlo and Manilva contain no biostratigraphic references during the Bonarelli Level and the inferred extinction levels in figure 3 were therefore not used. The FAD of P. praehelvetica, 1st and 2nd isotope peaks (the dates of which are taken from isotopic correlations with the well dated Pueblo Section) and the FAD of H. helvetica provides the basis for a sedimentation rate estimate for these sections. The isotope excursion and plateau termination is abrupt in both sections related to low sedimentation rates. Regionally, these types of problems are common. In Gubbio, Italy, the positive isotope excursion is equally rapid, but nevertheless comparable to Pueblo's curve [Tsikos, et al., 2004]. The resulting datum points in these deeper sections are open to question but nevertheless represent the best possible attempt to construct a sedimentation rate that, even if in error, gives a more realistic record for phosphorus than using mere concentrations.

Separate runs were made for both P_{total} and P-speciation as the former could be done more rapidly and therefore at a higher resolution and over a greater extent of the section. The time consuming P-speciation concentrates on the changes from immediately before the $\delta^{13}C$ excursion to the mid-stages of the $\delta^{13}C$ plateau.

Analysis of organic carbon abundance (TOC) and maturity (Hydrogen Index, HI) was conducted on all samples using Rock-Eval 6™ with instrumental precision of < 2 % [see [Espitalié, et al., 1985].

A detrital index (DI) was obtained by dividing the sum of quartz, feldspar, plagioclase and phyllosilicates intensities by calcite. Lower DI values therefore correspond to less delivery of terrigenous material from continental sources and/or increased dilution due to a greater marine influence. The mineralogical bulk-rock analysis used to calculate the detrital index were carried out on a SCINTAG XRD 2000 diffractometer at the University of Neuchatel, Switzerland, following the procedures outlined by [Kübler, 1987; Adatte, et al., 1996]. Accuracy was better than 5%.

C.4. Results

C.4.1. Planktonic foraminiferal biostratigraphic

This study concentrates on the Late Cenomanian and particularly the $\delta^{13}C$ excursions that mark the upper part of the Rotalipora cushmani and the *Whiteinella archaecretacea* biozones and the correlation of this interval at Mohammed Plage with sequences at Pueblo, Eastbourne, Manilva and Furlo (Fig. 3). The biostratigraphy of Mohammed Plage, Pueblo and Eastbourne are discussed in Keller et al., (2001), Keller and Pardo (2004) and Mort et al. (in press). These three sequences are easily correlated based on planktic foraminiferal biozones and the first and last appearances of index species, as indicated in Fig. 3. Correlation with Furlo and Manilva is difficult because of carbonate dissolution during the Bonarelli Level. Correlation lines are therefore tentatively drawn (hatched line) based on carbon isotope stratigraphy. The first appearance of *Praeglobotruncana praehelvetica* is tentatively used as a correlation datum below the $\delta^{13}C$ excursion. However, the first appearance of this species may vary across the region. The extinction of *Rotalipora greenhornensis* consistently marks a level in the earliest part of the $\delta^{13}C$ excursion (Fig.

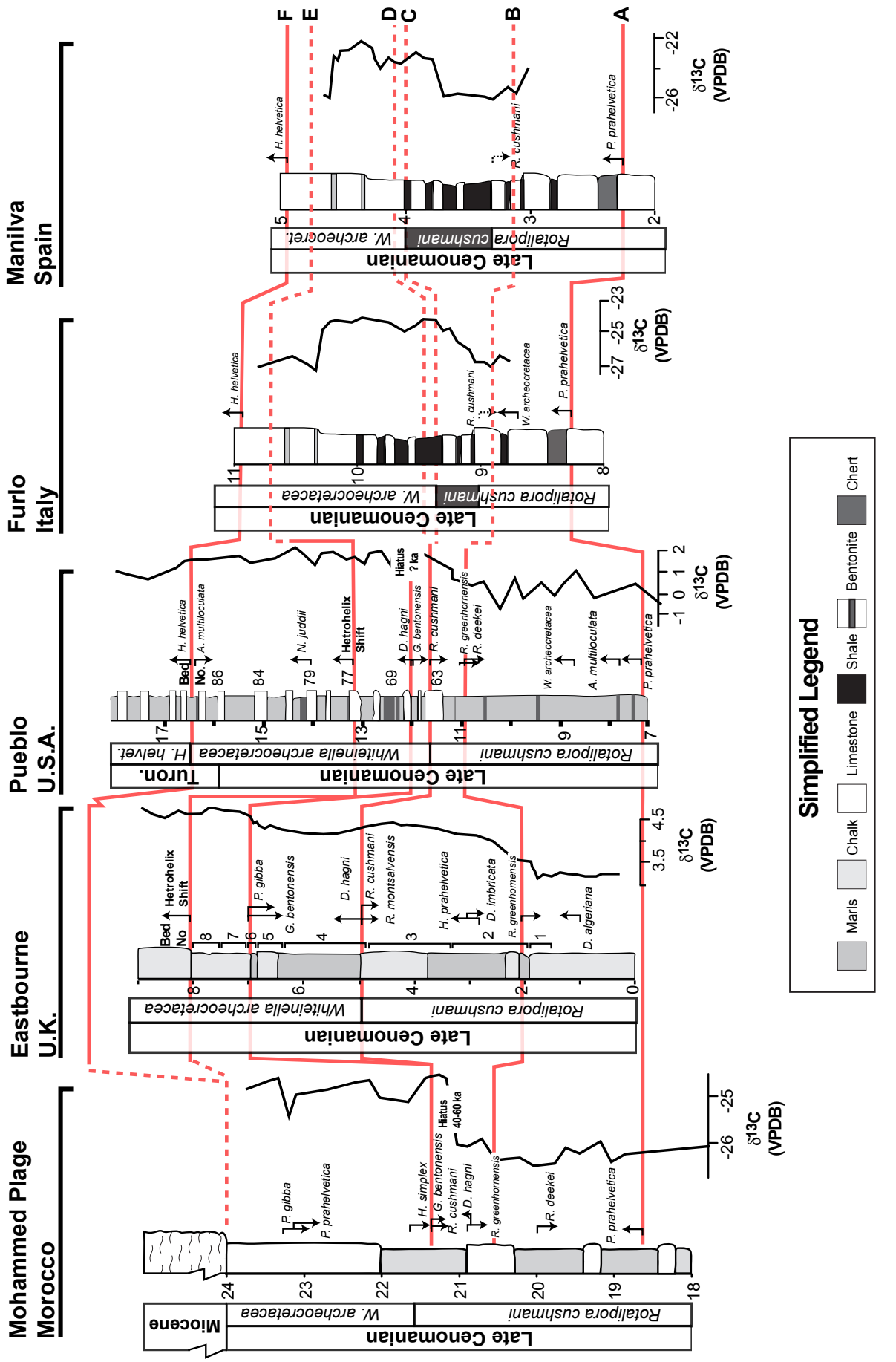

Figure 3. An integrated planktonic foraminiferal and isotopic framework used to calibrate phosphorus mass accumulation rates.

C

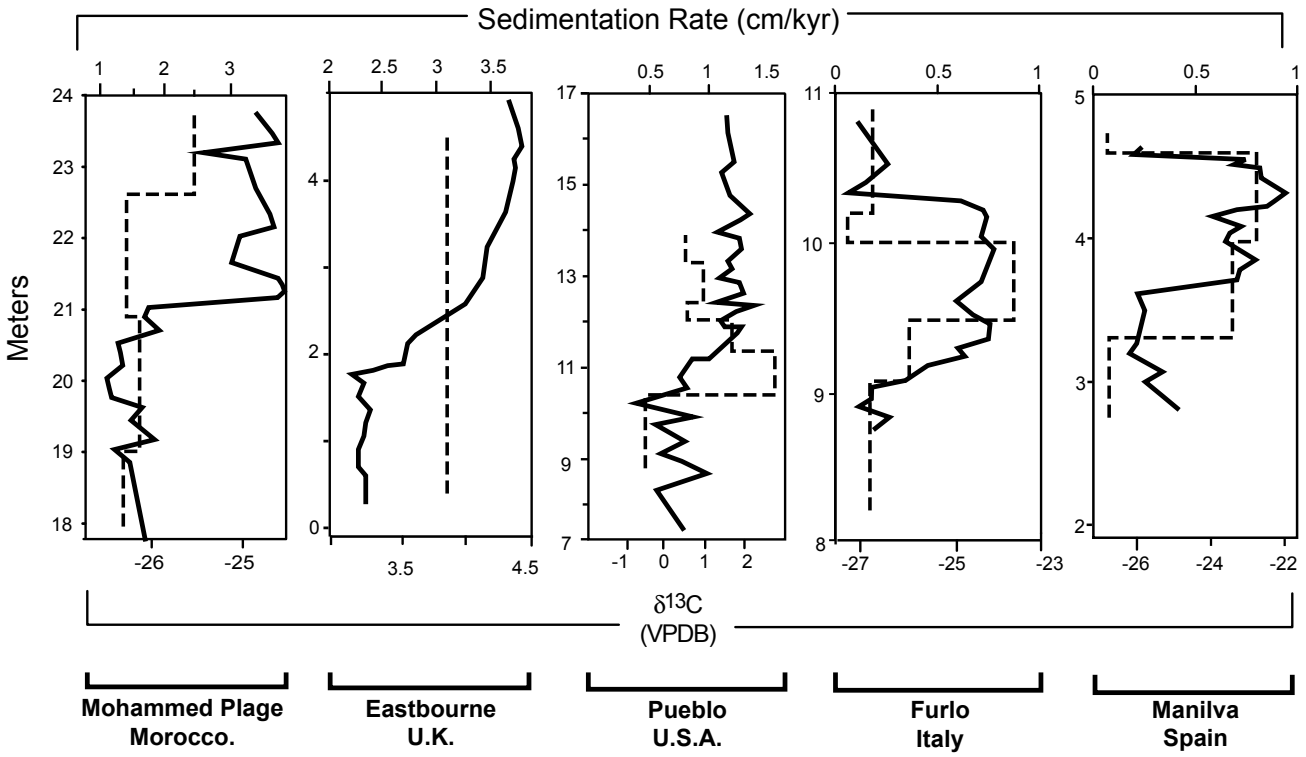

Figure 4. Sedimentation rates calculated for the five sections, based on isotopic, foraminiferal and cyclostratigraphic data.

3). In the trough between the first and second $\delta^{13}C$ peaks is marked by the extinction of *R. cushmani*. Within the *W. archeocretacea* zone, correlation can be based on the extincton of G. bentonensis and followed by the *Heterohelix* shift (onset of dominant and nearly monospecific low oxygen tolerant assemblage). The latter is a consistent and very reliable global marker (Leckie et al., 2002; Keller and Pardo, 2004). The top of the sections is tentatively correlated based on the first appearance of *Helvetoglobotruncana helvetica*, which marks the Cenomanian-Turonian boundary. The correlation is tentative because this species is rare at the onset of its range and therefore may not always be found.

C.4.2. Sedimentation Rate and Carbon-Isotope Stratigraphic Comparisons

Each section possesses sedimentation rates that are distinctly different to the others (figure 4). In Mohammed Plage the sedimentation rates are based on the obliquity cyclostratigraphic framework constructed by Kuhnt et al., [1997]. Values are stable varying between 1.5-1.7 cm/kyr. During the $\delta^{13}C$ plateau at 22.6 meters there is a calculated increase to 2.5 cm/kyr.

In Eastbourne, there is a change in lithology from the Grey Chalk into the Plenus Marls (the base of the isotope excursion). This may suggest the presence of a small hiatus, probably caused by a maximum flooding surface [Jarvis, et al., 2006; Voigt, et al., 2006]. However previous studied using planktonic foraminifera where not able to confirm this [Keller, et al., 2001]. Sedimentation rates calculated for Eastbourne therefore remain constant at 3.1 cm/kyr between the studied interval (0-4 meters). The distance between $\delta^{13}C$ excursion onset and first peak in Eastbourne is approximately 2 meters. In other sections, this part of the excursion is represented by < 1 meter of sedimentation. This gives a good idea of how much more expanded Eastbourne is compared to the other sections.

Prior to the $\delta^{13}C$ excursion sedimentation rates in the Pueblo section are 0.5 cm/kyr. During the excursion values increase to ~ 1.5 cm/kyr before decreasing gradually to between 0.6-0.8 cm/kyr.

The sedimentation rate in Furlo remains largely unchanged until the first isotope peak,

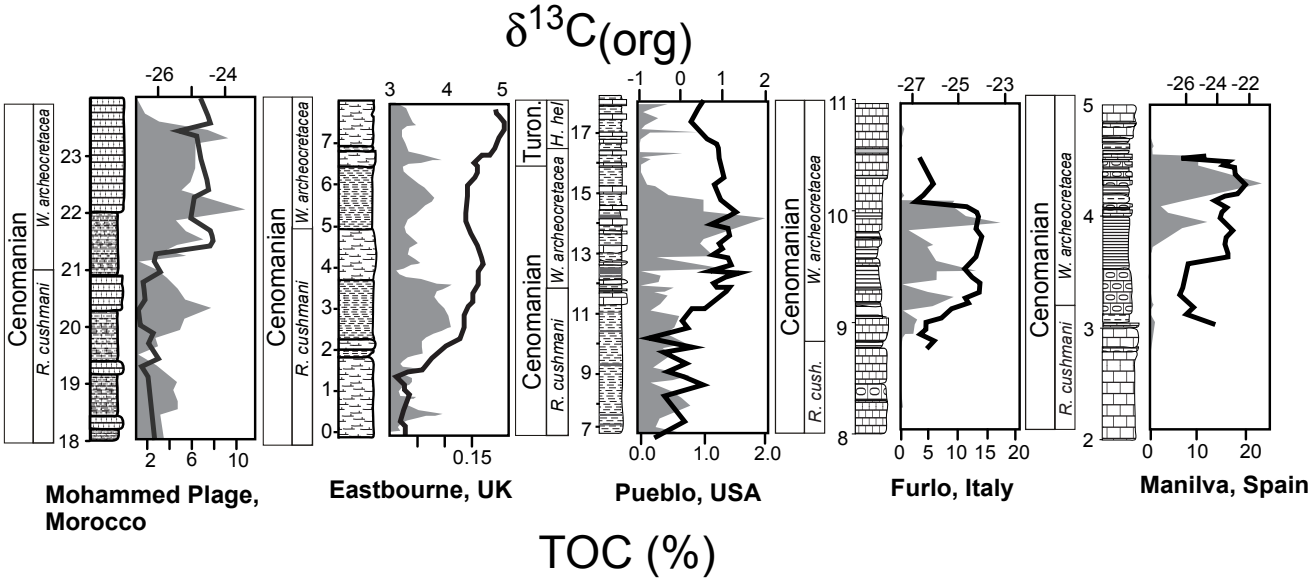

Figure 5. The relationship between $\delta^{13}C$ and TOC content. In general TOC increases most significantly within the isotope plateau as apposed to the excursion itself.

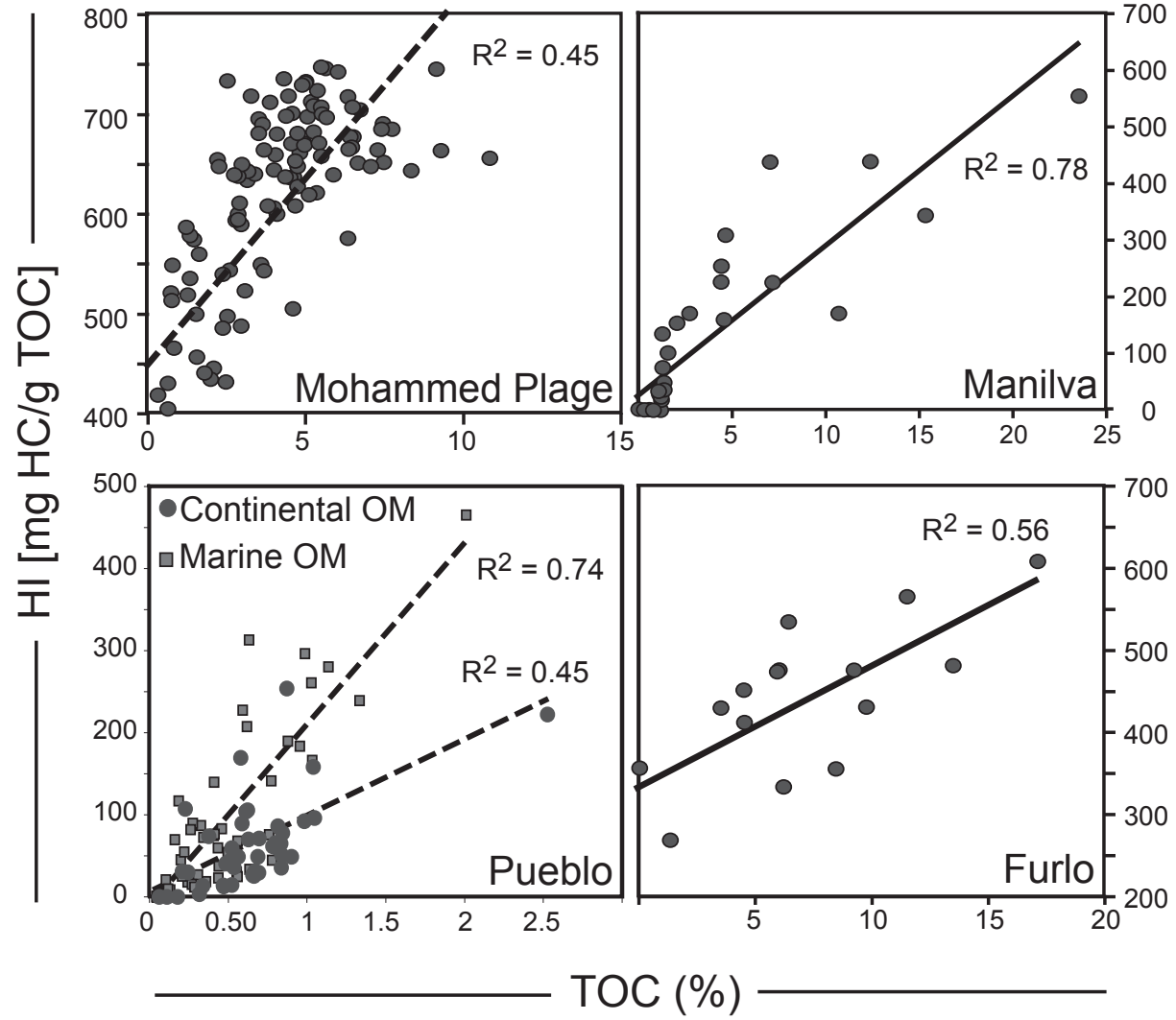

Figure 6. Scatter graph made between organic carbon content (TOC) and hydrogen index (HI).

C

where it increases from 0.3 cm/kyr to 0.9 cm/kyr. Values return to lower than pre-excursion values after the second isotope peak. In Manilva the sedimentation rate increases considerably before the $\delta^{13}C$ onset from 0.1 cm/kyr to 0.6 and to 0.7 at the first isotope peak. The values drop at the end of the isotope plateau to pre-excursion values.

C.4.3. Influence of Sedimentation rate on MARs

Occasionally it is possible that sedimentation rate may exert a strong influence on the accumulation rate of P to the extent that results solely reflect changes in sedimentation. We are able to preclude this possibility based on a number of grounds. P uncorrected for sedimentation rate (mg/g, figure 7) displays the same trend of peaking at the $\delta^{13}C$ excursion onset. Secondly, Mohammed Plage and Eastbourne see slightly negative or no change across the onset yet P ARs increase. Furlo's sedimentation rate only increases during the isotope excursion, whereas the P AR rises clearly before. In Manilva, the sedimentation rate does increase at the same time as the P AR. However, the sedimentation rate remains high throughout the entire isotope plateau in contrast to the P AR, which decreases rapidly.

C.4.4. Total Organic Carbon (TOC %)

With the exception of Eastbourne, which contains almost no organic matter, the time of maximum organic-carbon deposition occurred during the $\delta^{13}C$ plateau (figure 5). In the Mohammed Plage section, there are periodic variations prior to the isotope excursion, with TOC values averaging 4 %. The highest TOC values in the section are found at 22 m (during the $\delta^{13}C$ plateau).

Although permanently low (< 2 %) TOC content in Pueblo appears to vary as a function of lithology, with limestone mg/cm2/kyr possessing much lower concentrations of organic matter than that of the intervening shaley marls. There is greater variability in TOC above the isotope excursion (Bridge Creek Limestone) than below (Hartland Shale Member). On average TOC % values are lower above the isotope excursion, but excluding the limestone mg/cm2/kyr (as is done in figure 5), values increase noticeably from about 0.5 % to 1.7 %, with a maximum value of 2 %, at 14 meters.

In Furlo and Manilva, TOC values are zero before the isotope excursion. Furlo's TOC increases from 0-10% during the isotope excursion. This if followed by another two increases during the isotope plateau, the second of which records the highest value in the section (16 %) towards the end of the isotope plateau. In Manilva, TOC increases shortly after the isotope excursion and reaches again a maximum near the end of the plateau, with values up to 20 %.

C.4.5. Total Organic Carbon and Hydrogen Index Correlation (TOC/HI)

There is a reasonable positive correlation seen between TOC content and HI values (figure 6). The highest R^2 value is 0.78, in Manilva. Furlo and Manilva show good correspondence but a limited number of data points. The entore 24 m of the Mohammed Plage section are correlated (this study on features results from the top 6 m) . The relationship is less strong ($R^2 = 0.45$). A previous study on the Pueblo section has identified a significant switch the in the origin of organic matter, from continental to marine at the $\delta^{13}C$ excursion onset [Keller, et al., 2004]. To distinguish between the two types of organic matter, two correlations were made: one using samples below the $\delta^{13}C$ excursion and one using samples from above. There is a distinct improvement in the correlation when distinguishing between the marine and continental datasets (R^2 increases from 0.45 to 0.74).

C.4.6. Total Phosphorus Mass Accumulation Rates (P_{total} MARs)

High-resolution trends in P_{total} MARs show a remarkable similarity in each of the four sections analysed (figure 7). Although there are differences in the exact detail, the trend can be described as follows. Before the $\delta^{13}C$ isotope onset P_{total} MARs

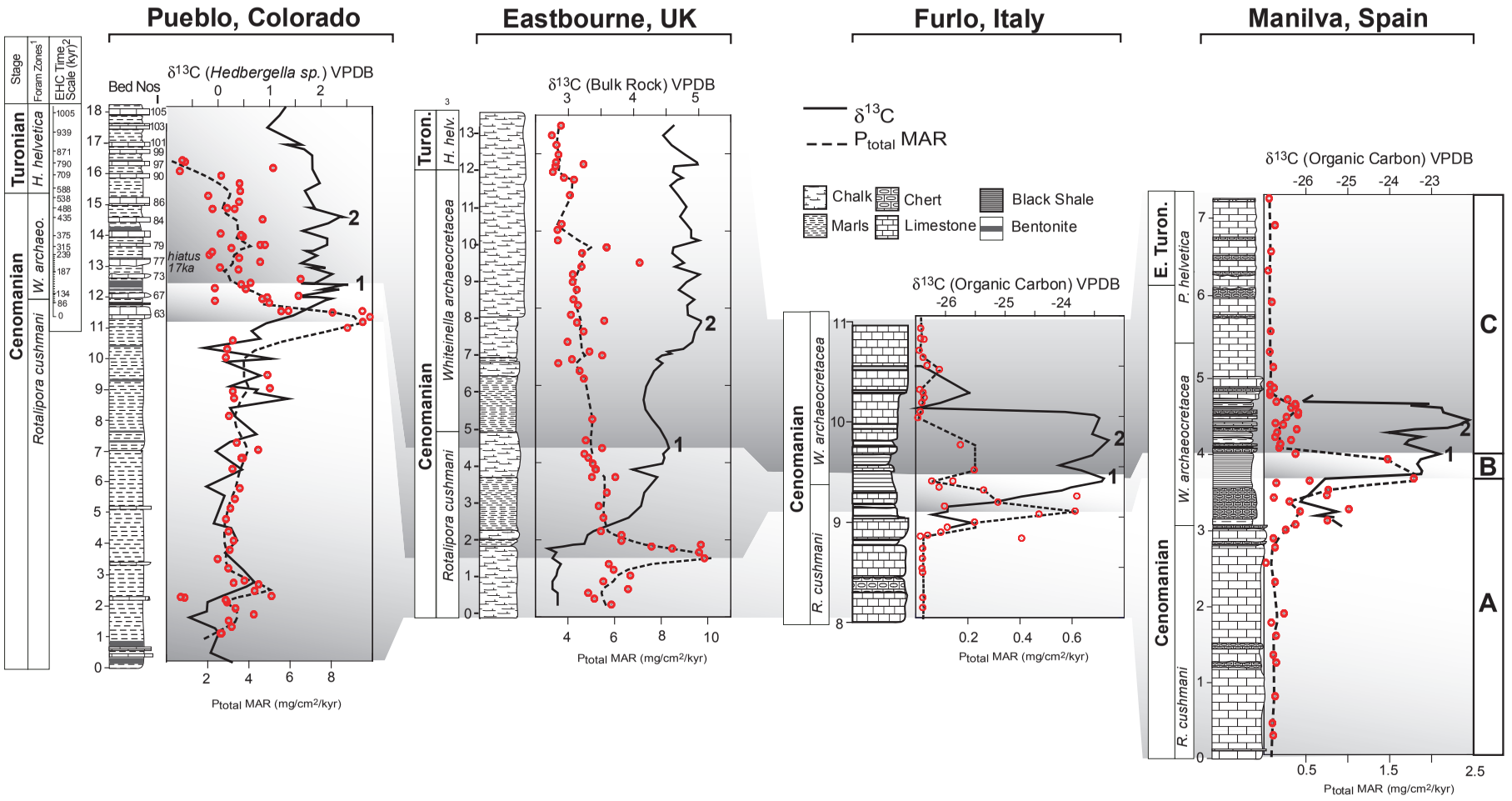

Figure 7. P_{total} MARs and $\delta^{13}C$ for Pueblo, Eastbourne, Furlo and Manilva, based on the total P extraction technique. The three shaded areas correlate the distinct pattern in the P_{total} trend. The lower area represents pre-excursion values. The second area is the interval between the peak in P MARs and the first peak in $\delta^{13}C$. The upper area represents the period of minimal P MARs, during the $\delta^{13}C$ plateau. [1]Biostratography from Keller et al., [2004]. [2]Cyclostratigraphic framework from Sageman et al., 2006. [3]Biostratography from Keller et al., [2001]. The number '1' and '2' represent estimates of the 1st and 2nd isotope peaks, commonly referred to in the text.

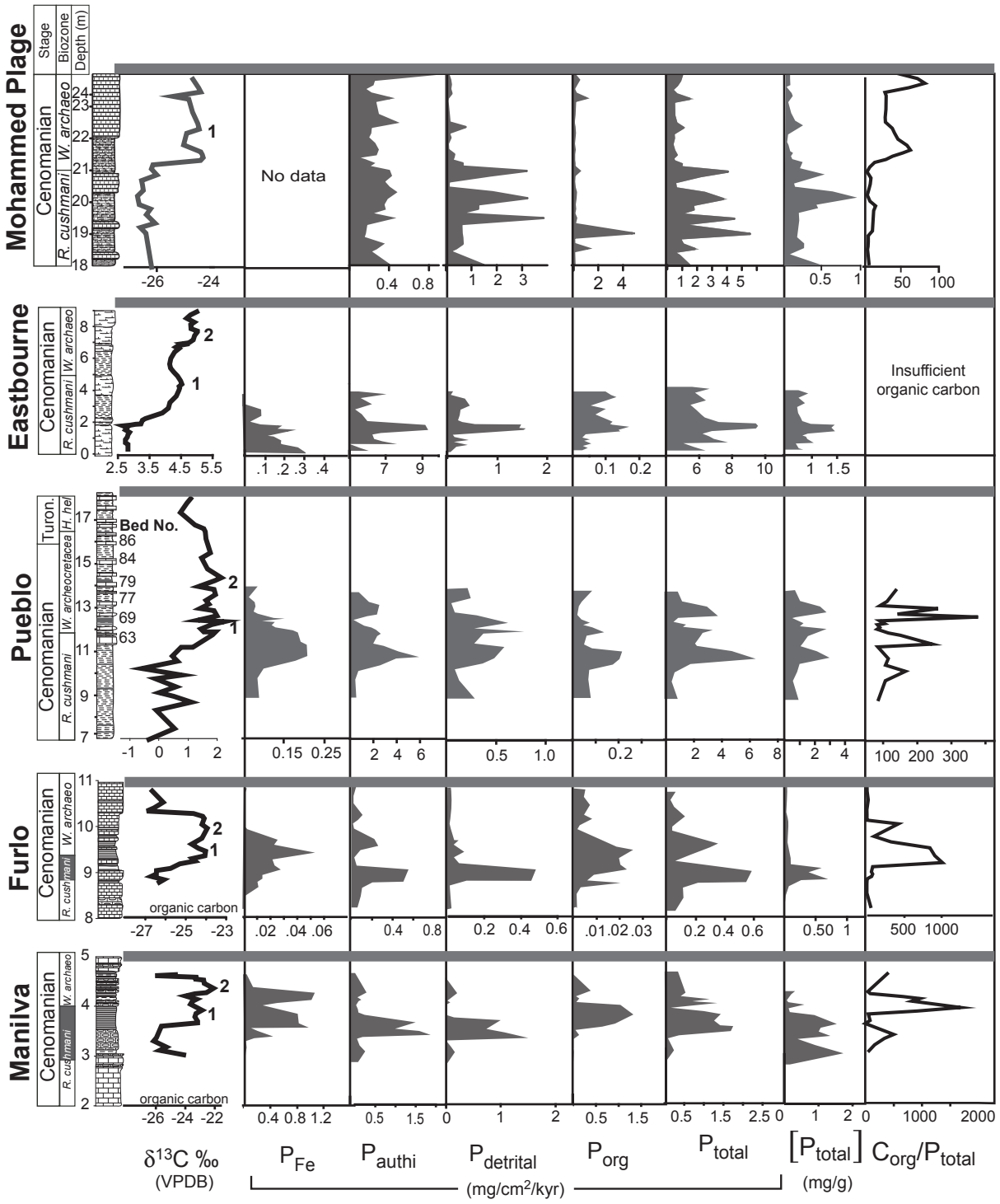

Figure 8. P MARs for iron associated to iron oxy-hydroxides (P_{Fe}), authigenic minerals, Ca-P ($P_{authigenic}$), terrigenous material ($P_{detrital}$) and organic matter ($P_{organic}$). P concentration (mg/g) and the carbon/phosphorus (C_{org}/P_{total}) Redfield

are stable and maybe referred to as 'background' values. These values remain stable until immediately before or at the $\delta^{13}C$ excursion onset. At this point there is a 4-to 6-fold increase in the MAR of P_{total} in all the sections, reaching maximum ARs before the first peak in $\delta^{13}C$ values. Furthermore, background values are almost restored by the time the first peak in $\delta^{13}C$ is reached. Values continue to decrease higher in the excursion plateau.

There are subtle differences in the four sections. In Pueblo, Furlo and Manilva, it is not clear whether maximum P_{total} ARs are attained at the excursion onset, or during the excursion. In the

latter two sections, this is uncertainty is due to the brevity of the excursion itself which occurs only over one or two samples. In Pueblo the uncertainty is in the exact position of the onset itself due to the variability of the $\delta^{13}C$ curve. In contrast, Eastbourne's P_{total} MAR peak is clearly constrained by five points to having occurred at the excursion onset and not during the excursion itself.

C.4.7. Phosphorus Speciation

Concentrations of the various phases of P used to construct the mass accumulation rates in Fig. 8, can be found in table 2 data on page 47. This is to allow other sedimentation rates that are based on other dating schemes to be applied to our data [e.g. Gradstein, et al., 2004].

C.4.7.1. Iron-bound phosphorus (P_{Fe})

At the time of writing P_{Fe} data have not been measured for the Mohammed Plage section due to technical problems. The P_{Fe} MAR in Eastbourne is seen to decline from the beginning of the section up until the end of analysis (4 meters, 1st isotope peak). There is a small increase exactly at the $\delta^{13}C$ onset (figure 8). Values are low, falling from 0.4 - 0 mg/cm^2/kyr. Pueblo sees values increase from 0.05 mg/cm^2/kyr before the excursion onset, to 0.25 at the excursion onset or during the excursion itself. Values return to pre-excursion values at, or immediately after the first $\delta^{13}C$ peak. A similar trend is observed in Furlo, where there is an increase from 0 mg/cm^2/kyr, before the excursion, to 0.05. However, this peak is clearly at the start of the isotope plateau and not at the excursion onset. Manilva records two enrichments of P_{Fe}. At the excursion onset were there is relatively a large enrichment (background values are almost zero) to 0.8 mg/cm^2/kyr . Values decrease and fluctuate during the first phases of the isotope excursion before increasing again to approximately 1 unit in two samples near the second $\delta^{13}C$ peak. After this peak in P_{Fe} MAR, values return to pre-excursion levels.

C.4.7.2. Authigenic Phosphorus ($P_{authigenic}$)

Mohammed Plage records a fluctuating trend in $P_{authigenic}$ with no significant overall increase or decrease in accumulation. The last sample of the section registers a doubling in the accumulation rate of $P_{authigenic}$, but this should be treated with caution due to the potential of alteration and contamination from the overlying Miocene grainstones (not displayed). Eastbourne sees an increase in $P_{authigenic}$ from the base of the section to the isotope excursion onset. Above this, $P_{authigenic}$ decreases from 9 - 6 mg/cm^2/kyr . The peak is more pronounced than the P_{Fe} described above, whose accumulation is already elevated towards the base of the section. In Pueblo, $P_{authigenic}$ has a background value of approximately 0.25 mg/cm^2/kyr and increases to 6 mg/cm^2/kyr, at or immediately after the isotope excursion onset. The accumulation rate rapidly decreases after this point staying below 2 mg/cm^2/kyr by the time the first isotope peak is reached. The $P_{authigenic}$ peak in Furlo is constrained by 2 points at the base of the isotope excursion, which represents a 10-fold increase relative to background values (0.08 - 0.8 mg/cm^2/kyr). Values return to below 0.2 mg/cm^2/kyr for the remainder of the section analysed. The same is seen in Manilva, although values increase from 0.2 - 1.75 mg/cm^2/kyr and the peak it constrained by 4 points at the excursion onset. Values decrease rapidly before the first isotope peak is reached.

C.4.7.3. Detrital Phosphorus ($P_{detrital}$)

In Mohammed Plage the $P_{detrital}$ AR is best described in terms of the amount of fluctuation. From 18 - 21 m values vary from 0.5 to 4 mg/cm^2/kyr . The $\delta^{13}C$ onset (21 m) marks a removal in this fluctuation and $P_{detrital}$ stays below 0.2 mg/cm^2/kyr for the remainder for the section. $P_{detrital}$ in Eastbourne shows a strong resemblance with its $P_{authigenic}$ phase, although overall unit values are lower. $P_{detrital}$ increases from almost zero to 1.8 mg/cm^2/kyr , a peak constrained by four points at the $\delta^{13}C$

Table 2 (overleaf): Raw data containing the measured concentrations of the 4 species of Phosphorus measured in this study. This is to allow the application of other sedimentation rates, based on different time scales to be applied to this data. Note that authigenic and detrital-P are added together as the majority of measured detrital-P is considered to be recrystalized authigenic-P (see text for

Sed. Rates and MARs: MOHAMMED PLAGE

Depth	Sed Rate	Sample	P-authi	P-detr	Porganic	Ptotal	Preactive MAR
meters	(cm/kyr)	ID	mg/g				mg/cm2/kyr
17.750	1.7	MB 82	0.100	0.371	0.020	0.491	2.00
18.20	1.7	MB 85	0.051	0.037	0.012	0.101	0.41
18.30	1.7	MB 86	0.000	0.002	0.018	0.021	0.09
18.45	1.7	MB 87	0.083	0.163	0.014	0.260	1.06
18.65	1.7	MB 88	0.036	0.159	1.195	1.390	5.67
18.80	1.7	MB 89	0.000	0.002	0.056	0.058	0.24
19.10	1.7	MB 90	0.043	0.150	0.017	0.209	0.85
19.30	1.7	MB 91	0.106	0.964	0.035	1.105	4.51
19.45	1.7	MB 92	0.051	0.127	0.026	0.205	0.83
19.60	1.7	MB 93	0.089	0.318	0.043	0.450	1.84
19.75	1.7	MB 94	0.085	0.318	0.050	0.453	1.85
19.95	1.7	MB 95	0.094	0.802	0.024	0.920	3.75
20.15	1.7	MB 96	0.116	0.462	0.015	0.592	2.42
20.30	1.7	MB 97	0.099	0.024	0.023	0.146	0.59
20.50	1.7	MB 98	0.087	0.027	0.123	0.237	0.97
20.70	1.7	MB 99	0.104	0.435	0.021	0.560	2.29
20.85	1.7	MB 100	0.099	0.796	0.020	0.915	3.73
21.00	1.7	MB 101	0.046	0.160	0.014	0.221	0.90
21.10	1.7	MB 102	0.059	0.165	0.012	0.236	0.96
21.20	1.7	MB 103	0.040	0.059	0.012	0.111	0.45
21.30	1.7	MB 104	0.017	0.072	0.012	0.100	0.41
21.40	1.7	MB 105	0.067	0.079	0.015	0.160	0.65
21.55	1.7	MB 106	0.072	0.019	0.017	0.107	0.44
21.75	2.5	MB 107	0.063	0.015	0.021	0.099	0.60
21.95	2.5	MB 108	0.047	0.043	0.026	0.116	0.70
22.1	2.5	MB 109	0.052	0.025	0.015	0.093	0.56
22.3	2.5	MB 110	0.054	0.195	0.026	0.275	1.65
22.45	2.5	MB 111	0.117	0.032	0.014	0.163	0.98
22.7	2.5	MB 112	0.072	0.026	0.015	0.113	0.68
23.15	2.5	MB 114	0.064	0.014	0.023	0.101	0.61
23.25	2.5	MB 115	0.102	0.016	0.022	0.140	0.84
23.4	2.5	MB 116	0.054	0.053	0.014	0.121	0.73
23.55	2.5	MB 117	0.037	0.039	0.017	0.093	0.56
23.7	2.5	MB 118	0.058	0.048	0.014	0.120	0.72
23.85	2.5	MB 119	0.062	0.040	0.021	0.124	0.74
24.05	2.5	MB 120	0.219	0.019	0.065	0.304	1.82

Sed. Rates and MARs: PUEBLO

Depth	Sed Rate	Sample	PFe	Pauthi+detr	Porganic	Ptotal	Preactive MAR
meters	(cm/kyr)	ID	mg/g				mg/cm2/kyr
8.85	0.581	PC-45	0.030	0.445	0.061	0.536	0.72
9.7	0.581	PC-48	0.025	0.215	0.050	0.289	0.39
10.12	0.581	PC-50	0.032	0.348	0.046	0.425	0.57
10.4	1.7	PC-51	0.030	0.341	0.041	0.412	1.61
10.7	1.7	PC-52	0.037	1.413	0.048	1.498	5.86
11	1.7	PC-53	0.038	1.022	0.051	1.111	4.34
11.22	1.7	PC-54	0.037	0.453	0.019	0.509	1.99
11.35	1.34	PC-55	0.042	0.565	0.013	0.620	1.91
11.75	1.34	PC-58	0.039	0.709	0.018	0.766	2.36
11.85	1.34	PC-60	0.037	0.681	0.043	0.761	2.34
12.02	0.95	PC-62	0.033	1.403	0.012	1.448	3.16
12.1	0.95	PC-63	0.031	0.454	0.034	0.519	1.13
12.22	0.95	PC-64	0.033	0.385	0.018	0.435	0.95
12.27	0.95	PC-65	0.019	0.593	0.032	0.644	1.41
12.4	1.088	PC-66	0.038	0.044	0.011	0.093	0.23
12.4	1.088	PC-66	0.027	0.079	0.013	0.119	0.30
12.57	1.088	PC-67	0.012	0.254	0.035	0.301	0.75
12.7	1.088	PC-68	0.011	1.359	0.007	1.377	3.45
13.08	1.088	PC-71	0.010	1.090	0.010	1.111	2.78
13.27	0.941	PC-74	0.006	0.473	0.018	0.496	1.07
13.77	0.941	PC-77	0.020	0.291	0.040	0.351	0.76
13.77	0.941	PC-77	0.016	0.270	0.039	0.325	0.70

Sed. Rates and MARs: EASTBOURNE

Depth	Sed Rate	Sample	PFe	Pauthi+detr	Porganic	Ptotal	Preactive MAR
meters	(cm/kyr)	ID	mg/g				mg/cm2/kyr
0.350	3.1	EB 1	0.036	0.842	0.003	0.881	6.28
0.50	3.1	EB 2	0.035	0.725	0.007	0.767	5.47
0.65	3.1	EB 3	0.025	0.669	0.004	0.698	4.98
0.75	3.1	EB 4	0.024	1.050	0.007	1.080	7.70
0.95	3.1	EB 5	0.024	0.905	0.004	0.933	6.65
1.10	3.1	EB 6	0.019	0.892	0.007	0.917	6.54
1.25	3.1	EB 7	0.011	0.822	0.003	0.836	5.96
1.40	3.1	EB 8	0.043	0.888	0.005	0.936	6.67
1.55	3.1	EB 9	0.028	1.400	0.019	1.447	10.31
1.70	3.1	EB 10	0.020	1.351	0.017	1.387	9.89
1.80	3.1	EB 11	0.025	1.096	0.023	1.144	8.16
1.85	3.1	EB 12	0.023	1.058	0.022	1.102	7.86
1.90	3.1	EB 13	0.015	1.391	0.016	1.421	10.13
1.92	3.1	EB 14	0.011	0.991	0.014	1.017	7.25
2.15	3.1	EB 15	0.000	0.833	0.016	0.849	6.06
2.25	3.1	EB 16	0.000	0.803	0.015	0.818	5.83
2.60	3.1	EB 17	0.011	0.769	0.009	0.789	5.62
2.90	3.1	EB 18	0.010	0.725	0.013	0.749	5.34
3.25	3.1	EB 19	0.000	0.886	0.007	0.893	6.37
3.65	3.1	EB 20	0.000	0.774	0.016	0.790	5.63
3.85	3.1	EB 21	0.000	0.926	0.015	0.941	6.71
4.00	3.1	EB 22	0.000	0.731	0.012	0.743	5.30

Sed. Rates and MARs: FURLO

Depth	Sed Rate	Sample	PFe	Pauthi+detr	Porganic	Ptotal	Preactive MAR
meters	(cm/kyr)	ID	mg/g				mg/cm2/kyr
8.2	0.19	FU-7	0.0000	0.129	0.002	0.131	0.057
8.49	0.19	FU-10	0.0000	0.217	0.003	0.220	0.096
8.69	0.19	FU-12	0.0232	0.209	0.005	0.237	0.104
8.79	0.19	FU-13	0.0214	1.113	0.043	1.177	0.514
8.81	0.19	FU-14	0.0275	0.424	0.014	0.465	0.203
8.85	0.19	FU-16	0.0281	0.381	0.015	0.424	0.185
8.9	0.19	FU-17	0.0333	0.297	0.013	0.343	0.150
8.95	0.19	FU-18	0.0308	0.528	0.018	0.577	0.252
9.06	0.38	FU-20	0.0282	0.700	0.026	0.754	0.659
9.15	0.38	FU-22	0.0237	0.046	0.022	0.091	0.080
9.3	0.38	FU-24	0.0223	0.025	0.020	0.067	0.059
9.47	0.88	FU-27	0.0243	0.040	0.012	0.076	0.153
9.6	0.88	FU-28	0.0101	0.121	0.009	0.139	0.282
9.72	0.88	FU-30	0.0111	0.130	0.018	0.160	0.323
9.99	0.055	FU-33	0.0182	0.166	0.014	0.198	0.025
10.07	0.055	FU-36	0.0029	0.174	0.016	0.192	0.024
10.19	0.19	FU-38	0.0017	0.134	0.016	0.151	0.066
10.3	0.19	FU-41	0.0000	0.264	0.009	0.273	0.119
10.51	0.19	FU-43	0.0000	0.071	0.013	0.084	0.037
10.7	0.19	FU-46	0.0000	0.042	0.009	0.050	0.022
10.88	0.19	FU-49	0.0073	0.113	0.010	0.130	0.057

Sed. Rates and MARs: MANILVA

Depth	Sed Rate	Sample	PFe	Pauthi+detr	Porganic	Ptotal	Preactive MAR
meters	(cm/kyr)	ID	mg/g				mg/cm2/kyr
2.82	0.067	MA-25	0.000	0.107	0.001	0.108	0.017
3.05	0.067	MA-28	0.076	1.455	0.164	1.695	0.261
3.17	0.067	MA-31	0.233	0.849	0.061	1.142	0.176
3.3	0.067	MA-33	0.087	0.314	0.035	0.435	0.067
3.35	0.68	MA-34	0.082	0.124	0.009	0.216	0.337
3.38	0.68	MA-35	0.248	1.127	0.087	1.462	2.286
3.45	0.68	MA-36	0.042	1.195	0.016	1.253	1.959
3.5	0.68	MA-37	0.109	0.954	0.028	1.090	1.705
3.54	0.68	MA-39	0.052	0.170	0.382	0.604	0.944
3.57	0.68	MA-38	0.554	0.621	0.033	1.208	1.889
3.6	0.68	MA-40	0.089	0.235	0.552	0.876	1.370
3.66	0.68	MA-41	0.472	0.942	0.112	1.526	2.386
3.79	0.68	MA-44	0.000	0.149	0.790	0.939	1.468
3.85	0.68	MA-45	0.457	0.042	0.073	0.572	0.895
3.92	0.68	MA-46	0.000	0.054	0.073	0.127	0.199
4	0.8	MA-47	0.129	0.029	0.519	0.677	1.246
4.05	0.8	MA-48	0.239	0.041	0.033	0.313	0.576
4.1	0.8	MA-49	0.493	0.093	0.072	0.657	1.210
4.14	0.8	MA-50	0.133	0.045	0.014	0.192	0.353
4.2	0.8	MA-51	0.089	0.026	0.035	0.150	0.275
4.24	0.8	MA-52	0.518	0.149	0.195	0.862	1.587
4.6	0.057	MA-64	0.091	0.154	0.032	0.278	0.036

excursion onset. Pre-excursion values are restored during the first phase of the isotope excursion. The $P_{detrital}$ signal in Pueblo also is similar to the section's $P_{authigenic}$ curve, albeit slightly 'noisier'. The peak at the excursion onset it noticeable but is not significantly elevated above background values (0.6 versus 0.4 mg/cm^2/kyr). Values decrease with some fluctuation within the $\delta^{13}C$ excursion. Furlo and Manilva display an extremely strong correspondence (almost point for point) between $P_{authigenic}$ and $P_{detrital}$. The increase in $P_{detrital}$ AR in Furlo, is from 0.02 mg/cm^2/kyr to 0.5 mg/cm^2/kyr at the excursion onset. The decrease occurs immediately after these two points and is even more pronounced than the reduction in $P_{authigenic}$, which fluctuates slightly. In Manilva the similarity between $P_{authigenic}$ and $P_{detrital}$ is again striking and a point-for-point correlation is observed. ARs increase from 0 to 1.5 mg/cm^2/kyr. The peak is constrained by four points at the excursion onset and decreases immediately thereafter.

C.4.7.4. $P_{detrital}$ and $P_{authigenic}$ recrystalization

Terrigenous input is commonly seen as an import initial driver of productivity during OAE 2, thus the signal generated for $P_{detrital}$ MARs is also considered to be important. However the $P_{detrital}$ data in figure 7 are counter-intuitive. Firstly the shallow sections (Eastbourne and Pueblo) appear to have accumulation rates of $P_{detrital}$ similar to the deeper sections (Furlo and Manilva) despite sedimentation rates being one order of magnitude higher in Eastbourne and Pueblo, and their paleobathymetric situation making them more likely to have received larger amounts of detrital material, especially in Pueblo. This similarity between the sections may be explained if we consider the possibility that a considerable amount of $P_{authigenic}$ was diagenetically recrystallized and therefore extracted with the chemically similar $P_{detrital}$ fraction. The conversion of $P_{authigenic}$ into $P_{detrital}$ has been documented in younger sediments

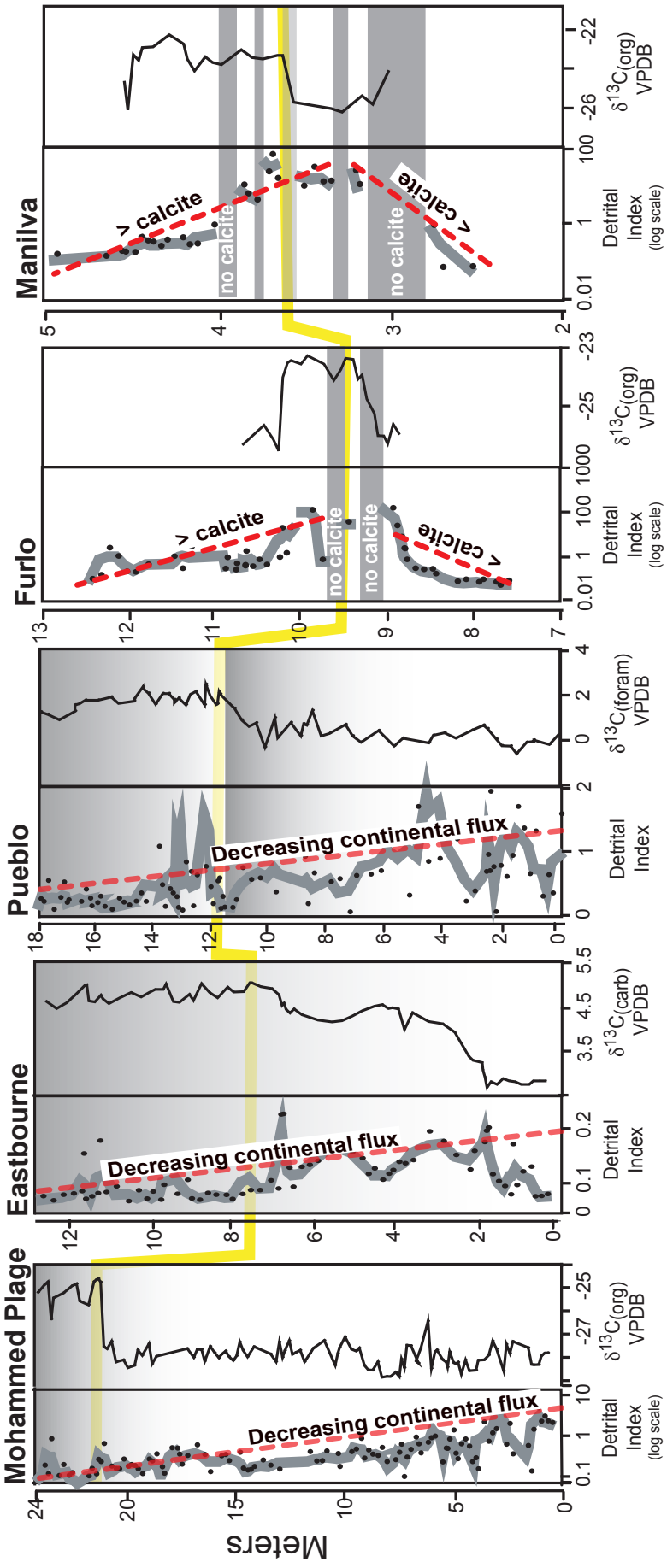

Figure 9. A 'detrital index' (DI) used to give an idea of the relative amount of continental flux of material into the ocean over time. See text for details.

C

[Filippelli and Delaney, 1995; Föllmi, et al., 2005]. This processes certainly appears to have been the case in Furlo, Manilva and Eastbourne, where the $P_{authigenic}$ and $P_{detrital}$ curves are almost identical in shape and value. This would be highly improbable if both are primary signals. Very low $\delta^{18}O$ values in Pueblo (-5-9 ‰) suggest that fresh water input and diagenesis were factors in creating these values [Keller, et al., 2004]. In this case, it is likely that some of the measured $P_{detrital}$ was derived from $P_{authigenic}$ in Pueblo as well.

The peak in $P_{detrital}$ is conveniently placed in each of the sections to support well-developed theories pertaining to increased nutrient input either from continental sources (also proposed for other OAEs) or nutrient remobilisation from land flooded by the late Cenomanian transgression [Hilbrecht, et al., 1992; Davey and Jenkyns, 1999; Larson and Erba, 1999a; Sugarman, et al., 1999; Jarvis, et al., 2006]. However, given the general uncertainty in interpreting the true source of $P_{detrital}$ it is important to exercise discretion when interpreting the results.

C.4.7.5. Organic Phosphorus ($P_{organic}$)

For the majority of the Mohammed Plage section $P_{organic}$ AR is surprisingly low given the abundance of organic carbon. There is a peak at the base of the section (one point measuring 5 mg/cm^2/kyr) although values do not exceed 0.8 mg/cm^2/kyr for the rest of the section. In Eastbourne, values increase in a similar way to $P_{authigenic}$ and $P_{detrital}$ at the isotope excursion onset. ARs decrease after this point but only to approximately double pre-excursion values (0.8 mg/cm^2/kyr). In Pueblo a peak is observed slightly before that of the other P phases (increase in ARs from 0.09 - 0.2 mg/cm^2/kyr). Values decrease to slightly less than pre-excursion levels (0.05 mg/cm^2/kyr). $P_{organic}$ AR is more widespread in Furlo with the enrichment occurring during the excursion or at the first $\delta^{13}C$ peak, extending into the isotope plateau. Values decrease gradually returning to near pre-excursion values towards the end of the plateau. In Manilva, the same is observed, with $P_{organic}$ increasing immediately after the peaks in the other phases and from 0.01 - 1.5 mg/cm2/kyr.

C.4.7.6. Comparing P_{total} from the complete extraction and P_{total} from the speciation

See figs. 7 and 8; P_{total} MARs derived from the total extraction technique ($P_{total}{}^1$) show a reasonable agreement in values when compared to the sequential extraction technique ($P_{total}{}^2$). It is inevitable that some deviation will be incurred from the two methods but this does not detract from the virtues of either one. Even so, the values of $P_{total}{}^1$ for Eastbourne, Pueblo, Furlo and Manilva and within the same order or magnitude. For example, Pueblo sees an increase in $P_{total}{}^1$ from 2 - 9 mg/cm^2/kyr. $P_{total}{}^2$ increases from 1 - 8 mg/cm^2/kyr indicating a slight loss in the amount of phosphorus from one or more of the extraction steps. The other three sections compare very well with P_{total} AR increasing and decreasing by very similar mg/cm^2/kyr. Despite some discrepancies the overall trends are replicated well in both extraction techniques.

C.4.8. Detrital Index (DI)

A log scale is needed for three sections to effectively see the trend in lower DI values, as some points are extremely high. Mohammed Plage, Eastbourne and Pueblo all see a decrease in the DI values from bottom to top of section (figure 9). The long-term trends is most easily seen in Mohammed Plage and Pueblo where the majority of the section is below the $\delta^{13}C$ excursion (20 m and 10 m respectively). Pueblo does see an interruption in the downward trend, with a significant increase in the DI during the isotope excursion. In Eastbourne, the decrease in DI occurs from the excursion onset and above. In Furlo and Manilva the DI increases prior to the isotope excursion and decreases after the first isotope peak. However, it should be noted that the increase in DI is an artifact of calcite dissolution and therefore cannot, in this case, be used as a proxy for changes in detrital input.

C.5. Discussion

C.5.1. Organic Carbon Deposition

The behaviour of TOC is different in each of the five sections and probably reflects the different palaeoenvironmental regimes existing in each

locality. The deposition of organic carbon at the Mohammed Plage section is cyclical and maybe partly driven by obliquity (39 ka) forcing [Kuhnt, et al., 2004; Kolonic, et al., 2005] . TOC fluctuates considerably in Pueblo but this is likely a result of it's shallow palaeoenvironment and varying amounts of continental organic matter input, possibly controlled also by Milankovitch forcing [Elder and Kirkland, 1985; Kennedy and Cobban, 1991; Ricken, 1994; Sageman, et al., 1997; Sageman, et al., 1998; Keller, et al., 2004]. Furlo and Manilva have noticeably higher amounts of organic carbon due to their paleodepth and better organic matter preservation. However, those sections with a significant quantity of organic matter do share some features described in the results. Organic matter reaches a maximum in each section (except Eastbourne) within the $\delta^{13}C$ plateau but does not increase immediately at the excursion onset. Caution must be given to the precise meaning of the isotope curve in Furlo, Manilva, and Mohammed Plage, which is based on organic carbon, instead of carbonate. Although the carbon is derived from two different reservoirs for the purposes of this study it is reasonable to assume that fluctuations in $\delta^{13}C$ in carbon derived carbon in organic matter and carbonate are both indicators of changes in productivity. If this can be assumed then it has significant repercussions. Given that TOC does not follow $\delta^{13}C$ in its increase then this means the productivity did not have an immediate effect on TOC content (figure 5). Oxic benthic waters would have led to the effective breakdown of organic matter via high rates of scavenging and bacteria remediation. If the productivity that caused the positive $\delta^{13}C$ excursion was sustained (indicated by the plateau) then this may have eventually caused the gradual consumption of bottom water oxygen content via eutrophication processes and the ineffective breakdown of organic matter. New organic matter arriving would then have the chance to accumulate, as it would be arriving faster than it was being removed. This can be inferred by the increase in TOC content, apparent in Pueblo, Furlo, Manilva and to a lesser extent in Mohammed Plage.

The correlation between TOC and HI provides addition evidence for this idea, indicating a direct link between organic matter immaturity (better preservation) and TOC content. If the consumption of bottom water oxygen was the determining factor in when significant organic carbon accumulation started, then preservation would have occurred in a stepwise fashion as the oxygen minimum zone expanded and intensified. This expansion can be seen in the progressive disappearance of microfossil fauna in OAE 2 sequences globally [Leckie, 1985; Jarvis, et al., 1988; Gebhardt, 1997; Jolet, et al., 1997; Huber, et al., 1999; Kassab and Obaidalla, 2001; Keller, et al., 2001; Coccioni and Luciani, 2004; Gebhardt, et al., 2004; Keller and Pardo, 2004]. Organic carbon accumulation models for the Furlo and Manilva sections suggest that it is difficult to generate the observed amount of TOC assuming a productivity-based system only [Mort, et al., in press]. Although the model used in this study cannot be assumed to reflect reality, it does suggest that redox processes played an important role.

C.5.2. Reducing Conditions at the Start of OAE 2

Phosphorus burial efficiency (PBE) is postulated to be reduced in sediments that are overlain by oxygen deficient waters [Ingall and Van Cappellen, 1990; Ingall, et al., 1993; Ingall and Jahnke, 1994; Van Cappellen and Ingall, 1994, 1996; Colman and Holland, 2000; Schenau, et al., 2005]. As argued above, the accumulation of organic matter seems partly controlled by the progressive decreases in oxygen availability as productivity advanced. The increase in P MARs appears to occur at or just prior to the $\delta^{13}C$ excursion onset. The cause of this increase it not certain but the delivery of nutrients from continental sources currently provides the best explanation (see below). $P_{detrital}$ maybe used in this case but, as discussed above, it may partly represent recrystallized $P_{authigenic}$. P_{Fe} and $P_{authigenic}$ can be recycled and become bioavailable when reduced (see above references). The drop in accumulation rates of the these phases is coeval with an increase in the Redfield molar ratio value ($C_{organic}/P_{total}$) in all sections; an indication that, regardless of environmental situation, P was being fluxed from the sediment into the water column on a large scale during this time. This behavior has been inferred

when studying Pliocene sapropels and modern ocean basins [Slomp, et al., 2002; Slomp, et al., 2004; Schenau, et al., 2005] and has significant repercussions for our understanding of how OAE 2 evolved. The first inference of this kind, based on measured P data during OAE 2 was observed in drill core S13, near the Mohammed Plage beach section in Morocco [Nederbragt, et al., 2004] where a drop in P and in increase in C_{org}/P_{total} ratio was observed at the $\delta^{13}C$ excursion onset. Modelling in the same study demonstrates that in order to achieve the measured amounts of TOC, preservation is probably required and a change in rate of phosphorus burial is in the correct order of magnitude to explain organic-carbon burial during OAE 2 quantitatively.

C.5.3. Causes and Consequences of P MAR trends

C.5.3.1. Eustatic Sea-level transgression

The partitioning of carbon between organic and carbonate carbon sinks as caused by relative sea-level rise transgression and regression phases is another commonly sited mechanism by which $\delta^{13}C$ can be used to represent first-order rises in eustatic sea-level [Scholle and Arthur, 1980; Jenkyns, et al., 1994; Weissert, et al., 1995; Voigt and Hilbrecht, 1997; Weissert, et al., 1998; Jarvis, et al., 2001]. [Jarvis, et al., 2006] presents a compilation of carbon isotope values from Cenomanian to Santonian successions in England. The resulting curve corresponds closely to eustatic sea-level curves from Russia, India and northwest Europe [Sahagian, et al., 1996; Gale, et al., 2002]. In the sea-level change model, rapid rises may have caused the reworking of sediments on coastal areas, promoting a nutrient flux into the oceans, enhanced productivity and subsequently higher organic matter burial. It is certainly conceivable that continent to ocean inorganic P flux may have been greatly enhanced during this time, adding to the bioavailable P budget of the ocean. Unreactive P phases reworked from continents may also account for increases in P_{Fe}, $P_{authigenic}$ and $P_{detrital}$ P ARs. The rate of the sea-level transgression is crucial in this model. A relative rapid rise would be required to rework the necessary nutrients into stimulating productivity (see Fig. 11). [Voigt, et al., 2006] calculated a the rate of 0.2 - 0.3 m/kyr based on transgressive system tracts (TSTs) within cyclostratigraphic frameworks from the UK [Gale, et al., 1999; Gale, et al., 2002] with a total rise of 22-28 m having occurred within in the isotope excursion. As transgression rates diminished this would have led to new sediments covering drowned continental regions, capping nutrient flux and therefore reducing productivity [see Jarvis, et al., 2006 for a more detailed summary of this process].

This conceptual model may (in part) explain our observed increases in P MAR. The most conservative estimates for residence time of P in the oceans range from 20 - 100 ka [Ruttenburg, 1993; Delaney and Filippelli, 1994]. This is probably an overestimation [see Ruttenburg, 1993; Van Cappellen and Ingall, 1994; Colman and Holland, 2000; see Latimer, et al., 2006] but is nevertheless a period which is currently a good estimate for the time elapsed between the peak in P MARs and the first peak in $\delta^{13}C$ values. However, there remains some observations that a sea-level driven/ productivity driven model may find challenging.

TOC content increases during the isotope excursion plateau and not so much during the isotope excursion itself (figure 5). The reasonable correlation between TOC and HI (figure 6) indicates that reducing conditions played a role preserving organic matter. Both of these observations are difficult to reconcile by a productivity-driven scenario. Furthermore, with the exception of Mohammed Plage and Pueblo, $P_{organic}$ AR is more sustained that the inorganic phases. In a sea-level driven model, continental reworking of $P_{inorganic}$ and primary production should go hand-in-hand. The apparent offset suggests a decoupling between carbon and phosphorus cycles. Given the evidence for dysoxic conditions it likely that reducing conditions led to decreased phosphorus burial efficiency (PBE), which ultimately led to the preservation of organic matter through a benthic nutrient regeneration - productivity - dysoxia feedback loop.

In addition to this, the detrital index (DI, figure 9) shows a distinct long-term deepening with

no major decrease, which would have suggested a rapid sea-level transgression. This does not exclude the possibility that there was a rapid increase in eustatic sea level immediately prior to OAE 2, but simply raises questions about how to reconcile mineralogical data with current sequence stratigraphic interpretations. Our understanding of how either/both tool(s) can be used during OAE 2, may need to be revised in light of this contradiction.

C.5.3.2. Autocyclic fluctuations

The high ratio of shallow to deep ocean basins in the ocean during the Cretaceous, generally high sea-level and atmospheric CO_2 content [Jenkyns, 1980] has been used to model the behavior of phosphorus a being caused by a series of self-sustaining oscillations [Handoh and Lenton, 2003]. Arguing that the oceans may have been predisposed to the occurrence of OAE's merely as a result of the aforementioned characteristic of the Cretaceous ocean, the authors present an internally consistent model that associates the phosphorus and oxygen cycles. The oscillations are maintained by a positive feedback between phosphorus recycling, productivity and dysoxia: versus increasing atmospheric O_2 concentrations which would have eventually acted as a negative feedback to oxidize and bury phosphate decreasing the overall bioavailable P in the oceans. Handoh and Lenton's [2003] model is appealing because is makes several falsifiable predictions which are borne out by our data. These predictions include, 1) A decrease in the PBE during OAEs (i.e. a decrease in P accumulation rate). 2) A consequent increase in $C_{organic}/P_{reactive}$ ratio during the start of an OAE. 3) Decreases in P_{Fe} and $P_{authigenic}$ should occur at the same time as increases in $P_{organic}$ (an indication of sink switching). This can be observed by carefully looking at Eastbourne, Furlo and Manilva, where $P_{organic}$ increase slightly after the inorganic phases. The same does not occur in Mohammed Plage or Pueblo. These sites are associated with upwelling activity [Bush and Philander, 1997; Gebhardt, et al., 2004] and high detrital input [Pratt, 1985; Ricken, 1991; Keller, et al., 2004] respectively. This may have stopped these sections from being an effective recorder of sink switching.

Handoh and Lenton's [2004] model does make a fourth prediction, which has not been tested by the five sections in this study. After an OAE, P accumulation should increase due to oxic conditions causing enhanced PBE. With the exception of Manilva, our sections are not sampled high enough to interrogate this possibility. This prediction would most easily be tested in a section whose paleodepth is sufficient enough to have probably been immersed in the OMZ during the main stages of OAE 2 and emerge again after. Both Furlo and Manilva are highly condensed sections with large paleodepths and may not have effectively recorded a later increase in $P_{inorganic}$.

In a recent study [Gertsch, et al., in prep] P_{total} has been measured across the OAE 2 interval at the shallow water Whadi El Ghaib section, Egypt (figure 10). This is not speciation P data, however, the section contains several oysters beds and therefore it can safely be assumed that the majority of the P_{total} is bound to inorganic phases. Gertsch, et al., [in prep] observe an increase in P concentration during the final stage of the $\delta^{13}C$ decline in the early Turonian. This provides compelling evidence to support a decoupling of the P and C cycles as an important driver at the start of OAE 2 as well as for their later re-coupling at the end of OAE 2 due to the return of more oxidizing conditions. The timing of the increase in [P] at Whadi El Ghaib also adds strong empirical evidence that the model of Handoh and Lenton [2004] is correct, in so far as a positive and negative feedback operated in controlling during of OAE 2. The author's notion of a self-sustaining positive-negative feedback oscillation still needs to be probed with further geochemical measurements.

C.5.4. Conceptual Model

Using the data obtained from this study and incorporating ideas related to eustatic sea-level change and the feedback mechanisms associated with an autocyclic fluctuation, it is possible to make a four-stage model for how OAE 2 unfolded (figure 11). In this model, a rapid transgression prior to OAE 2 caused the mega-scale reworking of continental

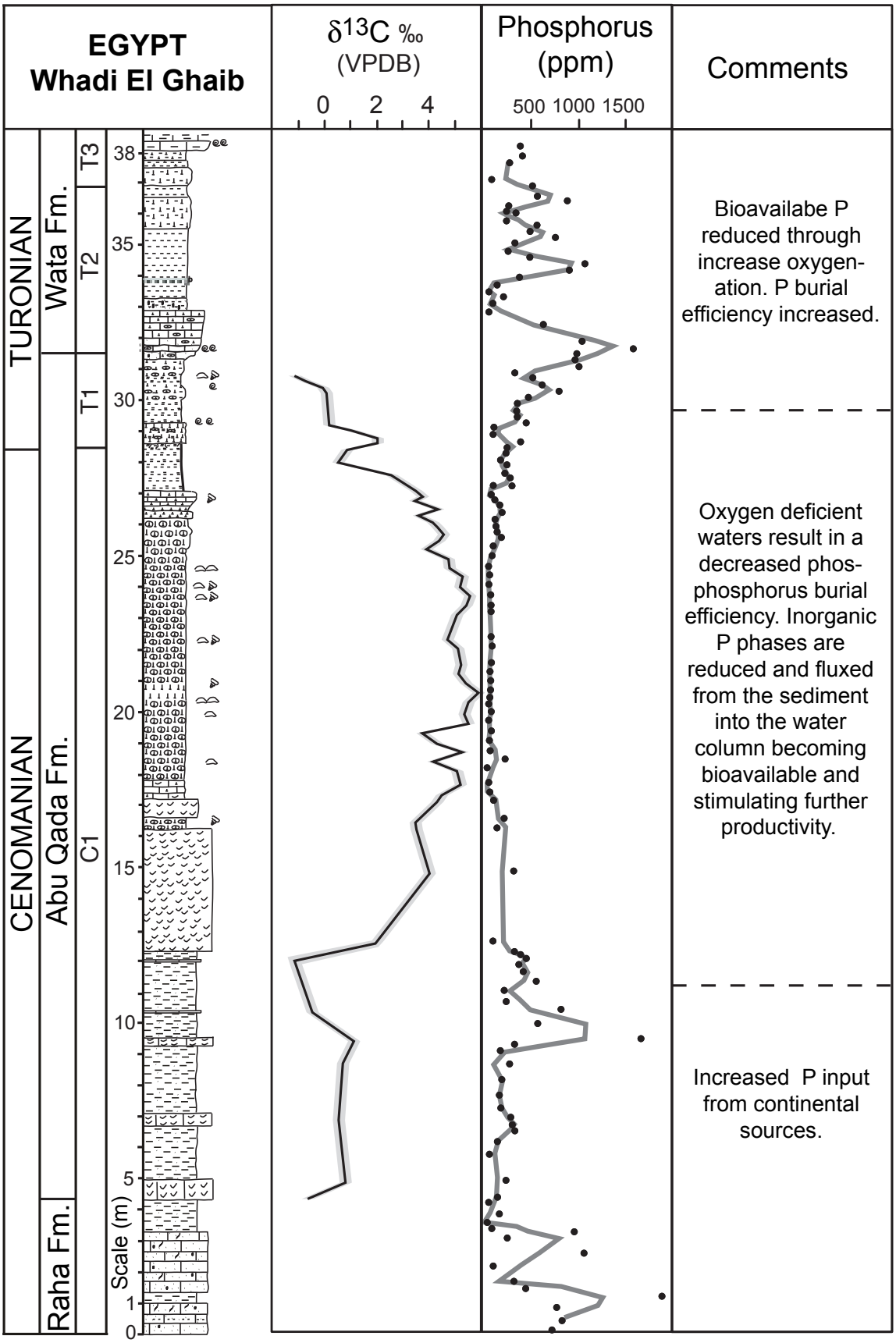

Figure 10. The P concentration (ppm) for the Whadi El Ghaib section, Egypt (after Gertcsh et al, in prep)

C

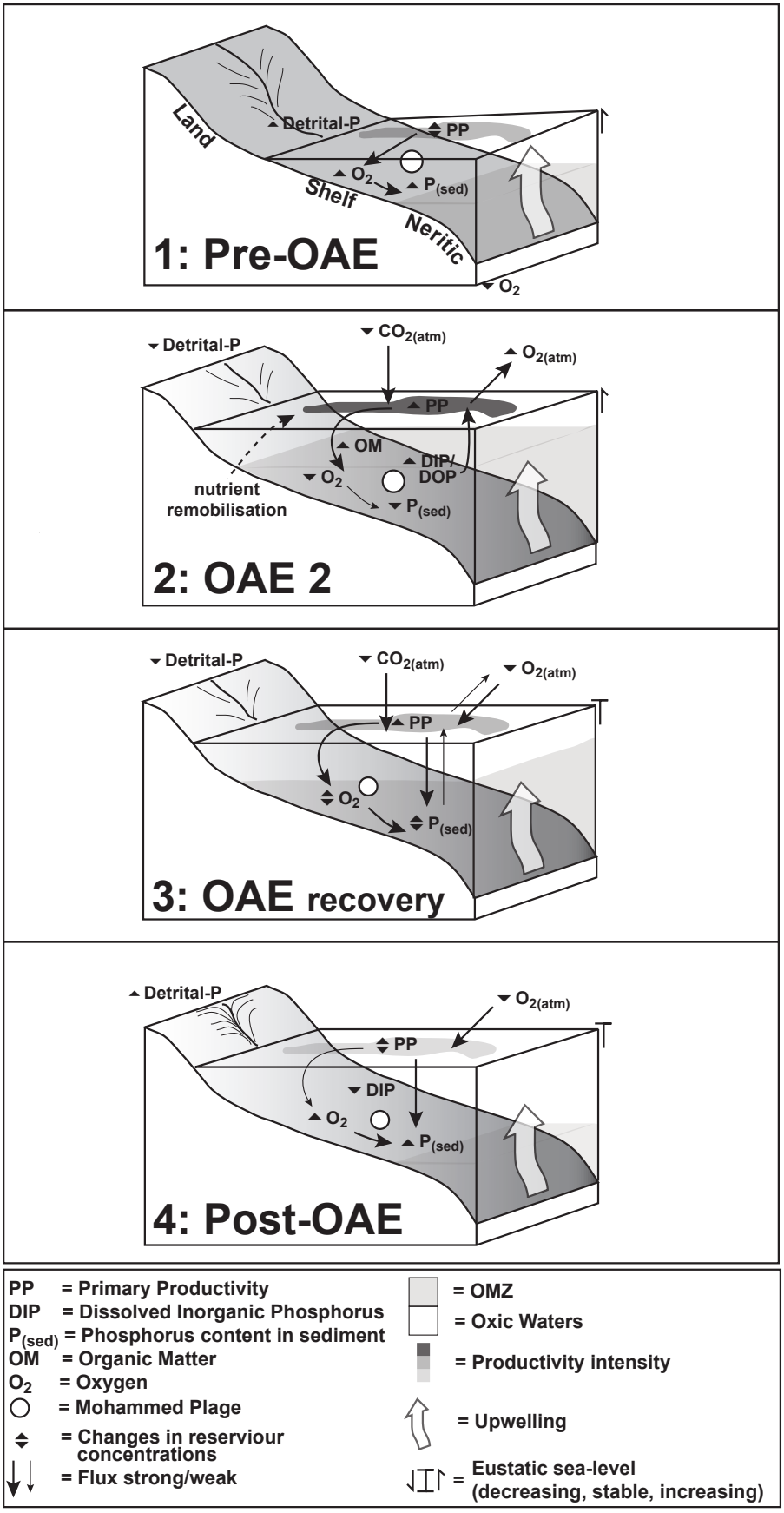

Figure 11. A conceptual model to explain the observed decline in P MARs during the $\delta^{13}C$ excursion onset and it's later recovery at the end of OAE 2.

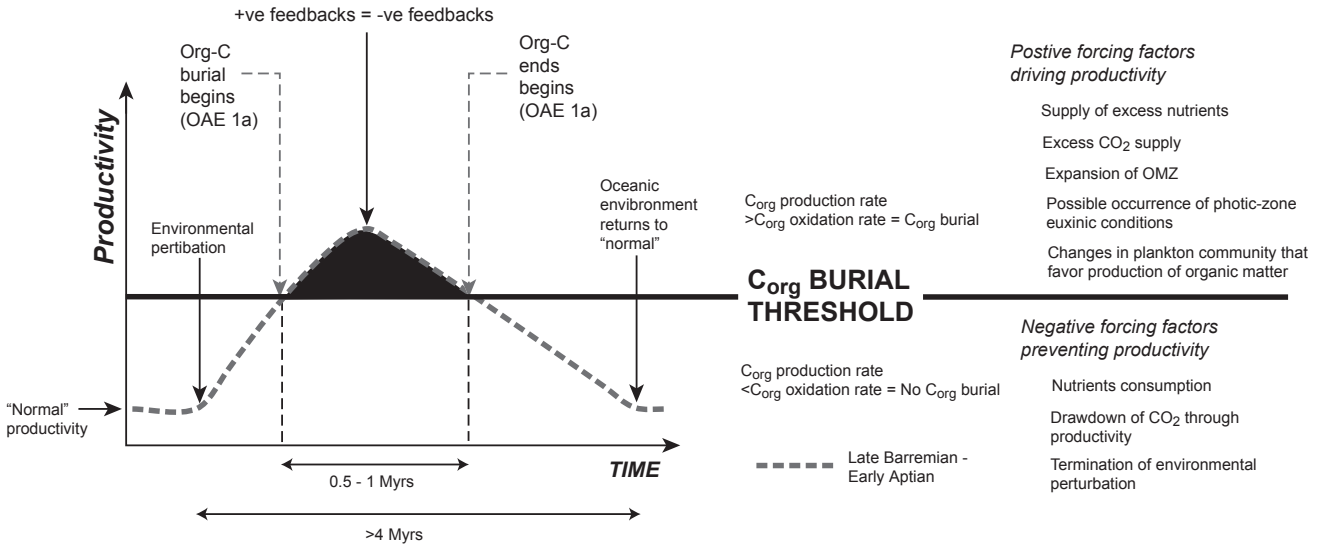

Figure 12, after Robinson et al (2004) explaining the relationship between productivity, time, and black shale deposition for OAE 1a (Late Barremian - Early Aptian)

sediments. The Cretaceous ocean was predisposed to anoxia by virtue of high atmospheric CO_2 and shallow seas. Mechanically reworked nutrients were mostly bio-unavailable and caused the increase in P MARs. Nutrients, that were desorped from the matrices of sediments, were more soluble and therefore more bioavailable. This desorped fraction is probably what initially drove the increase in productivity (step 1-2, Fig 11). The decrease in $P_{inorganic}$ MARs may have been partly caused by a deceleration in eustatic sea-level rise capping the delivery of $P_{unreactive}$. However, our data suggests that dysoxic conditions restricted the mineralization of P once it had been removed through the oxidation of organic matter, causing a decrease in $P_{inorganic}$ MAR. The sustained productivity continued throughout the $\delta^{13}C$ plateau, despite the hypothetical capping of drowned continental sediments. Step 2 in Fig. 11 explains this by the decreased burial efficiency of phosphorus under reducing condition, causing it to be bioavailable, sustaining primary production of organic matter and creating a positive feedback. Eventually, over hundreds of thousands of years, the O_2, built up in the atmosphere to such an extent that its pO_2 exceeded the pCO_2 in the photic zone of the ocean. The resulting flux of oxygen into the mixing layer caused the large-scale oxidation and burial of nutrients, reducing the oceans budget of bioavailable P. At the same time, the consumption of bottom water oxygen, needed to oxidize the massive amounts of organic matter, decreased the efficiency of organic matter degradation, enhancing the preservation of organic matter (step 3, Fig. 11). $P_{inorganic}$ (as is seen in Whadi El Ghaib, Egypt) would increase as the sorption of P into Fe and Mn oxyhydroxides and the mineralization into authigenic minerals, was again permitted under more oxic conditions (step 3-4, Figure 11)

C.5.5. A New Perspective for the Cretaceous Ocean

That preservation may have played an important role in the formation of organic-rich deposits is not a new concept [Bralower and Thierstein, 1984; Crumiere, et al., 1990; Pedersen and Calvert, 1990; Ingall, et al., 1993; Calvert, et al., 1996; Van Cappellen and Ingall, 1996; Damste and Koster, 1998; Rimmer, et al., 2004; Föllmi, et al., 2005]. However this is first time Cretaceous modelling ideas of biogeochemical cycling and feedback [Van Cappellen and Ingall, 1996; Ingall and Jahnke, 1997; Handoh and Lenton, 2003; Robinson, et al., 2004] have been tested. A deeper understanding into the nature of black shale deposits gives us new insights into how the ocean follows homeostatic principles (i.e. Gaia) [Lovelock, 1989], bringing itself back into equilibrium from environmental perturbations. The model outline by Robinson et al., [2004] views black shales as the last step an ocean may go through when reacting to a disturbance in its 'steady state' (figure 12). A

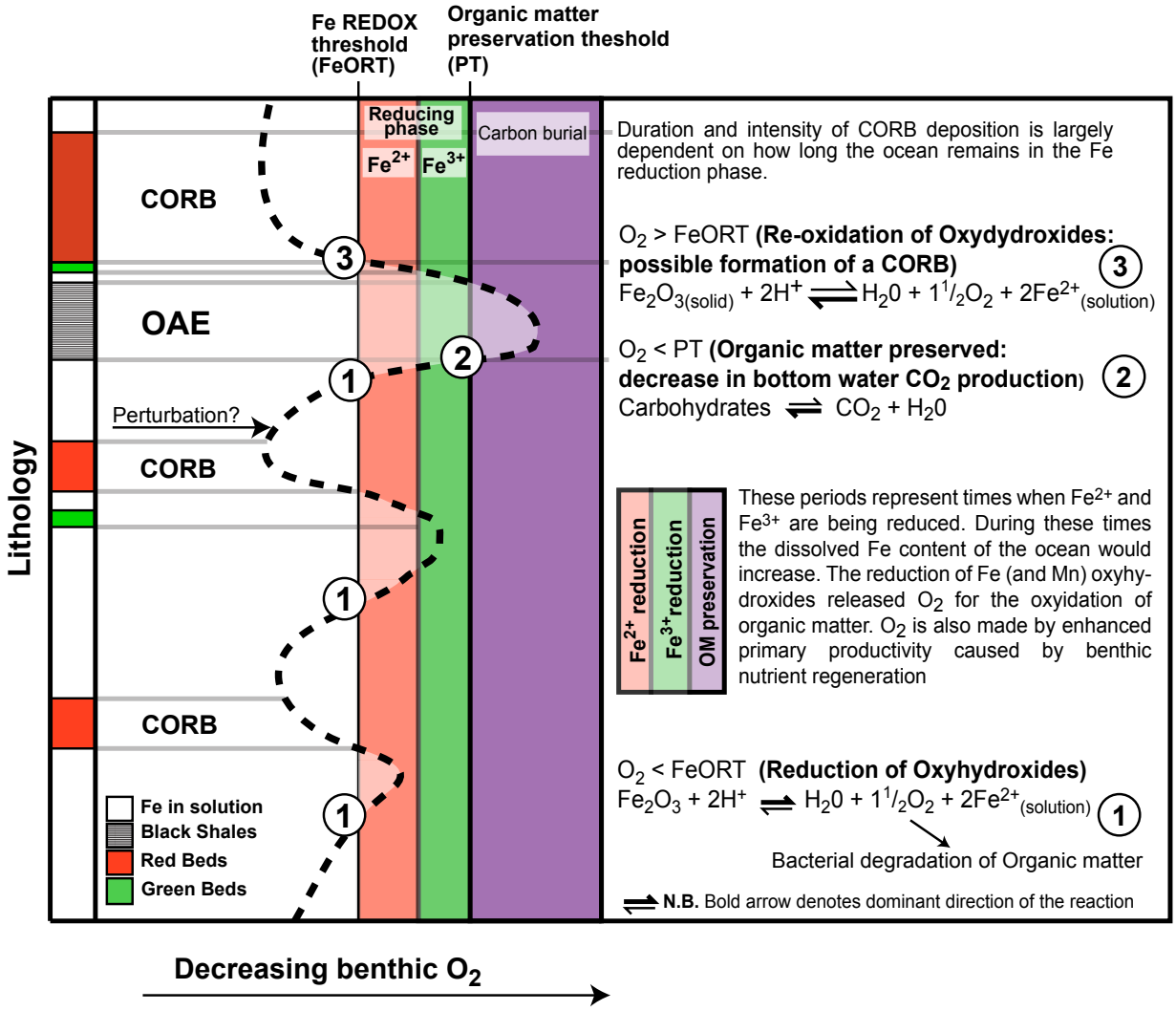

Figure 13. Conceptual model to explain the formation of Cretaceous Oceanic Red Beds (CORBs) as a series of homeostatic fluctuations the ocean may go through, either autocyclically or as a result of an environmental perturbation. Each stage of the increasing dysoxia produces oxygen, which acts against the perturbation and benthic nutrient regeneration. It is the crossing of redox thresholds that cause decreases and increasing in redox sensitive elements and nutrients

critical threshold is passed where production of organic carbon exceeds the rate it is being oxidized, thus a causing stabilization and reduction in the atmospheric/oceanic CO_2 as carbon is sequestered at higher burial rates. Robinson et al., [2004] do not address the the build-up if atmospheric and oceanic O_2 levels that would be essential in driving the reactions that would explain the later increase in phosphorus in Egypt.

The evidence of water column dysoxia impacting on the P cycle is strong and therefore raises questions about the behaviour of other redox sensitive productivity limiting nutrients, for example nitrogen (N) and iron (Fe). These elements are already know to be sensitive to changes in benthic oxygenation state [Karl, et al., 1997; Duarte, et al., 2004; Mills, et al., 2004]. The observation that P accumulation appears intimately linked to changes in the redox state of the ocean makes it reasonable to predict that N and Fe accumulation would follow similar patterns to P depending on how easily it is to reduce their associated oxides. The sedimentary colour change from brown to green is known to represent the transition where Fe^{3+} has been reduced to Fe^{2+} in pore waters [Lyle, 1983]. Given the parallel between the processes affecting P and Fe accumulation it is therefore valid to use changes in sediment colour (i.e. Fe redox state) as an additional test to the models supported by our data. The distribution of so-called

'Cretaceous Oceanic Red Beds' (CORBs) may add or detract support from notions of a homeostatic ocean, which logically follows from the discussion of the P accumulation data. From the homeostatic perspective, the reduction of ferric minerals liberates oxygen (step 1, figure 13) that is used for the oxidative breakdown of organic matter. Oxygen consumption would continue in benthic waters, reducing N each of which generates increased O_2 in their reduction, delaying the preservation of organic matter, whilst stimulating productivity when becoming bioavailable. Eventually, organic matter would become preserved, removing CO_2 from the biosphere (step 2, figure 13). The O_2, built up in the earlier stages of the perturbation would then have become a strong oxidizing agent of N, P and Fe decreasing the concentration of these nutrients in the water column. The transition between the termination of organic-matter preservation and conditions becoming sufficiently oxic enough to precipitate Fe-oxides, would not be immediate. The higher electropositivity of Fe^{3+} would insure that it became oxidized first (creating a relatively brown colour). Fe^{2+} would be oxidizes next creating a red coloured pigment (step 3, figure 13). The build-up of Fe in the oceans during dysoxic-anoxic conditions would mean that at the later oxidation threshold, Fe could have been precipitated in large quantities forming a CORB.

This model to explain CORB deposition stems directly from the interpretation that the P MARs are predominantly controlled by changes in the redox state of the Cretaceous ocean. It is therefore fully testable.

C.6. Conclusion

In the past conceptual and numerical models have been put forward which attempt to explain the formation and termination of black shales during OAE 2 and other OAEs in the Cretaceous. Very often these models fell into two categories; productivity or preservation. This study is the first attempt to rigorously test the former hypothesis. There is a decrease in P AR at the start of OAE 2, evidence of sink switching from $P_{inorganic}$ to $P_{organic}$, and an increase in P AR the end of the $\delta^{13}C$ plateau. OAE 2 therefore appears to represent a decoupling of the C and P cycles under reducing conditions, in line with previous models [Ingall, et al., 1993; Van Cappellen and Ingall, 1994; Calvert, et al., 1996; Slomp, et al., 2002; Handoh and Lenton, 2003; Nederbragt, et al., 2004; Robinson, et al., 2004; Meyers, 2006].

The implication of these data directly impacts our perspective on other geochemical cycles in the ocean (e.g. N and Fe) in that they would be expected to behaviour in a similar fashion to P given their various redox thresholds. The successive reduction of each nutrient resulted in sustained productivity and higher atmospheric O_2 concentrations. Once the atmospheric pO_2 exceeded the pO_2 in the oceans this would have oxidized many of the bioavailable nutrients in the water column. Similarly, once organic matter preservation commenced, CO_2 would have been sequestered in black shale deposits. This brought the ocean back into equilibrium. This proposal is testable when studying the relationship between OAEs and Cretaceous Oceanic Red Beds (CORBs).

Future studies should carry out higher resolution P and Fe speciation work across an entire OAE interval to test see if the results of this study are replicatable in other parts of the world. Whilst it can be confidently predicted that the peak in P MARs will be positioned at the $\delta^{13}C$ onset in most other OAE 2 sections, so far we only have one section showing a peak at the end of the isotope plateau. The veracity of this observation needs to be carried out by geochemically analysing other sections.

Acknowledgements

We thank Stuart Robinson for his permission to reproduce figure 12. This project was supported by the Swiss National Fund, No. FN21-67702.02 and US National Science Foundation Grant No. 0115357 (GK).

References

Abdallah, H., et al. (2000), Sequential stratigraphy and paleography at the Cenomanian-Turonian boundary in the Gafsa-Chotts region (Central Tunisia), Cretaceous Research, 21, 35-106.

Adatte, T., et al. (1996), Lithostratigrahical and mineralogic correlations of near K/T boundary clastic sediments in northeastern Mexico: Implications for origin and nature of deposition., Geological Society of America Special Paper, 307, 211-226.

Anderson, D. L., and M. L. Delaney (2000), Sequential extraction and analysis of phosphorus in marine sediments: streamlining of the SEDEX procedure, Limnol Oceanogr, 45, 509-515.

Arthur, M., and I. Premoli-Silva (1982), Development of widespread organic rich strata in Mediterranean Tethys., in Nature and Orgin of Cretaceous Carbon-rich Facies., edited by A. Schlanger and M. B. Cita, pp. 7-54, Academic Press, London/New York/Paris.

Attewell, P. B., and I. W. Farmer (1976), Principles of engineering geology, Chapman and Hall, London.

Barron, E. J., et al. (1985), Cretaceous rhythmic bedding sequences: a plausiable link between orbital variations and climate., Earth and Planetary Science Letters, 72, 327-340.

Berner, R. A., et al. (1993), The nature of burial in modern marine sediments, in Interaction of C, N, P and S Biogeochemical Cycles and Global Change, edited by R. Wollast, et al., pp. 365-378, Springer.

Bodin, S., et al. (2006), The late Hauterivian Faraoni oceanic anoxic event in the western Tethys: Evidence from phosphorus burial rates, Palaeogeography, Palaeoclimatology, Palaeoecology, 235, 245-264.

Bortolotti, V., et al. (1970), The miogeosynclinal sequences., Sedimentary Geology, 4, 341-344.

Bralower, T. J., and H. Thierstein, R. (1984), Low productivity and slow deep-water circulation in Mid-Cretaceous oceans, Geology, 12, 614-618.

Bush, A. B. G., and S. G. H. Philander (1997), The late Cretaceous: simulation with a coupled atmosphere-ocean general circulation model., Paleoceanography, 12, 495-516.

Calvert, S. E., et al. (1996), Influence of water column anoxia and sediment supply on the burial and preservation of organic carbon in marine shales, Geochim Cosmochim Ac, 60, 1577-1593.

Caron, M. (1985), Cretaceous planktonic foraminifera, in Plankton stratigraphy, edited by H. M. Bolli, et al., pp. 17-86, Cambridge University Press, Cambridge.

Caron, M., et al. (2006), High-resolution stratigraphy of the Cenomanian–Turonian boundary interval at Pueblo (USA) and Wadi Bahloul (Tunisia): stable isotope and bio-events correlation, Geobios-Lyon, 39, 171-200.

Coccioni, R., et al. (1991), Litho- and biostratigraphy of the Livello Bonarelli close to the Cenomanian/Turonian boundary (Umbria-Marche Apennines, Italy) and possible paleoceanographic significance, Géologie Alpine, Mémoire Hors Série, 17, 25-26.

Coccioni, R., and S. Galeotti (2003), The mid-Cenomanian Event: prelude to OAE 2, Palaeogeography, Palaeoclimatology, Palaeoecology, 190, 427-440.

Coccioni, R., and V. Luciani (2004), Planktonic formainifera and environmental changes across the Bonarelli Event (OAE 2, latest Cenomanian) in it type area. A high resolution study from the Tethyan reference Bottaccione Section (Gubbio, Central Italy), J Foramin Res, 34, 109-129.

Coleman, A. S., and H. D. Holland (1994), the global diffusive flux from marine sediments into the oceans., Eos, Transations of the American Geophysical Union, 75, 96.

Coleman, A. S., and H. D. Holland (2000), The global diagenetic flux of phosphorus from marine sediments to the oceans: Redox sensitivity and the control of atmospheric oxygen levels., in Marine Authigenesis: From Microbial to Global., edited by C. Glenn, et al., pp. 53-75, SEPM Special Publication.

Colman, A. S., and H. D. Holland (2000), The global diagenetic flux of phosphorus from marine sediments to the oceans: Redox sensitivity and the control of atmospheric oxygen levels., in Marine Authigenesis: From Microbial to Global., edited by C. Glenn, et al., pp. 53-75, SEPM Special Publication.

Compton, J. S., et al. (1993), Origin and age of phosphorite from the south-central Florida platform: relation of phosphogenesis to sea-level fluctuations and d13C excursions., Geochim Cosmochim Ac, 57, 131-146.

Cresta, S., et al. (1989), Mesozoic - Cenozoic stratigraphy in the Umbria-Marche area, Memoire Cartagraphica Geolgia de Italia, 39, 185.

Crumiere, J. P., et al. (1990), Cyclic Preservation of Amorphous Organic-Matter in Sediments of the Vocontian Basin (Southeastern France), around the Cenomanian-Turonian Boundary - Paleoceanographic Controls, B Soc Geol Fr, 6, 469-478.

Curiale, J. A. (1994), High-Resolution Organic Record of Bridge Creek Deposition, Northwest New-Mexico, Organic Geochemistry, 21, 489-507.

Damste, J. S. S., and J. Koster (1998), A euxinic southern North Atlantic Ocean during the Cenomanian/Turonian oceanic anoxic event, Earth and Planetary Science Letters, 158, 165-173.

Davey, S. D., and H. C. Jenkyns (1999), Carbon-isotope stratigraphy of shallow-water limestones and implications for the timing of Late Cretaceous sea-level rise and anoxic events (Cenomanian-Turonian of the peri-Adriatic carbonate platform, Croatia), Eclogae Geol Helv, 92, 163-170.

Delaney, M. L., and G. M. Filippelli (1994), An apparent contradition in the role of phosphorus in Cenozoic chemical mass balances for the world ocean, Paleoceanography, 9, 513-527.

Duarte, C. M., et al. (2004), The effect of nutrient additions on the partitioning of nutrients in an experimental coastal Mediterranean system, Biogeochemistry (Dordrecht), 68, 153-167.

Eaton, A. D., et al. (1995), Standard methods for the examination of water and wastewater, 19 ed., American Public Health Association, New York.

Eicher, D. L., and R. Diner (1989), Origin or the Cretaceous Bridge Creek cycles in the Western Interior, United States., Palaeogeogr Palaeocl, 74, 127-146.

Eicher, D. L., and R. Diner (1991), Environmental factors controlling Cretaceous limestone-marlstone rhythums., 79-93 pp., Springer Verlag, Berlin.

Eijsink, L. M., et al. (1997), The use of sequential extraction techniques for sedimentary phosphorus in eastern Mediterranean sediments, Mar Geol, 139, 147-155.

El Albani, A., et al. (1999), Palaeoenvironmental evolution of the late Cretaceous sequence in the Tarfaya Basin (southwest of Morocco), in The Oil and Bas Habitats of the South Atlantic. Special Publication Geological Society of London, edited by N. R. Cameron, et al., pp. 223-240.

Elder, W. P., and J. I. Kirkland (1985), Statigraphy and depositional environment of the Bridge Creek

Limestone Member of the Greenhorn Formation at Rock Canyon Anticline near Pueblo, Colorado, Society of Economic Paleontologists and Mineralogists, Tulsa.

Espitalié, J., et al. (1985), La pyrolyse Rock-Eval et ses applications, Revue de l'Institut Français du Pétrole, 40, 563-579.

Filippelli, G. M. (2001), Carbon and phosphorus cycling in anoxic sediments of the Saanich Inlet, British Columbia, Mar Geol, 174, 307-321.

Filippelli, G. M., and M. L. Delaney (1995), Phosphorus geochemistry, diagenesis and mass balances of the Miocene Monterey Formation at Shell Beach California, in Evolution of sedimentary basins/ onshore oil and gas investigations - Santa Maria Province, edited by M. A. Keller, pp. G1-G11, U.S. Geological Survey Bulletin.

Filippelli, G. M., et al. (1994), Phosphorus Accumulation Rates in a Miocene Low-Oxygen Basin - the Monterey Formation (Pismo Basin), California, Mar Geol, 116, 419-430.

Föllmi, K. B. (1995), 160 m.y. record of marine sedimentary phosphorus burial; coupling of climate and continental weathering under greenhouse and icehouse conditions, Geology, 23, 859-862.

Föllmi, K. B., et al. (2005), Phosphogenesis and organic-carbon preservation in the Miocene Monterey Formation at Naples Beach, California - The Monterey hyphothesis revisited., GSA Bulletin, 117, 589-619.

Gale, A. S., et al. (2002), Global correlation of Cenomanian (Upper Cretaceous) sequences: evidence for Milankovitch constrol on sea level., Geology, 30, 291-294.

Gale, A. S., et al. (1993), Chemostratigraphy versus biostratigraphy - data from around the Cenomanian-Turonian boundary, J Geol Soc London, 150, 29-32.

Gale, A. S., et al. (1999), Orbital tuning of Cenomanian marly chalk successions: towards a Milankovitch time-scale for the Late Cretaceous., Philosophical Transactions of the Royal Society of London Series A, 357, 1815-1829.

Gebhardt, H. (1997), Cenomanian-Turonian foraminifera from Ashaka (NE Nigera): quantitative analysis and palaeoenvironmental interpretation, Cretaceous Research, 1997, 17-36.

Gebhardt, H., et al. (2004), Formainiferal responce to sea level change, organic flux and oxygen deficiency in the Cenomanian of the Tarfaya Basin, southern Morocco, Marine Micropalaeontology, 53, 133-157.

Gertsch, B., et al. (in prep), Cenomanian-Turonian transition in shallow water sequences of the Sinai, Egypt.

Gonsiorczyk, T., et al. (2001), Mechanisms of phosphorus release from the bottom sediment of the oligotrophic Lake Stechlin: Importance of the permanently oxic sediment surface., Archaeology and Hydrobiology, 151, 203-219.

Gradstein, F. M., et al. (2004), A Geological Time Scale 2004, 600 pp., Cambridge University Press.

Gächter, R., et al. (1988), Contribution of bacteria to release and fixation of phosphorus from marine sediments, Limnol Oceanogr, 33, 1542-1558.

Handoh, I. C., and T. M. Lenton (2003), Periodic mid-Cretaceous oceanic anoxic events linked by oscillations of the phosphorus and oxygen biogeochemical cycles, Global Biogeochemical Cycles, 17, doi:10.1029/2003GB002039.

Hardenbol, J., et al. (1998), Mesozoic and Cenozoic sequence chronostrigraphic framework of European Basins., in Mesozoic and Cenozoic Sequence Stratigraphy of European Basins, edited by J. Graciansky and T. Hardenbol, pp. 3-13, SEPM Special Publication.

Hilbrecht, H., et al. (1992), Biogeography of planktonic-foraminifera and regional carbon isotope variations - productivity and water masses in Late Cretaceous Europe, Palaeogeogr Palaeocl, 92, 407-421.

Hu, X., et al. (2006), Mid-Cretaceous oceanic red beds in the Umbria-Mache Basin, central Italy: Constraints on paleoceanography and paleoclimate, Palaeogeogr Palaeocl, 233, 163-186.

Huber, B. T., et al. (1999), Foraminiferal assemblage and stable isotopic change across the Cenomanian-Turonian boundary in the subtropical North Atlantic, J Foramin Res, 29, 392-417.

Ingall, E., and R. Jahnke (1994), Evidence for enhanced phosphorus regeneration from marine-sediments overlain by oxygen depleted waters, Geochim Cosmochim Ac, 58, 2571-2575.

Ingall, E., and R. Jahnke (1997), Influence of water-column anoxia on the elemental fractionation of carbon and phosphorus during sediment diagenesis, Mar Geol, 139, 219-229.

Ingall, E. D., et al. (1993), Influence of Water Column Anoxia on the Burial and Preservation of Carbon and Phosphorus in Marine Shales, Geochim Cosmochim Ac, 57, 303-316.

Ingall, E. D., et al. (1990), The Nature of Organic Phosphorus in Marine-Sediments - New Insights from P-31 Nmr, Geochim Cosmochim Ac, 54, 2617-2620.

Ingall, E. D., and P. Van Cappellen (1990), Relation between Sedimentation-Rate and Burial of Organic Phosphorus and Organic-Carbon in Marine-Sediments, Geochim Cosmochim Ac, 54, 373-386.

Jarvis, I., et al. (1988), Microfossil assemblages and the Cenomanian-Turonian (late Cretaceous) oceanic anoxic event., Cretaceous Research, 9, 3-103.

Jarvis, I., et al. (2006), Secular variation in late Cretaceous carbon isotopes: a new d13C carbonate reference curve for the Cenomanian-Campanian (99.6-70.6 Ma), Geol Mag, 143, 561-608.

Jarvis, I., et al. (2001), Geochemistry of pelagic and hemipelagic carbonates: criteria for identifying systems tracts and sea-level change, J Geol Soc London, 158, 685-696.

Jenkyns, H. C. (1980), Cretaceous anoxic events, from continents to oceans, Journal of the Geological Society of London, 137, 171-188.

Jenkyns, H. C. (1991), Impact of Cretaceous Sea-Level Rise and Anoxic Events on the Mesozoic Carbonate Platform of Yugoslavia, Aapg Bulletin-American Association of Petroleum Geologists, 75, 1007-1017.

Jenkyns, H. C., et al. (1994), Carbon-Isotope and Oxygen-Isotope Stratigraphy of the English Chalk and Italian Scaglia and Its Paleoclimatic Significance, Geol Mag, 131, 1-34.

Jensen, H. S., and B. Thamdrup (1993), Iron-bound phosphorus in marine-sediments as measured by bicarbonate-dithionite extraction, Hydrobiology.

Jolet, P., et al. (1997), New biostratigraphic data on the Cenomanian-Turonian boundary. The Cassis section (SE France): proposal for a European hypostratotype, Cr Acad Sci Ii A, 325, 703-709.

Kaiserli, A., et al. (2002), Phosphorus fractionation in lake sediments - Lakes Volvi and Koronia, N. Greece, Chemosphere, 46, 1147-1155.

Karl, D. M., et al. (1997), The role of nitrogen fixation in biogeochemical cycling in the subtropical North Pcific Ocean, Nature, 388, 533-538.

Kassab, A. S., and N. A. Obaidalla (2001), Integrated biostratigraphy and inter-regional correlation of the Cenomanian–Turonian deposits of Wadi Feiran, Sinai, Egypt, Cretaceous Research, 22, 105-114.

Keller, G., et al. (2001), Palaeoenvironment of the Cenomanian-Turonian transition at Eastbourne, England, Cretaceous Research, 22, 391-422.

Keller, G., and A. Pardo (2004), Age and paleoenvironment of the Cenomanian-Turonian global stratotype section and point at Pueblo, Colorado, Marine Micropalaeontology, 51, 95-128.

Keller, G., et al. (2004), Cenomanian - Turonian d13C, d18O, Sea level and salinity variations at Pueblo, Colorado, Palaeogeography, Palaeoclimatology, Palaeoecology, 211, 19-43.

Kennedy, W. J., and W. A. Cobban (1991), Stratigraphy and Interregional Correlation of the Cenomanian-Turonian Transition in the Western Interior of the United-States near Pueblo, Colorado, a Potential Boundary Stratotype for the Base of the Turonian Stage, Newsl Stratigr, 24, 1-33.

Kerr, A. C. (1998), Oceanic plateau formation: a cause of mass extinction and black shale deposition around the Cenomanian-Turonian boundary? Journal of the Geological Society London, 155, 619-626.

Kleeberg, A., and G. E. Dudel (1997), Changes in extent of phosphorus release in a shallow lake (Lake Grober Müggelsee; Germany, Berlin) due to climatic factors and load., Mar Geol.

Kolonic, S., et al. (2002), Geochemical characterization of Cenomanian/Turonian black shales from the Tarfaya Basin (SW Morocco) - Relationships between palaeoenvironmental conditions and early sulphurization of sedimentary organic matter, J Petrol Geol, 25, 325-350.

Kolonic, S., et al. (2005), Black shale deposition on the northwest African shelf during the Cenomanian/ Turonian oceanic anoxic event: Climate coupling and global organic carbon burial., Paleoceanography, 20.

Krajewski, K. P., et al. (1994), Biological processes and apatite formation in sedimentary environments, Eclogae Geol Helv, 87, 701-745.

Kuhnt, W. (1992), Abyssal Recolonization by Benthic Foraminifera after the Cenomanian Turonian Boundary Anoxic Event in the North-Atlantic, Mar Micropaleontol, 19, 257-274.

Kuhnt, W., et al. (1990), Distribution of Cenomanian-Turonian Oragnic Facies in the Western Mediterranean and Along the Adjacent Atlantic Margin, in Deposition of Organic Facies, edited by A. Y. Huc, pp. 133-160, AAPG Studies in Geology.

Kuhnt, W., et al. (2004), Orbital scale record of the late Cenomanian-Turonian Oceanic Anoxoc Event (OAE 2) in the Tarfaya Basin (Morocco), Int J Earth Sci, 94, 147-159.

Kuhnt, W., et al. (2005), Orbital-scale record of the late Cenomanian-Turonian oceanic anoxic event (OAE-2) in the Tarfaya Basin (Morocco), Int J Earth Sci, 94, 147-159.

Kuhnt, W., et al. (1997), Cyclicity of Cenomanian-Turonian organic-carbon-rich sediments in the Tarfaya Atlantic Coastal Basin (Morocco), Cretaceous Research, 18, 587-601.

Kübler, B. (1987), Cristallinite de l'illite, méthods normalisées de préparations, méthodes normalisées de mesures, Cahier Insitut de Géologie, 1, 13.

Larson, R. L., and E. Erba (1999a), Onset of the mid-Cretaceous greenhouse in the Barremian-Aptian: Igneous events and the biological, sedimentary, and geochemical responses, Paleoceanography, 14, 663-678.

Larson, R. L., and E. Erba (1999b), Onst of the mid-Cretaceous greehouse in the Barremian-Aptian: Igenous event and the biological, sedimentary, and geochemical responces., Paleoceanography, 14, 663-678.

Latimer, J. C., et al. (2006), Opal-associated particulate phosphorus: Implications for the marine P cycle., Geochim Cosmochim Ac, 70, 3843-3854.

Leckie, M. R., et al. (2002), Oceanic anoxic events and plankton evolution: Biotic response to tectonic forcing during the mid-Cretaceous, Paleoceanography, 17, 1-29.

Leckie, R. M. (1985), Foraminifera of the Cenomanian-Turonian Boundary Interval, Greenhorn Formation, Rock Canyon Anticline, Pueblo, Colorado., Field Trip Guidebook ed., 139-149 pp., SEPM Bulletin.

Lovelock, J. E. (1989), Geophysiology, the science of Gaia, Reviews of Geophysics, 27, 215-222.

Luderer, F., and W. Kuhnt (1997), A high resolution record of the Rotalipora extinction in laminated organic-rich limestones of the Tarfaya Atlantic coastal Basin (Morocco), Ann. Soc. Géol. Nord., 5, 199-205.

Lyle, M. (1983), The brown-green color transition in marine sediments: A marker of the Fe(III)-Fe(II) redox boundary., Limnol Oceanogr, 28, 1026-1033.

Meyers, P. A. (2006), Paleoceanographic and paleoclimatic similarities between Medierranean sparopels and Cretaceous black shales, Palaeogeogr Palaeocl, 235, 305-320.

Meyers, S. R., et al. (2001), Integrated quantitative stratigraphy of the Cenomanian-Turonian Bridge Creek Limestone Member using evolutive harmonic analysis and stratigraphic modeling, J Sediment Res, 71, 628-644.

Mills, M. M., et al. (2004), Iron and phosphorus co-limit nitrogen fixation in the eastern tropical North Atlantic, Nature, 429, 292-294.

Mort, H. P., et al. (in press), The Cenomanian-Turonian anoxic event in Italy and Spain: enhanced productivity and/ or better preservation, Cretaceous Research.

Mort, H. P., et al. (submitted), Phosphorus and the roles of productiviity and nutrient recycling during Oceanic Anoxic Event 2, Geology.

Nederbragt, A. J., et al. (2004), Modelling oceanic carbon and phosphorus fluxes: implications for the cause of the late Cenomanian Oceanic Anoxic Event (OAE 2), Journal of the Geological Society, London, 141, 721-728.

Nijenhuis, I. A., et al. (1999), Organic matter and trace element rich sapropels and black shales: a geochemical comparison, Earth and Planetary Science Letters, 169, 277-290.

Paul, C. R. C., et al. (1999), The Cenomanian–Turonian boundary at Eastbourne (Sussex, UK): a proposed European reference section, Palaeogeography, Palaeoclimatology, Palaeoecology, 150, 83-121.

Pedersen, T. F., and S. E. Calvert (1990), Anoxia vs. Productivity: what controls the formation of organic carbon-rich sediments and sedimentary rocks? Bulletin of the American Association of Petroleum Geologists, 74, 454-466.

Pratt, L. M. (1985), Isotopic studies of organic matter and carbonate in rocks of the Greenhorn marine cycles. In: Pratt. L.A., Kauffman, E.G. and Zelt, F.B. (Eds.) Fine grained Deposits and Biofacies of the

Cretaceous Western Interior Seaway: Evidence of cyclic Sedimentary Processes, in Fine grained Deposits and Biofacies of the Cretaceous Western Interior Seaway: Evidence of cyclic Sedimentary Processes, edited by L. M. Pratt, et al., pp. 38-48, Tulsa Society of Economic Paleotologists and Mineralogists.

Pratt, L. M., et al. (1993), Paleoceanographic cycles and events during the late Cretaceous in the Western Interior Seaway of North America, in Evolution of the Western Interior Basin, edited by M. W. Caldwell and E. G. Kauffman, pp. 333-354, St John's Geological Association of Canada Special Paper.

Racki, G., and T. Wrzolek (2001), Causes of mass extinctions, Lethaia, 34, 200-202.

Rao, J.-L., and R. A. Berner (1997), Time variation of phosphorus and sources of sediments beneath the Chang Jiang (Yangtze River), Mar Geol.

Redfield, A. C. (1958), The biological control of chemical factors in the environment., American Scientist, 46.

Reicherter, K., et al. (1994), Mid-Cretaceous paleogeography and paleoceanography of the Betic Seaway (Betic Cordillera, Spain), Palaeogeogr Palaeocl, 107, 1-33.

Ricken, W. (1991), Variations of sedimentation rates in rhythmically bedded sediments - distinction between depositional types., 167-187 pp., Springer Verlag, Berlin.

Ricken, W. (1994), Complex rhythmic sedimentation related to third order sea-level variations: Upper Cretaceous, Western Interior Basin, USA., in Orbital Forcing and Cyclic Sequences., edited by P. L. deBoer and D. G. Smith, pp. 167-193, International Association of Sedimentologists Special Publication., Oxford.

Rimmer, S. M., et al. (2004), Multiple controls on the preservation of organic matter in Devonian-Mississippian marine black shales: geochemical and petrographic analysis, Palaeogeogr Palaeocl, 215, 125-154.

Robaszynski, F., and M. Caron (1979), Atlas de foraminifers planctonique du Crétacé moyen (Mer Boreale et Tethys) première partie., Cahier de Micropaleonotologie, 1.

Robinson, S. A., et al. (2004), Fluctuation in biosiliceous production and the generation of Early Cretaceous oceanic anoxic events in the Pacific Ocean (Shatsky Rise, Ocean Drilling Program Les 198), Paleoceanography, 19, PA2024.

Ruttenberg, K. C. (1992), Development of a sequential extraction method for different forms of phosphorus in marine sediments., Limnol Oceanogr, 37, 1460-1482.

Ruttenburg, K. C. (1993), Reassessment of the oceanic residence time of phosphorus, Chemical Geology, 107, 405-409.

Rydin, E. (2000), Potentially mobile phosphorus in Lake Erken sediment, Water Resources, 34, 2037-2042.

Sageman, B. B., et al. (2006), Orbital time scale and new C-isotope record for the Cenomanian-Turonion boundary stratotype, Geology, 34(2), 125-128.

Sageman, B. B., et al. (2003), A tale of shales: the relative roles of production, decomposition and dilution in the accumulation of organic-rich strata, Middle-Upper Devonian, Appalachian Basin, Chemical Geology, 195, 229-273.

Sageman, B. B., et al. (1997), Evidence for Milankovitch periodicities in Cenomanian-Turonian lithologic and geochemical cycles, western interior USA, J Sediment Res, 67, 286-302.

Sageman, B. B., et al. (1998), Multiple Milankovich cycles in the Bridge Creek Limestone (Cenomanian-Turonian), Western Interior Basin., in Concepts in Sedimentology and Paleontology, edited by W. E. Dean and M. A. Arthur, pp. 153-171, Society for Sedimentary Geology.

Sahagian, D., et al. (1996), Eustatic curve for the middle Jurassic-Cretceous based on Russion platform and Siberian stratigraphy: zonal resolution., American Association of Petroleum Geologists, 80, 1433-1458.

Sanudo-Wilhelmy, S. A., et al. (2001), Phosphorus limitation of nutrient fixation by Trichodesmium in the central Atalntic Ocean, Nature, 411, 66-69.

Schenau, S. J., et al. (2005), Phosphorus burial as a function of paleoproductivity and redox conditions in Arabian Sea sediments, Geochim Cosmochim Ac, 69, 919-931.

Schlanger, S. O., et al. (1981), Volcanism and Vertical Tectonics in the Pacific Basin Related to Global Cretaceous trangressions, Earth and Planetary Science Letters, 52, 435-449.

Scholle, P. A., and M. A. Arthur (1980), Carbon isotope fluctuations in Cretaceous pelagic limestones: potential stratigraphic and petroleum exploration tool, American Association of Petroleum Geologists, 64, 67-57.

Schootbrugge, B. V. d., et al. (2003), Decoupling of P- and Corg-burial following Early Cretaceous (Valanginian-Hauterivian) platform drowning along the NW Tethyan margin, Palaeogeogr Palaeocl, 199, 315-331.

Schwenke, W., and W. Kuhnt (1992), Subsidence history and continental margin evolution of the Western Pyrenean and Basque Basins, Palaeogeogr Palaeocl, 95, 297-318.

Sinton, C. W., and R. A. Duncan (1997), Potential links between ocean plateau volcanism and global ocean anoxia at the Cenomanian-Turonian boundary, Econ Geol Bull Soc, 92, 836-842.

Slomp, C. P., et al. (2002), Enhanced regeneration of phosphorus during formation of the most recent eastern Mediterranean sapropel (S1), Geochim Cosmochim Ac, 66, 1 April 2002.

Slomp, C. P., et al. (2004), Controls on phosphorus regeneration and burial during formation of eastern Mediterranean sapropels, Mar Geol, 203, 141-159.

Snow, L. J., et al. (2005), Trace element abundance in the Rock Canyon Anticline, Pueblo, Colorado, marine sedimentary section and their relationship to Caribbean plateau construction and Oceanic Anoxic Event 2, Paleoceanography, 20, doi: 10.1029/2004PA001093.

Sugarman, P. J., et al. (1999), The Cenomanian/Turonian carbon burial event, Bass River, NJ, USA: Geochemical, paleoecological, and sea-level changes, J Foramin Res, 29, 438-452.

Tamburini, F., et al. (2003), Investigating the history of East Asian monsoon and climate during the last glacial-interglacial period (0-140 000 years): mineralogy and geochemistry of ODP Sites 1143 and 1144, South China Sea, Mar Geol, 201, 147-168.

Tsikos, H., et al. (2004), Carbon-isotope stratigraphy recorded by the Cenomanian-Turonian Oceanic Anoxic Event: correlation and implications based on three key localities., J Geol Soc London, 161, 711-719.

Valladares, I., et al. (1996), Sequence stratigraphy and stable isotopes (delta C-13,delta O-18) of the late

Cretaceous carbonate ramp of the western margin of the Iberian chain (Soria, Spain), Sedimentary Geology, 105, 11-28.

Van Cappellen, P., and E. D. Ingall (1994), Benthic Phosphorus Regeneration, Net Primary Production, and Ocean Anoxia - a Model of the Coupled Marine Biogeochemical Cycles of Carbon and Phosphorus, Paleoceanography, 9, 677-692.

Van Cappellen, P., and E. D. Ingall (1996), Redox stabilization of the atmosphere and oceans by phosphorus-limited marine productivity, Science, 271, 493-496.

Van Cappellen, P., and E. D. Ingall (1996), Redox stabilization of the atmosphere and oceans by phosphorus-limited marine productivity, Science, 271, 493-496.

Voigt, S., et al. (2006), Sea-level chane, carbon cycling and palaeoclimate during the Late Cenomanian of northwest Europe; an integrated palaeoenvironmental analysis., Cretaceous Research, doi:10.1016/j.cretres.2006.04.005.

Voigt, S., and H. Hilbrecht (1997), Late Cretaceous carbon isotope stratigraphy in Europe: Correlation and relations with sea level and sediment stability, Palaeogeogr Palaeocl, 134, 39-59.

Wallmann, K. (2003), Feedbacks between oceanic oceanic redox states and marine productivity: A model perspective focused on benthic phosphorus cycling, Global Biogeochemical Cycles, 17, 10-11 - 10-18.

Wang, C., et al. (2005), Upper Cretaceous oceanic red beds in southern Tibet: a major change from anoxic to oxic, deep-sea environments., Cretaceous Research, 26, 21-32.

Weissert, H., et al. (1998), Correlation of Early Cretaceous carbon isotope stratigraphy and platform drowning events: a possible link? Palaeogeogr Palaeocl, 137, 89-203.

Weissert, H., et al. (1995), Correlation of Early Cretaceous carbon isotope stratigraphy and carbon isotope stratigraphy and platform drowning events: a possible link? Palaeogeogr Palaeocl, 137, 189-203.

Wignall, P. B. (2001), Large igneous provinces and mass extinctions, Earth-Science Reviews, 53, 1-33.

Willems, H., et al. (1996), Stratigraphy of the Upper Cretaceous and Lower Tertiary Strata in the Tethyan Himalayas of Tibet (Tingri area, China), Geol Rundsch, 85, 723-754.

- D -

Organic carbon deposition and phosphorus accumulation during Oceanic Anoxic Event 2 in Tarfaya, Morocco

Submitted for publication to Cretaceous Research

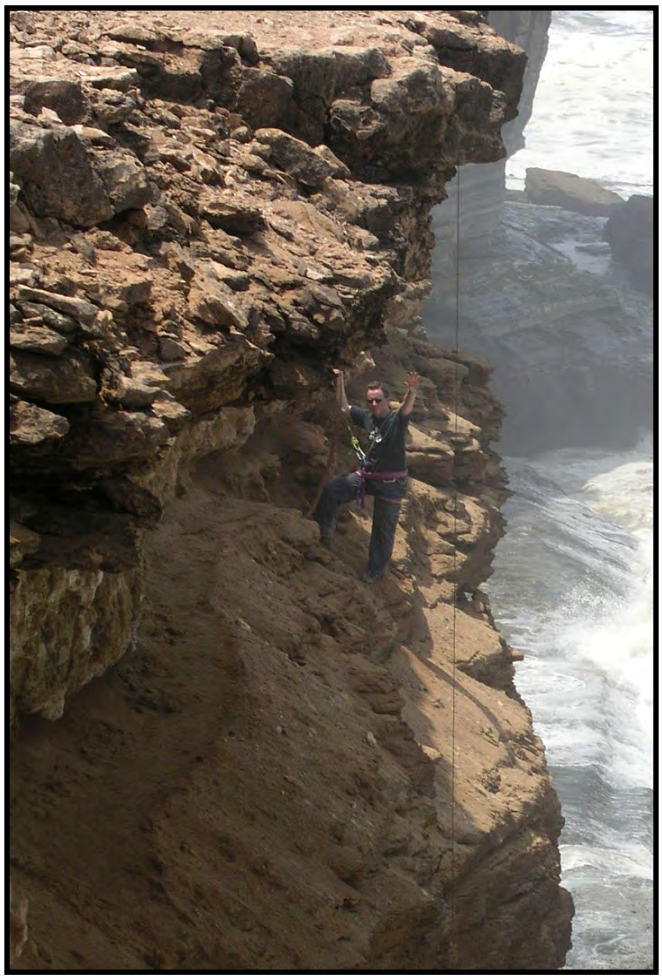

Having identified a phenomenon, which appears global in scale, we now move on to consider, in more detail, the sedimentological and geochemical processes that are thought occurred in a zone of upwelling activity in the late Cretaceous. In this paper the 'Mohammed Plage' section in Morocco is studied using a range of geochemical techniques. A planktonic foraminiferal stratigraphy is also constructed. Using $\delta^{13}C$, Rock-Eval, bulk and clay mineralogy, phosphorus speciation, and ICP-MS analysis an attempt is made to reconstruct the palaeoenvironment of the Tarfaya coast, leading up to and including the start of OAE 2. The discussion considers the global implications by making a comparison between the other sections in this project.

Left: The author risking life and limb to bring you critical samples for the following paper: by abseiling down the Mohammed Plage section.

The most exciting phrase to hear in science, the one that heralds new discoveries, is not 'Eureka!' (I found it!) but 'That's funny ...'

Isaac Asimov

Organic carbon deposition and phosphorus accumulation during Oceanic Anoxic Event 2 in Tarfaya, Morocco

Haydon P. Mort[1], Thierry Adatte[1], Gerta Keller[2], David Bartels[2], Karl B. Föllmi[1], Philipp Steinmann[1], Zsolt Berner[3], E.H. Chellai[4]

[1] Rue Emile Argand 11, Institute of Geology, University of Neuchatel, Case postale 158, CH-2009 Neuchatel, Switzerland
[2] Department of Geosciences, Princeton University, Guyot Hall, Princeton, NJ 08544-1003, USA
[3] Institut für Mineralogie und Geochemie, Universität Karlsruhe, 76128 Karlsruhe, Germany
[4]University Cadi Ayyad, Faculty of Sciences Semlalia, Marrakech, Morocco

Abstract

An attempt is made to constrain productivity and bottom-water redox conditions and their effects on the phosphorus accumulation rate at the Mohammed Plage section on the Tarfaya coast, Morocco, during Oceanic Anoxic Event (OAE 2). A distinct $\delta^{13}C_{org}$ isotope excursion of +2.5 ‰ occurs close to the top of the section. The abrupt shift of the isotope excursion and disappearance of several planktonic foraminiferal species *(*e.g. *Rotalipora cushmani and Rotalipora greenhornensis*) in this level suggests a hiatus of between 40 - 60 kyrs at the excursion onset. Nevertheless, it was possible to determine the long-term environmental history as well as the processes that took place immediately prior to and during OAE 2. TOC % values increase gradually from the base of the section to the top (from ~2.5 % to ~10 %). This is interpreted as the consequence of a long-term eustatic sea-level rise and subsidence causing the encroachment of less oxic waters into the Tarfaya Basin. Similarly a reduction in the mineralogically constructed 'detrital index' can be explained by the decrease in the continental flux of terrigenous material due to a relative sea-level rise. A speciation of phosphorus in the upper part of the section, which spans the start and mid-stages of OAE 2, shows overall higher abundances of $P_{reactive}$ mass accumulation rates before the isotope excursion onset and lower values during the plateau. Due to the probable short hiatus, the onset of the decrease in phosphorus content relative to the isotope excursion is uncertain, although the excursion plateau already contains lower concentrations. The C_{org}/P_{total} and V/Al ratios suggests that this reduction was caused by a decrease in bottom water oxygen availability (probably as a result of higher productivity) and a corresponding fall in the phosphorus retention ability of the sediment. Productivity appears to have remained high during the isotope plateau possibly due to a combination of increased aridity (increased K/Al and Ti/Al ratios) and higher dissolved inorganic phosphorus content in the water column as a result of P recycling. The evidence for decreased P-burial has been observed in many other palaeoenvironments during OAE 2. Tarfaya's unique upwelling paleosituation provides strong evidence that the nutrient recycling was a global phenomenon and therefore a critical factor in starting and sustaining OAE 2.

Keywords: **Cenomanian-Turonian, OAE 2, geochemistry, phosphorus, TOC, mineralogy, biotic changes, transgression, dysoxia, benthic nutrient regeneration**

D.1.1. Introduction

At least seven so-called 'anoxic events' punctuated various intervals in the Cretaceous the one of which was in the latest Cenomanian (Bonarelli Level) dated around 93.5 Ma. Generally these events are characterized by enhanced organic rich shale deposition and positive $\delta^{13}C$ excursions (Schlanger and Jenkyns, 1978; Jenkyns, 1980). Although the fundamental causal mechanisms have remained enigmatic, there have been no shortages of ideas that have, at least in part, helped to explain these events. The causal nature of each OAE is likely to be subtly different given the differing sea-level positions, tectonic and paleogeographic situations (Haq et al., 1987; Jenkyns, 1991; Hallam and Wignall, 1999; Aguilera-Franco et al., 2001) and ocean chemistry at each point in time. In terms of the amount and rate of organic carbon sequestration OAE 2 was probably the largest of the anoxic events that punctuated the Cretaceous. Often the debate has centred on the role of preservation and productivity in producing the characteristic positive $\delta^{13}C$ excursion and black shales. Ideas revolving around increased anoxia and the expansion of the oxygen minimum zone (OMZ) find universal agreement (e.g. Damste and Koster, 1998; Keller et al., 2001) when explaining black shale formation. However, disagreement remains as to the driving force of the increased anoxic conditions; whether it is productivity driven (i.e. organic rich sediments were formed only through the rate at which organic matter was arriving at the sea-floor) (e.g. Kuypers et al., 2002), or preservation where productivity itself would not have been enough to produce black shales. Bacterial respiration of organic matter and the resulting decrease in oxygen availability inhibited the breakdown of organic matter (Sinton and Duncan, 1997; Racki and Cordey, 2000; Mort et al., in press).

Increased continental nutrient run-off triggered by elevated CO_2 driven temperatures, evaporation, precipitation and weathering have been the most commonly cited mechanism to explain increased productivity (e.g. Larson and Erba, 1999). This model fails to reconcile conflicting clay mineral data obtained from OAE 2 sequences, which suggest increased aridity rather than chemical weathering (Jeans et al., 1991; Sellwood et al., 1994). The sea-level transgression, leading up to OAE 2, probably played a significant role, potentially decreasing the erosional capacity of rivers due to higher base levels, flood and leaching nutrients on previous dry land and causing the encroachment of waters with low oxygen availability higher onto the shelf. Clearly there are great uncertainties and inconsistencies in our knowledge as to how the ocean/atmosphere system has lead to the repeated occurrence of OAEs during the Cretaceous.

D.1.2. Previous work

D.1.2.1. Geological and Tectonic setting.

Mohammed Plage is a coastal section located at the northern end of the Tarfaya Basin, Morocco. The Tarfaya Basin extends along the southern coast of Morocco between 28°N and 24°N. The basin is situated at the tectonically stable western margin of the Saharan Platform (Fig. 1A and 1B). The Mohammed Plage section is situated on the eastern flank of a wide synclinal structure. Throughout the region, during the late Cenomanian to early Turonian, laminated, organic-rich siltstones, limestones, and marls were deposited in an open shelf environment to depths of 200-300 m (Kuhnt *et al.*, 2001). According to Gebhardt *et al.* (2004), the palaeoenvironment shallows to the north of the basin. Thus, at Mohammed Plage the depositional setting was likely interpreted as being near the paleocoastline associated with high terrigenous input.

Eustatic sea-level rises inferred from the Russian Platform and Western Europe are in the order of 70 m during the Cenomanian (Sahagian et al., 1996; Gräfe, 2002). Therefore out of the total reported 150 m of relative sea-level rise in the Tarfaya Basin, 80 m could be accounted for by subsidence alone (El Albani et al., 1999a; El Albani et al., 1999b; Gebhardt et al., 2004).

This gradual subsidence appears to have been punctuated by at least 9 sea-level lowstands (Gebhardt et al., 2004), as indicated by the abundance of shallow water benthic foraminifera (tolerance range 20-100 m; *Bolivina anambra*, *Lenticulina spissocosta* and *Spiroplactammina*

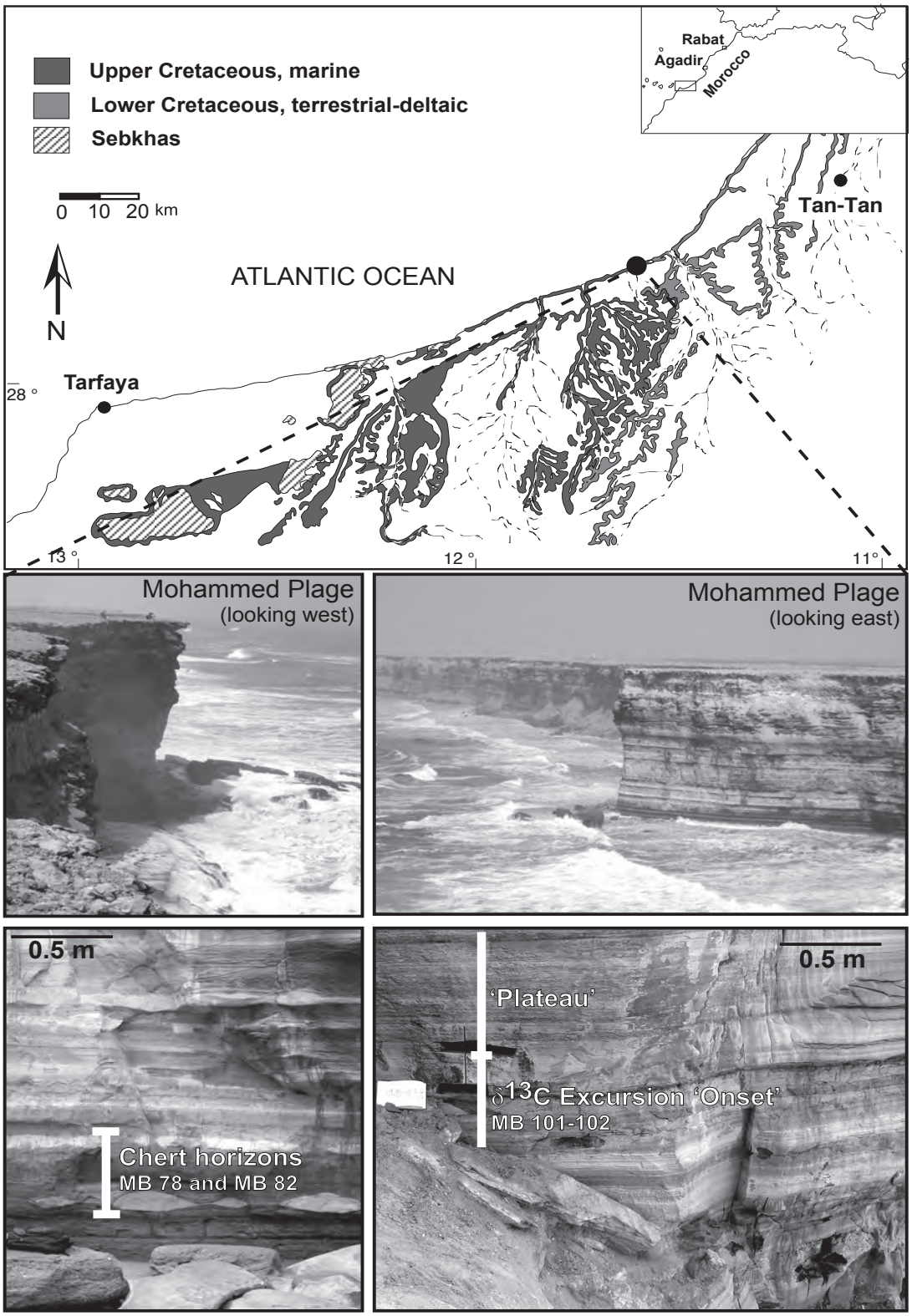

Photographs of the lithologies towards the top of the Mohammed Plage section. See text for details

Fig. 1A: Position of the Mohammed Plage section on the modern coastline. Adapted from Gebhardt et al., (2004). Outcrop photographs show different perspectives of the section along with lithological details of the $\delta^{13}C_{(org)}$ excursion and chert nodule layer.

sp.). Despite these regressions, the migration of ostracod species indicates that a Trans-Saharan seaway may have existed flowing south to north especially during the late Cenomanian (Gebhardt, 1999).

D.1.2.2. Geochemistry and Cyclostratigraphy

Modern (Kuhnt et al., 1999; South China Sea) and ancient studies (on the Tarfaya coast; Holbourn et al., 1999; Holbourn and Kuhnt, 2002) show that benthic foraminiferal assemblages are strongly modulated by carbon flux and oxygenation fluctuations. Given that the oxidation of organic matter is decelerated when the oxygen minimum zone impinges on the shelf sea during sea-level highstands, the gradual relative sea-level (RSL) rise (150 m) could explain the gradual increase in total organic carbon (TOC) contents throughout the Mohammed Plage section (Kolonic et al., 2002; Gebhardt et al., 2004). (Kuhnt et al., 1997) noted that maximum organic carbon burial corresponds to benthos-free laminated sediments, which indicates bottom water anoxia.

In the same study, Kuhnt et al constructed the first cyclostratigraphic framework for the Cenomanian-Turonian sediments in the region, by using density logs from six exploration wells. The attributed cyclic fluctuations in organic carbon and pelagic carbonate content were presumed to have

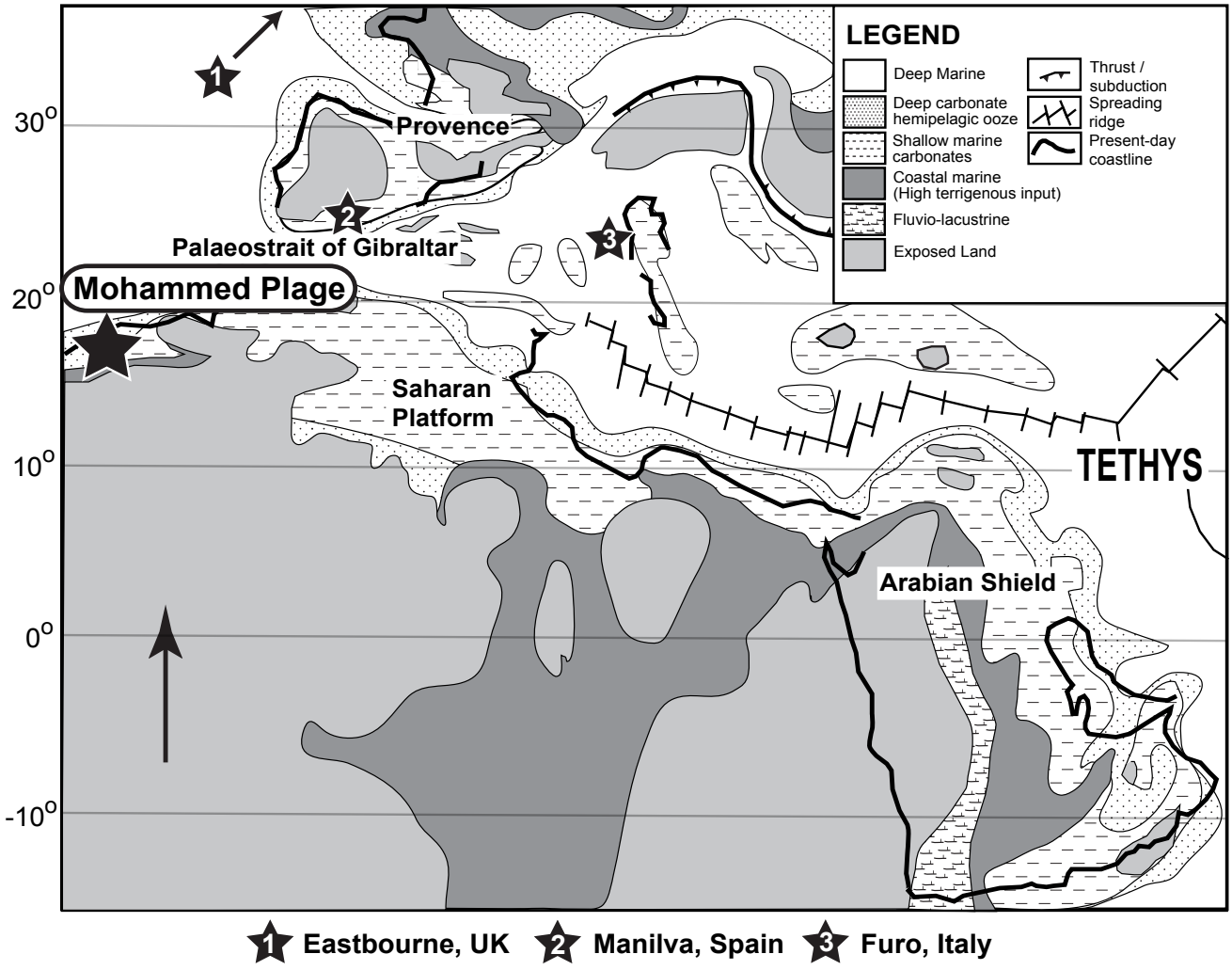

Fig. 1B: Palaeogeographical map detailing the main depositional environments of the Peri-Tethyan realm, including North Africa in the late Cenomanian (94.7-93.5 Ma). Modifed after (Philip, 2003). The Mohammed Plage section is indicated. Also shown are the section of Eastbourne, Manilva and Furlo to which comparisons are made in the discussion.

arisen from climate changes driven by Cretaceous obliquity (39 ka) Milankovitch cycles. Kolonic et al. (2005) extrapolated this well correlation to the Mohammed Plage section to calculate bulk sedimentation rates, which were then used to generate mass accumulated rates for TOC and redox sensitive metals. High amplitude variations in these proxies lead the authors to conclude that this geochemical response resulted from short-term fluctuations in the upwelling (El Albani et al., 1999b) of oxygen depleted, nutrient-rich intermediate waters coupled to enhanced marine productivity. Climate forcing supposedly drove photic zone and bottom water euxinia, alternating with periods of better water column oxygenation.

General circulation models (GCMs) also predict the location of a major upwelling zone on the North African margin during much of the late Cretaceous (Bush and Philander, 1997). The presence of this zone made the Tarfaya Basin an extremely productive area of the ocean.

In this study, a variety of traditional and novel proxies is employed in order to more accurately reconstruct the late Cenomanian palaeoenvironmental history of the Tarfaya Basin. A better understanding of the environmental factors that lead to the development of OAE 2 may be generated by evaluating the behaviour of geochemical proxies prior to and during the $\delta^{13}C$ excursion.

D.2. Material and Methods

The Mohammed Plage section was measured and sampled at closely spaced intervals of 10 to 30 cm. For this study a total of 121 samples was analyzed, which span the mid-late Cenomanian including the critical OAE 2 interval that starts ~17 m above the base of the cliff (Fig. 2). The vertical face of the cliff was sampled using climbers' rope.

Foraminifera were prepared for biostratigraphic analysis using standard methods at the University of Princeton, N.J, U.S.A. (see Keller et al., this vol.). Because of the high organic content foraminifera were difficult to free from the indurated bituminous and slightly silicified chalk and therefore no quantitative analysis could be obtained. Thin sections were made for every second sample for biostratigraphic analyses. The resultant species ranges and relative abundance estimates are based on thin sections and washed residues.

Bulk rock and clay mineralogical analyses were carried out on a SCINTAG XRD 2000 diffractometer at the University of Neuchatel, Switzerland, following the procedure outlined by (Kübler, 1987; Adatte et al., 1996). Accuracy was better than 5%. Bulk rock contents were obtained using standard semiquantitative techniques based on external standardization. XRD analysis was also made on the < 2μm sediment fraction to determine the abundance of major clay mineral components.

A detrital index (DI) was obtained by dividing the sum of quartz, feldspar, plagioclase and phyllosilicates intensities by calcite. Lower DI values therefore correspond to less delivery of terrigenous material from continental sources and/or increased dilution due to a greater marine influence.

The abundance of the different phosphorus phases was quantified following the sequential extraction (SEDEX) procedure (Ruttenberg, 1992; Eijsink et al., 1997; Anderson and Delaney, 2000). This method has been successfully applied to a wide range of geological and modern settings (Eijsink et al., 1997; Anderson and Delaney, 2000; Tamburini et al., 2003a; Tamburini et al., 2003b). Measurements for $P_{authigenic}$, $P_{detrital}$ and $P_{organic}$ were conducted with a UV/Vis Perkin Elmer Lambda 10 spectrophotometer at the University of Neuchâtel. Error margins are < 5%. P_{total} was calculated by the addition of the measured concentrations (mg/g) of the phases derived from the SEDEX method.

Published sedimentation rates based on cyclostratigraphy were used for the Mohammed Plage section (Kuhnt et al., 1997; Kolonic et al., 2005). These sedimentation rates served to calculate mass accumulation rates for phosphorus by multiplying [P] mg/g by the sedimentation rate (cm/ka) and rock density (Attewell and Farmer, 1976).

100-200 mg of powder were exposed to two hydrochloric (HCl) and hydrofluoric (HF) acid washes to leach silicate and non-silicate elements

respectively. The residue was left to dry in a sunbath. 5 ml of hot 1 M HCl was added to the sediments and allowed to cool. The solutions was transferred to a 25 ml volumetric flask and analyzed with a Perkin Elmer Instruments Optima 4300 DV Inductively Coupled Plasma-Optical Emission Spectrometer (ICP-OES) at the University of Princeton, NJ, USA.

The quantity of barium that is not associated with the aluminosilicate fraction (Ba*) was calculated using the method outlined by (Thompson and Schmitz, 1997). Ba* is assumed to be derived from the formation of biogenic barite through the following calculation.

$$Ba_{(normalised)} = Ba/Al_2O_{3(sample)} \times Al_2O_{3(average\ crust)}$$

$$Ba^* = Ba_{(normalised)} - Ba_{(aluminosilicate)}$$

Analysis of organic carbon abundance and type was conducted on all samples using Rock-Eval 6™ with instrumental precision of < 2 % (see (Espitalié et al., 1985) for details).

D.3. Results

D.3.1. Lithology

The Mohammed Plage section predominantly consists of alternating limestones, marly limestones and shales. There are frequently siltstones, especially towards the base of the section. Limestone units often show erosive lower contacts, which mark tempestite accumulation at many horizons. Bioturbation is common, particularly within limestone units, below 12 m.

The sediments attributed to the upper Cenomanian at Mohammed Plage consists of dark to light, organic-rich marls and limestones with chert nodules in some lower beds. This study focuses on OAE 2, the beginning of which can be taken as the start of the isotope excursion (MB 100). Samples 74-121 (17-24 m) cover pre-OAE and a considerable part of the excursion plateau. A 10 cm thick, organic-rich limestone layer embedded with chert nodules defines the base of this interval. At the top of this layer is an erosional surface, followed by a 65 cm thick marly shale. A 20 cm thick, bedded marly limestone overlies this. This pattern of rhythmically bedded marly limestone and black shale repeats with few exceptions.

This lithologic sequence is similar to published lithologies of the Tarfaya Basin (e.g. Kuhnt et al, 2001; Gebhardt et al, 2004), suggesting that the Mohammed Plage section was deposited in a paleo-shelf environment. The erosive contacts between beds and the alternation between siltstone and limestone are indicative of sea level fluctuation. *The base of this section corresponds to approximately 35 m on the lithology by Gebhardt et al, (2004)*.

D.3.1. Biostratigraphy

D.3.1.1. Rotalipora reicheli zone

At the Mohammed Plage section sediments attributed to the Cenomanian planktic foraminiferal zones *Rotalipora reicheli, R. cushmani* and *Whiteinella archaeocretacea* (the latter two are shown in Fig. 3) were studied. The *R. reicheli* zone spans the range of the nominate taxon and the top coincides with the first appearance of *R. cushmani*. Two $\delta^{13}C$ excursions mark this biozone in the Mohammed Plage section. The nannofossil biozone boundary CC9c/CC10a coincides with the top of the first excursion (sample MBa12) and the first appearance of *R. cushmani* is observed in the trough above the second excursion (sample MB30, Fig. 3). These two $\delta^{13}C$ excursions appear to be the two mid-Cenomanian anoxic events (MCE 1 and 2), which Rodriguez et al. (1998) identified within the *R. reicheli* zone based on the Leioa section of the Basque basin in Spain. However, Coccioni and Galeotti (2003) placed the MCE events in the lower part of the *R. cushmani* zone based on the Bottaccione Gorge and Contessa quarry sections in Italy. The reason for the discrepancy in the zonal assignment is unclear at this time.

D.3.1.2 Rotalipora cushmani zone

The top of the *R. cushmani* zone is defined by the extinction of the nominate taxon. In the Tarfaya basin subsurface cores and Tazra outcrop this extinction was observed after the $\delta^{13}C$ shift that characterizes OAE 2, and more precisely in the trough between the first

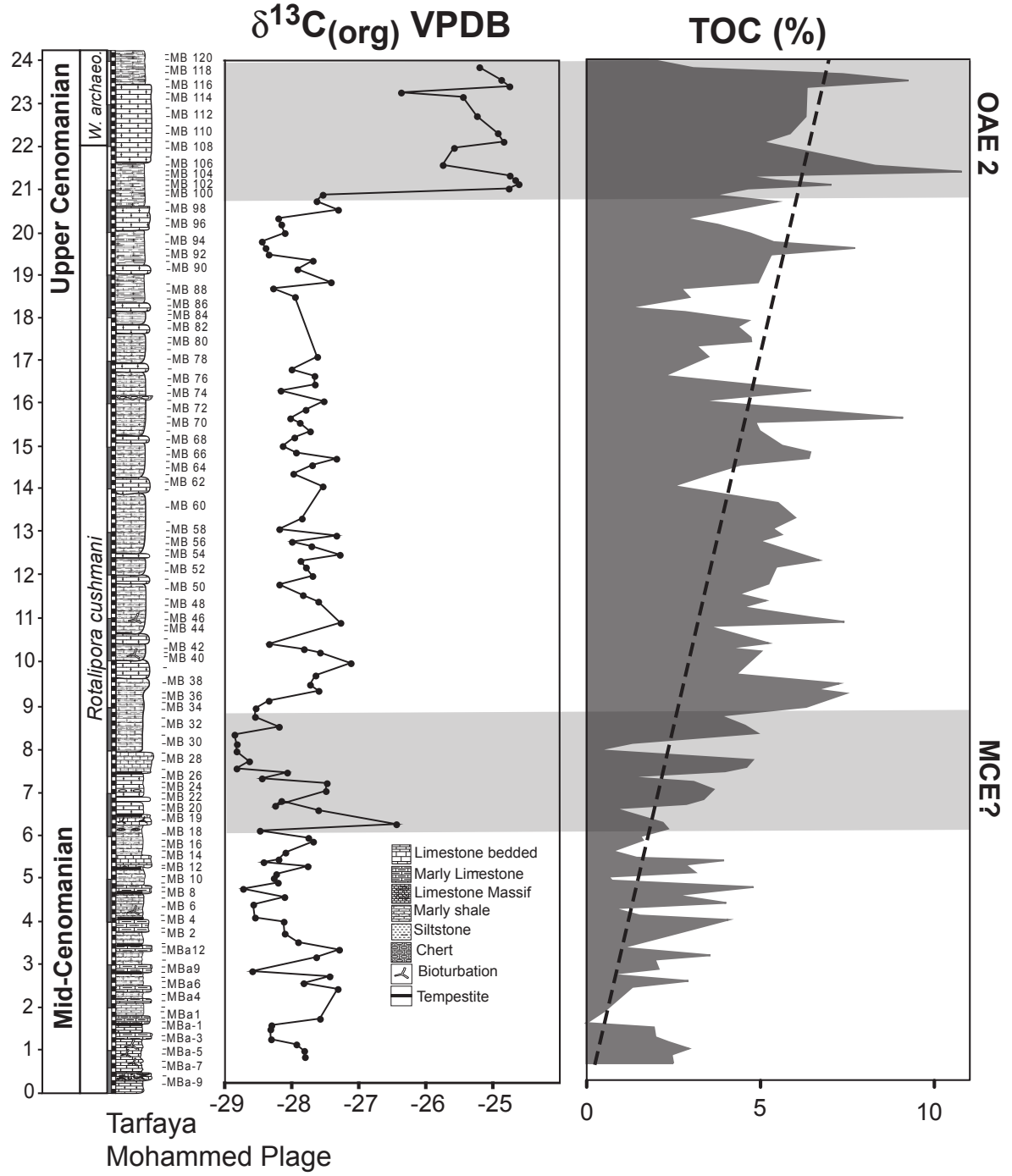

Fig. 2. Lithology with major sedimentary features and sample distribution plotted alongside $\delta^{13}C_{(org)}$ and TOC %. Note the gradual increase in TOC% values from the base-top of the section and the + 2.5‰ $\delta^{13}C_{(org)}$ excursion at 21 m.

and second $\delta^{13}C$ peaks about 70-90 cm above the maximum $\delta^{13}C_{carb}$ excursion (Luderer and Kuhnt, 1997). At Mohammed Plage the last *R. cushmani* was observed 60 cm above the maximum excursion (sample MB103) and just below the trough. The absence of *R. cushmani* in the trough in our samples is likely due to poor preservation and the rarity of this species at the end of its range. *Rotalipora greenhornensis* disappears at the abrupt shift in $\delta^{13}C_{org}$, coincident with the onset of dominant low-oxygen tolerant biserial species (*Heterohelix moremani* and *H. reussi*) and a lithological change from limestone to dark shale (Fig. 3). This suggests the presence of a short hiatus.

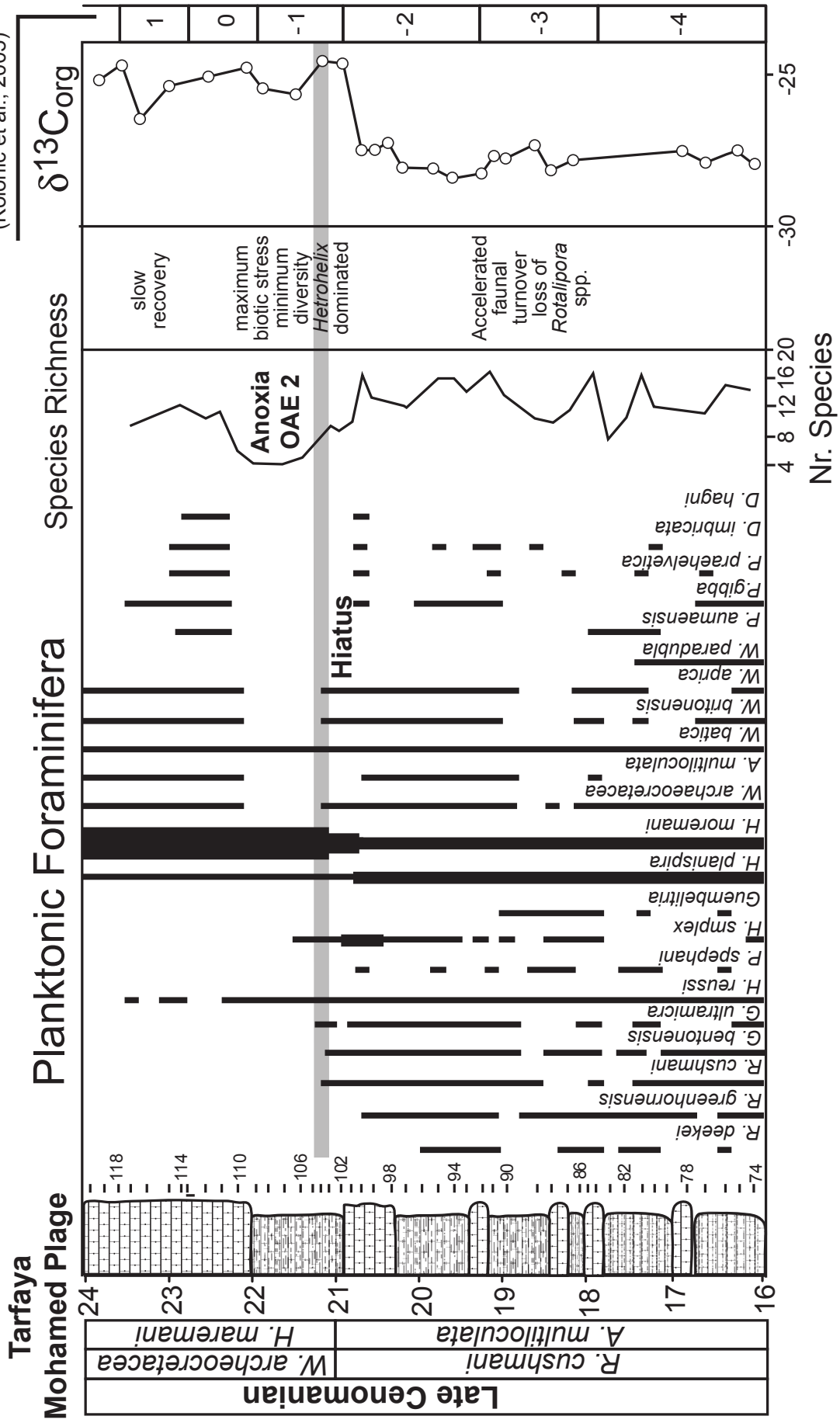

Fig. 3. Planktonic foraminiferal biostratigraphy showing the faunal changes before and during OAE 2 at Mohammed Plage. Note that the sharp faunal change coincident with the rapid $\delta^{13}C_{(org)}$ shift and the lithological change marks a short hiatus that probably spans most of the onset of the excursion. However, the disappearance of R. cushmani at this level is likely an artifact of poor preservation and rarity of this species at the end of its range.

D.3.1.3. Whiteinella archeocretacea Zone

This biozone spans the interval from the *Rotalipora cushmani* extinction to the first appearance of *Helvetoglobotruncana helvetica*, which marks the Cenomanian/Turonian (C/T) boundary. The uppermost part of the Mohammed Plage section does not reach the C/T boundary. The *Whiteinella archeocretacea* Zone is characterized by high abundance of *Heterohelix*, low species diversity and anoxic to dysoxic conditions. At Mohammed Plage the shift to dominant low oxygen tolerant *heterohelicids* (~60%, sample 101) begins at the top of a limestone layer and is coincident with the δ^{13}Corg shift. A further increase to ~80% begins near the base (sample 103, Fig. 3) of the overlying dark shale. This shift to low oxygen tolerant *Heterohelix* dominated assemblages is globally recognized and marks the onset of the *H. moremani* subzone (Keller and Pardo, 2004). The lower part of this subzone is characterized by minimum diversity and maximum biotic stress. The upper part sees the return of *Whiteinella*, *Dicarinella* and *Praeglobotruncana*.

D.3.2. Stable Carbon Isotopes (Organic Carbon)

For the majority of the Mohammed Plage section δ^{13}C values remain low, fluctuating between -28.5 ‰ and -27.5 ‰ (see Fig. 2), except for two exceptions. The first shift represents the mid-Cenomanian Event (MCE), which consists of a small peak in δ^{13}C values (-26.4 ‰) in sample MB 18, followed by a trough (-28.82 ‰) in samples MB 26-30 (total shift -2.42 ‰). The second shift represents the OAE 2 and consists of an abrupt + 2.59 ‰ shift in sample MB 97, ~21 m above the base of the section. This shift, marked by four initial points, represent the first of two δ^{13}C peaks separated by a trough, as documented in many previous studies (Gale et al., 1993; Paul et al., 1999; Keller et al., 2001; Tsikos et al., 2004). The following 'plateau' values show similar amplitude variations (~1 ‰) to those lower in the section. The abrupt nature of the OAE 2 isotope excursion suggests a significant hiatus between samples MB 100 and MB 101. A comparison with the $\delta^{13}C_{org}$ and $\delta^{13}C_{carb}$ curves of nearby subsurface cores S13, S57 and S75 (Kuhnt et al., 2004; Tsikos et al., 2004; Kolonic et al., 2005) provides an approximate duration for the hiatus. In Mohammed Plage, the top of the δ^{13}C (the 'first peak') occurs in the middle of cycle 1. In cores S13, S57 and S75 this peak is seen at the transition between cycles 0 and 1. This difference of 1.5 obliquity cycles suggests ~60 kyrs is missing from the sedimentary record. Due to uncertainties in the exact positioning of the 'first peak' in Mohammed Plage, 50-80 kyrs is a safer estimate for the duration of the hiatus.

D.3.3. Organic-carbon and organic matter composition

Total organic-carbon content rhythmically fluctuates throughout the section (Fig. 2). However, a stepwise increase from base to top is observed, as also noted in a previous study (Gebhardt et al., 2004). In the lower part of the section (0-8 m) TOC values fluctuate between 0-5 % followed by more elevated values above 3-11 %. A slight increase in TOC % is observed during the isotope excursion or plateau, although the highest value is observed just above the 'first peak' in δ^{13}C values (10.7 %).

Hydrogen and Oxygen Index (HI/OI) values display an inverse correlation and evolve in three distinct phases (Fig. 4). Phase 1 (0-8 m) shows a scattered, but easily identifiable increase in HI values, with less scatter towards the top. A similar though inverse pattern is observed in OI values. Phase 2 marks a period of stability in both HI and OI values up to approximately 16 m. In Phase 3, HI values increasing scatter near the top of the section. HI and OI values broadly show inverse trends. The most accurate way to describe the evolution of HI and OI values is as a function of varying degrees of scatter. OI values show the least scatter of values with the majority of points within the minimum scatter zone (dark rectangle). However, HI shows very few values within the dark rectangle during phases 1 and 3. Despite this in phase 2, all HI values are within the dark rectangle.

A scatter plot between OI and HI (Fig. 5) shows type II organic matter (marine) dominant with the highest TOC contents associated with higher HI's and lower OI's. The lower HI values tend to be towards the base of the section. In this case low HI values are probably not indicative of greater

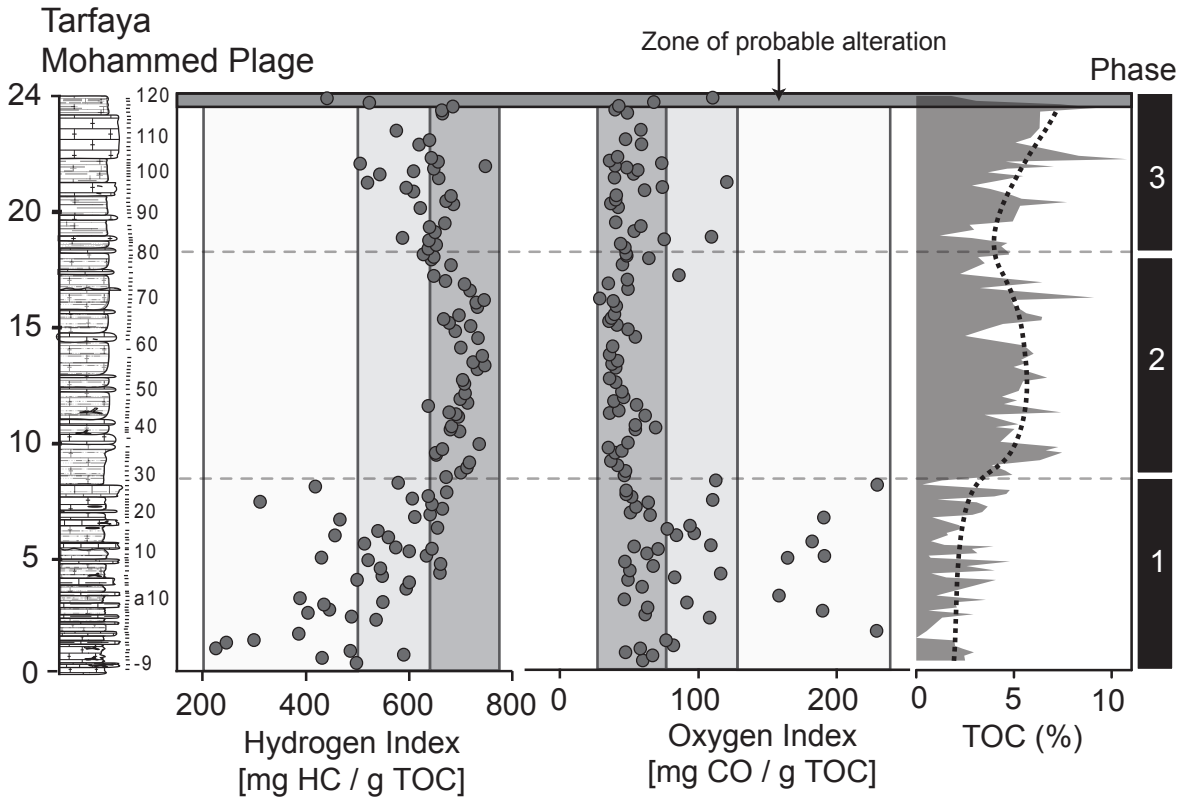

Fig. 4. Hydrogen index (HI) and oxygen index (OI) plotted against depth. The shaded rectangles represent degree of scatter, which are high in phases 1 and 3.

continental organic matter input, but rather reflect effective oxygenation of the water column, which causes the degradation of marine organic matter, making it appear similar to type III (continental, see arrow in Fig. 5).

D.3.4. Bulk rock mineralogy (0-24 m)

Quartz values fluctuate greatly at the base of the section and decrease steadily towards the top (Fig. 6). The lowest values occur above the isotope excursion (<2 %). The detrital index (plotted against a logarithmic scale) also decreases gradually from the base to the top of the section, corresponding with the gradual increase in sea level (Gebhart et al, 2004). At the $\delta^{13}C$ excursion, the detrital index shows increased fluctuation.

Calcite content remains high throughout the section, although the variability decreases considerably up-section. Between 0 and 7 m values vary from a high of 99 % to a low of 20 %. From 7 to 18 m calcite values remain above 70 % and increase to above 85% from 18 to 24 m. There is

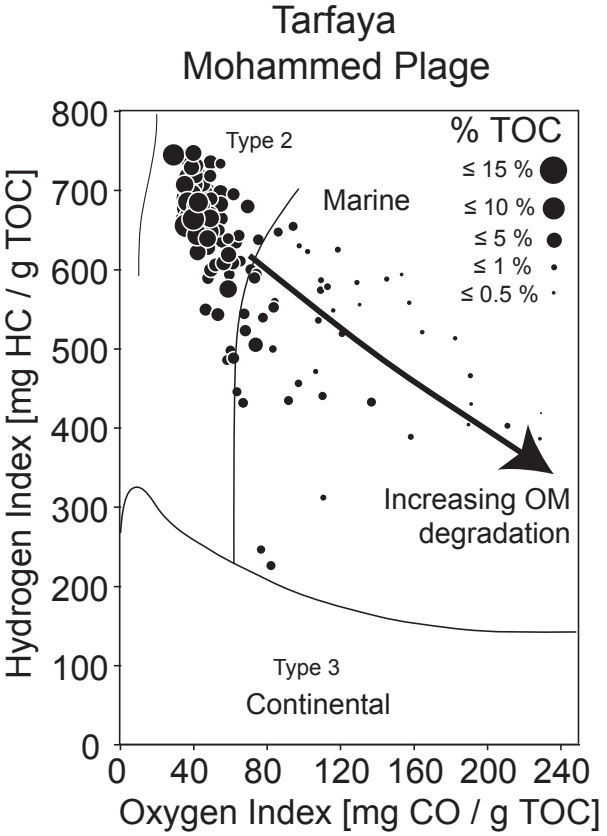

Fig. 5. HI/OI plot demonstrates that the dominant source of organic matter is of marine origin.

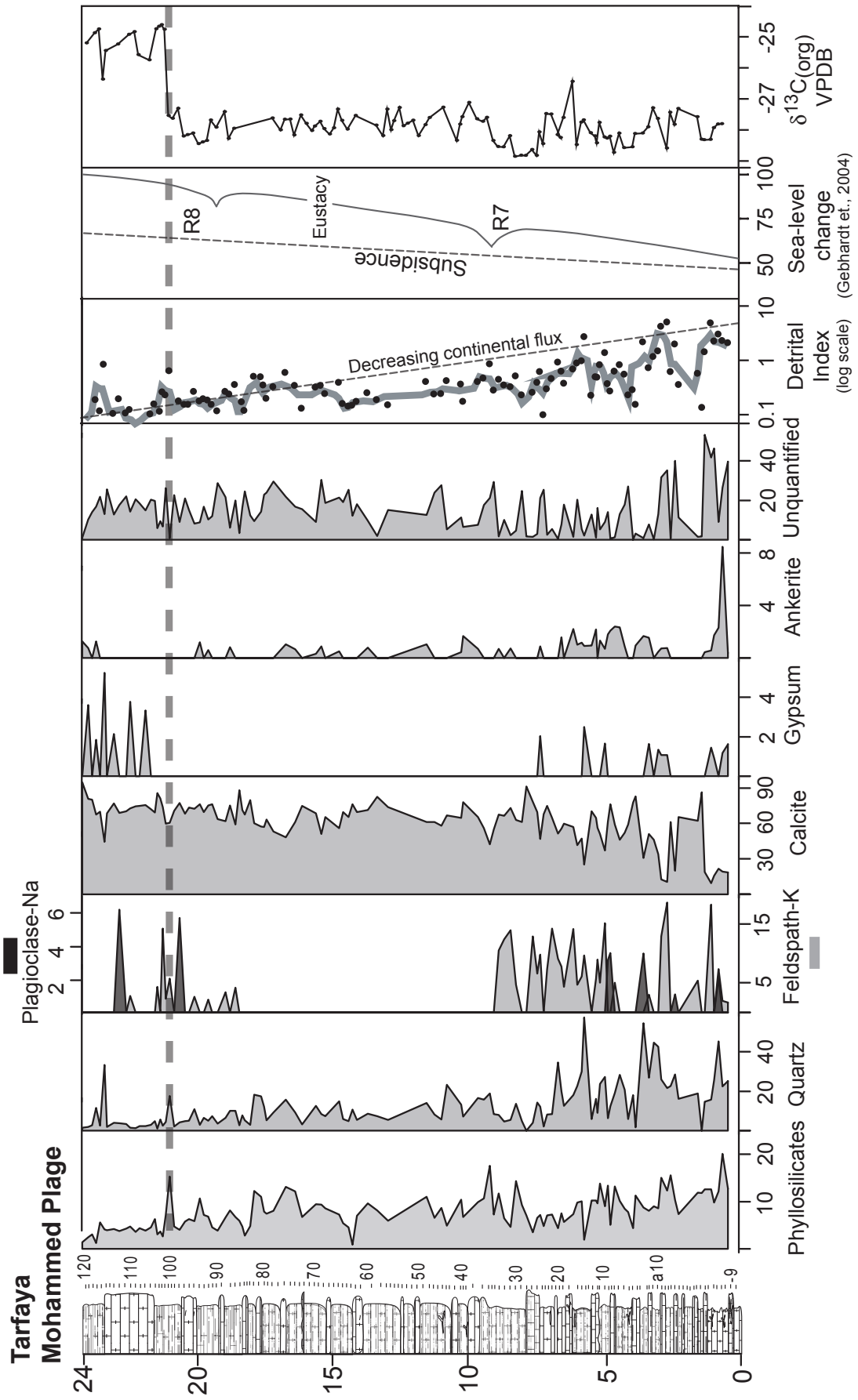

Fig. 6. Bulk rock mineralogy from XRD analysis with detrital index, relative sea-level curve (calculated using percentages of planktonic foraminifera by

a near perfect inverse relationship between calcite and quartz contents.

Phyllosilicate contents are more or less constant around 8 to 10 % until MB 82 There is then a decrease to values of around 5 %.

K-Feldspar content shows 3 distinct phases. In the lower part of the section (0-9 m), values remain mostly below 13%, but fluctuate greatly. In the middle part, (9-18.5 m) feldspar accumulation practically ceased (<5%). In the upper part of the section near the $\delta^{13}C$ shift (21m) there is an isolated peak of 10%. No K-Feldspar is observed above 22.5m. Small spikes in plagioclase content are seen between 0 and 5 m (1.8 %) and from 21 to 23 m (4-6 %). Between 5 and 21 m there is total absence of plagioclase.

Ankerite content remains below 5 % for the most of the section, but with a noticeable spike of 25 % in the second sample from the base.

Secondary gypsum is relatively abundant at the base of the section reaching a maximum value of approximately 4 % (Fig. 6). There is a complete absence of gypsum above 7.5 m, except near the top of the section (22-24 m) where it reaches 6 %.

D.3.5. Clay Mineralogy (< 2μm) 18-24 m

Smectite percentages average around 10 % for the top of the section with two samples at 19.6 and 20.1 m reaching 40 % and 20% respectively (Fig. 7). There is a small increase at the onset of the isotope excursion (15 %). Illite/smectite (I/S) ratios remain relatively constant at approximately 20 % from 18 to 22.75 m and drop to zero above this interval. Kaolinite content is negligible throughout the section (including below 18 m: not shown), except for minor enrichments (< 15 %) at 19.75 m, 21 m and 23.1 M. Chlorite contents are generally higher between 18 and 21 m (20-30%), and drops below 20% at the onset of the $\delta^{13}C$ excursion and for the remainder of the section. The fine fraction of mica is more abundant above the isotope excursion (> 60 %, as apposed to 30 % before the excursion).

D.3.6. Phosphorus Speciation and Redfield Ratios (18-24 m)

There appear to be two phases of P accumulation in the Mohammed Plage section. Figure 8 separates the lower part of the section (relatively abundant P accumulation) and the upper part (relatively depleted). The exception to this is $P_{authigenic}$, which remains relatively consistent (0.2 - 0.4 mg/cm^2/kyr) throughout the section.

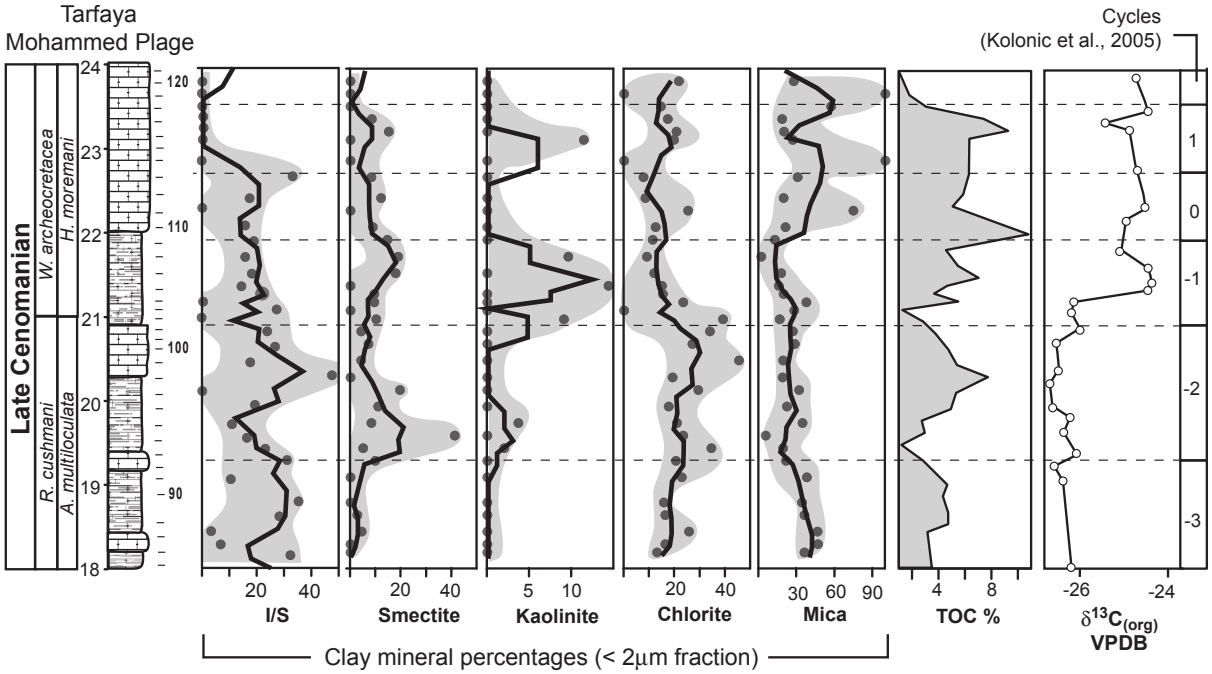

Fig. 7. Relative abundance of major clay minerals in the <2 μm sediment fraction before and during OAE 2.

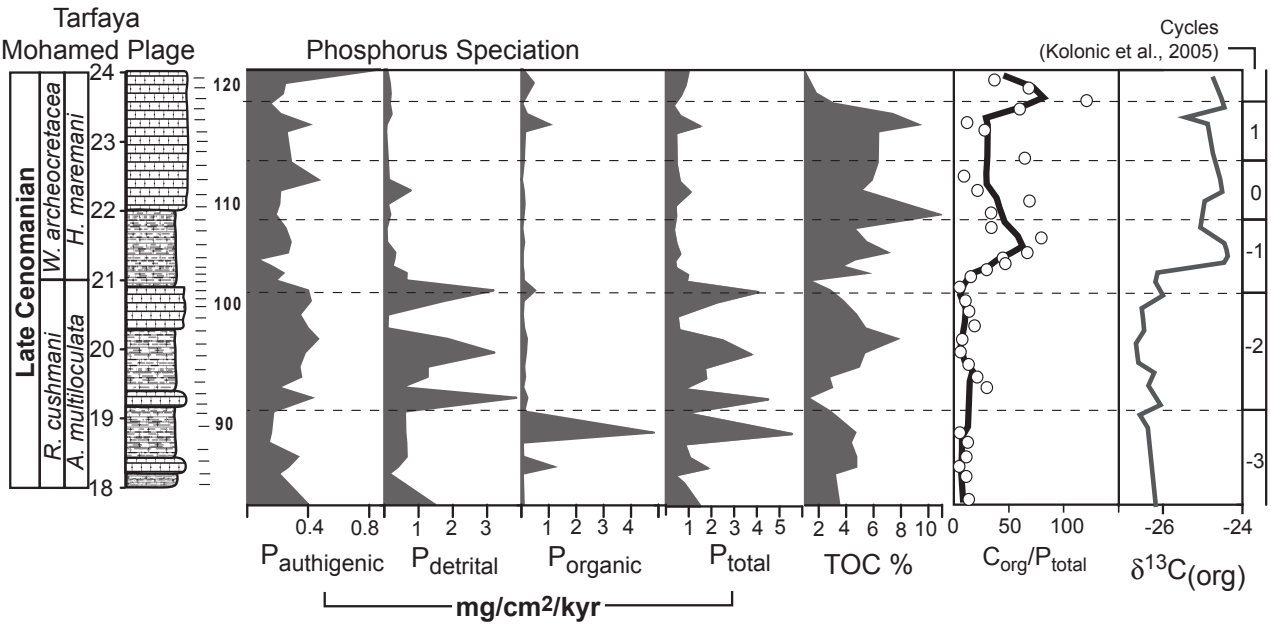

Fig. 8. Results from a sequential extraction of phosphorus (including $P_{authigenic}$ apatite, $P_{detrital}$ and $P_{organic}$). $P_{reactive}$ is taken as an addition of these phases. Corg/Preactive (Redfield) ratios are also calculated and included alongside TOC and $\delta^{13}C_{(org)}$ data

The switch between P-rich and P-poor sediments is coeval with the start of the positive $\delta^{13}C$ shift and a re-introduction of higher TOC values.

There are some significant differences between the behaviour of the P phases. For example $P_{organic}$ appears not to contribute significantly to the P_{total} total, despite the high amount of organic matter. Only one sample (MB 90) registers a significant elevation in $P_{organic}$ MARs (5 mg/cm^2/kyr). Otherwise, the values never exceed 1 mg/cm^2/kyr and usually stay below 0.2 mg/cm^2/kyr. $P_{detrital}$ contributes most significantly to the P_{total} with 4 values above 2 mg/cm^2/kyr prior to the isotope excursion. $P_{detrital}$ fluctuates substantially up to this point before reducing to minimal values in the post-isotope excursion.

There is a sharp decrease in TOC values in the topmost samples (MB 119-121) preceding a 2-fold increase in $P_{authigenic}$ ARs (MB 121). See table 1 for the P-speciation MAR data. C_{org}/P_{total} ratios increase substantially at the onset of the isotope excursion and remain relatively high for the remainder of the section. The increase is from approximately 10 to 75, which is still considerably lower than the average value in today's oceans (~111).

$P_{detrital}$ is susceptible to having been diagenetically transformed from $P_{authigenic}$ (e.g. Filippelli and Delaney, 1995; Föllmi et al., 2005). It also in no way correlates with the detrital index described above. It is therefore reasonable, for the purposes of this study, to assume that the majority of measured $P_{detrital}$ is recrystalized $P_{authigenic}$ and thus was bioavailable. It is with this argument that $P_{detrital}$ is included into the C_{org}/P_{total} ratio.

D.3.7. ICP-MS Geochemistry

Fig 9 shows the ICP-MS results for the carbonate fraction of the sediments between 17 and 24 m, encompassing the positive $\delta^{13}C$ excursion.

Ba* shows three periods of enrichment with values reaching 2200 ppm at 17 m, 2500ppm at 20.5 m (immediately prior to the isotope excursion) and 3000 ppm at 23 m (during the excursion plateau). V/Al ratios are significantly enriched during the isotope excursion and for a short interval during the first stages of the isotope plateau reaching values of 0.2 (21.4 – 22 m). Above this interval, V/Al ratios decrease close to, but still above, pre-excursion values. Sr/Ca ratios remain stable through the samples analyzed, except for a minor exception during the isotope excursion at 22.5 m where ratios increase from 0.08 to 0.2. The K/Al and Ti/Al ratio values are also stable, except for the

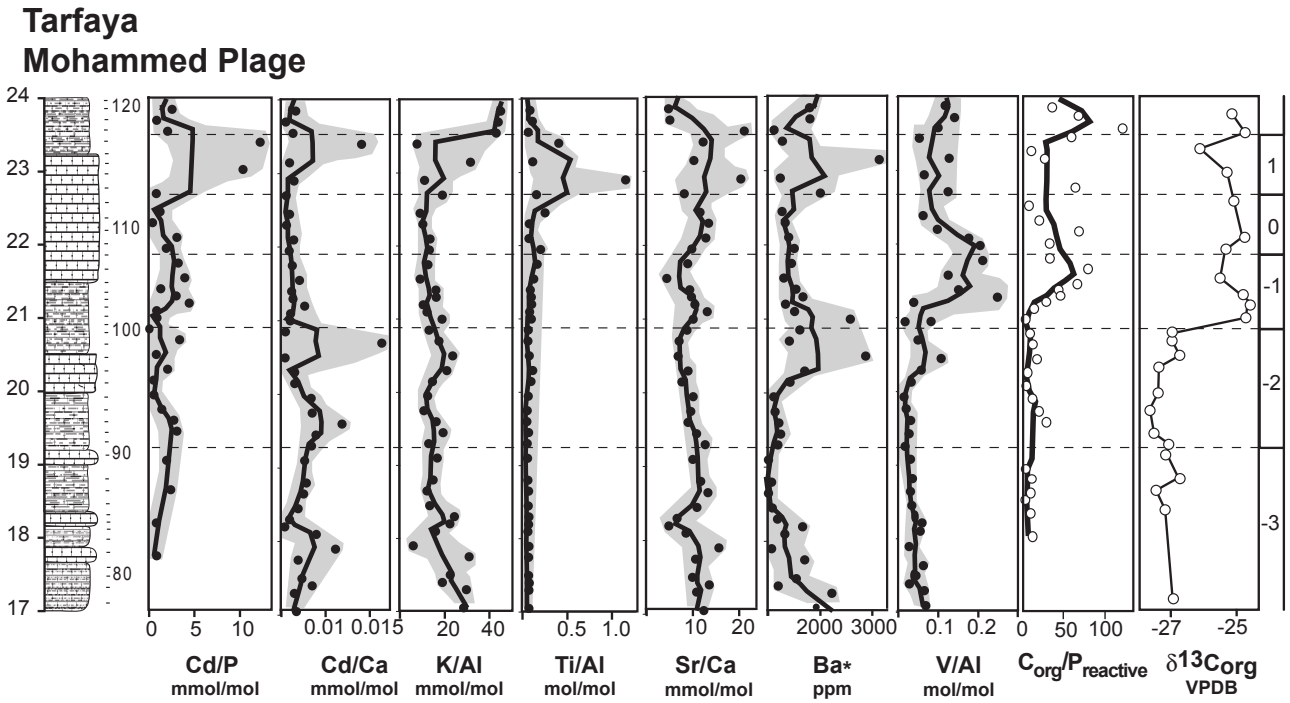

Fig. 9. ICP-MS data from the carbonate fraction of the sediment. The dashed and shaded area corresponds to the dashed areas in the scatter plot beneath which illustrates the difference between carbon and silicate fraction elemental concentrations, using vanadium (V) as an example.

top of the section (23-24 m) where they increase significantly.

D.4. Discussion

D.4.1. Long-term depositional history

The increase in TOC values from the base of the Mohammed Plage section and stable $\delta^{13}C$ values (Fig 2) suggest that productivity was not the primary control on OC accumulation. Gebhardt et al, (2004) drew the same conclusion pointing to the oxygen minimum zone impingement on shelf seas during sea-level highstands as the primary reason for the inhibition of organic-matter oxidation. The gradual increase in HI values (phase 1, Fig. 4) could support this explanation, if they were caused by an increase in organic matter of marine origin and/or better preservation of organic matter. A shift from a continental to marine influence is also indicated by the decrease and increase in quartz and calcite values respectively (Fig. 6). A gradual increase in sea-level is perhaps best indicated by the gradual decrease in the detrital index (Fig. 6), which suggests a gradual decrease in terrigenous input and/or a rising sea-level, greater paleodepth and increased dilution of the terrigenous material. In the upper part of the section, the thinly laminated siltstones and marly limestone beds with horizontally aligned foraminifera also suggest low energy currents consistent with a higher sea level. The decrease in the frequency of siltstone beds from the bottom to the top of the section also supports this interpretation. The small positive isotope excursion, shortly followed by a trough in sample MB 18 (Fig. 2) may represent the so-called 'mid-Cenomanian event' (MCE) (Coccioni and Galeotti, 2003)..

As noted above, the Tarfaya paleo-coast is widely regarded as having had a major upwelling cell offshore (Einsele and Wiedmann, 1975, 1982; Bush and Philander, 1997; Gustafsson et al., 2003). This interpretation is supported by the quantification of different phosphorus phases. For example, $P_{authigenic}$ behaves differently compared to other P phases in that it is relatively constant throughout the section. This observation is consistent with a reliable upwelling zone, which provides abundant nutrients (including dissolved inorganic P), which can then precipitate onto pellets, skeletal material or other binding sites forming $P_{authigenic}$ (Van Cappellen and Ingall, 1994;

Mackenzie et al., 1998). However, out of all the phases $P_{authigenic}$ is the least abundant, despite the favourable upwelling-zone environment. These lower than expected values may be symptomatic of the higher relative sea level in the upper-part of the section, which caused the OMZ to encroach further onto the continental shelf and thus resulted in a consistent, but limited, accumulation rate of $P_{authigenic}$ due to lower oxygen availability.

D.4.2. Oceanic Anoxic Event 2

Immediately prior to the isotope excursion there is a noticeable enrichment in Ba* in two samples (~20.5 m) coincident with a small peak in species richness (Figs. 3 and 9). The increase in biodiversity is primarily due to the temporary reintroduction of less common planktonic foraminifera which make an appearance precisely at the $\delta^{13}C$ excursion onset (e.g. *P. gibba*, *P. praehelvetica*, *D. imbricata* and *D. hagni*). Together with the disappearance of *R. cushmani and R. greenhornensis* in short succession of one another points to a time of maximum faunal turnover, which also marks the start of some profound geochemical changes in the sediments. For example, the coeval enrichment of Cd/Ca values with Ba*. The Cd/P ratio is used as a proxy for sea-surface phosphate utilization due to the constant fractionation of P relative to Cd in primary productivity (Rickaby and Elderfield, 1999; Elderfield and Rickaby, 2000). These authors performed their analyses on planktonic foraminifera, whereas we use bulk-rock measurements, which provide less sensitive values. Nevertheless, our results suggest that the role of Cd as a micronutrient became significant for a short time (this is only seen in one sample) at the excursion onset. At this point, P MAR values drop considerably along with the Cd/Ca ratio. This may have been caused by an increase in dissolved inorganic phosphate (DIP) in the water column as a result of P recycling from sediments overlain by oxygen-depleted waters.

V/Al values show a similar trend as the positive $\delta^{13}C$ excursion before reducing to values still elevated relative to pre-OAE 2 values (Fig. 9). $P_{detrital}$ and $P_{organic}$ contents almost completely disappear from the sediment and the average $P_{reactive}$ AR is reduced by approximately 3 times. This transition is marked by a considerable drop in planktonic foraminiferal diversity and an increase in the opportunistic low oxygen tolerant species *H. moremani*, both suggesting a period of biotic stress. The increased V/Al and biotic stress combined with the decrease in P MARs is further evidence that oxygen depletion was crucial in limiting P accumulation.

The sharp increase in the $C_{org}/P_{reactive}$ ratio at the excursion onset is also a good indication that phosphorus was being lost and/or prevented from accumulating in sediments. Given that the Tarfaya Basin is an upwelling region with an apparently strong bio-pump (Gustafsson et al., 2003), it would seem likely that this excess DIP could have become reintroduced into surface waters, stimulating further primary productivity. This idea has been proposed in the past (Ingall and Van Cappellen, 1990; Ingall et al., 1993; Ingall and Jahnke, 1994; Van Cappellen and Ingall, 1994, 1996) and has tentatively been suggested as applicable to the Cretaceous OAEs (Nederbragt et al., 2004).

If increased DIP acted as a driver for productivity, this would have caused the continued formation of biogenic barite (for which Ba* is used as a proxy in this study). However, our data shows only a brief increase in Ba* formation prior to the $\delta^{13}C$ excursion onset. Ba* formation appears restricted within the isotope plateau despite almost certainly representing high productivity in this interval. This is probably due to a drop in barite production due to an oxygen-deficient water column (Dickens, 2001; Castellini et al., 2006).

What caused these changes? Sea levels appear to have been increasing steadily for several million years prior to the isotope excursion onset. Although this leaves climate change as an obvious choice, there is little evidence to suggest that there was an increase in humidity or weathering. Two proxies could conceivably be called upon to infer an increase in continental input. OI's (figure 4) becomes slightly more scattered at the top of the section, suggesting a fluctuation in the abundance of continentally derived OM or more likely the hydraulic alteration via water percolating through the overlying Miocene grainstones. However, in

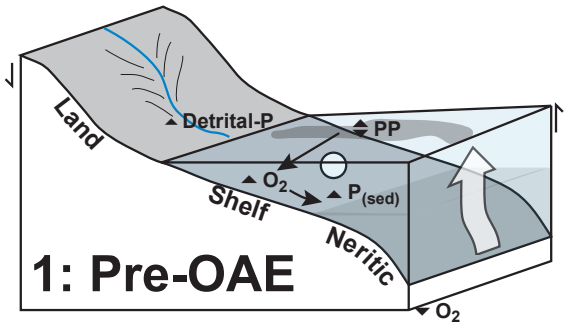

Relatively low sea-level means a relatively high rate of erosion and delivery of $P_{detrital}$. Eustatic sea-level rise combined with subsidence.

Mohammed Plage relatively oxic. OM easily oxidised and the resulting DIP readily incorporated into $P_{authigenic}$. $P_{detrital}$ is the most abundant P phase due to proximity to coastline.

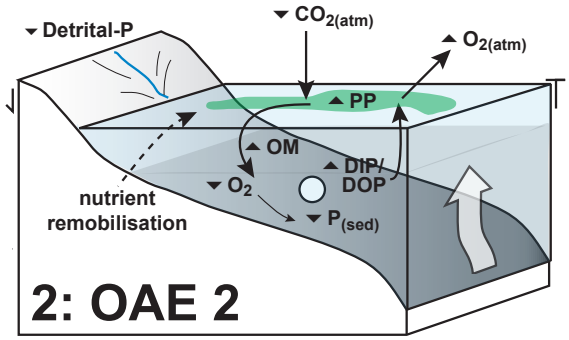

Sea-level rise inundates land, remobilising nutrients. This produces more bio-available nutrients but simultaneously decreases $P_{detrital}$ delivery.

Increase in productivity and OMZ inpingement onto the continental shelf prevents the effective retention of P in sediments. DIP budget is consequently increased promoting further PP. OM distributed over a larger area due to greater depositional area. This also lower $P_{organic}$ AR.

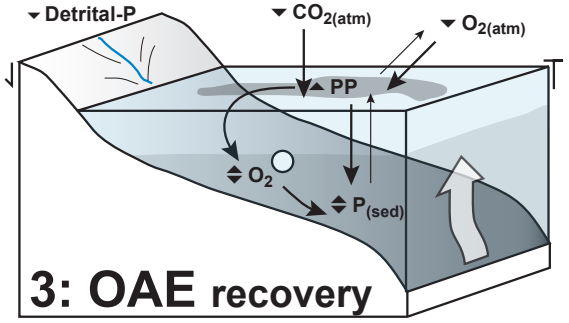

Eustatic sea-level stabilises. Subsidence continues

Nutrient sources become depleted. $pO_{2(atm)} > pO_{2(sea\ surface)}$ so oceans start to become more oxic. $P_{detrital}$ and $P_{organic}$ remains low due to high sea-level. $P_{authigenic}$ may increase due to high DIP and DOP in the presence of less dysoxia

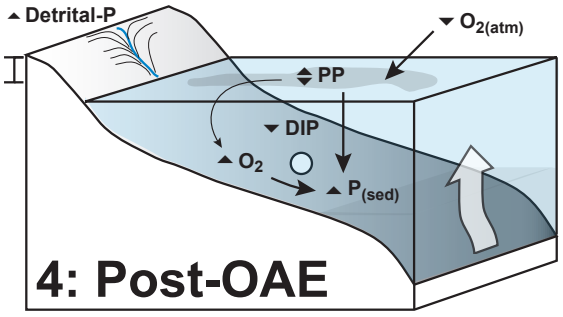

Nutrient sources become depleted. $pO_{2(atm)} > pO_{2(sea\ surface)}$ so there is a rapid introduction of O_2 into the water column pushing down the OMZ and allowing other productivity-limiting nutrients to become oxidised. Subsequent decreasing in DIP. Increase in $P_{detrital}$ due to long-term erosion of the land.

Region returns to a more steady state situation with upwelling as the primary control on productivity.

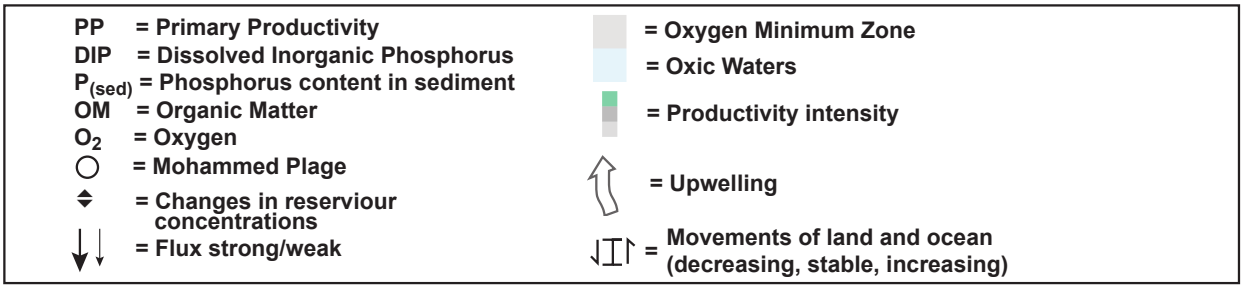

Fig. 10. Conceptual model outlined in the discussion.

the same samples we see elevated gypsum intensity values. We may assume that the gypsum does not represent dry conditions, but rather the conversion of pyrite (FeS_2) into gypsum ($CaSO_4(OH)$) via OM remediation. This is more likely to account for the observed decrease in OI values

Clay minerals maybe used to infer more humid or arid conditions (Lu et al., 1998; Bolle et al., 2000; Bolle and Adatte, 2001). Kaolinite increases at the $\delta^{13}C$ onset, but values do not exceed 15 % (seen in one sample). The inferred increase in humidity and continental weathering from a 15 % abundance in kaolinite is unlikely to have had a significant impact on productivity. A more likely source for the small increase in kaolinite at the $\delta^{13}C$ excursion onset is a relatively rapid sea-level transgression, which results in reworking of sediments that were previously existed on dry land (Fig, 10). This idea was earlier proposed by Hilbrecht et al., (1996). Gebhardt et al, (2004) used planktonic foraminifera to calculate a brief regression followed by a transgression prior to the excursion onset (Fig. 6). This may well have increased productivity by remobilising nutrients. In addition, the most dominant clay minerals in Mohammed Plage are smectite and mica, which point to a drier climate where sediments would have been more susceptible to reworking and erosion by the encroaching sea. The inundation of dry land would have had other effects. The elevated base level of rivers and the corresponding reduction in erosional capacity probably reduced $P_{detrital}$ MARs (Fig. 8). Lower $P_{organic}$ values may have resulted from OC deposition occurring over a larger shelf area.

A more expansive shallow sea has a greater ability to produce the oxidative regeneration of nutrients (Schlanger and Jenkyns, 1976; Jenkyns, 1980) creating a region of high primary productivity. Therefore, a shallow sea, especially in an upwelling area with abundant nutrients, such as the Tarfaya basin, was probably predisposed to becoming dysoxic.

The mode of OC accumulation appears to have changed during and after the $\delta^{13}C$ excursion. Fluctuations in TOC may partly be orbitally controlled. The boundary between the finish and

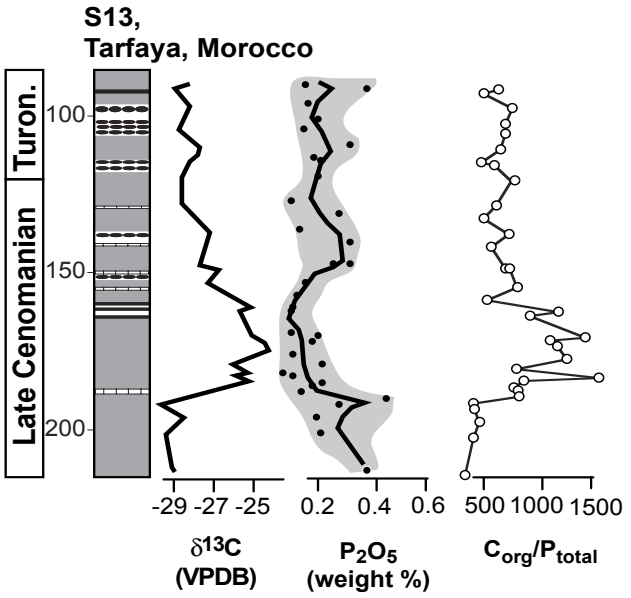

Fig. 11. A comparison of the Phosphate and C_{org}/P_{total} from drill hole S13, also in the Tarfaya basin. Modified after Nederbragt et al, (2004).

start of the 39 ka obliquity cycles from Kuhnt et al. (1997) (Fig. 8) coincides reasonably well with periods of minimum OC content. The base of the isotope $\delta^{13}C$ excursion coincides with a transition from obliquity cycle -2 to -1 and the corresponding minimum in TOC. TOC values begin to rise, but not as rapidly as $\delta^{13}C$ values.

D.4.3 Phosphorus recycling during OAE 2: A global phenomenon?

Nederbragt et al, (2004) modelled the behaviour of P under anoxic conditions, concluding that a change in the oceanic phosphorus cycle was the most realistic way to generate a substantial positive $\delta^{13}C$ excursion. In the same study, empirical data from the Tarfaya drill hole S13 was presented. A decrease in weight % total phosphate at the onset of OAE 2's positive carbon isotope excursion was observed, as was an increase in $C_{org}/P_{reactive}$ molar ratios (Fig. 11). Other recent studies (Mort et al., in press, submitted) show the same correlation in four other localities (the Pueblo CT GSSP, Colorado; Eastbourne, UK; Furlo, Italy; Manilva, Spain). These studies also used MARs calculated from isotopic, biostratigraphic and cyclostratigraphic datasets. Figure 12 illustrates a correlation between the Mohammed Plage's $\delta^{13}C$ and $P_{reactive}$ AR curves

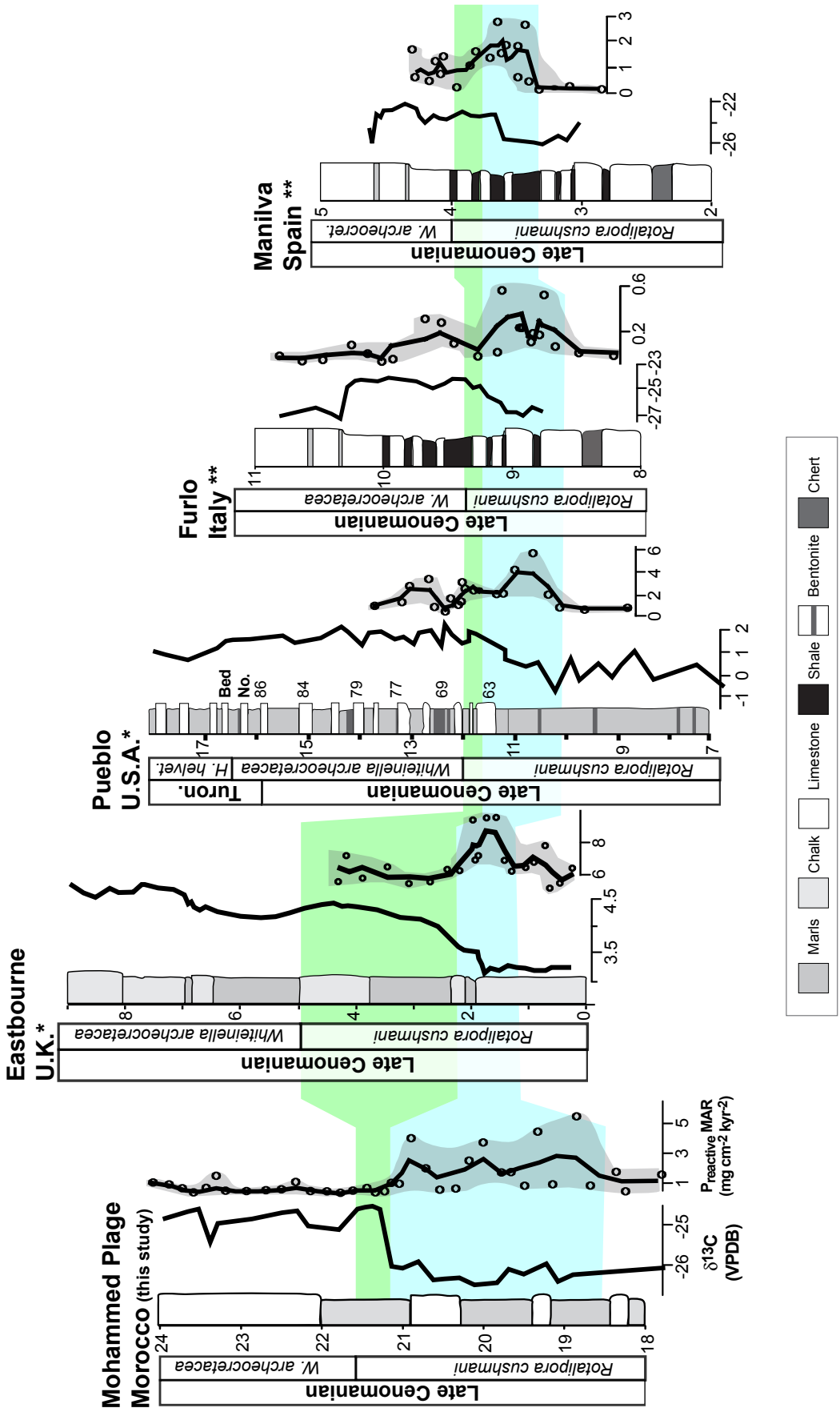

Fig. 12. Correlation of phosphorus mass accumulation rates with four other sections (3 from Europe and 1 from the Cenomanian-Turonian GSSP in Pueblo, Colorado). *(Mort et al., submitted)). (Mort et al., in press). Lithology for Mohammed Plage has been simplified to conform with other lithologies presented. Lighted shaded area highlights the main phase of P accumulation, prior to and during the isotope excursion. The dark shaded area covers the fall in P accumulation until the extinction of Rotalipora cushmani. During and after this time, it is likely that dysoxia had reduced the nutrient retention ability of the

and those of the 4 sections. Because the drop in P MAR is coevally observed in such a diversity in palaeoenvironments, it is very likely that this signature, if interpreted correctly, represents a critical factor in the processes that lead to the development of OAE 2.

D.4.4 Termination of OAE 2

The termination of OAE 2 is not documented in the sediments at Mohammed Plage. In previous studies, the final phase of OAE 2 seems to have occurred in the early Turonian with the rapid radiation of deep water agglutinated foraminifera (Kuhnt, 1992) indicating a return to more oxygenated waters (Kolonic et al., 2005). Eight species of planktonic foraminifera disappear at or during the $\delta^{13}C$ excursion (precise location is uncertain due to probable hiatus) and reappear later, signalling the end of *maximum* environmental stress (Fig. 3). $C_{org}/P_{reactive}$ ratios also decrease somewhat during this recovery phase, pointing to regional water column dysoxia as an important control on species abundance. However the fall in the $C_{org}/P_{reactive}$ ratio is not due to an increase in P content, but rather a decrease in OC content due to degradation (see below).

TOC values reach their maximum during OAE 2, but are still highly variable, suggesting Milankovitch climate forcing. Alternatively, the proximity of Mohammed Plage to the paleocoastline (albeit at a deep paleodepth) makes it an effective recorder of local changes in OC flux from continental sources. OI values fluctuate in the upper part of the section (phase 3, Fig. 4), thus suggesting fluctuations in the delivery of continental organic matter or oxygenation. However, the overlying porous Miocene deposits may have been conductive to the percolation of water in the highest Cenomanian bed resulting in its alteration. This is a more convincing explanation for the dramatic fall in TOC percentages in the uppermost samples, although not the increased in $P_{authigenic}$. Due to these types of complications, it is very difficult to identify with certainty any precursors to the end of OAE 2.

D.5 Conclusions

OAE 2 is a global phenomenon and its overall cause must therefore also be global in scale. The event is represented (at least partially) in the Mohammed Plage section by a + 2.5 ‰ shift in $\delta^{13}C$ values, marking the regional expression of this global event. There is no direct evidence to link events in this area of the Tarfaya basin to the direct cause of OAE 2 itself. However, it is possible to conclude that the long-term eustatic sea-level rise and subsidence resulted in a large shallow continental shelf sea, which combined with an abundant nutrient source (provided by upwelling) made this area susceptible to dysoxia via global mechanisms that caused OAE 2 (e.g., sea level change, upwelling).

Mohammed Plage shows a distinct long-term deepening trend, which was caused by a mixture of sea-level rise and shelf subsidence. This is seen in decreases in quartz, phyllosilicates and feldspar, increases in quartz and a systematic fall in detrital and organic matter indices.

OAE 2 is clearly expressed by an abrupt + 2.5 ‰ shift in $\delta^{13}C$ values. A rapid sea-level rise, superimposed on the long-term rise may have leached continentally stored nutrients, stimulated productivity, created bottom dysoxia and prevented the accumulation of P through the expansion and intensity of the OMZ. This may have led to regeneration of P and other redox-sensitive nutrients. Nutrients recycled would have increased the DIP content of the water, further sustaining primary productivity. If this interpretation is correct, then the global significance of this mechanism is apparent when compared to other OAE 2 phosphorus studies in the Tarfaya basin and in sections from Europe and America (Figs. 11 and 12). Productivity would have produced more atmospheric O_2 simultaneously drawing down CO_2 from the atmosphere. Eventually the abundance of O_2 in the atmosphere may have acted as a negative feedback to halt the cycle of productivity - anoxia - P recycling - productivity. Once nutrient supply fell (due to consumption and burial and/or fall in supply) this would have led to a return of more oxygenated bottom waters and a termination to OAE 2.

Acknowledgements

We thank Wolfgang Kuhnt and Jens Wendler for constructive reviews. This report is based upon work supported by the Swiss National Fund No. FN21-67702.02 (TA), the US National Science Foundation under Grant NSF INT 0115357 (GK), and the German Science Foundation grant STU 169/10-1 to 3 (DS).

References

Adatte, T., Stinnesbeck, W., Keller, G., 1996. Lithostratigrahical and mineralogic correlations of near K/T boundary clastic sediments in northeastern Mexico: Implications for origin and nature of deposition. Geological Society of America Special Paper 307, 211-226.

Aguilera-Franco, N., Hernandez-Romano, U., Allison, P.A., 2001. Biostratigraphy and environmental changes across the Cenomanian-Turonian boundary, southern Mexico. Journal of South American Earth Sciences 14, 237-255.

Anderson, D.L., Delaney, M.L., 2000. Sequential extraction and analysis of phosphorus in marine sediments: streamlining of the SEDEX procedure. Limnology and Oceanography 45, 509-515.

Attewell, P.B., Farmer, I.W., 1976. Principles of engineering geology, Chapman and Hall, London.

Bolle, M.-P., Adatte, T., 2001. Palaeocene-early Eocene climate evolution in the Tethyan realm: clay mineral evidence. Clay Minerals.

Bolle, M.-P., Tantawy, A.A., Pardo, A., Adatte, T., Burns, S.J., Kassab, A., 2000. Climateic and environmental changes documented in the upper Paleocene to lower Eaocene of Egypt. Eclogae Geologicae Helvetiae 93, 33-51.

Bush, A.B.G., Philander, S.G.H., 1997. The late Cretaceous: simulation with a coupled atmosphere-ocean general circulation model. Paleoceanography 12, 495-516.

Castellini, D.G., Dickens, G.R., Snyder, G.T., Ruppel, C.D., 2006. Barium cycling in shallow sediment above active mud volcanoes in the Gulf of Mexico. Chemical Geology 1, 1-30.

Coccioni, R., Galeotti, S., 2003. The mid-Cenomanian Event: prelude to OAE 2. Palaeogeography, Palaeoclimatology, Palaeoecology 190, 427-440.

Damste, J.S.S., Koster, J., 1998. A euxinic southern North Atlantic Ocean during the Cenomanian/Turonian oceanic anoxic event. Earth and Planetary Science Letters 158, 165-173.

Dickens, G.R., 2001. Sulphate profiles and barium fronts in sediment on the Blake Ridge: Present and past methane fluxes through large gas hydrate reservoir. Geochimica et Cosmochimica Acta 65, 529-543.

Eijsink, L.M., Krom, M.D., de Lange, G.J., 1997. The use of sequential extraction techniques for sedimentary phosphorus in eastern Mediterranean sediments. Marine Geology 139, 147-155.

Einsele, G., Wiedman, J., 1975. Faunal and sedimentatological evidence for upwelling in the Upper Cretaceous coastal basin of Tarfaya, Morocco: 9th International Congress on Sedimentology, 67-72.

Einsele, G., Wiedman, J., 1982. Turonian black shales in the Moroccan coastal basins: first upwelling in the Atlantic Ocean? In: von Rad, U., Hinz, K., Sarnthein, M., and Seibold, E., (Eds) Geology of the Northwest African Continental Marin: Berlin-Heidelberg-New York, Springer-Verglag, 396-414.

El Albani, A., Kuhnt, W., Luderer, F., Herbin, J.P., Caron, M., 1999a, Palaeoenvironmental evolution of the late Cretaceous sequence in the Tarfaya Basin (southwest of Morocco). In: Cameron, N.R., Bate, R.H., and Clure, V.S., (Eds.), The Oil and Bas Habitats of the South Atlantic. Special Publication Geological Society of London, 223-240.

El Albani, A., Vachard, D., Kuhnt, W., Chellai, E.H., 1999b. Signature of hydrodynamic activity caused by rapid sea level changes in pelagic organic rich sediments, Tarfaya Basin (southern Morocco). Science de la Terre Planetes 329, 397-404.

Elderfield, H., Rickaby, R.E.M., 2000. Oceanic Cd/P ratio and nutrient utilization in the glacial Southern Ocean. Nature 405, 305-310.

Espitalié, J., Deroo, G., Marquis, F., 1985. La pyrolyse Rock-Eval et ses applications. Revue de l'Institut Français du Pétrole 40, 563-579.

Filippelli, G.M., Delaney, M.L., 1995. Phosphorus geochemistry, diagenesis, and mass balances of the Miocene Monterey Formation at Shell Beach, California: U.S. Geological Survey Bulletin (1995), G1-G11.

Föllmi, K.B., Badertscher, C., de Kaenel, E., Stille, P., John, C., Adatte, T., Steinmann, P., 2005. Phosphogenesis and organic-carbon preservation in the Miocene Monterey Formation at Naples Beach, California – the Monterey hypothesis revisited. Geological Society of America Bulletin, 117, 589-619.

Gale, A.S., Jenkyns, H.C., Kennedy, W.J., Corfield, R.M., 1993. Chemostratigraphy versus biostratigraphy - data from around the Cenomanian-Turonian boundary. Journal of the Geological Society 150, 29-32.

Gebhardt, H., 1999. Cenomanian to Coniacian biogeography and migration of North and West African ostracods. Cretaceous Research 20, 215-229.

Gebhardt, H., Kuhnt, W., Holbourn, A., 2004. Formainiferal responce to sea level change, organic flux and oxygen deficiency in the Cenomanian of the Tarfaya Basin, southern Morocco. Marine Micropalaeontology 53, 133-157.

Gräfe, K.U., 2002. Stratigraphische Korrelation und Steuerungsfaktoren sedimentärer Zyklen in auserwählten borealen und tethyalen Becken des Cenoman/Turon Europas und Nordwestafrikas. Berlin Fachbereich Geowiss University Bremen 198, 1-197.

Gustafsson, M., Holbourn, A., Kuhnt, W., 2003. Changes in Northeast Atlantic temperature and carbon flux during the Cenomanian/Turonian paleoceanographic event: the Goban Spur stable isotope record. Palaeogeography Palaeoclimatology Palaeoecology 3182, 1-16.

Hallam, A., Wignall, P.B., 1999. Mass extinctions and sea-level changes. Earth-Science Reviews 48, 217-250.

Haq, B.U., Hardenbol, J., Vail, P.R., 1987. Chronology of fluctuating sea levels since the Triassic. Science 235, 1156-1167.

Hilbrecht, H., Frieg, C., Troger, K.A., Voigt, S., Voigt, T., 1996. Shallow water facies during the Cenomanian-Turonian anoxic event: Bio-events, isotopes, and sea level in southern Germany. Cretaceous Research 17, 229-253.

Holbourn, A., Kuhnt, W., 2002. Cenomanian-Turonian palaeoceanographic change on the Kerguelen Plateau: a comparison with Northern Hemisphere records. Cretaceous Research 23, 333-349.

Holbourn, A., Kuhnt, W., El Albani, A., Ly, A., Gomez, R., Herbin, J.P., 1999. Palaeoenvironments and palaeobiogeography of the Late Cretaceous Casamance transect (Senegal, NW Africa): distribution patterns of benthic foraminifera, organic carbon and terrigenous flux. Neues Jahrbuch für Geologie und Palaontologie-Abhandlungen 212, 335-377.

Ingall, E., Jahnke, R., 1994. Evidence for enhanced phosphorus regeneration from marine-sediments overlain by oxygen depleted waters. Geochimica et Cosmochimica Acta 58, 2571-2575.

Ingall, E.D., Bustin, R.M., Van Cappellen, P., 1993. Influence of Water Column Anoxia on the Burial and Preservation of Carbon and Phosphorus in Marine Shales. Geochimica Et Cosmochimica Acta 57, 303-316.

Ingall, E.D., Van Cappellen, P., 1990. Relation between Sedimentation-Rate and Burial of Organic Phosphorus and Organic-Carbon in Marine-Sediments. Geochimica Et Cosmochimica Acta 54, 373-386.

Jeans, C.V., Long, D., Hall, M.A., Bland, D.J., Cornford, C., 1991. The Geochemistry of the Plenus Marls at Dover, England - Evidence of Fluctuating Oceanographic Conditions and of Glacial Control During the Development of the Cenomanian-Turonian Delta-C-13 Anomaly. Geological Magazine 128, 603-632.

Jenkyns, H.C., 1980. Cretaceous anoxic events, from continents to oceans. Journal of the Geological Society of London 137, 171-188.

Jenkyns, H.C., 1991. Impact of Cretaceous Sea-Level Rise and Anoxic Events on the Mesozoic Carbonate Platform of Yugoslavia. AAPG Bulletin-American Association of Petroleum Geologists 75, 1007-1017.

Keller, G., Han, Q., Adatte, T., Burns, S.J., 2001. Palaeoenvironment of the Cenomanian-Turonian transition at Eastbourne, England. Cretaceous Research 22, 391-422.

Keller, G., Pardo, A., 2004. Age and paleoenvironment of the Cenomanian-Turonian global stratotype section and point at Pueblo, Colorado. Marine Micropalaeontology 51, 95-128.

Kolonic, S., Damste, J.S.S., Bottcher, M.E., Kuypers, M.M.M., Kuhnt, W., Beckmann, B., Scheeder, G., Wagner, T., 2002. Geochemical characterization of Cenomanian/Turonian black shales from the Tarfaya Basin (SW Morocco) - Relationships between palaeoenvironmental conditions and early sulphurization of sedimentary organic matter. Journal of Petroleum Geology 25, 325-350.

Kolonic, S., Wagner, T., Forster, A., Damste, J.S.S., et al., 2005. Black shale deposition on the northwest African shelf during the Cenomanian/Turonian oceanic anoxic event: Climate coupling and global organic carbon burial. Paleoceanography 20.

Kuhnt, W., 1992. Abyssal Recolonization by Benthic Foraminifera after the Cenomanian Turonian Boundary Anoxic Event in the North-Atlantic. Marine Micropaleontology 19, 257-274.

Kuhnt, W., Hess, S., Jian, Z., 1999. Quantitative composition of benthic foraminiferal assemblages as a proxy indicator for organic carbon flux rates in the South China Sea. Marine Geology 156, 123-127.

Kuhnt, W., Luderer, F., Nederbragt, A., Thurow, J., Wagner, T., 2004. Orbital scale record of the late Cenomanian-Turonian Oceanic Anoxoc Event (OAE 2) in the Tarfaya Basin (Morocco). International Journal of Earth Sciences 94, 147-159.

Kuhnt, W., Nederbragt, A., Leine, L., 1997. Cyclicity of Cenomanian-Turonian organic-carbon-rich sediments in the Tarfaya Atlantic Coastal Basin (Morocco). Cretaceous Research 18, 587-601.

Kuypers, M.M.M., Pancost, R.D., Nijenhuis, I.A., Damste, J.S.S., 2002. Enhanced productivity led to increased organic carbon burial in the euxinic North Atlantic basin during the late Cenomanian oceanic anoxic event. Paleoceanography 17, art. no.-1051.

Kübler, B., 1987. Cristallinite de l'illite, méthods normalisées de préparations, méthodes normalisées de mesures. Cahier Institut de Géologie 1, 13.

Larson, R.L., Erba, E., 1999. Onst of the mid-Cretaceous greehouse in the Barremian-Aptian: Igenous event and the biological, sedimentary, and geochemical responces. Paleoceanography 14, 663-678.

Lu, G., Adatte, T., Keller, G., Ortiz, N., 1998. Abrupt climatic, oceanographic and ecological changes near the Paleocene-Eocene transition in the deep Tethys basin: The Alademilla section, southern Spain. Eclogae Geologicae Helvetiae 91, 293-306.

Luderer, F., Kuhnt, W., 1997. A high resolution record of the Rotalipora extinction in laminated organic-rich limestones of the Tarfaya Atlantic coastal Basin (Morocco). Ann. Soc. Géol. Nord. 5, 199-205.

Mackenzie, F.T., Lerman, A., Ver, L.M.B., 1998. Role of the continental margin in the global carbon balance during the past three centuries. Geology 26, 423-426.

Mort, H.P., Jaquat, O., Adatte, T., Steinmann, P., Föllmi, K., Matera, V., Berner, Z., Stuben, D., in press. The Cenomanian-Turonian anoxic event in Italy and Spain: enhanced productivity and/or better preservation. Cretaceous Research.

---. submitted. Phosphorus and the roles of productiviity and nutrient recycling during Oceanic Anoxic Event 2. Geology.

Nederbragt, A.J., Thurow, J., Vonhof, H., Brumsack, H.J., 2004. Modelling oceanic carbon and phosphorus fluxes: implications for the cause of the late Cenomanian Oceanic Anoxic Event (OAE 2). Journal of the Geological Society, London 141, 721-728.

Paul, C.R.C., Lamolda, M.A., Mitchell, S.F., Vaziri, M.R., Gorostidi, A., Marshall, J.D., 1999. The Cenomanian-Turonian boundary at Eastbourne (Sussex, UK): a proposed European reference section. Palaeogeography Palaeoclimatology Palaeoecology 150, 83-121.

Philip, J., 2003. Peri-Tethyan neritic carbonate areas: distribution through time and drving factors. Palaeogeography, Palaeoclimatology, Palaeoecology 3082, 1-19.

Racki, G., Cordey, F., 2000. Radiolarian palaeoecology and radiolarites: is the present the key to the past? Earth-Science Reviews 52, 83-120.

Reicherter, K., Pletsch, T., Kuhnt, W., Manthey, J., Homeier, G., Wiedmann, J., Thurow, J., 1994. Mid-Cretaceous paleogeography and paleoceanography of the Betic Seaway (Betic Cordillera, Spain). Palaeogeography Palaeoclimatology Palaeoecology 107, 1-33.

Rickaby, R.E.M., Elderfield, H., 1999. Plankonic foraminferal Cd/Ca: Paleonutrients or Paleotemperature. Paleoceanography 14, 293-303.

Ruttenberg, K.C., 1992. Development of a sequential extraction method for different forms of phosphorus in marine sediments. Limnology and Oceanography 37, 1460-1482.

Sahagian, D., Pinous, O., Olferiev, A., Zakaharov, V., Beisel, A., 1996. Eustatic curve for the middle Jurassic-Cretaceous based on Russian platform and Siberian stratigraphy: zonal resolution. American Association of Petroleum Geologists 80, 1433-1458.

Schlanger, S.O., Jenkyns, H.C., 1976. Cretaceous oceanic anoxic events: Causes and consequences. Geol. Mijnbouw 55, 179-184.

Schwenke, W., Kuhnt, W., 1992. Subsidence history and continental margin evolution of the Western Pyrenean and Basque Basins. Palaeogeography Palaeoclimatology Palaeoecology 95, 297-318.

Sellwood, B.W., Price, G.P., P.J., V., 1994. Cooler esimates for Cretaceous temperatures. Nature 370, 453-455.

Sinton, C.W., Duncan, R.A., 1997. Potential links between ocean plateau volcanism and global ocean anoxia at the Cenomanian-Turonian boundary. Economic Geology and the Bulletin of the Society of Economic Geologists 92, 836-842.

Tamburini, F., Adatte, T., Föllmi, K., Bernasconi, S.M., Steinmann, P., 2003a. Investigating the history of East Asian monsoon and climate during the last glacial-interglacial period (0-140 000 years): mineralogy and geochemistry of ODP Sites 1143 and 1144, South China Sea. Marine Geology 201, 147-168.

Tamburini, F., Föllmi, K., Adatte, T., 2003b. Sedimentary phosphorus record from the Oman margin: New evidence of high productivity during glacial periods. Paleoceanography 18, 1015, doi:10.1029/2000PA000616.

Thompson, E.I., Schmitz, B., 1997. Barium and the late Paleocene $\delta^{13}C$ maximum: Evidence of increased marine surface productiviity. Paleoceanography 12, 239-254.

Tsikos, H., Jenkyns, H.C., Walsworth-Bell, B., Petrizzo, M.R., et al., 2004. Carbon-isotope stratigraphy recorded by the Cenomanian-Turonian Oceanic Anoxic Event: correlation and implications based on three key localities. Journal of the Geological Society 161, 711-719.

Van Cappellen, P., Ingall, E.D., 1994. Benthic Phosphorus Regeneration, Net Primary Production, and Ocean Anoxia - a Model of the Coupled Marine Biogeochemical Cycles of Carbon and Phosphorus. Paleoceanography 9, 677-692.

Van Cappellen, P., Ingall, E.D., 1996. Redox stabilization of the atmosphere and oceans by phosphorus-limited

- E -

The Cenomanian/Turonian anoxic event at the Bonarelli Level in Italy and Spain: enhanced productivity and/or better preservation

Submitted and in press for Cretaceous Research

Above: A photo of the OAE 2 black shales (Bonerelli Level) in Furlo, Italy. Right: In Manilva, Spain

So far, we have uncovered good evidence that reducing conditions were and important factor in the chemical cycling of nutrients during OAE 2. After a sedimentological, biostratigraphic, and geochemical investigation of the Furlo section, Italy, a simple question is posed: ***Is productivity alone, sufficient to explain the observed accumulations of organic matter during OAE 2?*** To try and answer this question a study is made comparing two sections (Furlo, Italy and Manilva, Spain) that contain high amounts of organic matter in the 'Bonerelli Level' (the regional term for the how OAE 2 is expressed in the geological record). The model incorporates a carbon isotope fraction constant in order to predict the quantity of organic matter that would resulted from the observed carbon isotope excursions (i.e. it assumes that the organic matter in the sediment comes only from productivity and that preservation played no role in the quantity present). This is a simple model and the paper stresses that it should not taken to reflect reality. However, the model outputs have implications for the other papers in this thesis because they suggests that preservation (i.e. reducing conditions) were probably needed to produce the observed amount of organic matter.

Where we have strong emotions, we're liable to fool ourselves.

Carl Sagan

The Cenomanian/Turonian anoxic event at the Bonarelli Level in Italy and Spain: enhanced productivity and/or better preservation?

Haydon Mort[1], Olivier Jaquat[3], Thierry Adatte[1], Philip Steinmann[1], Karl Föllmi[1], Virginie Matera[1], Zsolt Berner[2] and Doris Stüben[2]

1. Institut de géologie, Emile Argand 11, 2007, Neuchâtel, Switzerland.
2. Institut für Mineralogie und Geochemie, Universität Karlsruhe, 76128 Karlsruhe, Germany.
3. Institute of Terrestrial Ecology ETH SGC D11, Grabenstrasse 3, CH-8952 Schlieren, Switzerland

Abstract

The upper Cenomanian pelagic sediments of Furlo in the northern Apennines are characterized by a 1.5 m-thick organic-rich stratigraphic horizon called the Bonarelli Level, which represents the second major oceanic anoxic event in the Cretaceous (OAE 2). The Bonarelli Level is depleted in carbonates and consists essentially of biogenic quartz, phyllosilicates, and organic matter, with values of TOC reaching 18%. The age of the Furlo section is constrained by correlating its $\partial^{13}C$ curve with that of the well-dated Pueblo (USA) and Eastbourne (UK) sections. The presence of all the planktonic foraminiferid zones and details of the OAE 2 $\delta^{13}C$ excursion indicates a relatively continuous but reduced sedimentation rate across the Cenomanian/Turonian (C/T) boundary. Sediment and TOC mass accumulation rates have been calculated and suggest a sedimentation break in the upper Bonarelli Level. This may be an artifact of the diachronous FAD of the planktonic foraminiferid Helvetoglobotruncana helvetica and suggests that in some sections the $\partial^{13}C$ curve may provide more reliable age control for dating the C/T boundary. In order quantitatively to explain the carbon-isotope curve and the measured TOC mass accumulation rate, a simple dynamic model of the isotope effects of organic versus inorganic carbon burial was developed. In order to verify the consistency of the model we correlated the modeled output of the Furlo section with that of the Manilva section, in southeast Spain. The modelling shows that increasing productivity only partially explains the measured $\partial^{13}C$ excursion and is not the only factor relevant to black shales deposition. Preservation may play a central role, especially in the later stages of OAE 2. Phosphorus and TOC accumulation patterns in the Bonarelli Level in both Furlo and Manilva suggest a similar process, although other factors may also be involved.

Key Words: **Cenomanian/Turonian, stable isotopes, organic matter, modelling, Furlo, Italy, Manilva, Spain.**

E.1 Introduction

During the Cretaceous, the deposition of organic-rich black shales (with >5 % total organic carbon (TOC) was common throughout the world in various palaeogeographic settings. These black shales reflect episodes of anomalous environmental conditions, which have been called "oceanic anoxic events" (OAEs). Two major OAEs are recorded in the Cretaceous: during the Aptian/Albian transition (OAE 1a-c) and OAE 2 at the C/T transition, also known as the "Cenomanian/Turonian Boundary event" (CTBE) (Schlanger and Jenkyns, 1976; Ryan and Cita, 1977; Jenkyns, 1980). The CTBE occurred during a peak global greenhouse interval, thought to be caused by a period of major oceanic

crust production and volcanism which coincided with a eustatic sea level rise of nearly 300 m, relative to present levels (Schlanger et al., 1981; Larson, 1991; Kauffman, 1995). The biogenic carbonate fraction and organic matter from CTBE marine sediments record a 2 ‰ positive excursion in carbon stable isotope ratios (Schlanger et al., 1987; Kuhnt et al., 1988; Pratt et al., 1993; Accarie et al., 1996; Kolonic et al., 2002; Tsikos et al., 2004). Biostratigraphic studies suggest that the isotopic excursion represents a global oceanic geochemical event that can be used as a stratigraphic tool (Schlanger et al., 1987; Thurow et al., 1988).

The relative roles of productivity and preservation in the organic-rich sediments of the CTBE are poorly understood. Some workers interpret this enrichment as caused by higher primary productivity, a consequently strong oxygen depletion, especially in deep waters, leading to enhanced preservation (Kuhnt et al., 1990; Pedersen and Calvert, 1990; Caron et al., 1999; Premoli-Silva et al., 1999). Intensified upwelling and increased ecological niche availability are some factors that can lead to higher productivity (Martinez et al., 1996).

Alternatively, a model involving reservation views sluggish circulation and associated anoxia as the primary cause of improved preservation, which is not necessarily associated with productivity. In this model, a decreased oxygen exchange between the different water masses separated by a pycnocline, or a poor chemical and/thermal stratification (e.g., the stagnant basin of the Black Sea) is the primary cause (Shimkus and Trimonis, 1974; Demaison and Moore, 1980; Bralower and Thierstein, 1984).

In the Umbria-Marche Apennines, the CTBE resulted in the deposition of an organic-rich horizon which consists of black mudstone and shale alternating with black-grey radiolarian-rich mudstone (chert). This horizon is called the Bonarelli Level (BL) and represents a regional marker. Its age is close to the C/T boundary and it varies in thickness between 1 and 2 metres. The BL occurs in the uppermost part of the Scaglia Bianca Formation, which consists of pelagic limestones of mainly Cenomanian age (Bortolotti et al., 1970; Jenkyns, 1980; Arthur and Premoli-Silva, 1982; Coccioni et al., 1991). A correlation with the principle geochemical proxies was made with the C/T boundary in the Manilva section, southeast Spain, whose regional expressions in the Betic Cordillera have been studied by Kuhnt et al. (1990) and by Reicherter et al. (1994). The lithology and proposed palaeobathymetry of Manilva are similar to those of Furlo. By directly comparing the two sections firmer conclusions can be made.

The aim of this study is to evaluate the

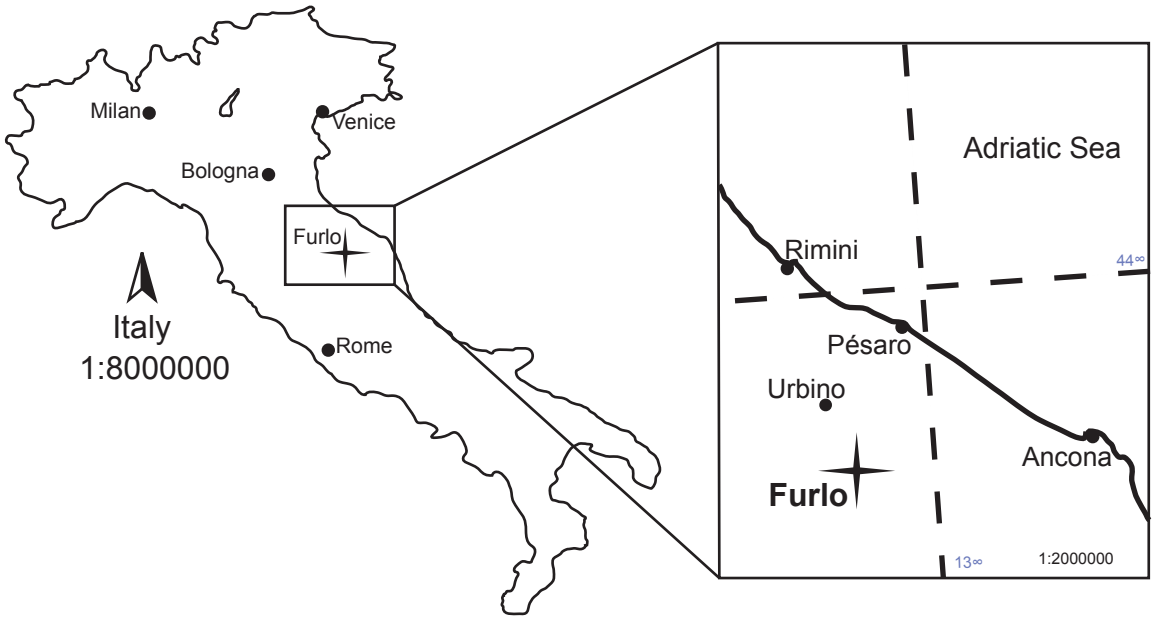

Fig. 1a. Geographical situation of the Furlo Section, Italy.

Figure. 1b. General view of the Furlo Section. The Bonarelli Level and the top of the sampled section are highlighted.

mechanisms of organic matter accumulation and preservation during the C/T transition. For this purpose, planktonic foraminiferid biostratigraphy, organic matter, bulk-rock isotope and phosphorus analyses were conducted on the Furlo section, in the northern Apennines, Italy (figure 1). Based on these data, a quantitative model of isotopic and organic matter interactions in a surface water ocean was developed. The comparison between our analyzed and calculated data provides some insights into the relative roles of productivity and preservation during the CTBE. In addition, we present results ran on the same model for the Manilva section in order to get a better understanding of the significance of our model output. Correlating the model with TOC and P data from both sections has enabled a greater understanding of the geochemical processes involved in the generation of the modeled outputs.

E.2 Methods

The Furlo Section was sampled at high resolution (10 cm intervals) with a total of 111 samples collected from the Scaglia Bianca Formation, including the BL. Thin sections were made for all samples for microfacies observations and micropalaeontological analysis. The hard limestones do not allow examination of planktonic foraminiferids in washed residues and hence biostratigraphic analysis merely examines the presence or absence of different species found in thin sections.

For stable isotope analysis samples from the BL were first decarbonated and then analyzed at the stable isotope laboratory of the Department of Mineralogy and Geochemistry at the University of Karlsruhe, Germany, using an Optima (Micromass, UK) gas mass spectrometer. This was equipped with an online organic matter preparation line (Carlo Erba, CSN 1030) and with an online carbonate preparation line (MultiCarb) for other samples. Separate capsules were used for each sample. The results were calibrated to PDB scale with standard errors of < 0.06‰ for $\delta^{13}C$.

The origin and amount of organic matter were determined by Rock-Eval pyrolysis using a Rock-Eval 6 at the Geological Institute of the University of Neuchâtel, Switzerland. Errors were < 0.1%. Standard notations are used: TOC content in weight %; hydrogen index (HI = S_2/TOCx100) in mg hydrocarbons per g of TOC; oxygen index (OI = S_3/TOCx100) in mg CO_2 per g of TOC.

Bulk rock XRD analysis was also conducted at the Geological Institute of the University of

Fig. 2. General and detailed log of the Furlo Section and Bonarelli Level with associated main microfacies. The grey scale of the sedimentary column was chosen according to the field observations. Thin section Fu-83: typical chert layer with radiolarians and organic matter, Fu-5: wackestone with high diversity of foraminifera (i.e.Rotalipora, Hedbergella genus) below the Bonarelli Level, Fu-20: black shale with radiolarians and biogenic phosphate fragments , respectively with a fish vertebrate, Fu-31: laminated black shale with phosphate microfilms, Fu- 35: black shale/mudstone, indicating carbonate production, Fu-56: Wackestone with renewal of foraminiferal assemblages (i.e. Dicarinella, Whiteinella genus).

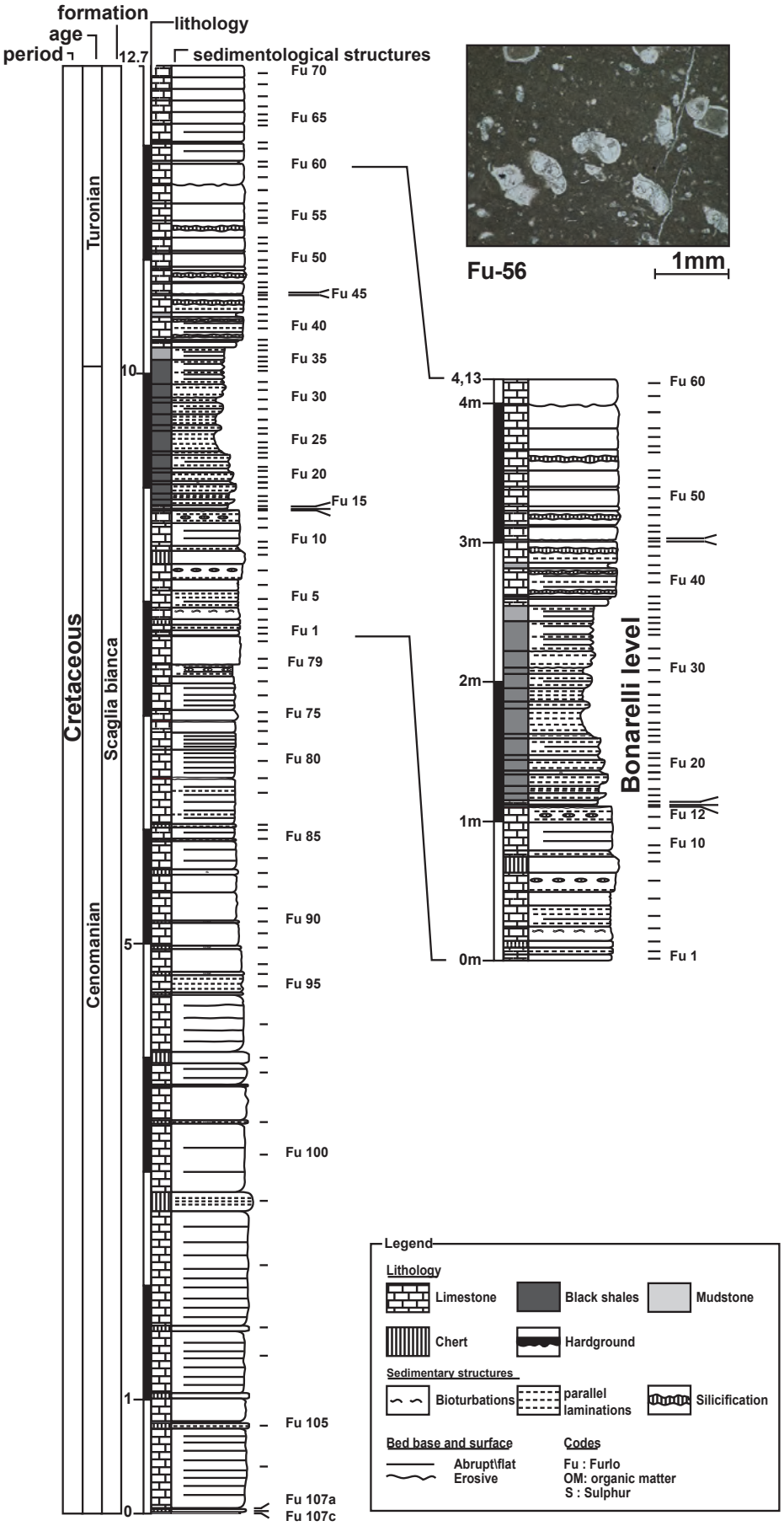
formation
age
period
lithology
sedimentological structures
Cretaceous
Turonian
Cenomanian
Scaglia bianca
12.7
10
5
1
0
Fu 70
Fu 65
Fu 60
Fu 55
Fu 50
Fu 45
Fu 40
Fu 35
Fu 30
Fu 25
Fu 20
Fu 15
Fu 10
Fu 5
Fu 1
Fu 79
Fu 75
Fu 80
Fu 85
Fu 90
Fu 95
Fu 100
Fu 105
Fu 107a
Fu 107c
4,13
4m
3m
2m
1m
0m
Bonarelli level
Fu 60
Fu 50
Fu 40
Fu 30
Fu 20
Fu 12
Fu 10
Fu 1
Legend
Lithology
Limestone
Black shales
Mudstone
Chert
Hardground
Sedimentary structures
Bioturbations
parallel laminations
Silicification
Bed base and surface
Abrupt\flat
Erosive
Codes
Fu : Furlo
OM: organic matter
S : Sulphur

Fu-56
1mm


Fu-35
1mm


Fu-31
1mm

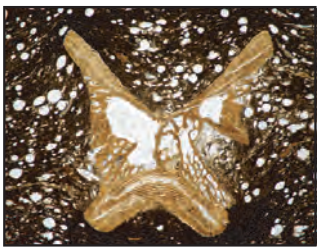
Fu-20
1mm

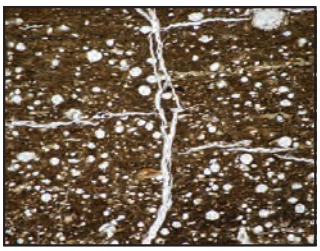
Fu-20
1mm

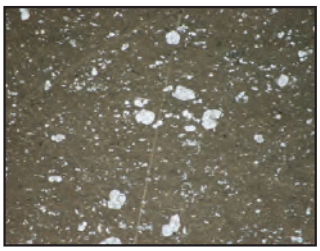
Fu-5
1mm

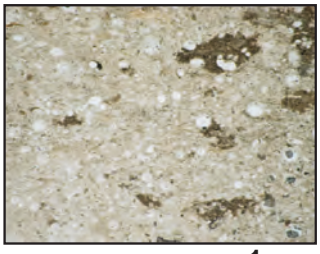
Fu-83
1mm

Neuchâtel, Switzerland, using a SCINTAG XRD 2000 Diffractometer following the procedure outlined by (Kübler, 1987; Adatte et al., 1996). Errors were < 5%. Bulk rock contents were obtained using standard semiquantitative techniques based on external standardization. Analysis of total phosphorus was conducted with a UV/Vis Perkin Elmer Lambda 10 spectrophotometer at the University of Neuchâtel, using the ascorbic acid molybdate blue developed by (Eaton et al., 1995). Errors were < 5%

E.3 Results

E.3.1 Lithology

The Furlo section is located on the southwestern flank of the Furlo anticline, between the summit of the Monte Pietralata and the village of Furlo, where the Via Flaminia crosses the Bottaccione Gorge (Fig. 1). The strata dip at 40° southwest without any visible major tectonic disturbance. Samples were taken from a 12.70 m thick sequence at 10 cm intervals (Fig. 1B).

The Furlo section is part of the Scaglia Bianca Formation, which consists mainly of white limestone and mudstones (Fig. 3). At the base of the section, chert layers, varying from 1-2 cm to 5 cm thick, are common alternating with white limestone layers that range from 10 cm to 70 cm. The cherts consist of radiolarian-rich layers generally of a grey-black colour and are thinly laminated. The upper part of the Scaglia Bianca formation, the black BL (Bortolotti et al., 1970; Cresta et al., 1989) is 1.5 metres thick and contains mainly thin laminated organic-rich dark shales and radiolarian sands. Above the BL, the lithology consists of rhythmically bedded 10–20 cm-thick non-bioturbated white limestones, which occasionally contain chert nodules or 1–8 cm-thick chert layers (Figs. 2A,B). Microfacies analysis shows high faunal diversity, with common large planktonic foraminiferids in the white limestones, and abundant siliceous organisms, such as radiolarians, silicoflagellates or diatoms, in the chert layers.

Just below the last chert layer (Fu-8) beneath the BL, foraminiferids rapidly decrease in abundance (Fu-6 and Fu-5) and become almost totally absent in sample Fu-7. This was also observed for chert-limestone layers above and below the BL. At the base of the BL and up to sample Fu-23, within the BL, radiolarians are abundant and diverse, occurring with large amounts of biogenic fragments consisting of vertebrate (fish) remains, surrounded by laminated organic matter. In the upper part of the BL, phosphatic fish fragments are still present, though radiolarians and silicoflagellates (not shown) are less common. Above this interval, the sediments change from black to orange-brown in colour, indicating that phosphorus is still present but perhaps not bound to organic matter. Both the black and orange-brown sediments consist mainly of organic matter and quartz/opal CT due to the presence of siliceous organisms and near-absence of large foraminiferids (Figs. 2, 3).

E.3.2 Biostratigraphy

The biostratigraphy of the Furlo section is based on planktonic foraminiferids. These are abundant and provide an additional tool for global correlation. Due to the palaeogeographic setting (deep sea basin), no ammonites were found. Relative abundances of planktonic foraminiferids, radiolaria, silicoflagellates and diatoms were estimated from thin sections. A total of 19 planktonic species were identified; smaller species of the genera *Hedbergella, Globigerinelloides* or *Heterohelix* were not identified to species level (Fig. 3). The base of the section (samples Fu-107c to Fu-98) is part of the upper *Rotalipora reicheli* Zone. The *Rotalipora cushmani* Zone is recognized above this interval (Fu-98 to Fu-8). The *Helvetoglobotruncana helvetica* Zone, the base of which marks the C/T boundary, appears in the top metre of the section (Fu-64) along with a species belonging to the genus *Marginotruncana*. Between the *Rotalipora cushmani* and *Helvetoglobotruncana helvetica* zones, the *Whiteinella archeocretacea* Zone (Fu-8 to Fu-64) is tentatively identified. This interval corresponds primarily to the BL and planktonic foraminiferids are mostly absent up to sample Fu-48 (Fig.3). In the upper part of the *W. archeocretacea* zone, larger species are present, including *Dicarinella hagni*, *Marginotruncana sigali, Praeglobotruncana gibba* and *P. stephani*.

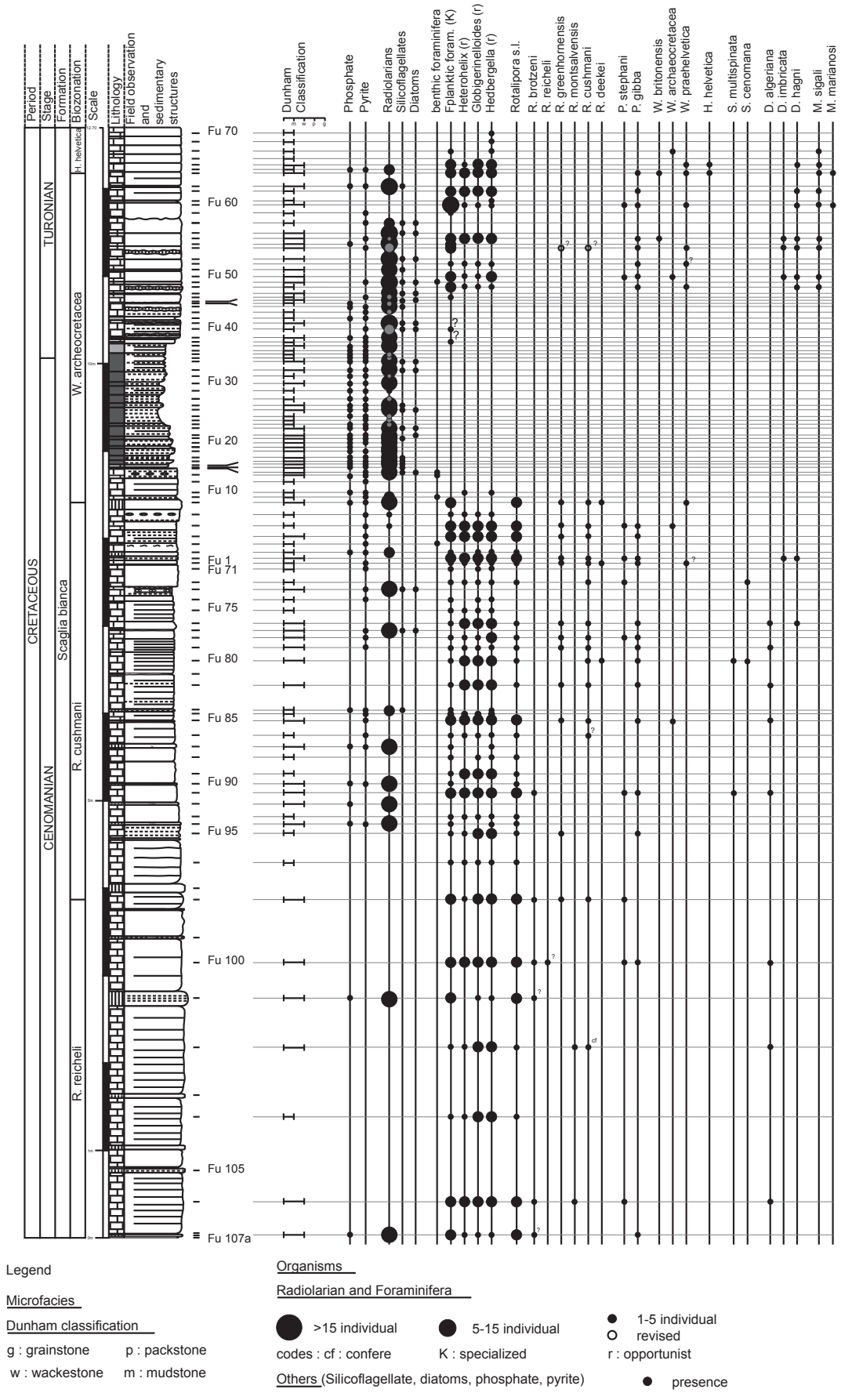

Fig. 3. Foraminiferal distribution and biostratigraphy across the Cenomanian - Turonian boundary at Furlo.

The larger and more complex, ornate foraminiferid species (K-species) are generally more sensitive to changing environmental conditions. This is due largely to their highly specialized niche selection, generally subsurface habitat, and preference for oligotrophic conditions. In the Furlo section, the K-species taxa (belonging to the genera *Rotalipora, Dicarinella* and *Praeglobotruncana*) are present above and below the BL where environmental conditions were favourable. The smaller species, belonging to the genera *Whiteinella*, *Hedbergella, Globigerinelloides* and *Heterohelix* were more tolerant of environmental changes (R-species), including changes in oxygen, salinity and nutrients. R-species taxa generally reproduce rapidly, are very abundant, inhabit surface and subsurface waters and hence are considered opportunists (McArthur and Wilson, 1967; Caron, 1983). These species are generally common in the organic-rich shales of the late Cenomanian $\delta^{13}C$ excursion (Leckie, 1985, 1987; Keller et al., 2001). In the Furlo section, however, these stress tolerant species are nearly absent in the BL, possibly due to dissolution.

E.3.3 Stable carbon isotopes and age control

The observed $\delta^{13}C$ trends are very similar to published curves based on bulk rock, fine fraction carbonates, planktonic foraminiferids and organic matter across OAE 2 (Scholle and Arthur, 1980; Accarie et al., 1996; Nederbragt and Fiorentino, 1999; Paul et al., 1999; Keller et al., 2001; Keller and Pardo, 2004). The major features of the organic matter $\delta^{13}C$ OAE 2 excursion at Furlo are: (l) a rapid increase of 3‰ towards a first peak; (2) a 0.7‰ decrease forming a trough; (3) a 1‰ increase to form the second peak; and (4) prolonged high $\delta^{13}C$ values into the early Turonian (Fig. 4). The same features have been identified at the Pueblo GSSP (Pratt, 1985; Keller et al., 2004) and at Eastbourne, England (Gale et al., 1993; Paul et al., 1999; Keller et al., 2001), suggesting that this pattern reflects a series of widespread or global oceanographic events (Fig. 4). Whilst it is true that carbon isotope values derived from organic matter are subject to the origin of the organic matter, we are confident that the signal is productivity-derived due to the

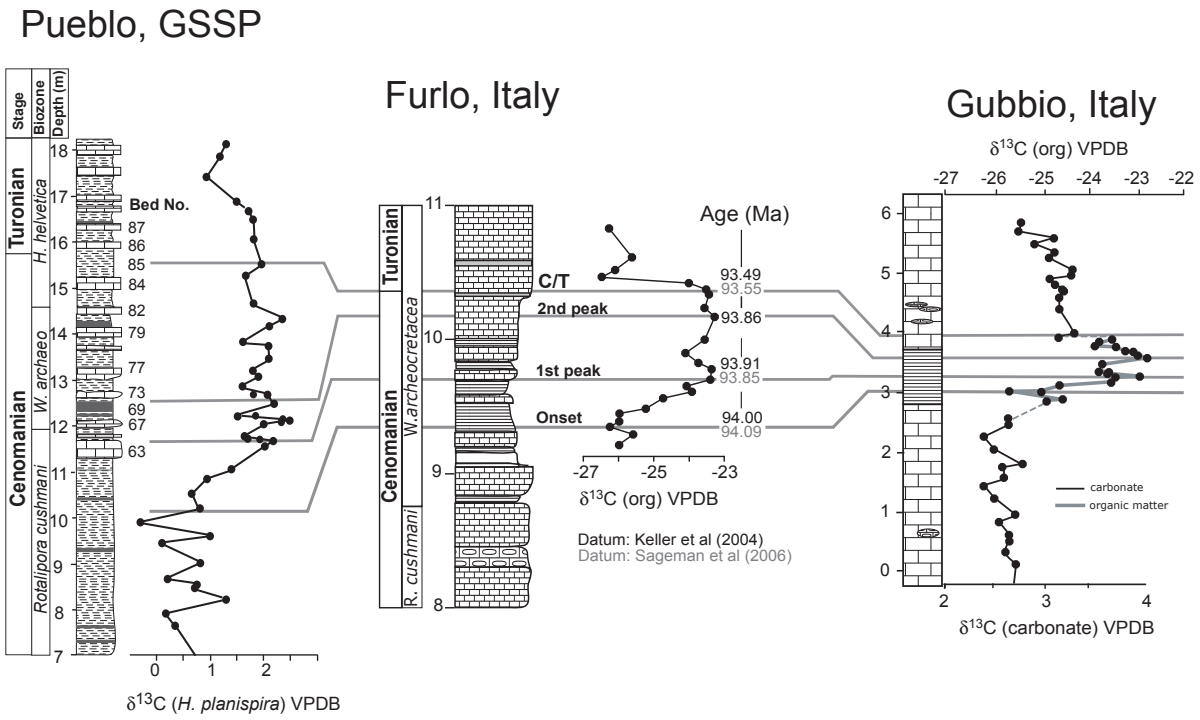

Fig. 4. Variations in $\delta^{13}C$ isotopic composition through the Bonarelli Level at Furlo and Gubbio (Tsikos et al., 2004), correlated with the Pueblo Section GSSP. Also plotted are the ages assigned to the various points

similarities with the signatures from Pueblo and Eastbourne. In the absence of carbonate it provides the best proxy we have for measuring productivity. Carbonate carbon isotope values below and above the Bonarelli Level are stable without considerable variation. This also indicates that the excursion seen in Furlo has longer term significance. The nature of the $\delta^{13}C$ excursion is, however, different from those in these shallower sections and more similar to deeper more pelagic sediments such as those found close by in the Gubbio Section (Tsikos et al., 2004). In these types of sections, where $\delta^{13}C$ is invariably measured using organic matter, the isotope plateau tapers off extremely rapidly. (Tsikos et al., 2004) explained this through changes in regional productivity or hiatuses, although this has not been tested. However this rapid tapering does not concern this study, which focuses on the basal part of the section, of which the isotope stratigraphy appears intact.

In both sections, planktonic foraminiferid datum events and the structure of the $\delta^{13}C$ excursion are comparable. Age estimates for species first and last appearances, $\delta^{13}C$ excursions and depositional and environmental events have been calculated by Keller and Pardo, (2004). These are based on ages of various ammonite and planktonic foraminiferid datum events extrapolated from the radiometric dates (Hardenbol et al., 1998) and are compatible (Keller et al., 2004) with three $^{40}Ar/^{39}Ar$ ages determined from bentonite layers (Obradovitch, 1993; Kowallis et al., 1995; Snow et al., 2005).

The Furlo section is calibrated with the Pueblo section using ages given by planktonic foraminiferid biostratigraphy and $^{40}Ar/^{39}Ar$ dating from bentonites (Hardenbol et al., 1998; Keller et al., 2001; Keller and Pardo, 2004). Assigned ages are as follows: the isotopic onset (94.00 ± 0.2 Ma), the two-peaked $\delta^{13}C$ shifts (93.91 ± 0.2 and 93.89 ± 0.05 Ma respectively), and the C/T boundary level corresponding to the first appearance of the ammonite *Watinoceras devonense* (93.49 ± 0.2 Ma) or, in our case, to the prolonged high $\delta^{13}C$ values (Fig. 4). The onset of the rapid $\delta^{13}C$ excursion at Furlo begins at the base of the BL (Fu-19), and reaches a maximum at Fu-25 (see Fig. 6 for sample distribution). The isotopic values then decrease rapidly from Fu-34 corresponding to the last black shale level, or to the C/T boundary, which is estimated at Furlo based on a correlation with the Pueblo section.

In the Furlo section, the last appearance of *R. cushmani* in sample Fu-8 significantly predates the first $\delta^{13}C$ shift, the extinction datum of this species in other sections (e.g., Tunisia, Italy, Spain, France, England, USA (Lamolda et al., 1994; Nederbragt and Fiorentino, 1999; Paul et al., 1999; Keller and Pardo, 2004). This is probably an environmental effect at Furlo associated with the removal of carbonate at the BL. Similarly, *Helvetoglobotruncana helvetica* appears later at Furlo, due either to environmental changes, difficulties in determining the evolutionary transition from *Praeglobotruncana praehelvetica* to *H. helvetica*, or to diachronous evolutionary transition of these species. For these reasons, the correlation with the Pueblo section is based largely on a combination of biostratigraphy and the $\delta^{13}C$ curve. This correlation suggests that the Furlo Section is condensed but reasonably complete, similar to the Gubbio section (Tsikos et al. 2004). The timing of the CTBE can therefore be constrained by using the ages associated to the $\delta^{13}C$ peaks (Keller et al., 2001; 2004).

E.3.4 Mineralogy

Bulk rock mineralogy is determined for 60 samples encompassing the BL (Fig. 5). Quartz, calcite, phyllosilicates, and 'non-quantified' were the four major groups observed. Minerals such as gypsum, Na-plagioclase, or K-feldspar were also identifiable in smaller quantities. Quartz quantities appeared very low but increase rapidly up-section through the BL. Calcite concentrations are inverse to those of quartz, with very low values in the BL. Non-quantified minerals represent the sum of minerals/phases that were not recognized by XRD analysis. However, in this study the non-quantified phases correspond mainly to organic matter and nearly amorphous to microcrystalline biogenic quartz (Fig.5).

Based on the results obtained, we separate the section into two parts: the Bonarelli Level and the white limestones. The BL is composed

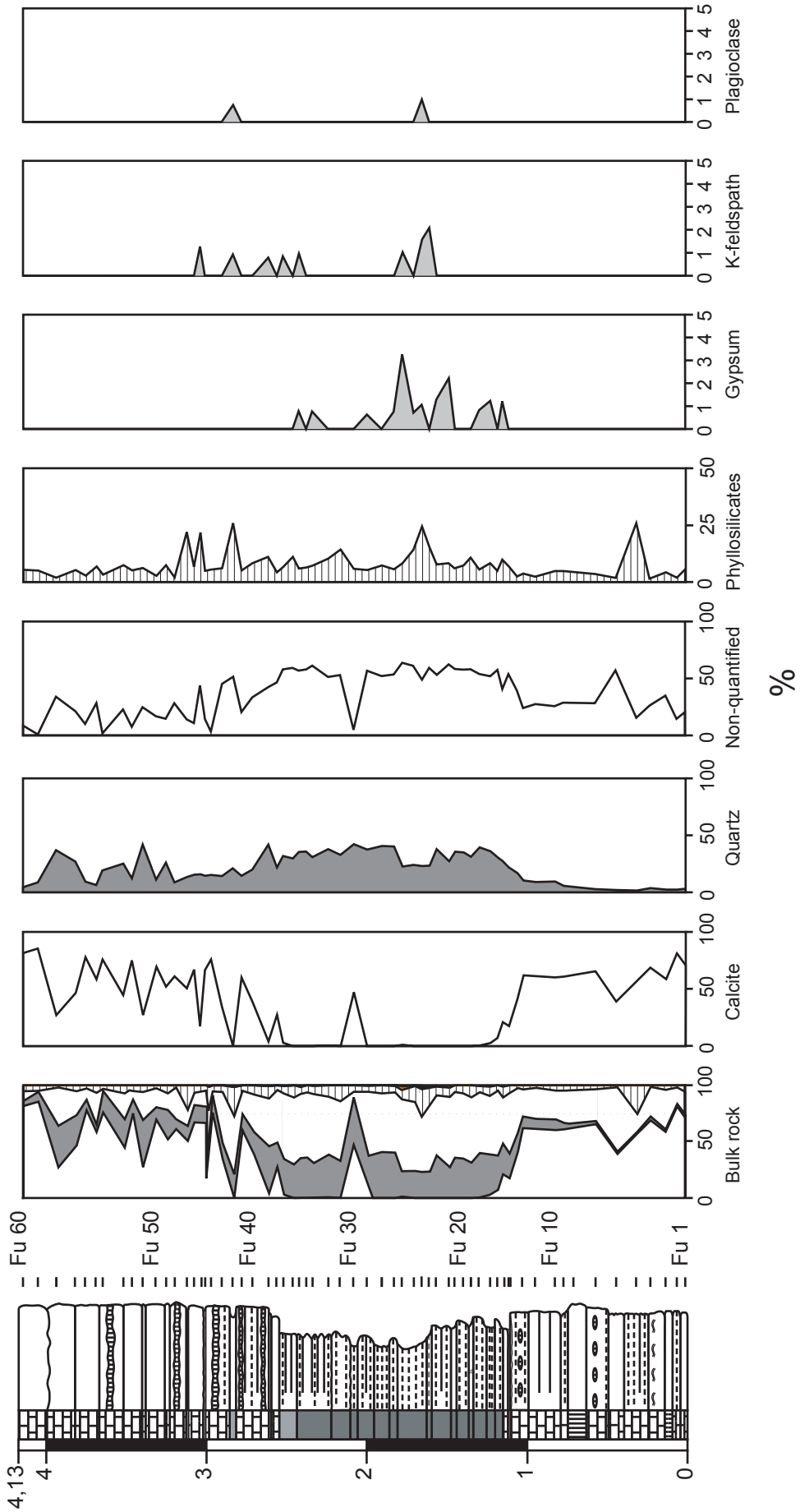

Fig. 5. Bulk mineralogy of the Bonarelli Level. Non-quantified minerals correspond mainly to organic matter and nearly amorphous biogenic quartz.

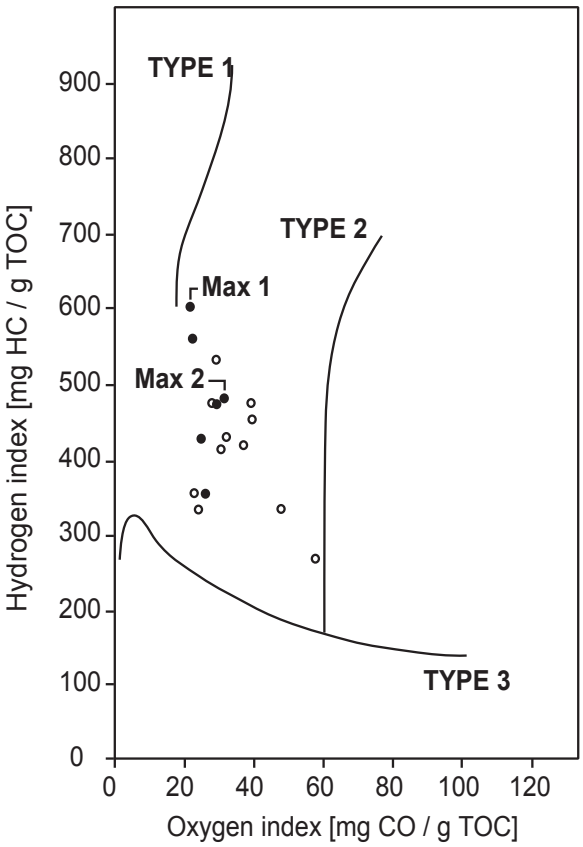

Fig. 6. Espitalié diagram. All data are within the type 2 field, indicating organic matter of marine origin. Maximum 1 indicates Fu- 31, and Maximum 2 Fu-26. Black points refer to values bigger than 8

essentially of organic matter and quartz/opal CT. The presence of radiolaria explains the high quartz/opal CT content. Planktonic foraminiferids are rare in the BL. The large amount of organic matter present in bottom waters results in acidification and dissolution, which may explain the near-absence of foraminiferids in the BL. After carbonate removal, rare silicified ghosts of foraminiferids have been recognized in the insoluble residue. Before and after the BL, white limestones with lower quartz content and diverse foraminiferid assemblages indicate an oligotrophic pelagic environment.

E.3.5 Organic matter

The BL is nearly devoid of carbonate (<7.05 %), except for the basal and uppermost parts, which contain up to 21% and 28% respectively (Fig. 6). The TOC record reflects the quantity of organic matter, although it should be kept in mind that organically bound oxygen, hydrogen, sulphur and nitrogen can contribute up to 50% of the total sedimentary organic matter (Tissot and Welte, 1984). The TOC content is highly variable, ranging from 0.66% to 17.09% (Fig. 6). The TOC content increases gradually in the BL to a first maximum at Fu-22 (9.25% TOC). After some fluctuations, the second maximum is reached at Fu-26 (13.58% TOC), with the maximum value recorded in sample Fu-31 (17.09% TOC).

Information on the composition and maturity of organic carbon can be achieved by pyrolytic measurements (Espitalié et al., 1985; Crumiere et al., 1990). With this method, the type of organic matter is determined by the hydrogen index (HI) and the oxygen index (OI), which approximate to the H/C atomic ratio and O/C atomic ratio respectively. Based on the observed range of HI-values (268 to 564 mg HC/g TOC) and of OI-values (23 to 57 mg CO_2/g TOC), the organic matter of the BL is distributed in the field of type 2 organic matter (Fig.7), which is associated with marine environments (Espitalié et al., 1985). The high HI values also suggest well-preserved organic matter. Temperatures of maximum pyrolytic hydrocarbon yield (Tmax) are in the range of 402–433°C for samples having an organic-richness higher than 0.75% TOC. This indicates that the organic matter did not experience strong burial and is still immature with respect to oil-generation.

E.3.6 Sedimentation and mass accumulation rate (MAR)

Ages obtained by biostratigraphic and carbon stable isotope correlation with the Pueblo section allow calculation of the average sedimentation and mass accumulation rates (MAR) for the different intervals. Each layer for which an age was determined was separated into two parts to improve the resolution. The first dated interval (identified as 'A'; Fu-19 to Fu-25) was calculated to have a non-decompacted sedimentation rate of 0.38 cm/ky. Interval B (Fu-25 to Fu-31), sees the sedimentation rate more than double to 0.88cm/ky. In interval C (Fu-31 to Fu-34), the sedimentation rate drops to a minimum value of 0.055 cm/ky. The average sedimentation rate calculated for the whole interval (A to C) is 0.19cm/ky.

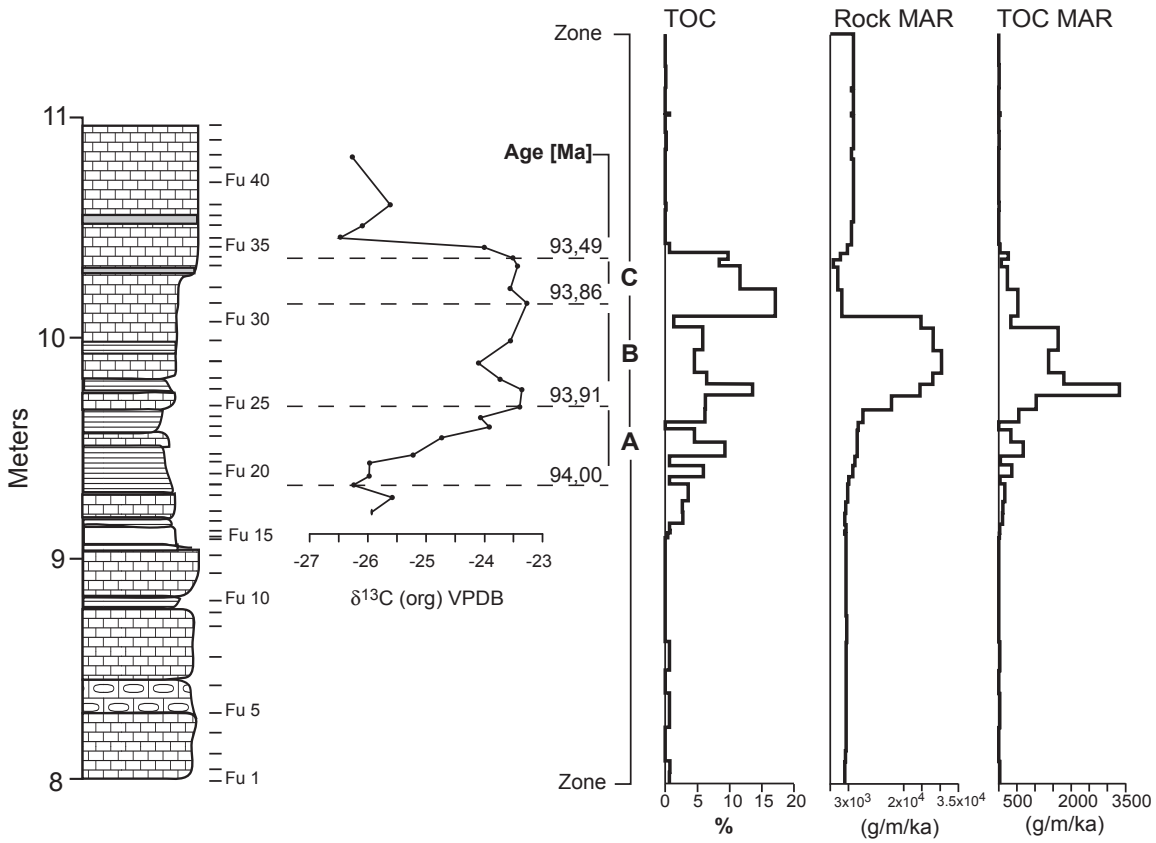

Fig. 6. □13C isotopic composition and related correlated age, with TOC values and respective rock and TOC mean accumulation rate (MAR).

To better estimate the contribution of the various lithologies, the MAR in g/m²/ky was calculated for each layer from A to C (Fig. 6). The rock densities for black shales, marls, cherts and limestones were taken from Attewell and Farmer, (1976). To avoid a different MAR for the same sample, the following corrections were applied. The MAR for dated horizons (Fu-19, Fu-25, Fu-31, and Fu-34) taken as the average of the upper and lower MARs. The curve was then smoothed to constrain the proposed MAR for each zone. Although inherently imperfect, the resulting curve corresponds better to the probable environmental conditions. The last age of 93.49 Ma (Fu-34), with an error margin of 0.2 Ma, generates an error because the lower error limit of 93.29 Ma is chosen, in which case the MAR doubles. The MAR curves for both rock and TOC represent maximum values, assuming that the calculated ages are reliable. However, this correction does not change the general shape of the curve, because the thickness for interval 'C' remains small. The other intervals are more precise (error margins of 0. 2 or 0.05 Ma), and therefore no correction factor was applied.

The MAR of TOC was calculated in the same way (Fig. 6), multiplying TOC values with rock MAR. Both values of rock and TOC MARs increase gradually from the basal part of the BL, then decrease rapidly in the uppermost layers, around Fu-31. The lower sedimentation rate, for interval 'C', may be due to decreased biogenic productivity and/or non-deposition. However, as previously mentioned, based on correlations with the Pueblo section, the Furlo section though condensed, still seems relatively complete. The average rate of 0.19 cm/ky compares well with the average rates of 0.5-1.0 cm/ky (Elder and Kirkland, 1985), 0.9 cm/ky (Scott et al., 1998) and 0.57 cm/ky (Sageman et al., 1998) for the shallower environment of the Pueblo section. The major sedimentary break or discontinuity between the B and C intervals may be a biostratigraphic artifact (e.g. delayed or variable first appearance of *H. helvetica* (93.49 or 93.29 Ma given by (Hardenbol et al., 1998), ± 0.05 Ma). A more precise age can be calculated based on the carbon-isotope shifts

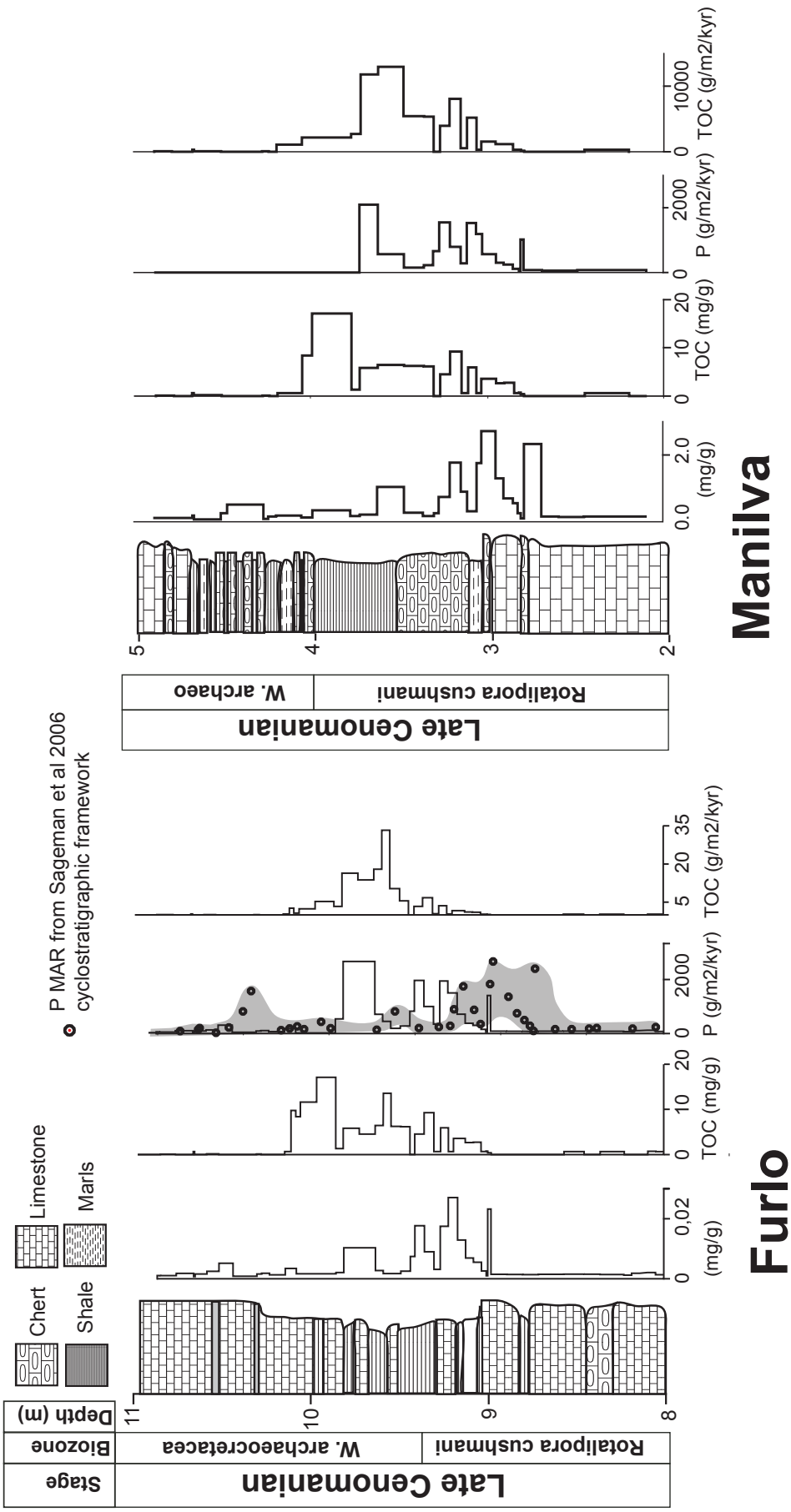

Fig. 8. Phosphorus and TOC contents (mg/g), phosphorus and TOC mass accumulation rates (g/m^2/ka) values for the Bonarelli Level in the Furlo and Manilva sections.

(error margin of 0.2 Ma, (Keller et al., 2004). The average sedimentation rates of the basal part of the Bonarelli Level (interval A: 0.38 cm/ky and B: 0.88 cm/ky), which are calculated using well-dated carbon-isotope shifts, show a significantly lower sedimentation rate than the figure of 10 cm/ky proposed by Beaudoin et al. (1996).

E.3.7 Phosphorus MAR

All samples from Furlo and Manilva were analyzed for total phosphorus content. In this paper, we present the data from within the Bonarelli Level only (Fig. 8). The concentration of phosphorus (mg/g) and mass accumulation rate (MAR) is calculated (mg/cm^2/kyr). A recent study by Sageman et al. (2006) constructed a high-resolution cyclostratigraphy timescale based on harmonic analysis developed by Meyers et al. (2001) and Meyers and Sageman (2004). The ages derived from this study were used to construct separate P MARs, which allowed us to better assess how sedimentation rates effects our phosphorus results.

Like organic matter, phosphorus (P) increases rapidly in the Bonarelli Level. With the appearance of black shales, the first peak is observed between Fu-19-23 (0.027 [mg/g] and 0.017 [mg/g] respectively (Fig. 8). Above this interval, values decrease rapidly and reach a second peak at Fu-29 (0.02 [mg/g]). In the uppermost part of the BL as well as in the white limestones, P is very low (0.005 [mg/g]). Precisely the same trend is observed in the Manilva section, although values of TOC and P MARs are considerably higher.

Sinks for phosphorus include organic matter, skeletal matter, iron and manganese oxyhydroxides, clays and phosphate minerals, incorporated into and preserved in sedimentary reservoirs (Föllmi, 1996). The increase in TOC and P MARs is concordant at Furlo and Manilva (possible slightly before in Manilva) but the origins of P are likely to be different. In the basal part of the black shales, rock and TOC MARs are low, contrary to those of phosphorus. P, therefore, does not appear to be bound principally to organic matter, even though there is an abundance of it. Biogenic phosphate fragments (fish vertebrates, fish bones), and biogenic fragments rimmed by phosphate, are common and associated with abundant radiolarians (bed 20, Fig. 2). Authigenic phosphorus is therefore likely to be the dominant phosphorus reservoir in the Furlo section.

P MARs calculated from the ages (see Fig. 4) given by Sageman et al., (2006) also generate the same general increase in P MAR prior to the $\delta^{13}C$ peak, albeit slight earlier, at 9 metres (Fu-14). The use of Sageman et al. (2006) creates a more consistent sedimentation rate. Assigning dates obtained by a high-resolution cyclostratigraphic framework onto a low-resolution $\delta^{13}C_{(org)}$ curve is difficult. Nevertheless, the results from this simple exercise support the assertion that variations in P MAR are *not* merely an artifact of changing sedimentation rate.

E.3.8 Modelling

The positive carbon stable isotope excursion during OAEs may be explained by depletion of the inorganic dissolved CO_2 pool in ^{12}C due to increased burial of organic matter. In order to test whether this hypothesis holds quantitatively in the Furlo section, a simple stock and flux model (called ISOAE) was developed and calculated using the modeling Stella Research© (High Performance Systems Inc.). The carbon isotope profile of the Manilva section in Spain was also used to generate a modeled output. The results may be comparable as both sections probably have similar depositional environments and palaeodepths.

The ISOAE model (Fig. 9) is based on two stocks or reservoirs in the upper layers of the ocean waters: the dissolved inorganic carbon reservoir (DIC) and the reservoir of carbon bound to dissolved or suspended organic matter (OM). Four fluxes are connected to the reservoirs:

- The supply of inorganic carbon (CO_2) into the DIC-reservoir (Fsupply, combining volcanic release and river input)
- The formation of OM from CO_2 i.e. photosynthesis (F_DIC_OC);
- The burial of carbonates (F_sed_IC) and burial of organic matter (F_sed_OC).

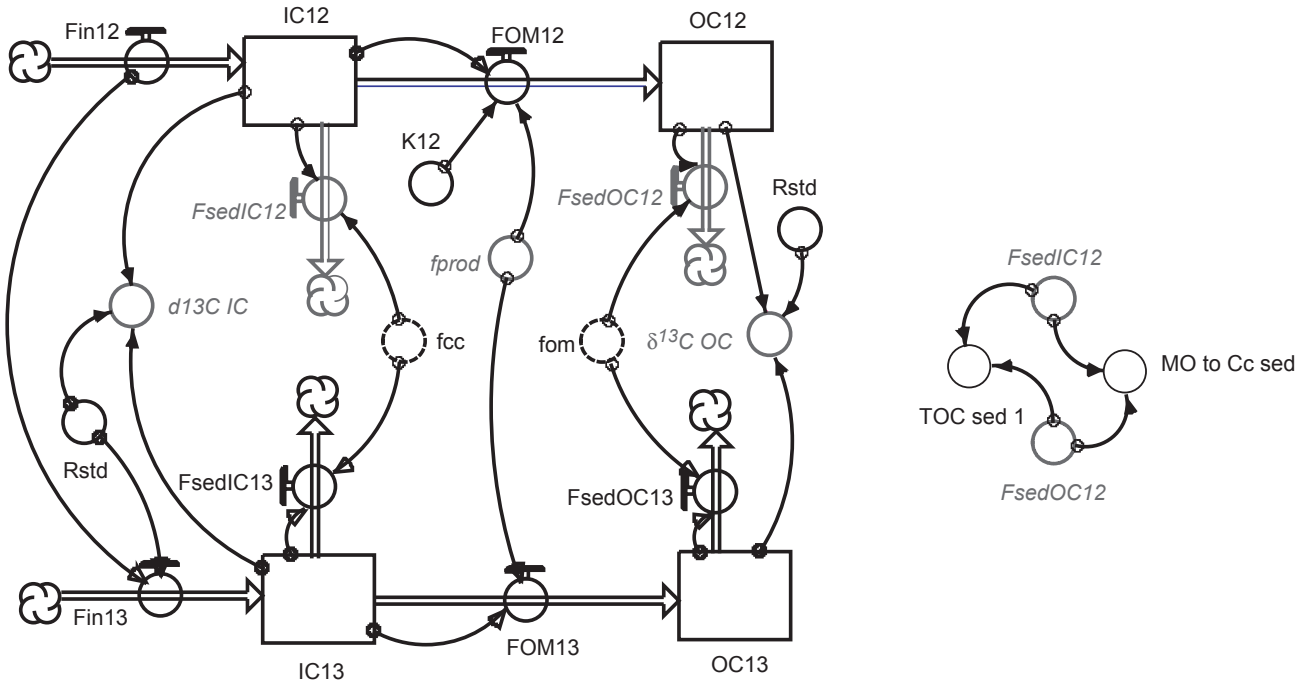

Fig. 9. The ISOAE Model design. The $\delta^{13}C$ curve for Furlo (and Manilva) is assumed to be produced by productivity alone. Using simple stock-flux mechanisms and fractionation constants, the model calculates the accumulation of organic matter. By comparing this modeled output with organic carbon values actually measured, we may make certain hypotheses as to the relative importance of productivity versus preservation. See text for details.

The carbonate burial rate is set to be proportional to the size of the DIC reservoir:

F_sed_IC = *f*Cc*DIC

Where *f*IC is the fraction of carbonate buried per unit of time. The (small) part of the DIC that enters the OC reservoir is proportional to the size of DIC and to a productivity factor *f*prod:

F_DIC_OC = DIC* *f*prod.

Finally, the burial of organic matter is set to be proportional to the OM reservoir:

F_sed_OC = OC* *f*OM.

The model is designed in such a way that each carbon isotope (^{12}C and ^{13}C) has it own reservoirs and fluxes. Thus it is possible to know at any time the isotopic ratio of each reservoir and flux. The isotopic fractionation during organic matter formation, i.e. the kinetics uptake of ^{12}C during photosynthesis, is included by a kinetic factor k12. As a consequence the equation for the flux from the DIC-pool to the OC-pool becomes:

F_DIC_OC_12 = DIC_12* *f*prod*k12.

Before simulation can be done, all parameters must be adjusted to run the system in steady state. For this, the size of the reservoirs and input fluxes are adopted from Siegenthaler and Sarmiento (1980) with 120'000 [GtC/Mioy] for Fsupply, 970 GtC for the DIC reservoir and 3 GtC for the OM reservoir. The factors *f*Cc, *f*prod, and *f*OM are calculated from the following equations describing the steady-state (input = output):

Fsupply = *f*Cc*DIC + *f*prod*DIC

*f*prod*DIC = *f*OM*OM

Moreover, the ratio of organic to carbonate

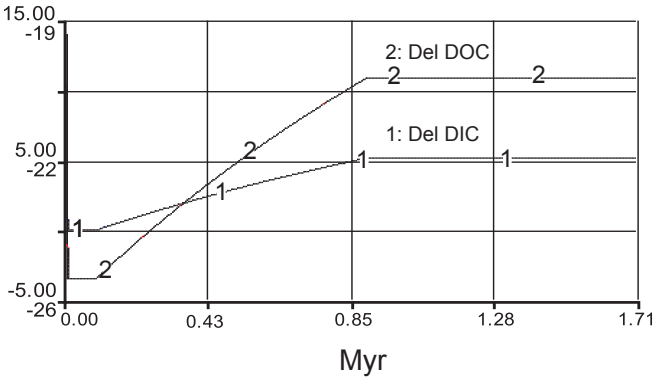

Fig. 10. Model behavior for a 10 times increase in fprod over 1.7 Ma.

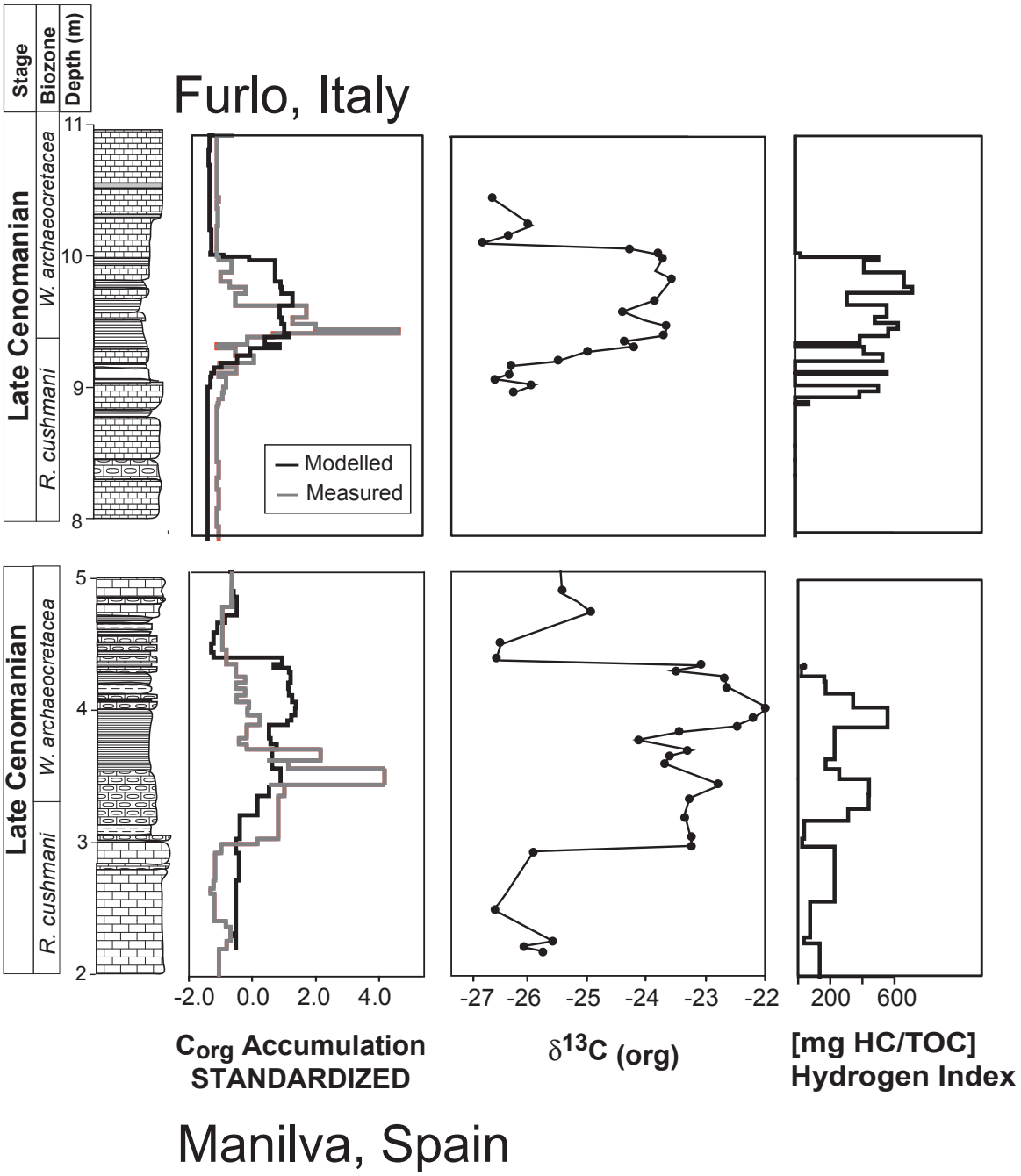

Fig. 11. From left to right: comparison of the measured and modeled data on for OC MAR and $\delta^{13}C$ isotopic fluctuations, hydrogen index for the Furlo and Manilva sections

carbon burial is taken to be

$$f\text{OM}*\text{OM} / f\text{Cc}*\text{DIC} = 0.06.$$

The ratio of 0.06 is given by Sarmiento et al. (2002) and also corresponds to the TOC/MINC ratio of the Fu-13 sample, which can be considered as a background ratio before the onset of the OAE 2. Finally, the $^{12}C/^{13}C$ ratio of Fsupply is adjusted to have an isotopic response of +1.5 permil in the DIC reservoir and the k12 rate constant is chosen such that the $\partial^{13}C$ value of the OC reservoir becomes -26 permil in the steady state. In this model, the $\partial^{13}C$ of the DIC reservoir increases when organic-carbon burial is increased. The $\partial^{13}C$ values of the OC reservoir follow those of the DIC reservoir, with an offset given by the kinetic factor k12 (Fig. 10). The dependence between the productivity (given by *f*prod) and the isotopic curves is almost linear.

Starting with these steady state parameters, a simulation was run, where the productivity factor (*f*prod) was varied so as to reproduce schematically

the $\partial^{13}C$ values measured in the Furlo Section. The resultant rate of organic carbon burial indeed shows a major increase in the Bonarelli Level. In Fig. 11, the normalised curves of the measured and calculated TOC accumulation rates are compared. In general, the model is able to explain the measured isotopic curve and the variations in the burial rate of organic carbon. According to the model, organic carbon burial (i.e. effect of productivity) must nearly triple (factor of 2.7) to obtain the measured isotopic excursion. Since we keep the inputs (Fsupply) constant, the ISOAE model implicitly diminishes the sedimentary flux of inorganic carbon during times of higher productivity. This may well correspond to the reality. The CTB may represent a time of global crisis in carbonate platform development (Ferrandini et al., 1985; Mermighis et al., 1991; Abdallah and Meister, 1997; Davey and Jenkyns, 1999; Buchbinder et al., 2000). With the drowning of the platforms this important sink of inorganic carbon would have been switched off (Weissert et al., 1998). In our simulation the flux of inorganic carbon is reduced by 9 % at maximum burial of organic matter. As a result, the ratio of IC to OC burial changes from 16 (before and after the isotopic excursion) to 5 (during the isotopic excursion). A similar trend is observed in the Manilva section (Fig. 12). Actual OM accumulation begins to exceed modeled values at the first peak in $\delta^{13}C$.

E.4 Discussion

The age of the Furlo section is well constrained, based on the shape of the $\delta^{13}C$ curve correlated with that of the Pueblo stratotype section Keller et al., (2004). At Furlo, the major planktonic foraminiferid zones, and details of the OAE 2 $\delta^{13}C$ excursion indicate a relatively continuous but slow sediment deposition across the C/T boundary, relative to Pueblo. The upper Cenomanian succession is characterized by the Bonarelli Level, which consists of a 1.5 m thick black shale layer with up to 18% TOC. This level coincides with a major positive $\delta^{13}C$ excursion, which is interpreted as having resulted from a depletion of ^{12}C in the water column due to high primary productivity and/or enhanced preservation of organic matter as a result of poorly oxygenated bottom waters (Arthur et al., 1995; Pratt, 1985).

From our simple model, it is reasonable to say that increasing the productivity factor (*f*prod) to meet the carbon isotopic constraints comfortably explains the OC burial in the basal part of the Bonarelli Level (Fu-16 to Fu-24). However, in the middle part (Fu-25 to Fu-28), the model values fall below the measured values. In other words, the ISOAE model finds it impossible that productivity alone can explain the organic carbon burial rate during this time. It is always during the $\delta^{13}C$ excursion that this discrepancy takes place in Furlo and Manilva (Fig. 11). Preservation may therefore also play a central role. This proposition is given weight when we observe the same trend in the Manilva section (Fig. 11). The very high hydrogen index values in Furlo and Manilva during the isotope excursion start and mid-plateau supports enhanced preservation over productivity.

The fact that P MARs increase more rapidly compared to TOC MAR in Furlo and Manilva (Fig. 8) supports the model in this respect, suggesting that increased productivity may be the main factor leading to the initial increased P, at the base of the BL. In contrast, in the upper BL, rock and TOC MARs are high and no phosphatic biogenic fragments are observed (bed 31 and 35, Fig. 2). The sediment consists mainly of organic matter and quartz/opal CT. In bed 31, the sediment changes in colour from black to orange-brown and is highly laminated, indicating that P is still present. In this upper part, microbial activity may control the rate of P accumulation. Patterns associated with productivity processes are no longer observed. Preservation may play a more central role during this stage of the event. Large increases in the HI values during the excursion plateau (Fig. 11) are consistent with increased preservation of organic matter compared to the lower part of the BL. P may therefore be concentrated in organic matter, which, in this case, would be preserved due to reduced oxygenation of bottom waters.

The model predicts that a 3-fold increase in productivity is required to cause the observed increased in measured $\delta^{13}C$ values. Therefore, productivity alone cannot explain the recorded increase in TOC MAR values. Phosphorus MAR values in the Furlo and Manilva sections are in good agreement with the modeled results, suggesting that this element is associated first with productivity and then with preservation.

All this, of course, does not help to explain what caused the increase in productivity in the first place. The apparent high productivity associated with the $\delta^{13}C$ excursion could be explained by a number of factors. For example, the complex interactions between the CTB sea level transgression, nutrient remobilization as well as CO_2 and P release from volcanic provinces may all have led to increased productivity and even eutrophic conditions in surface waters (Larson and Erba, 1999; Leckie et al., 2002). The increased accumulation of organic matter and depletion of oxygen in the water column could have led to the enhanced preservation of organic carbon, the extinction of environmentally sensitive planktonic species and the survival of low oxygen tolerant species.

Although there is good agreement between the data sets and the model, a number of additional factors should also be considered. These include:

- Inaccurate accumulation rates due to uncertainties in the assigned ages. Indeed, the slower sedimentation rate in the upper part (0.055 to 0.88 cm/ky), and the subsequent lower accumulation in this upper part of the Bonarelli Level, may be due to an overestimate for the first appearance datum of the ammonite *Watinoceras devonense*, where the error margin is greater than those for the $\partial^{13}C$ shift.
- Changes in the depositional patterns, i.e. changes in the lateral advection of OM into or out of the studied section. To improve the model a more detailed understanding of the oceanic circulation (e.g. inclusion of the deep ocean reservoir) and palaeogeography of the late Cretaceous is required.
- Changes in magnitude (e.g. due to increased pCO_2 in the atmosphere) and isotopic composition of the input flux.
- Changes in pCO_2 in the surface waters, due to changes in pH.

E.5 Conclusions

The Furlo section can be correlated with the Pueblo stratotype based on the $\delta^{13}C$ excursion. The isotope and planktonic foraminiferid biostratigraphy of the Furlo section show that it is condensed, yet relatively complete.

The C/T event is evaluated based on TOC MAR and $\delta^{13}C$ fluctuations. To approximate the observed measured $\delta^{13}C$ values, our model predicts that a 3-fold increase in productivity is required. Productivity alone seems unable to explain the recorded TOC MAR values; preservation may play a key role. Phosphorus MARs are in good agreement with the model results, suggesting that this element is associated first with productivity and then with preservation. The initial increase in productivity associated with the $\delta^{13}C$ excursion could be explained by the complex interaction of sea level rise, CO_2 release from volcanic provinces, and remobilization of nutrients in the oceans. However our data do not provide any insights into this. The increased accumulation of organic matter and depletion of oxygen in the water column may have led to enhanced preservation of organic carbon. In the future an attempt to incorporate additional factors into the model, such as the local palaeoenvironmental situation, should be made. The model also needs to be tested in different environmental settings. The ISOAE model results show promise as a tool for testing ideas regarding productivity-driven accumulation of organic matter. The model could be improved significantly by using other concepts, such as diffusion, as well as incorporating a better understanding of Cretaceous ocean-water chemistry.

Acknowledgements

We would like to thank Michèle Caron for training in foraminifera determination, Gesine Preuss for stable isotope laboratory assistance, André Villard for thin section preparation, F. Tamburini for helping to collect the samples and R. Coccioni for introducing us to the Furlo Section. Also to Silke Voigt for helpful reviews which greatly benefited this manuscript. This study was supported by FNRS No: 21-67702.02.

References

Abdallah, H., Meister, C., 1997. The Cenomanian-Turonian boundary in the Gafsa-Chott area (southern part of central Tunisia): biostratigraphy, palaeoenvironments. Cretaceous Research 18, 197-236.

Accarie, H., Emmanuel, L., Robaszynski, F., Baudin, F., Amedro, F., Caron, M., Deconinck, J. F., 1996. Carbon isotope geochemistry (delta C-13) as stratigraphic tool. A case study of the Cenomanian/ Turonian boundary in central Tunisia. Comptes Rendus De l'Académie des - Sciences Series IIA - Earth and Planetary Science 322, 579-586.

Adatte, T., Stinnesbeck, W., Keller, G., 1996. Lithostratigraphical and mineralogic correlations of near K/T boundary clastic sediments in northeastern Mexico: Implications for origin and nature of deposition. Geological Society of America Special Paper 307, 211-226.

Arthur, M., Premoli-Silva, I., 1982, Development of widespread organic rich strata in Mediterranean Tethys. In: Schlanger, A., and Cita, M. B., (Eds.), Nature and Origin of Cretaceous Carbon-rich Facies. Academic Press, London/New York/Paris, 7-54.

Attewell, P.B., Farmer, I. W., 1976. Principles of engineering geology, Chapman and Hall, London.

Beaudoin, B., M'Ban, E.P., Montanari, A., Pinault, M., 1996. Stratigraphie haute resolution (<20 ka) dans le Cenomanien du bassin de Marches-Ombrie (Italie) [High-resolution lithostratigraphy in the Cenomanian of the Umbria-Marche Basin (Italy)]. Académie de Sciences, Comptes Rendus 323, 689-696.

Bortolotti, V., Passerini, P., Sagri, M., Sestini, G., 1970. The miogeosynclinal sequences. Sedimentary Geology 4, 341-344.

Bralower, T.J., Thierstein, H., R., 1984. Low productivity and slow deep-water circulataion in the Mid-Cretaceous oceans. Geology 4, 341-444.

Buchbinder, B., Benjamini, C., Lipson-Benitah, S., 2000. Sequence development of Late Cenomanian-Turonian carbonate ramps, platforms and basins in Israel. Cretaceous Research 21, 813-843.

Caron, M., 1983. La spéciation chez les foraminifères planctiques: une réponse adaptée au contrainte de l'environnement. Zitteliana 10, 671-676.

Caron, M., Robaszynski, F., Amedro, F., Baudin, F., Deconinck, J.F., Hochuli, P., Salis-Perche Neilsen, K.V., Tribovillard, N., 1999. Estimation de la duree de l'evenement anoxique global au passage Cenomanien/Turonien. Approche cyclostratigrphique dans la formation Bahloul en Tunisie centrale. Bulletin de la Société Géologique de France 170, 145-160.

Coccioni, R., Erba, E., Premoli-Silva, I., 1991. Litho- and bisotratigraphy of the Livello Bonarelli close to the Cenomanian/Turonian boundary (Umbria-Marche Apennines, Italy) and possible paleoceanographic significance. Géologie Alpine, Mémoire Hors Série 17, 25-26.

Cresta, S., Monechi, S., Parisi, G., Baldamza, A., Reale, V., 1989. Mesozoic - Cenozoic stratigraphy in the Umbria-Marche area. Memoire Cartagraphica Geolgia de Italia 39, 185.

Crumiere, J.P., Crumiereairaud, C., Espitalie, J., 1990. Cyclic Preservation of Amorphous Organic-Matter in Sediments of the Vocontian Basin (Southeastern France), around the Cenomanian-Turonian Boundary - Paleoceanographic Controls. Bulletin de la Société Géologique de France 6, 469-478.

Davey, S.D., Jenkyns, H.C., 1999. Carbon-isotope stratigraphy of shallow-water limestones and implications for the timing of Late Cretaceous sea-level rise and anoxic events (Cenomanian-Turonian of the peri-Adriatic carbonate platform, Croatia). Eclogae Geologicae Helvetiae 92, 163-170.

Demaison, G.T., Moore, G.T., 1980. Anoxic environments and oil source bed genesis. Organic Geochemistry 2, 9-31.

Eaton, A.D., Clesceri, L.S., Greenberg, A.E., 1995. Standard methods for the examination of water and wastewater, American Public Health Association, New York.

Elder, W.P., Kirkland, J.I., 1985. Statigraphy and depositional environment of the Bridge Creek Limestone Member of the Greenhorn Formation at Rock Canyon Anticline near Pueblo, Colorado. Fine grained deposits and biofacies of the Cretaceous Western Interior Seaway: Evidence of cyclic sedimentary processes. Field Trip Guidebook, 4, Society of Economic Paleontologists and Mineralogists, Tulsa.

Espitalié, J., Deroo, G., Marquis, F., 1985. La pyrolyse Rock-Eval et ses applications. Revue de l'Institut Français du Pétrole 40, 563-579.

Ferrandini, M., Philip, J., Babinot, J. F., Ferrandini, J., Tronchetti, G., 1985. The Cenomanian-Turonian Carbonate Platform in the Erfoud-Errachidia Area (Southeastern Morocco) - Stratigraphy and Paleoenvironments. Bulletin de la Société Géologique de France 1, 559-564.

Föllmi, K.B., 1996. The phosphorus cycle, phosphogenesis and marine phosphate-rich deposits. Earth-Science Reviews 40, 55-124.

Gale, A.S., Jenkyns, H.C., Kennedy, W.J., Corfield, R.M., 1993. Chemostratigraphy Versus Biostratigraphy - Data from around the Cenomanian-Turonian Boundary. Journal of the Geological Society 150, 29-32.

Hardenbol, J., Thierry, J., Farley, M.B., Jacquin, T., De Graciansky, P.-C., Vail, P. R., 1998, Mesozoic and Cenozoic sequence chronostrigraphic framework of European Basins. In: Graciansky, J., and Hardenbol, T., (Eds.), Mesozoic and Cenozoic Sequence Stratigraphy of European Basins, Society of Economic Paleontologists and Mineralogists Special Publication, 3-13.

Jenkyns, H.C., 1980. Cretaceous anoxic events, from continents to oceans. Journal of the Geological Society of London 137, 171-188.

Kauffman, E.G., 1995, Global Change Leading to Biodiversity Crisis in a Greenhouse World: The Cenomanian-Turonian (Cretaceous) Mass Extinction, Effects of Global Change on Life. Panel on Effects of Past Global Change on Life, National Research Council, 47-71.

Keller, G., Han, Q., Adatte, T., Burns, S. J., 2001. Palaeoenvironment of the Cenomanian-Turonian transition at Eastbourne, England. Cretaceous Research 22, 391-422.

Keller, G., Pardo, A., 2004. Age and paleoenvironment of the Cenomanian-Turonian global stratotype section and point at Pueblo, Colorado. Marine Micropalaeontology 51, 95-128.

Keller, G., Stueben, D., Berner, Z., Adatte, T., 2004. Cenomanian - Turonian d13C, d18O, Sea level and Salinity variations at Pueblo, Colorado. Palaeogeography, Palaeoclimatology, Palaeoecology 211, 19-43.

Kolonic, S., Damste, J.S.S., Bottcher, M.E., Kuypers, M.M.M., Kuhnt, W., Beckmann, B., Scheeder, G., Wagner, T., 2002. Geochemical characterization of Cenomanian/Turonian black shales from the Tarfaya Basin (SW Morocco) - Relationships between palaeoenvironmental conditions and early sulphurization of sedimentary organic matter. Journal of Petroleum Geology 25, 325-350.

Kowallis, B.J., Christiansen, E.H., Deino, A.L., Kunk, M.J., Heaman, L.M., 1995. Age of the Cenomanian-Turonian Boundary in the Western Interior of the United-States. Cretaceous Research 16, 109-129.

Kuhnt, W., Herbin, J.P., Thurow, J., Wiedmann, J., 1988. Cenomanian-Turonian Organic Facies in the Western Mediterranean and Along the Adjacent Atlantic Margin. American Association of Petroleum Geologists 72, 1011-1011.

---, 1990, Distribution of Cenomanian-Turonian Oragnic Facies in the Western Mediterranean and Along the Adjacent Atlantic Margin. In: Huc, A. Y., ed., Deposition of Organic Facies. AAPG Studies in Geology, 133-160.

Kübler, B., 1987. Cristallinite de l'illite, méthods normalisées de préparations, méthodes normalisées de mesures. Cahier Insitut de Géologie 1, 13.

Lamolda, M.A., Gorostidi, A., Paul, C.R.C., 1994. Quantitative Estimates of Calcareous Nannofossil Changes across the Plenus Marls (Latest Cenomanian), Dover, England - Implications for the Generation of the Cenomanian-Turonian Boundary Event. Cretaceous Research 15, 143-164.

Larson, R.L., 1991. Geoogical consequences of superplumes. Geology 19, 963-966.

Larson, R.L., Erba, E., 1999. Onset of the mid-Cretaceous greenhouse in the Barremian-Aptian: Igneous events and the biological, sedimentary, and geochemical responses. Paleoceanography 14, 663-678.

Leckie, M.R., Bralower, T. J., Cashman, R., 2002. Oceanic anoxic events and plankton evolution: Biotic response to tectonic forcing during the mid-Cretaceous. Paleoceanography 17, 1-29.

Leckie, R.M., 1985. Foraminifera of the Cenomanian-Turonian Boundary Interval, Greenhorn Formation, Rock Canyon Anticline, Pueblo, Colorado. Fine-Grained Deposits and Biofacies of the Cretaceous Western Interior Seaway: Evidence of Cyclic Sedimentary Processes., 4, SEPM, 139-149 pp.

---. 1987. Paleoecology of mid-Cretaceous planktic foraminifera: A comparison of open ocean and epicontinental sea assemblages. Micropaleontology 33, 164-176.

Martinez, P.H., Bertrand, P.H., Bouloubassi, I., Bareille, G., et al., 1996. An intergrated view of inorganic and organic biogeochemical indicators of palaeoproductivity changes in a coastal upwelling area. Organic Geochemistry 24, 411-420.

McArthur, R.H., Wilson, E.O., 1967. The theory of island biogeography, Princeton University Press.

Mermighis, A., Philip, J., Tronchetti, G., 1991. Carbonate Platform Sequences and System Tracts at the Cenomanian-Turonian Boundary, Internal Hellenids (Peloponnesus, Greece). Bulletin de la Société Géologique de France 162, 547-552.

Meyers, S., Sageman, BB., 2004. Detection, quatification and significance of hiatuses in pelagic and hemipelagic strata. Earth and Planetary Science Letters 224, 55-72.

Meyers, S.R., Sageman, B.B., Hinnov, L.A., 2001. Integrated quantitative stratigraphy of the Cenomanian-Turonian bridge creek limestone member using evolutive harmonic analysis and stratigraphic modeling. Journal of Sedimentary Research 71, 628-644.

Nederbragt, A.J., Fiorentino, A., 1999. Stratigraphy and palaeoceanography of the Cenomanian-Turonian boundary event in Oued Mellegue, north-western Tunisia. Cretaceous Research 20, 47-62.

Obradovitch, J.D., 1993, A Cretaceous timescale. In: Caldwell, W.G.E., and Kauffman, E. G., (Eds.), Evolution of the Western Interior Basin. Geological Association of Canada Special Paper, 47-62.

Paul, C.R.C., Larnolda, M.A., Mitchell, S.F., Vaziri, M.R., Gorostidi, A., 1999. The Cenomanian–Turonian boundary at Eastbourne (Sussex, UK): a proposed European reference section. Palaeogeography, Palaeoclimatology, Palaeoecology 150, 83-121.

Pedersen, T.F., Calvert, S.E., 1990. Anoxia vs. Productivity: what controls the formation of organic carbon-rich sediments and sedimentary rocks? Bulletin of the American Association of Petroleum Geologists 74, 454-466.

Pratt, L.M., 1985, Isotopic studies of organic matter and carbonate in rocks of the Greenhorn marine cycles. In: Pratt. L.A., Kauffman, E.G. and Zelt, F.B. (Eds.) Fine grained Deposits and Biofacies of the Cretaceous Western Interior Seaway: Evidence of cyclic Sedimentary Processes. In: Pratt, L. M., Kauffman, E. G., and Zelt, F. B., (Eds.), Fine grained Deposits and Biofacies of the Cretaceous Western Interior Seaway: Evidence of cyclic Sedimentary Processes. Tulsa Society of Economic Paleotologists and Mineralogists, 38-48.

Pratt, L.M., Arthur, M.A., Dean, W.E., Scholle, P.A., 1993, Paleoceanographic cycles and events during the late Cretaceous in the Western Interior Seaway of North America. In: Caldwell, M.W., and Kauffman, E.G., (Eds.), Evolution of the Western Interior Basin. St John's Geological Association of Canada Special Paper, 333-354.

Premoli-Silva, I., Erba, E., Salvini, G., Locatelli, C., Verga, D., 1999. Biotic changes in Cretcaeous oceanic anoxic events of the Tethys. Journal of Foraminiferal Research 29, 352.

Reicherter, K., Pletsch, T., Kuhnt, W., Manthey, J., Homeier, G., Wiedmann, J., Thurow, J., 1994. Mid-Cretaceous paleogeography and paleoceanography of the Betic Seaway (Betic Cordillera, Spain). Palaeogeography Palaeoclimatology Palaeoecology 107, 1-33.

Ryan, W.B.F., Cita, M.B., 1977. Ignorance concerning episodes of ocean-wide stagnation. Marine Geology 23, 197-215.

Sageman, B.B., Meyers, S.R., Arthur, M.A., 2006. Orbital time scale and new C-isotope record for the Cenomanian-Turonion boundary stratotyoe. Geology 34(2), 125-128.

Sageman, B.B., Rich, J., Arthur, M.A., Dean, W.E., Savrda, C.E., Bralower, T.J., 1998, Multiple Milankovich cycles in the Bridge Creek Limestone (Cenomanian-Turonian), Western Interior Basin. In: Dean, W. E., and Arthur, M. A., (Eds.), Concepts in Sedimentology and Paleontology. Society for Sedimentary Geology, 153-171.

Sarmiento, J.L., Dunne, J., Gnanadesikan, R. M., Matsumoto, K., Slater, R., 2002. A new estimate of the CaCO3 to organic carbon export ratio. Global Biogeochemical Cycles 16, 1-12.

Schlanger, S.O., Arthur, M.A., Jenkyns, H.C., Scholle, P.A., 1987, The Cenomanian/Turonian anoxic event deposits. In: Einsele, G., and Seilacher, A., (Eds.), Cyclic and event stratification. Springer-Verlag, New York, 161-173.

Schlanger, S.O., Jenkyns, H.C., 1976. Cretaceous oceanic anoxic events: Causes and consequences. Geol. Mijnbouw 55, 179-184.

Schlanger, S.O., Jenkyns, H.C., Premoli-silva, I., 1981. Volcanism and Vertical Tectonics in the Pacific Basin Related to Global Cretaceous trangressions. Earth and Planetary Science Letters 52, 435-449.

Scholle, P.A., Arthur, M.A., 1980. Carbon isotope fluctuations in Cretaceous pelagic limestones: potential stratigraphic and petroleum exploration tool. American Association of Petroleum Geologists 64, 67-57.

Scott, R.W., Evetts, M.J., Franks, P.C., Bergen, J.A., Stein, J.A., 1998, Timing of mid-Cretaceous relative sea level changes in the Western Interior: Amoco No. 1 Bounds Core. In: Dean, W.E., and Arthur, M.A., (Eds.), SEPM Concepts in Sedimentology and Paleontology, 11-34.

Shimkus, K., Trimonis, E., 1974, Modern sedimentation in the Black Sea. In: Degens, E. T., and Ross, D. A., (Eds.), The Black Sea-geology, chemistry and biology. American Association of Petroleum Geologists, 249-278.

Siegenthaler, U., Sarmiento, J.L., 1980. Atmospheric carbon dioxide and the ocean. Nature 365, 119-125.

Snow, L.J., Duncan, R.A., Bralower, T. J., 2005. Trace element abundance in the Rock Canyon Anticline, Pueblo, Colorado, marine sedimentary section and their relationship to Caribbean plateau construction and oxygen anoxic event 2. Paleoceanography 20, doi: 10.1029/2004PA001093.

Thurow, J., Moullade, M., Brumsack, H.J., Masure, E., Taugourdeau-Lantz, J., 1988. The Cenomanian/ Turonian boundary event (CTBE) at hole 641A, ODP Leg 103 (compared with CTBE interval at site 398). The proceedings of the ocean drilling program, Scientific Results 103, 587-634.

Tissot, B.P., Welte, D., 1984. Petroleum formation and occurrence, Chapmand and Hall, London, 699 pp.

Tsikos, H., Jenkyns, H.C., Walsworth-Bell, B., Petrizzo, M.R., et al., 2004. Carbon-isotope stratigraphy recorded by the Cenomanian-Turonian Oceanic Anoxic Event: correlation and implications based on three key localities. Journal of the Geological Society 161, 711-719.

Weissert, H., Lini, A., Kuhnt, O., 1998. Correlation of Early Cretaceous carbon isotope stratigraphy and platform drowning events: a possible link? Palaeogeography Palaeoclimatology Palaeoecology 137, 89-203.


- F -
Conclusions and Outlook

Main Conclusions

This project has introduced a new angle in the debate surrounding the causes and consequences of oceanic anoxic event 2. Published models about the behavior of phosphorus in sub-oxic conditions, have been tested using the scientific method. As always in geology, the findings of these studies are open to multiple interpretations. Regardless of the interpretation adopted, a summary of the observations made in this study is as follows…

1. **There is a period of elevated P accumulation (in particular, inorganic-P) during the start of the $\delta^{13}C$ isotope excursion of OAE 2. This observation can be made in all the sections presented, although to a lesser extend in Mohammed Plage, which was possibly unique due to its upwelling palaeoenvironment.**
2. **The duration of this increase in P accumulation is short, not extending into the $\delta^{13}C$ plateau.**
3. **Significant organic carbon deposition does not start until after the decrease in P accumulation rates. Deeper sections observe a considerable offset between peaks in P-inorganic and P-organic, the latter occurring slightly later.**
4. **Where is has been possible (in sections with insignificant dissolution) there appears to be a steady, long-term decrease in detrital input, preceding OAE 2.**
5. **An further increase in total-P has been observed towards the end of OAE 2.**

The occurrence of the first enrichment in P generally occurs at what is widely considered to be a maximum flooding surface (the base of the isotope excursion). Given the simultaneous nature of the P enrichment, the rapid eustatic sea-level rise and the reworking of sediments on previously dry land offers the best explanation for the increase in P accumulation. There appears to be no evidence that an increase in humidity supplied P to the ocean via increased global weathering rates. The small increase in kaolinite (also plagioclase and feldspar), observed in Mohammed Plage is more consistent with the sediment reworking of clay minerals rather than a dramatic climate shift. This does not rule out the possibility of there being one, but simply questions the significance of any shift that may have taken place.

Given that organic matter starts forming, in any significant quantity, only after the peak in P accumulation and isotope excursion onset, this suggests the following. (1) The flux of organic matter from the surface of the ocean to the sea floor was slower than the rate as which it was being oxidized and that (2) the oceans were therefore still generally oxic enough to allow the effective breakdown of organic matter.

The decrease in inorganic-P accumulation occurs before the increase in organic matter. This is explainable in two ways. (1) After the maximum flooding surface, eustatic sea-level rise slowed allowing new marine sediments to form on top of drowned continental margins, capping the amount of unreactive-P being remobilized and/or (2) Oxygen was gradually consumed at the sediment-water interface, reversing the processes of P sorption in oxyhydroxides and preventing authigenesis. The reduction in oxygen also would have caused the deceleration in the rate of organic matter oxidation.

We are unable to rule out the first explanation, but it would appear a logical conclusion to make. We have evidence for the second explanation in the form of increase hydrogen indices that correlate reasonable well with TOC percentages and an offset in the accumulation of organic-P relative to inorganic-P, which also suggests a slowing in organic matter degradation.

The interplay between organic and inorganic-P leads us to the conclusion that during OAE 2 the bottom of the ocean underwent a transition from an oxidizing to a reducing environment. Dissolved inorganic phosphorous (DIP) would have become bioavailable to stimulate further primary productivity.

If the sedimentary capping of drowned continental margins was responsible for the fall in

P accumulation rates at the isotope excursion onset then an alternative source of nutrients would be required for primary producers. Nutrient recycling offers an alternative source.

Outlook

Further C/T boundary research

There is a strong case for nutrient recycling being a major driving force behind OAE 2. However each of the sections that have been studied almost certainly contains a hiatus somewhere during the $\delta^{13}C$ excursion onset or the isotope plateau due to a probable maximum flooding surface. It would therefore be ideal if we could find a complete, high-resolution record of the Cenomanian-Turonian transition. A good possibility would be to use ODP/IODP samples, perhaps from Shatsky Rise or Blake Nose. The importance of the research may justify a new cruise entirely.

Further work is especially required on sediments that document the end of OAE 2. A rise in phosphorus accumulation has been predicted but seen only once. Validation of this observation is required in other sections around the world.

Other timescales

In order to ascertain the potential significance of bottom-water oxygen depletion on phosphorus and nitrogen accumulation, it will be necessary to study other periods in the Earth's history where there is documented evidence for dysoxia. The model developed for OAE 2 is falsifiable in that if the same trends are not seen in other time periods, then is either means the model is wrong or incomplete or that the Cretaceous ocean was in someway different to other periods of time.

Potential timeframes that maybe chosen for studying the behavior of phosphorus include;

- Other OAEs (as well as Cretaceous Oceanic Red Beds). This is critical in accessing the role of eustatic sea-level changes in the formation of oceanic anoxia. OAE 2 takes place against the back-drop of a large trangression. Other OAEs do not, and therefore the mechanism put forward in this thesis is of little help when trying to explain the triggering mechanims of other OAEs.
- Paleocene/Eocene boundary (does the proposed disassociation of methane hydrates have an impact on the oxidation of nutrients which if reduced would be a further source of productivity?).
- Pliocene Mediterranean sapropels. There have been several studies discussing phosphorus recycling during the deposition of Pliocene sapropels and their similarities with OAE deposits. However, P-speciations needs to be carried out in more detailed to ascertan the true origin of P in these sediments.
- The modern ocean/large lakes. Detailed real time measurements could be taken from a boat crossing a basin transect with a well-defined oxygen minimum zone. Based on our interpretations of P signatures during OAE 2, pore water P content should decrease if overlain by oxygen deficient waters. Conversely, water samples taken from above the sediment-water

- G -

Appendix 1 - Affiliated Papers

The two papers presented in the following annex are multi-proxy studies of sections with a shallow water palaeoenvironmental setting, in Egypt and Morocco. Both sections in these papers contain oyster beds. Did sub-oxic conditions only develop in deeper environments or were shallow areas affected also? The answer has implications for our understanding about the extent of reducing conditions during OAE 2 or (as has recently been suggest) ocean circulation (Slomp and Van Cappellen., 2006). These implications are not directly addressed in the text, which is part of a different project to the one presented in this thesis.

Slomp, C. P. and Van Cappellen, P., 2006. The global marine phosphorus cycle: sensitivity to oceanic circulation. Biogeoscience discussions, 3, 1587–1629. www.biogeosciences-discuss.net/3/1587/2006/

Middle and Late Cenomanian Anoxia in shallow shelf environments of NW Morocco

The paper is in preparation and will be submitted for publication shortly

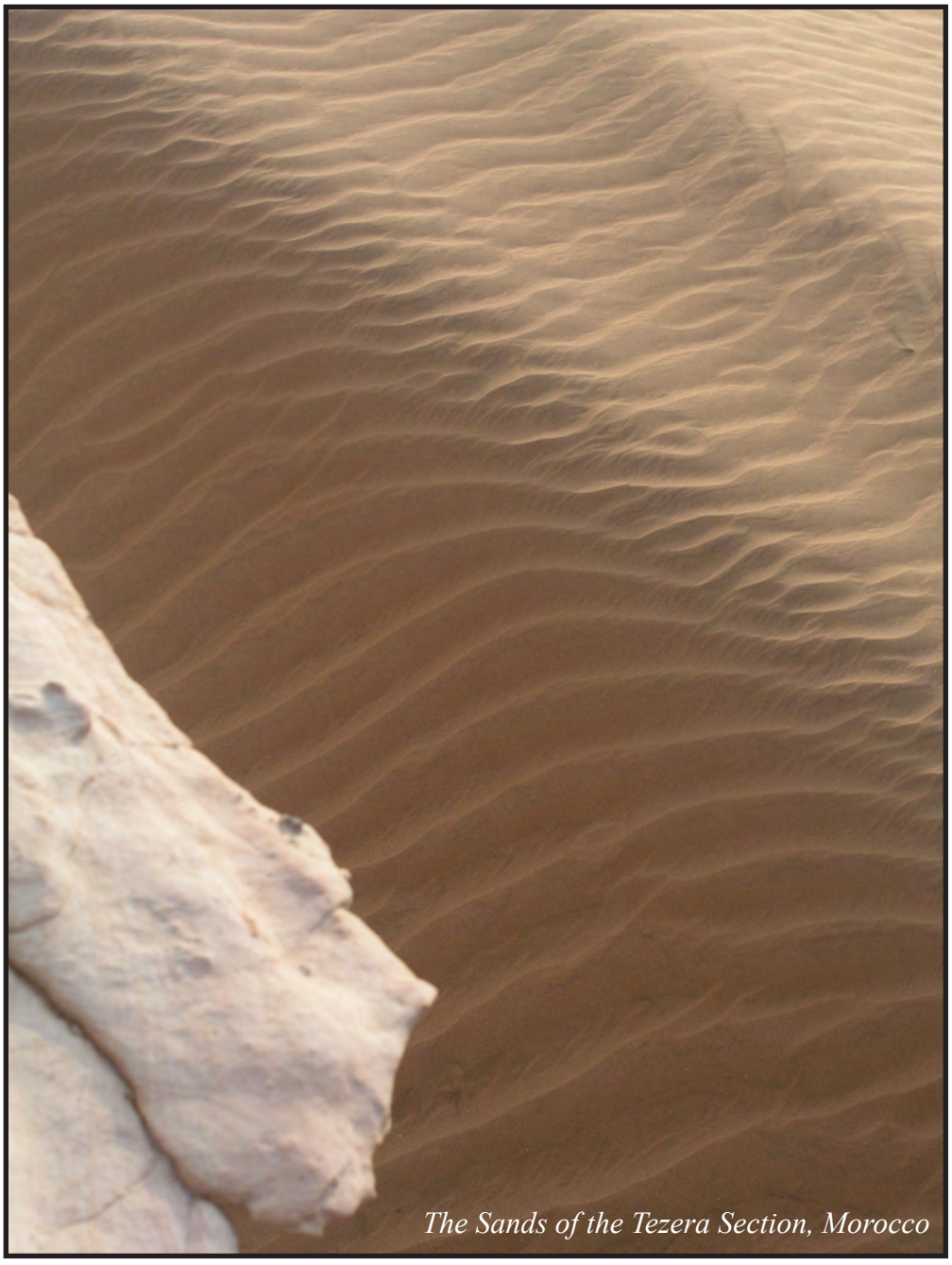

The Sands of the Tezera Section, Morocco

Middle and Late Cenomanian Anoxia in shallow shelf environments of NW Morocco

B. Gertsch[1], G. Keller[1], T. Adatte[2], Z. Berner[3], A.A.A.M. Tantawy[4], A.M. El-Sabbagh[4], H.P. Mort[2] and D. Stueben[3]

[1]*Department of Geosciences, Princeton University, Princeton NJ 08544, USA*

[2]*Geological Institute, University of Neuchatel, Neuchatel, CH-2007, Switzerland*

[3]*Institute for Mineralogy & Geochemistry, University of Karlsruhe, 76128 Karlsruhe, Germany*

[4]*Alexandria University, Faculty of Science, Department of Geology, Alexandria 21526, Egypt*

[5]*Department of Geology, Faculty of Science, South Valley University, Aswan 81528, Egypt*

Abstract

The mid-Cenomanian (MCE) and late Cenomanian to early Turonian (OAE2) ocean anoxic events were studied in shallow continental shelf environments characterized by oyster-rich limestones exposed near Azazoul, north of Agadir, Morocco. Biostratigraphy, stable isotopes, mineralogy, total organic content, rock eval and total phosphorous analyses were carried out and the results correlated with deeper water environments in the Tarfaya basin. Age control is based on nannofossils, foraminifera and carbon isotopes. Results show a 2‰ OAE2 δ13C excursion and two 1-1.5‰ MCE excursions, accompanied by low oxygen tolerant benthic and planktic foraminifera indicating dysoxic conditions. The growth of oyster-rich limestone beds during OAE2 suggests nutrient-rich water due to increased weathering and terrestrial runoff related to a more humid climate, as also indicated by the increase in kaolinite. Total phosphorus quantification indicates maximum concentrations at the onset of the carbon isotope excursion and decreasing values at the peak δ13C excursion. Similar observations were reported by Mort et al. (in press) from various deep-sea sections and interpreted as suggesting the decoupling of carbon and phosphorus cycles during OAE2 and thereby sustaining high productivity. This study suggests that the increased productivity may be linked to the major transgression, humid climate and increased terrigenous runoff associated with the latest Cenomanian.

Keywords: **Cenomanian, Anoxic Events, shallow shelf, Morocco**

A.P.1. Introduction

The middle to late Cretaceous was characterized by very warm climate and high sea level, which is commonly attributed to high concentration of greenhouse gases related to increased tectonic activity (Larson, 1991; Larson and Erba, 1999). During this time, low-latitude basins of the western Tethys and North Atlantic intermittently experienced times of black shale deposition known as oceanic anoxic events (OAEs) (Jenkyns, 1980; Arthur and al., 1988; Leckie et al., 2002). Two anoxic events are known from the middle Cenomanian (MCE, Jenkyns et al., l994; Coccioni et al., 2003), but perhaps the most extensive oceanic anoxic event, OAE 2, began near the end of the Cenomanian (~94-93.5Ma) and continued into the earliest Turonian. OAE2 was accompanied by a major sea level transgression that reached the highest Phanerozoic sea-level (Haq et al., 1987; Hallam, 1992), extremely warm ocean temperatures (Huber

et al., 1995; Clarke and Jenkyns, 1999; Huber et al., 2002; Norris et al., 2002), major faunal and floral turnovers (Erbacher et al., 1996; Leckie et al., 2002; Erba and Tremolda, 2002; Keller and Pardo, 2004), a positive 2‰ carbon isotope shift and black shale deposition (Hart and Leary, 1989; Ulicny et al., 1993; Paul et al., l999; Keller et al., 2004; Tsikos et al., 2004; Kuhnt et al., 2005). It was also a time of increasing eruptions of large igneous provinces in the Caribbean, Ontong Java and Madagascar (Wignall, 2001; Courtillot and Renne, 2003).

During OAE2, outer shelf and deep basin environments are characterized by deposition of organic-rich black shales. Factors influencing their deposition include: organic terrestrial influx, organic matter preservation, increased primary productivity, oxidation in the water column, rates of sedimentation, distance to the coast and water depth. The severity of the oceanic anoxia in the water column depends on which of these factors were prevalent. Deeper basins near upwelling areas, such as the northeast Atlantic off Morocco (e.g., Tarfaya basin), reveal the highest sedimentation rates and maximum organic contents reaching up to 8 cm/103yr (Kuhnt et al., 2005; Kolonic et al., 2005). These regions have been widely studied for their excellent biostratigraphic record, age control and variations in the intensity of anoxia (Kuhnt et al., 1997; Kolonic et al., 2005; Kuhnt et al., 2005; Keller et al., in press; Mort et al., in press). The shallower middle shelf environments (100-200 m depth), such as the U.S. Western Interior at Pueblo, Colorado (~100 m), and Eastbourne, England (50-100 m, Gale et al., 2000) reveal higher terrigenous influx and lower organic contents. These sections also provide excellent biostratigraphic control and a wealth of information on water column anoxia, the nature of the δ13C excursion and patterns of sedimentation (Paul et al., 1999; Keller et al., 2001; Leckie et al., 2002; Keller and Pardo, 2004; Sageman et al., 2006; Caron et al., 2006).

In contrast, sequences from inner shelf and coastal environments contain no black shales and have poor biostratigraphic records. These environments have received little attention to date and consequently are poorly understood with regards to the paleoenvironment during OAE2 (e.g., Drzewiecki and Simo, l997; Davey and Jenkyns, l999). Largely unanswered questions concern the overall response of shallow shelf environments to oceanic anoxia. Did the low oxygen water mass reach into inner shelf and coastal environments? If so, what were the biotic effects? At what rate did organic matter accumulate? Is the absence of black shale a matter of dilution by terrigenous influx or preservation? Investigation of shallow neritic and coastal sequences can provide some answers to these questions.

We hypothesize that OAE2 reached into very shallow waters, but that the effects were mitigated by oxygen uptake in surface waters such that the water column never reached the oxygen depletion of deeper shelves or basins. In addition, the signal was likely diluted by high terrigenous influx and generally poor organic matter preservation. If this hypothesis is right, then the seawater composition in shallow neritic environments should retain the δ13C signal that is characteristic oceanwide, even though other factors (e.g., biotic effects, TOC) may vary.

A.P.1.1. Aims

This study aims to test this hypothesis based on the shallow water coastal sequence at Azazoul north of Agadir, Morocco, and its correlation with published deeper basin sequences from the Tarfaya basin to the south. Investigations concentrate on: (1) stable isotopes (δ13C) to evaluate the shallow water response in relationship to the global oceanic productivity; (2) mineralogy, sedimentology and rock-eval to evaluate the depositional environment and understand climate evolution; (3) organic matter and phosphorus contents to glean information on primary productivity; (4) faunal turnovers to evaluate the biotic response to anoxia and environmental stress in general, and (5) biostratigraphy and age control.

A.P.2. Geological Setting and Location

The Azazoul section is exposed along the coast about 20 km north of Agadir. The section consists of two segments separated by a strike-slip fault

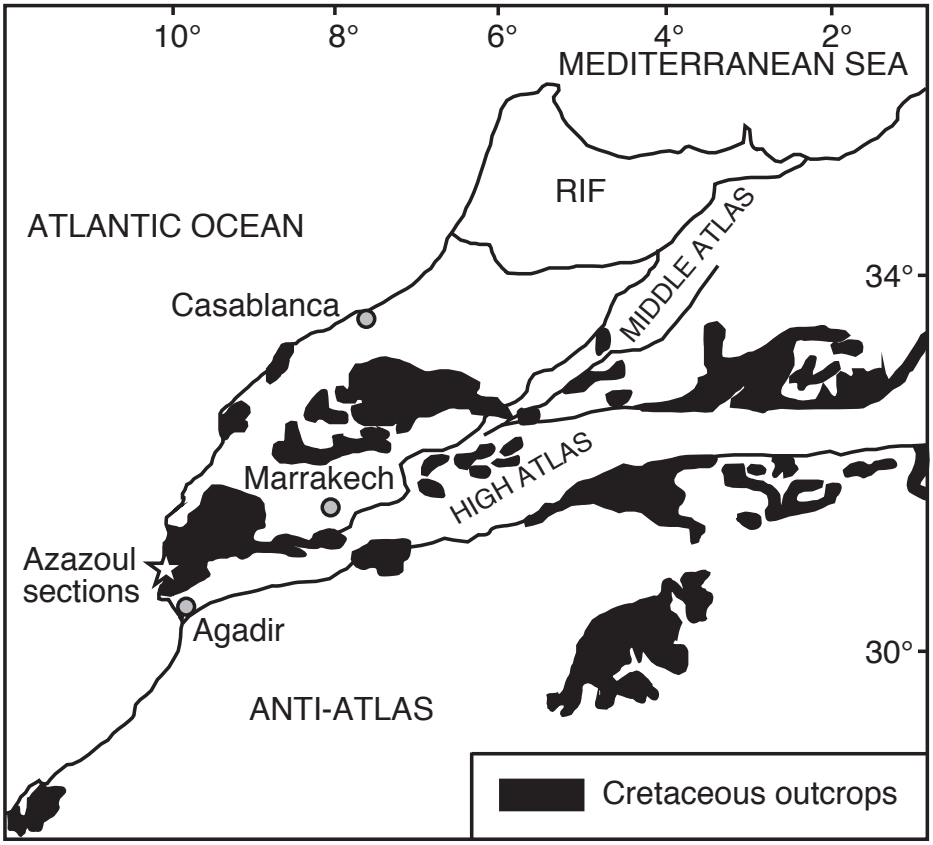

Figure 1: Geological map in north-western Morocco with Cretaceous outcrops (adapted from Ettachfini et al, 2005).

zone, which thrusts middle Cenomanian above late Cenomanian sediments. Consequently, the middle Cenomanian segment is exposed along the Agadir-Essaouira Road, whereas the late Cenomanian to Turonian segment is exposed along the beach (Fig. 1 and 2).

Geologically, the sections are situated on the rim of the Agadir and Essaouira basins, which form the northern part of the Tarfaya basin. During the late Cenomanian-early Turonian, the Agadir and Tarfaya basins were separated by a large marine seaway, which represents a failed rift arm of the North Atlantic Rift System (Luning et al., 2004). In the Agadir basin, sediments consist of organic-poor inner shelf deposits, including alternating marl-limestone layers and oyster-rich limestone beds. Deposition varied between inner to middle shelf environments without major upwelling (Wiedmann, 1978, 1982). Very little is known about these shallow water sequences. In contrast, the more widely studied Tarfaya basin to the south is characterized by thick units of organic-rich marls with high TOC (11-18%) and thin limestones during the late Cenomanian and early Turonian (Kuhnt et al., 1997; Kuypers et al., 2002; Gustaffson et al., 2003; Luning et al., 2004; Kolonic et al., 2005; Kuhnt et al., 2005; Keller et al., in press).

A.P.3. Methods

In the field, the sections were examined for lithological changes, burrows, macrofossils, hardgrounds and erosion surfaces, carefully described, measured and photographed. A total of 92 samples were collected at an average of 25 cm intervals for the Azazoul Beach section and 88 samples for the road outcrop at intervals of about 10 cm. In the laboratory, samples were processed for foraminiferal analysis using standard methods (Keller et al., 2001). Planktic foraminifera are generally rare and present mostly during relatively deeper intervals. Wherever present, 100-200 specimens were counted to obtain the benthic planktic ratio.

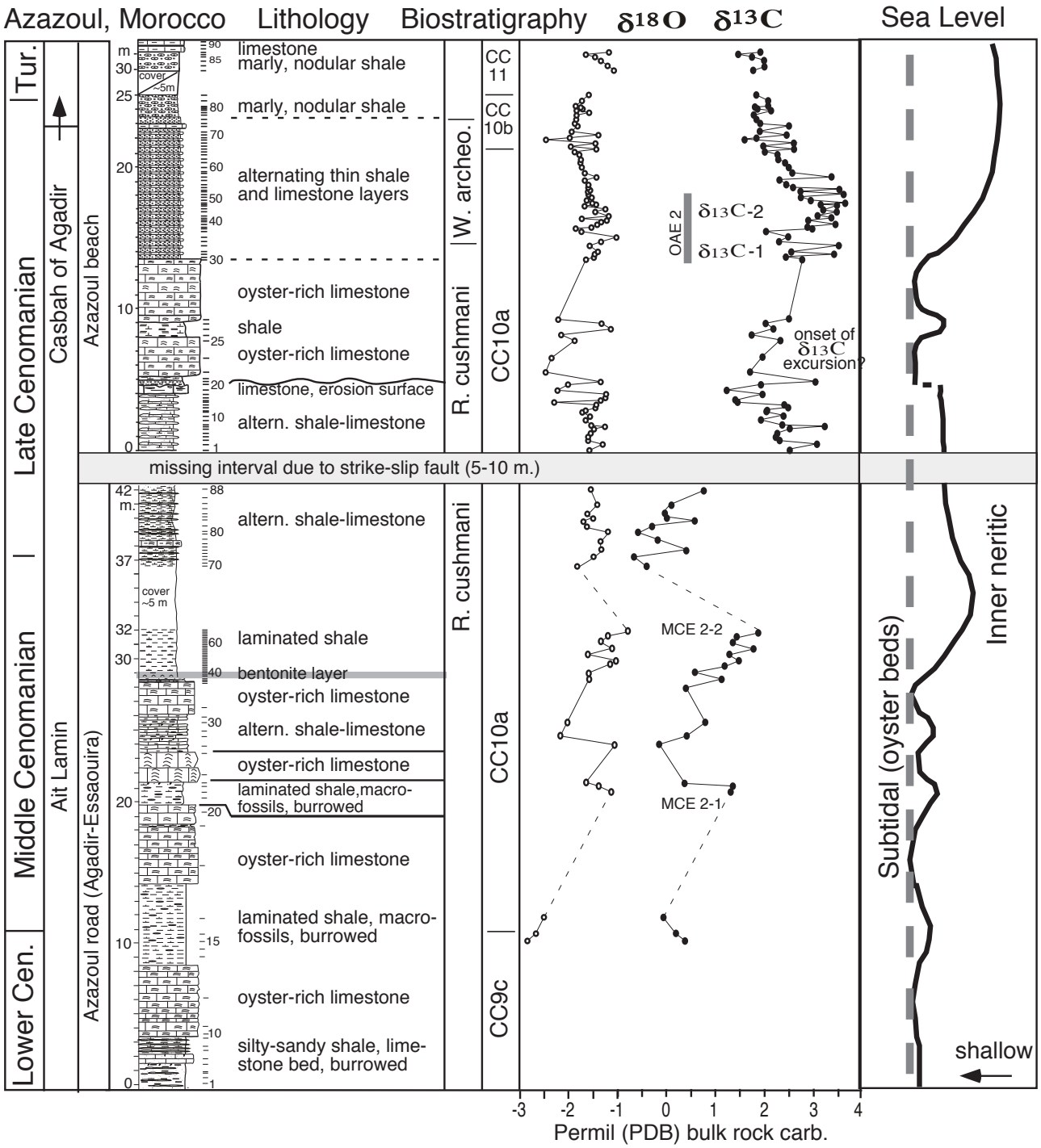

Figure 2:Lithological, biostratigraphic and isotopic results, and sea-level interpretation for the Azazoul sections. Distinction is made between limestone and shale results for carbon and oxygen isotopes.

Samples were processed for nannofossil analysis using methods described in Tantawy et al. (2003) and Perch-Nielsen (1985). Preservation and abundance of nannofossils is variable throughout the sections. In general, preservation is poor to moderate due to dissolution and calcite overgrowth, as evident by high abundance of Watznaueria barnesae (>50%) (Roth and Krumbach, 1986). Abundance of nannoliths in the samples is low (≤ 1 per field of view), though preservation and abundance improves in the upper part of the section.

Carbon and oxygen isotopes were carried out on powdered bulk rock samples at the stable isotope laboratory at the University of Karlsruhe, Germany, using an Optima (Micromass, UK) ratio mass spectrometer equipped with an online

carbonate preparation line (Multi Carb) with separate vials for each sample. The results were calibrated to the PDB scale with standard errors of 0.05 ‰ for δ13C and of 0.1‰ for δ18O.

Mineralogical, rock-eval and total phosphorus quantification analyses were carried out at the Geological Institute of the University of Neuchâtel, Switzerland. Bulk rock and clay mineral assemblages were analyzed by X-ray diffraction. (Scintag XRD 2000 Diffractometer) based on procedures described by Kubler (1983) and Adatte et al. (1996). This method permits the semi-quantification of whole-rock mineralogy based on XRD patterns of random powder samples by using external standards with an error margin between 5 and 10% for the phyllosilicates and 5% for grain minerals.

Clay mineral analysis follows the methods developed by Kubler (1987) and Adatte, et al. (1996). The intensities of the identified minerals are measured for a semi-quantitative estimate of the proportion of clay minerals, which is therefore given in relative percent without correction factors.

Total phosphorus quantification analysis was performed on bulk rock samples, following the procedure of Bodin et al. (2006). The concentration of PO4 in mg/l is obtained by calibration with known standards solutions, using a photospectrometer (Perkin Elmer UV/Vis Photospectrometer Lambda 10).

Rock Eval 6 was performed to obtain oxygen and hydrogen index (OI and HI), Mineral Carbon (MinC) and Total Organic Carbon (TOC) based on methods by Espitalie, (1985) and Behar (2001). Measurements were calibrated using the two standards IFP 160000 and VP143h.

A.P.4. Results

A.P.4.1. Lithology

The middle Cenomanian to early Turonian Azazoul sequence is exposed along the beach (Azazoul beach section) and along the Agadir-Essaouira Road (Azazoul road section) (Figs. 1, 2 and 3). The Azazoul road section spans the middle Cenomanian to the base of the upper Cenomanian. The Azazoul beach section encompasses the late Cenomanian to early Turonian interval. The two sections are tectonically detached by a strike-slip zone where an estimated 5-10 m is missing. Sediment deposition occurred in shallow inner to middle neritic environments, with sea level changes marked by thick oyster-rich limestone beds and alternating thin shale/limestone layers.

The basal 3.5 m of the Azazoul road section consist of burrowed silty-sandy shale layers with a 0.6 m thick limestone (Fig. 2). Above this interval are two, thick, oyster-rich limestone beds (3.5-8.5 m, 14-19.8 m), each overlain by burrowed laminated shale layers (8.5-14 m, 19.8-21.4 m). A 2 m thick oyster-rich limestone bed overlies this interval, followed by alternating shale/limestone layers (23.5-26 m) and another oyster-rich limestone bed (26-28.5 m). Above this sequence is a thin marly shale followed by a 5 cm thick bentonite layer and 3 m of dark laminated shale. For the next five meters the outcrop is covered. Above it, marly shale and thin limestone layers alternate to the top of the outcrop.

At the Azazoul beach outcrop, which continues the section above the strike-slip fault, marly shale and thin limestone layers mark the basal 4 m, followed by a 0.6 m thick burrowed limestone with an erosional surface at the top caused by a gravity-flow deposit made of oyster shells (Fig. 3A and 3B). Above it, are two thick oyster-rich limestones (5-13.5 m) separated by a 1 m thick shale layer (Fig. 3C). Rhythmically bedded thin shale and limestone layers (13.5-22.7 m) (Fig. 3D) mark a change in the depositional environment, followed by a 0.3 m thick limestone bed and marly shale (23-25 m, 30-31 m). A slump covers a 5 m interval of the marly shale (25-30 m). The upper part of the section consists of marly and nodular shale (Fig. 3E and 3F).

A.P.4.2 Stable Isotopes

StablePrimary environmental isotopic signals may be altered by post-depositional diagenetic alteration (e.g., dissolution, cementation, replacement reactions) (Jenkyns et al., 1994).

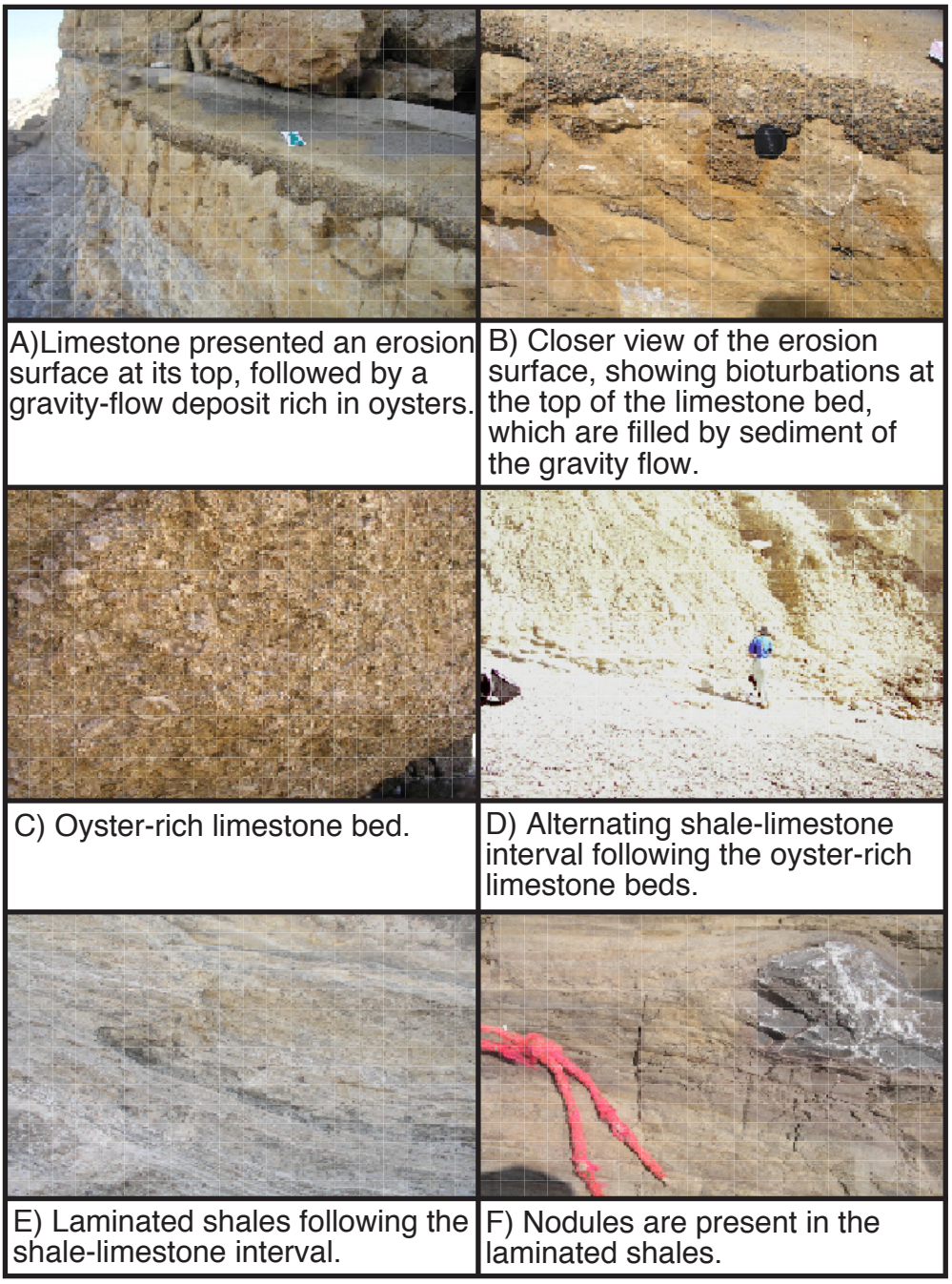

Figure 3:Illustrations of the Azazoul outcrops.

Carbon isotopic values are less prone to alteration during diagenesis than oxygen data due to the low carbon content of pore waters, but shifts can be important where organogenic carbon is incorporated (Marshall, 1992). Oxygen isotopes are more sensitive to diagenetic effects, which may lead to significant lowering of δ18O values due to recrystallization and/or pore water influence (Schrag et al., 1995). Shallow-water carbonates are more likely to undergo diagenesis as a result of meteoric-vadose diagenetic overprinting. However, various studies have demonstrated that the δ13C records of Cretaceous shallow-water sequences with strong diagenetic overprinting can be correlated with well-preserved deep-water sequences (Buonocunto et al., 2002; Davey and Jenkyns, 1999; Grotsch et al., 1998; Jenkyns, 1991).

A cross-plot of carbon- and oxygen-isotope values shows no significant trend for the Azazoul

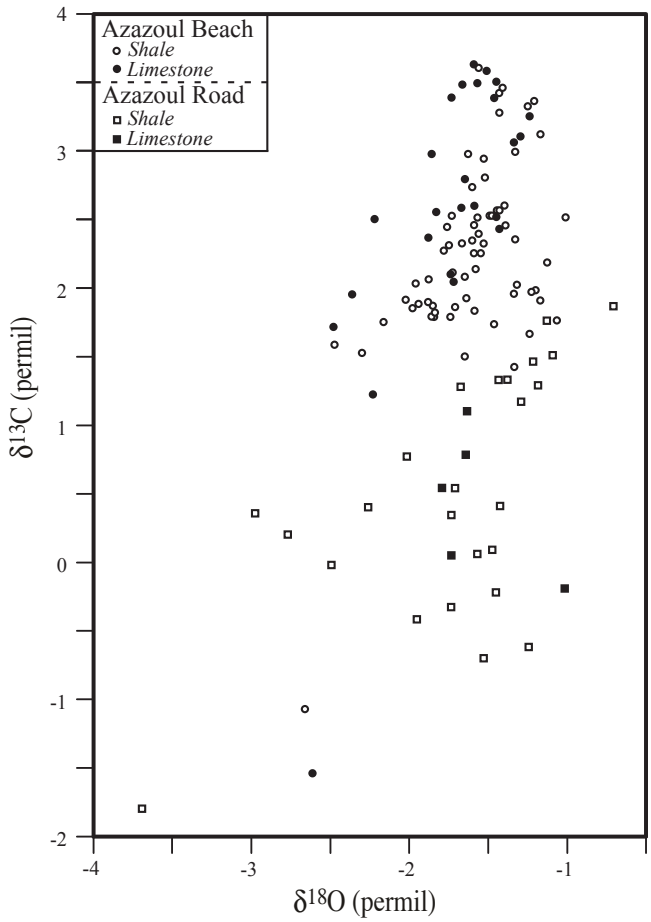

Figure 4:Oxygen versus carbon isotopes plot for Azazoul section with a distinction between shale and limestone. Distinction between results of each section, as well as shale/limestone is made to notice possible correlation.

Road and Azazoul Beach sections, where most δ18O and δ13C values fall in the range of -2.5 to -1‰ and -1 to 3.5‰, respectively, and no distinctive trends due to limestone or shale lithologies are apparent (Fig. 4). The relatively constant δ18O values (-2.5 to -1‰) suggest only minor diagenetic overprinting. Carbon isotopic data can be separated in two groups, with <2‰ in the Azazoul road section and >2‰ in the Azazoul beach section. The higher δ13C values in the Azazoul Beach section reflects the generally higher late Cenomanian values and OAE2 excursion, relative to the lower and middle Cenomanian.

A.P. 4.2.1. Carbon Isotopes

δ13C data of the Azazoul road outcrop are discontinuous due to a slump and poor outcrop exposure (12-18 m). Nevertheless, two δ13C excursions of 1.5‰ and 2.0‰ are apparent in laminated shale layers (Fig. 2). These excursions occur near the base of the middle Cenomanian, just above nannofossil zone CC10a and are characteristic of the two mid-Cenomanian δ13C events (MCE, Jenkyns et al., l994; Rodriguez-Lazaro et al., l998). Above this interval, δ13C values decrease to –0.5‰ and gradually increase to 0.8‰ towards the top of the outcrop.

In the shale/limestone layers (0-4 m) at the base of the Azazoul beach section, δ13C values generally vary between 2.0-2.5‰, except for two higher values (3.1‰, 3.2‰), then drop to 0.2-0.4‰ in the limestone below the erosional unconformity (Fig. 2). An isolated value of 3.0‰ is recorded at the unconformity. Above the unconformity, δ13C values gradually increase from 1.8‰ to 2.8‰ through the oyster-rich limestone and reach the first δ13C excursion maximum of 3.5‰ at the base of the overlying alternating shale/limestone interval. Above it, δ13C values drop to 2.0-2.2‰ (14.5-15.5 m) forming a trough. A rapid increase in δ13C values to 3.7‰ marks the second δ13C excursion with high values persisting from 15.5 m to 17.5 m (Fig. 2). Above the second δ13C excursion, values gradually decrease to around 2‰ by the top of the shale/limestone interval.

A.P.4.2.2. Oxygen Isotopes

Middle and Late Cenomanian δ18O values at the Azazoul road and beach sections narrowly fluctuate between –1 to –2‰. Overall, more positive δ18O values correlate with positive δ13C excursions, particularly during the MCE and OAE2 events (Fig. 2). (For the Azazoul road section, additional samples will be collected and analyzed to delineate the missing intervals in the two MCE events). In the lower part of the Azazoul Beach section, δ18O values decrease from –1.5 to –2.5‰ across the unconformity and increase again in the shale bed between the two oyster limestone layers. A short-term negative δ18O excursion coincides with the trough between the two OAE2 δ13C excursions. Thereafter, δ18O values gradually decrease to the top of the section in parallel with decreasing δ13C values.

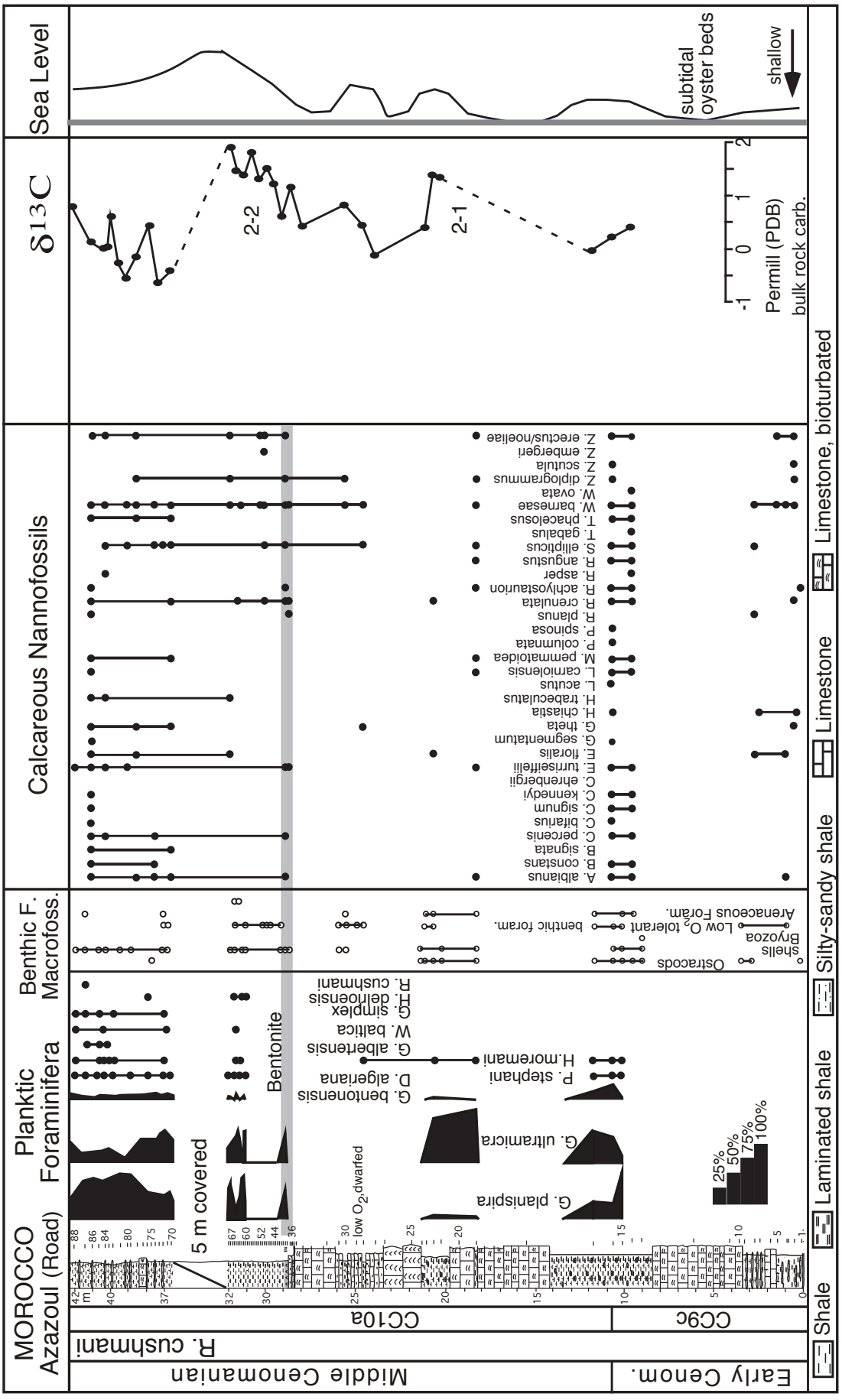

Figure 5:Planktic and benthic foraminifera, macrofossils and calcareous nannofossils results correlated with carbon isotope curve and sea-level changes for the Azazoul Road.

A.4.3. Biostratigraphy and Faunal Turnovers

A.4.3.1. Lower and Middle Cenomanian

Calcareous nannofossils and planktic foraminifera in the lower and middle Cenomanian Azazoul road section are sporadically present in the relatively deeper water shale intervals and mostly absent in the oyster-rich limestones. In the basal silty-sandy shale layers and limestones (0-8 m), planktic foraminifera are absent and rare nannofossils are restricted to the 2.5 m interval at the base (Fig. 5). The first relatively diverse nannofossil assemblage occurs in the laminated shale interval between 8.4-11.5 m, where the first appearance of Lithraphidites acutus at 10.5 m tentatively marks the boundary between CC9c and CC10a (Sissingh, l977; Perch-Nielsen, l985), or UC2/UC3 of Burnett (l996, l998). The overlying Zone CC10a spans the remainder of the Azazoul road outcrop (10.5-42 m), as indicated by the presence of Helena chiastia and co-occurrences of Axopodorhabdus albianus, Corollithion kennedyi and L.acutus.

Small planktic foraminifera first appear in the bioturbated shale between 10-12 m, with assemblages dominated by Globigerinelloides planispira, G. ultramicra and G. bentonensis, few Praeglobotruncana stephani and Heterohelix moremani, but no age diagnostic index species (Fig. 5). Ostracods, bivalves, oysters, bryozoa and low oxygen tolerant benthic foraminifera are also present. A similar impoverished assemblage dominated by G. ultramicra and rare nanofossils occurs between 18.5-21 m associated with elevated δ13C values, which may mark the first of two mid-Cenomanian δ13C events (MCE). Very rare nannofossils and dwarfed (<63μm) low oxygen tolerant planktic (H. moremani) and benthic foraminifera are present in the shale/limestone interval (24-26 m). A prominent bentonite layer above an oyster-rich limestone bed (at 29 m) marks the end of this impoverished interval.

In the alternating thin shale/limestone layers (29-32 m) above the bentonite, planktic foraminiferal and nannofossil assemblages are more diverse and associated with the second mid-Cenomanian δ13C excursion (MCE 2-2, Fig. 5). Whiteinella baltica first appears at the top of this interval, consistent with the middle Cenomanian age (CC10a) of the nannofossil assemblage. A slump covers the next five meters of the section. Above it, small planktic foraminifera are common to abundant and more diverse (e.g., Heterohelix moremani, Guembelitria albertensis, Whiteinella baltica, Hedbergella delrioensis, Globigerinelloides simplex. The first appearance of the deeper dwelling Rotalipora cushmani in this interval reflects the sea level transgression, rather than its evolutionary appearance. δ13C values are 2.5‰ lower above the covered interval and increase towards the top of the section. The Azazoul road section is truncated by a strike-slip fault, which physically offsets it from the Azazoul beach section. An unknown interval is missing between the two sections, which may be as little as 5-10 m.

A.4.3.2. Upper Cenomanian

The late Cenomanian exposed along the Azazoul beach (Fig. 2) continues with similar lithologies and impoverished nannofossil and planktic foraminiferal assemblages as the lower to middle Cenomanian interval (Fig. 6). More diverse microfossil assemblages are restricted to laminated shale intervals, whereas the prominent oyster-rich limestones (5-13 m) generally contain no microfossils. The low abundance of planktic relative to benthic foraminifera indicates a very shallow high stress environment. Nannofossil assemblages are characteristic of zone CC10a. The presence of Whiteinella archeocretacea, R. cushmani and R. greenhornensis at the base of the section (0-4.5 m) marks this interval as Late Cenomanian in age. An unknown interval is missing at the erosional unconformity at the top of the limestone (4.5 m).

The unconformity marks the onset of a gradual increase in δ13C values through the oyster-rich limestone beds and culminates in the first of two shifts at the base of a thinly bedded shale/limestone interval. Low diversity small planktic foraminifera dominate (e.g., Guembelitria cenomana, H. moremani, H. planispira) through the two δ13C shifts and high abundance of the low oxygen tolerant Heterohelix mark this interval as OAE2 and the W. archeocretacea zone (Heterohelix subzone of Keller et al., 2001; Keller and Pardo, 2004). Low oxygen tolerant benthic foraminifera dominate this

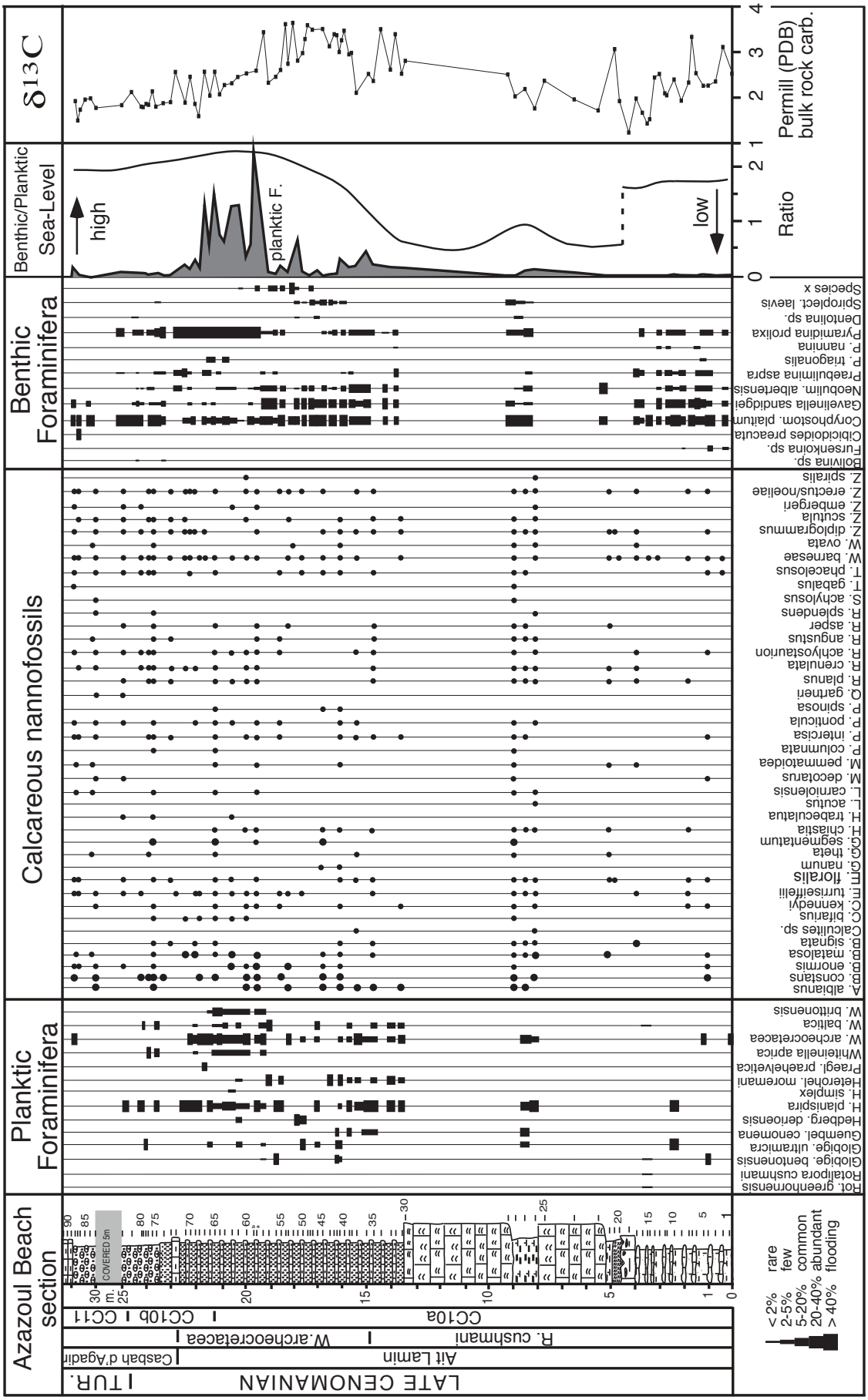

Figure 6:Planktic and benthic foraminifera, planktic/benthic foraminifera ratio and calcareous nannofossils results for the Azazoul Beach section, together with carbon isotope results and sea-level interpretation.

interval (e.g., Coryphostoma plaitum, Neobulimina albertensis, Gavelinella sandigei, Pyramidina prolixa, Fig. 6). An increase in planktic abundance indicates a rising sea level (Fig. 6). Rotalipora cushmani is absent making it difficult to mark the top of the R. cushmani zone. However, this species is known to disappear in the trough between the two δ13C shifts and nearly coincident with the onset of abundant Heterohelix, which places this boundary at about 15 m. Above the second δ13C shift, microfossils assemblages increase in diversity and abundance along with the gradual decrease in δ13C values. Increased abundance of W. archeocretacea and decreased abundance of low oxygen tolerant benthic species (19.5-22.5 m) mark a return to more normal oxic conditions. Sea level remained relatively high, as indicated by nodular shale deposition. The benthic/planktic ratio is low due to poor preservation of planktics and hence the relative increase in robust benthic species.

Nannofossil assemblages record the last occurrence of Helena chiastia, the marker for the CC10a/CC10b boundary at 21.3 m, A. albianus at 30 m and C. kennedyi at 24.6 m. The simultaneous LOs of A. albianus and H. chiastia are consistently observed and following the disappearance of C. kennedyi (Bralower, 1988; Burnett, 1998, Tantawy, in review). However, in the Azazoul Beach section, C. kennedyi seems to disappears above the LA of H. chiastia (Fig. 6), which may be due to reworking or the diachronous LA of this species as previously observed in North Africa and Italy (Robaszynski et al., 1990; Luciani and Cobianchi, 1999).

The Cenomanian-Turonian boundary is identified at 25 m within the plateau above the two δ13C shifts by the first appearance of Quadrum gartneri, which marks the base of CC11 (=UC7 of Burnett, l998). The stratigraphically consistent first appearance of Q. gartneri at or near the C/T boundary, as defined by ammonite stratigraphy, and within the δ13C plateau at Pueblo, Colorado (USA), Eastbourne, England, Gubbio, Italy and Tarfaya, Morocco, provides a reliable stratigraphic marker for the C/T boundary and the duration of OAE 2 (Tsikos et al., 2004; Kennedy et al., 2006). The planktic foraminifera C/T boundary marker H. helvetica was not observed.

A.P.4.4. Mineraological Analysis

A.P.4.4.1. Bulk rock

Calcite, quartz and phyllosilicate dominate in the Azazoul beach section (Fig. 7). Values are highly variable and reflect the alternating shale/ limestone layers, which represent very different depositional environments. To evaluate these environmental trends, shale and limestone signals can be viewed separately. Calcite in shales (white dots) varies between 20% and 60% in the upper half of the section, whereas in the limestone layers (black dots) calcite varies from 80% to 90%. Calcite also dominates in the limestone layers of the lower half of the section (80-90%), whereas the marly intervals vary between 60-80% calcite. Very low calcite values occur in the shale just below the first oyster-rich limestone bed (5 m) and in the laminated shale (<20%, 8-9 m) between the two thick limestone layers (Fig. 7).

Similar trends are seen in quartz and phyllosilicates + unquantified with quartz averaging between 5-10%, but reaching 20% in the shale intervals. Phyllosilicates plus the unquantified component were added together because they show similar trends, which suggest that most of the unquantified minerals correspond to phyllosilicates. Highest phyllosilicate + unquantified values correspond with high quartz and low calcite contents. In some intervals, K-Feldspar and Na-Plagioclase reach 3% and 7%, respectively (Fig.7). The Detritus/Calcite index (D/C=(quartz+phyllosilicates+K-feldspars+Na-Plagioclase/ Calcite) shows very low values in the lower half of the section, including the massive oyster-rich limestones, except for the marly shale between 8-9 m. Higher D/C ratios (0.5-2) mark the upper part of the section.

A.P.4.4.2. Clay minerals

Clay assemblages consist of kaolinite, chlorite, smectite, illite and I-S mixed layer (Fig. 8). A three-point average curve shows consistent overall trends with little local variation. Smectite dominates (70-80%) between 0-4 m. and 15-31 m, whereas kaolinite and chlorite dominate in the low smectite interval (4-15 m). Illite remains low with values

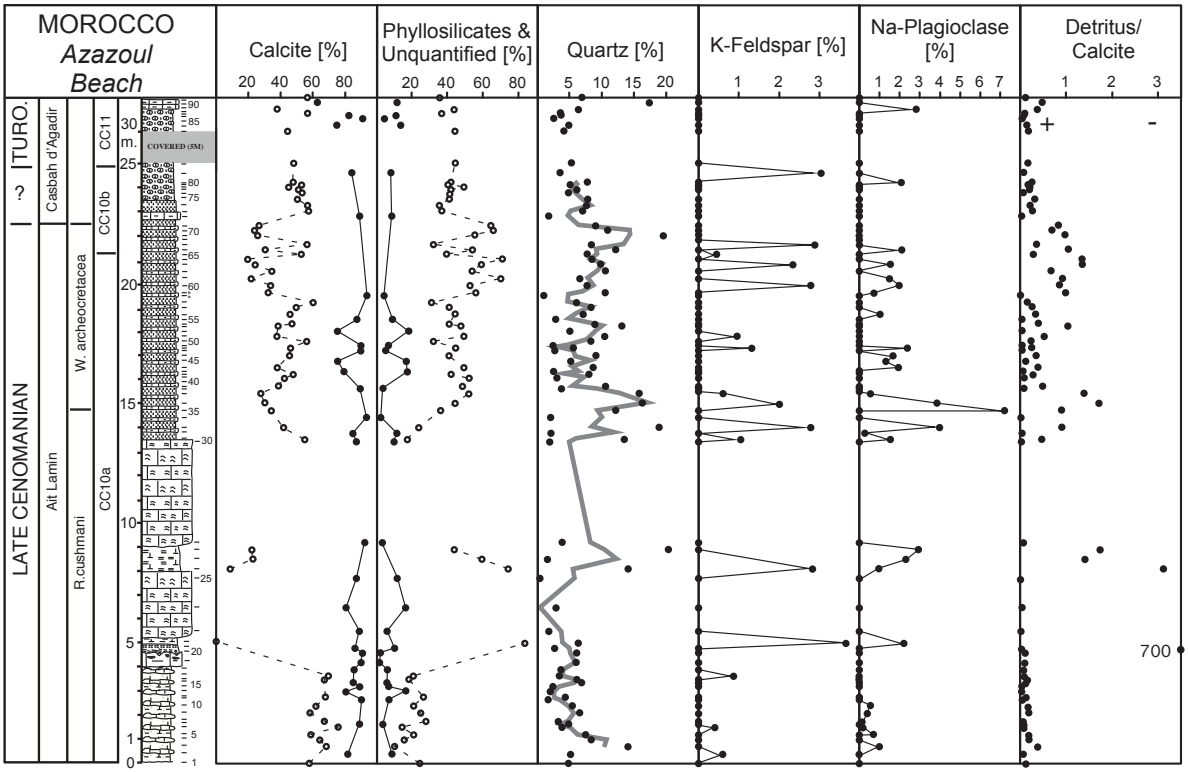

Figure 7: Bulk rock results for the Azazoul Beach section. Distinction is made between limestone (black dots) and shale (white dots) results for calcite, phyllosilicates and unquantified results.

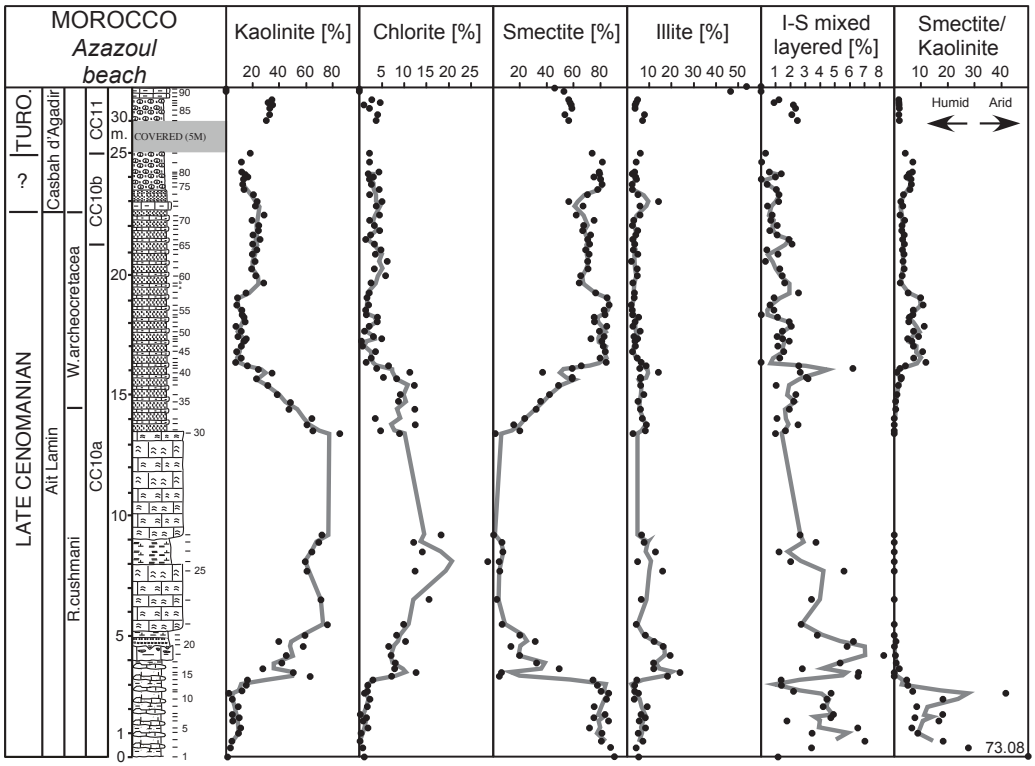

Figure 8: Clay mineralogy results for the Azazoul Beach section.

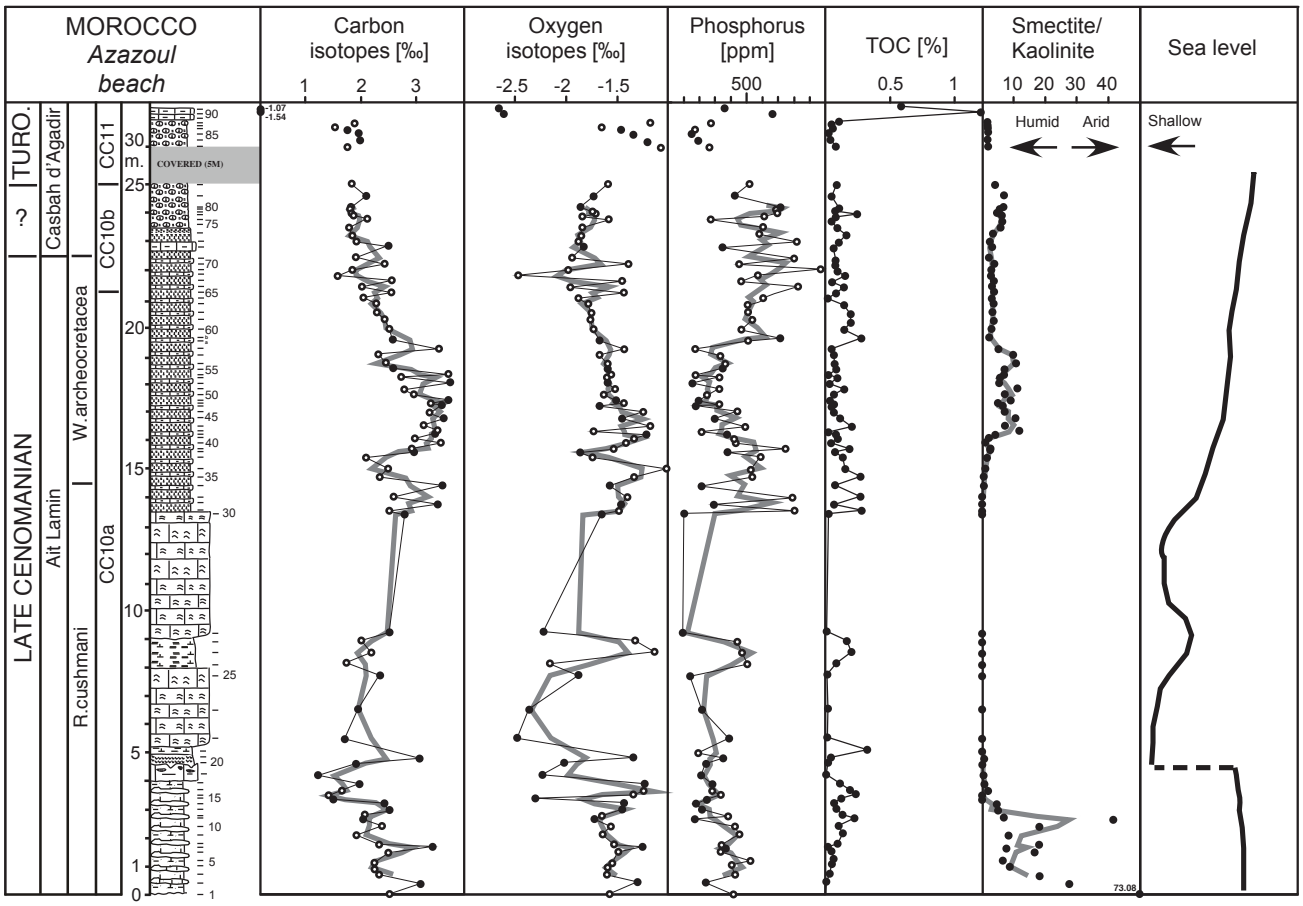

Figure 9:Summary figure with carbon and oxygen isotope curves, phosphorus concentrations, Total Organic Carbon, aridity index (smectite/kaolinite) and sea level interpretations for the Azazoul Beach section. Distinction is made between limestone (black dots) and shale (white dots) results for carbon and oxygen isotopes, and phosphorus concentrations.

around 5%, except in some shale and marly shale intervals (3.5-5 m. and 8-9 m) where values reach 20%. Maximum values (50%) are recorded at the top of the section. The smectite/kaolinite ratio is an aridity index (Chamley, 1989; Pardo et al., 1999), which shows high ratios (10 and 73) in the basal 4 m of the section and increased ratios (5-10) in the upper part.

A.P.4.5. Rock-Eval

Rock-Eval pyrolysis data of the Azazoul Beach section indicates that average total organic carbon (TOC) values are very low (0-0.3%), except for 0.6 and 1% in the last two samples at the top of the section (Fig 9). TOC values are at a minimum in the oyster-rich limestone. Origin and maturity of the organic matter can be deduced by pyrolytic measurements (Espitalie, 1985; Behar, 2001). Determination of the hydrogen index (HI) and oxygen index (OI) allows characterizing the type of organic matter. At Azazoul beach, organic matter has a terrestrial origin signal (type III), except for the two samples, which indicate marine organic matter origin (type II) (Fig. 10).

A.P.4.6. Total phosphorus analysis

Total phosphorus contents show values from 100 to 1000 ppm for the Azazoul Beach section (Fig. 9). From the base of the Azazoul beach section to the top of the second oyster bed, values between 200 and 500 ppm are recorded with the lowest data in the oyster beds. After the top of the second oyster bed, a first peak reaching value of 900 ppm is recorded, followed by a decrease to 200 ppm until 19 m. Although data show a lot of scatter near the top of the section, a second peak

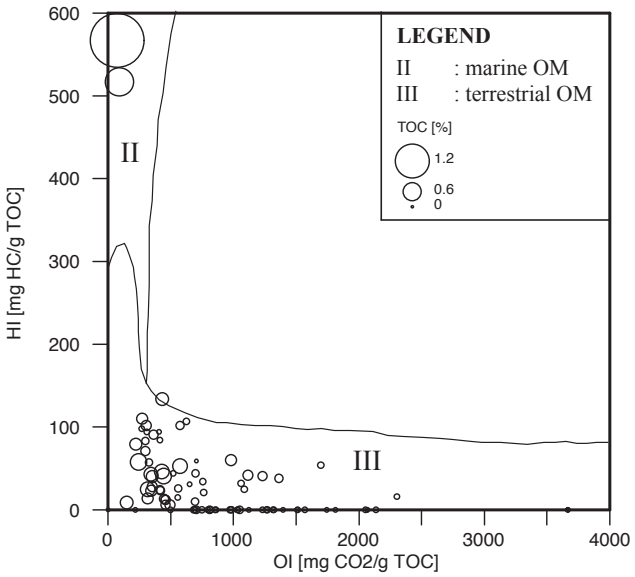

Figure 10: OI index versus HI showing the origin of the organic matter, together with the TOC.

occurs around 22 m, just 0.8 below the nannofossil defined C/T boundary.

A.P.4.7. Discussion

A.P.4.7.1. Paleoenvironment and Sea-level Changes

A.P.4.7.1.1. Oyster ecology

A key feature of the shallow water Azazoul sections is the presence of oyster-rich limestone beds during the middle and late Cenomanian, as also observed in the late Cenomanian of Egypt and Israel (Bauer et al., 2001; Gertsch et al., in prep). At Azazoul, these oyster beds are mainly thick tabular and laterally extensive oyster biostromes, indicative of shallow subtidal environments (Abed and Sadaqh, 1998). Exceptions are the thin oyster-rich beds above the unconformity at 4.5-5 m (Fig. 5) and at the onset of the late Cenomanian δ13C excursion. This oyster bed at 4.5-5 m has an eroded and bioturbated base, which suggests a gravity-flow deposit originating upward on the ramp due to a short-term sea-level regression.

In the Eastern Desert of Egypt, oyster biostromes and bioherms are characterized by low diversity and rapid growth as a result of reduced competition by other organisms for space and nutrients and lack of predation (Abed and Sadaqh, 1998). They are wave-resistant structures that formed in high-energy, shallow, faunally restricted environments and imply brackish conditions, similar to modern oysters, which tolerate a wide range of environmental conditions (Glenn and Arthur, 1990; Pufahl et al, 2006). Their success is largely a result of high reproduction rates, which enables these stress tolerant r-strategists to thrive by responding quickly to environmental perturbations, including low salinity, mesotrophic nutrient level and a turbid water column. In these aspects, oysters are opportunistic species, similar to the planktic foraminifera Guembelitria (a disaster opportunist that thrived in nutrient-rich surface waters) and Heterohelix (low oxygen tolerant, Keller and Pardo, 2004b). In addition, oyster communities play a key role in nutrient recycling through prolific feces production that stimulates filter feeders and supports extensive sea grass beds. Degradation of these organic-rich sediments under aerobic and dysaerobic conditions returns N and P to the water column (Froelich et al., 1979; Libes, 1992).

A.P.4.7.1.2. Sea-level change

The late Cenomanian/early Turonian is characterized by a major global sea-level transgression (Haq et al, 1987). Sea level changes in the Agadir area can be inferred from oysters and the foraminiferal planktic/benthic ratio (Fig. 2). Oyster beds indicate deposition in a subtidal environment at no more than 10 m depth. The frequent oyster-rich limestones in the lower and middle Cenomanian of the Azazoul road section indicate repeated subtidal environments alternating with drowning of oyster biostromes and the influx of open marine microplankton during higher sea levels (inner neritic depth). This is also indicated by the high abundance of low oxygen tolerant benthic foraminifera, dominated by Coryphostoma plaitum, Gavelinella sandidgei and Neobulimina albertensis in the shale layers, but absence in oyster-rich limestones (Figs. 5, 6). Major sea level transgressions are associated with the MCE (2-2) and OAE2 following oyster-rich limestone deposits. The late Cenomanian transgression was

larger and lasted longer, as indicated by a major increase in the planktic/benthic ratio, influx of open marine species and dysoxia in the water column (Fig. 6). Sea level remained relatively high into the early Turonian, as indicated by nodular marly shale deposition. The low benthic/planktic ratio in this interval is partly due to poor preservation.

A.P.4.7.1.2. Palaeoenvironment

The faunal and floral turnovers of the middle and late Cenomanian have been widely described from deeper water sequences (e.g., Colorado, England, Italy, Tunisia, and the Tarfaya Basin of Morocco). Biotic changes in shallow water sequences are more difficult to quantify due to sporadic occurrence of marine microfossils and rarity or absence of age diagnostic index species. This is also a problem in the Azazoul beach section, although it was possible to interpret the age and paleoenvironment based on the integration of macro- and microfossils, the carbon isotope record, sedimentology, mineralogy and geochemistry.

Benthic foraminiferal assemblages consists largely of abundant low oxygen tolerant species (e.g., Coryphostoma plaitum, Gavelinella sandidgei and Neobulimina albertensis, Pyramidina prolixa, Fig. 5 and 6) suggesting a generally dysoxic bottom environment, probably due to high nutrient influx. Planktic foraminiferal assemblages consist of small, high stress tolerant species able to thrive in low salinity environments (Hedbergella planispira, Keller and Pardo, 2004a), nutrient-rich surface waters (Guembelitria cenomena, Keller and Pardo, 2004b) and a low oxygen water column (Heterohelix moremani). Species unable to thrive in these environments and those requiring deeper neritic habitats are excluded or extremely rare in the Azazoul sections. Return to a more oxic water column after OAE2 is marked by the high percentages of Whiteinella archeocretacea (after sample 57) and by increased abundance of planktic foraminifera.

Paleoenvironmental information based on nannofossils is also limited by dissolution effects, as indicated by increased abundance of W. barnesae, one of the most solution resistant forms (Roth and Krumbach, 1986; Lamolda et al., 1994; Paul et al., 1994; Tantawy, in press). Zeugrhabdotus spp., an indicator for high surface water fertility or eutrophic conditions (Roth and Krumbach, 1986; Shafik, 1990; Watkins et al., 1996; Premoli Silva et al., 1999; Lees, 2002), is abundant in the alternating shale/limestone layers (upper CC10a) correlative with OAE2 and the δ13C excursion in the Azazoul beach section, as also observed in the Tarfaya basin (Tantawy, in press). Broinsonia spp. (B. signata + B. matalosa), indicators of shallow depth, reduced salinity or high fertility (Roth and Krumbach, 1986; Bralower, 1988; Paul et al., 1994, 1999) are present through the Azazoul sections.

Thus, planktic and benthic foraminifera and nannofossil assemblages indicate disoxic, brackish and mesotrophic conditions during inner neritic depths associated with shale deposition, and general absence of microfossils during subtidal (<10 m) oyster-rich limestone deposition. Return to more oxic conditions occurred after the OAE2 δ13C excursion, but prior to the Cenomanian/Turonian boundary.

A.P. 4.7.2. Carbon isotope geochemistry

The carbon isotope record of the OAE2 in shallow-water environments has been little studied. In the peri-Adriatic platform (Croatia, Davey and Jenkyns, 1999) and the carbonate platform of the south-central Pyrenees in Spain (Drzewiecki and Simo, 1997), the late Cenomanian δ13C excursion was observed to be comparable to deep-water sequences. However, at Azazoul the onset of the δ13C excursion is difficult to place because of the oyster-rich limestone beds where the excursion may be placed either in the shale layer between the two oyster-rich limestone beds, or above the unconformity below the base of the oyster-rich limestone interval. The latter would place the onset of the δ13C excursion at a hiatus. In this case, the oyster-rich limestone beds would have been deposited in a relatively short time period, which is consistent with rapid oyster growth (Abed and Sadaqah, 1998).

A.P. 4.7.3. Paleoclimatic evolution

A.P.4.7.3.1. Paleoclimatic evolution based on oxygen isotopes

Several physical processes can affect the evolution of δ18O: diagenesis, mixing between water masses with different salinities and isotopic compositions (Wolff et al., 1999), and changes in the precipitation-evaporation cycle. Diagenesis leads to significant lowering of δ18O due to recrystallization and/or pore water influence (Schrag et al., 1995). As noted above (section 5.4), the δ18O record of Azazoul does not present substantial diagenetic effect, although very low values at the top of section seem to be influenced by diagenesis. The precipitation-evaporation cycle, which is the most important process influencing δ18O trends in shallow waters, is caused by temperature changes and thus permits inferences regarding cooling and warming trends.

The consequences of mixing between water masses with different salinities and isotopic compositions are well illustrated by Keller et al. (2004). Based on δ18O, salinity-sensitive foraminifera (e.g. Hedbergella planispira) and mineralogy of the Cenomanian-Turonian interval at Pueblo, the δ18O trends were interpreted as a result of salinity changes due to freshwater influx into the shallow marine environment. Low δ18O values, high abundance of H. planispira and high clastic influx occurred at times when freshwater mixed with marine water, due to its lower δ18O. At Azazoul, salinity effects are difficult to see due to the poor and incomplete biostratigraphic record. Neverthless, the effects of salinity cannot be ruled out, because the sections were deposited in nearshore shallow marine environments. Hedbergella planispira, which is tolerant of salinity fluctuations, is present in the upper part of the section, but no correlation is apparent between their species abundance, low δ18O and high clastic influx. However, oysters-rich limestone beds, which were deposited in brackish waters (section 8.1.1), correlate with low δ18O and high clastic influx (section 8.3.2). Thus, this interval can be interpreted in terms of low salinity due to freshwater influx. Based on these considerations, temperature and salinity changes are inferred to have influenced the δ18O trends at Azazoul. Although it is difficult to differentiate salinity from temperature signals, it seems that, with the exception of the oyster-rich limestone beds, δ18O trends at Azazoul are mostly due to temperature changes.

δ18O variations indicate overall warm, but fluctuating conditions during the middle and late Cenomanian with relatively cooler temperatures prevailing during the MCE and OAE2 excursions (Fig. 2). Above the unconformity at 4.5 m, the oyster-rich limestone beds record lowest δ18O, possibly due to influx of low salinity water at the time of deposition. Relatively cool temperatures reached a maximum with the first δ13C peak just above the oyster beds and continued through the second δ13C peak, with warmer temperatures marking the trough. Above the δ13C excursion, climate gradually warmed up to the Cenomanian-Turonian boundary. This general trend of relatively constant cool temperatures from the middle Cenomanian to the end of the δ13C excursion, followed by warming that reached a maximum near the Cenomanian-Turonian boundary, is consistent with other studies (Wilson et al., 2002)

A.P.4.7.3.2. Paleoclimatic evolution inferred from mineralogy

Bulk rock mineralogy shows low detritus/calcite ratio (D/C<1), which suggests periods of low detrital input due to weak continental runoff, as observed at the Azazoul Beach section in the shale/limestone alternations of the basal 4 m of the section. However, in the oyster-rich limestone beds and marly shales (5-13.5 m) the very low D/C ratios are due to the dominance of oysters (90% calcite) and near absence of detritus, which cannot be interpreted in terms of weak continental runoff. The highest D/C ratios are seen in the marly shale between the two oyster-rich limestone beds. This suggests a period of high continental runoff due to increased humidity on the Western African margin. However, since oysters depend on nutrient-rich waters to grow and the nutrients in shallow shore environments are largely derived from continental runoff, we may assume that terrigenous runoff continued through the oyster-rich limestone beds. The alternating marl-limestone interval overlying

the oyster-rich limestone bed shows a lower D/C ratios suggesting weaker continental runoff, except for some periods.

The formation of clay minerals in terrestrial soils depends on the type of rocks and the climatic conditions, which vary with latitudes. Kaolinite and smectite are the major clay components. Kaolinite forms under humid conditions in equatorial soils. Smectite forms on tropical soils under dry, seasonal climate, or alteration of basalts (Chamley, 1989). Apart from climate, the distribution of clay minerals is influenced by authigenesis (Chamley, 1989; Kubler, 2000) and the differential settling of kaolinite versus smectite (Thiry, 2000; Godet et al., in press). Authigenesis, which refers to the recrystallization of new minerals during diagenetic processes, generally associated with tectonic activity and/or burial depth, may influence the composition of clay assemblages. However, authigenesis is not a significant influence in the clay composition of the Azazoul Beach section because of the weak tectonic history of the area and the low burial depth. Differential settling of smectite and kaolinite is difficult to evaluate in a single sequence and would benefit from comparison with deeper water sequences in the Tarfaya basin, though such data are not available to date. However, it seems reasonable to infer that no or only little differential settling occurred in the Azazoul paleoenvironment because no carbonate platform separates Azazoul from the Tarfaya basin to the south, except for the oyster reefs present in the Azazoul sections. Due to the high content of the main clay mineral (kaolinite for the lower part and smectite for the upper part), the clay minerals of the Azazoul Beach section therefore most likely reflect climatic conditions.

Within these constraints, the smectite-dominated 4 m at the base of the section can be interpreted as arid and seasonal climate. This interval is followed by a more humid period dominated by kaolinite from 4 to 15 meters spanning the oyster-rich limestone beds. In the upper half of the section, arid dry seasonal conditions returned (smectite dominance). These interpretations are consistent with previous conclusions based on bulk rock mineralogy, which shows stronger continental runoff due to more humid conditions coincident with oyster-rich limestone and abundant kaolinite.

Paleoclimate interpretations inferred from mineralogy and oxygen isotope suggest overall warming and increased humidity in the lower part of the section (4.5 m) below the unconformity. In the oyster-rich limestone beds, humid and cooler conditions prevailed. The alternating marls/limestone layers suggest gradual warming up to the Cenomanian-Turonian boundary, with a rapid change towards more arid and seasonal climate.

A.P.4.7.4. Paleoproductivity inferred by TOC and Phosphorus

TOC and total phosphorus quantification were carried out to test the hypothesis that the behavior of phosphorus (P) and carbon (C) during OAE2 can be used to evaluate the roles of productivity and nutrient cycling, and to understand the feedback between anoxic conditions, P regeneration and sustained productivity (Mort et al., in press).

TOC shows very low contents for the Azazoul Beach section, except for the two last samples. It is unclear whether organic matter contents are low due to weathering or to low bioproductivity. The origin of organic carbon in the section (Fig. 10) provides some clues and shows that organic matter is primarily of terrestrial origin, which is mainly due to the proximity of continents and high continental runoff during more humid periods. However, at the top of the section, two samples show a marine origin for the organic matter and many samples show high OI values (>500 mg CO2/g TOC) indicating alteration and oxidation of organic matter. Occurrence of marine organic matter and high TOC at the top of the section suggests that some samples with high OI of the organic matter, may have a marine origin, though were subsequently altered and oxidized (similar to Tazra, Keller et al., in press). Even though rare samples may contain altered marine organic matter, the origin of organic matter is mainly terrestrial.

These results suggest that terrestrial organic matter was carried from the continents to the coastal environments, where it was redeposited. Poor preservation of terrestrial and marine organic matter can be inferred from the low TOC in the sediments

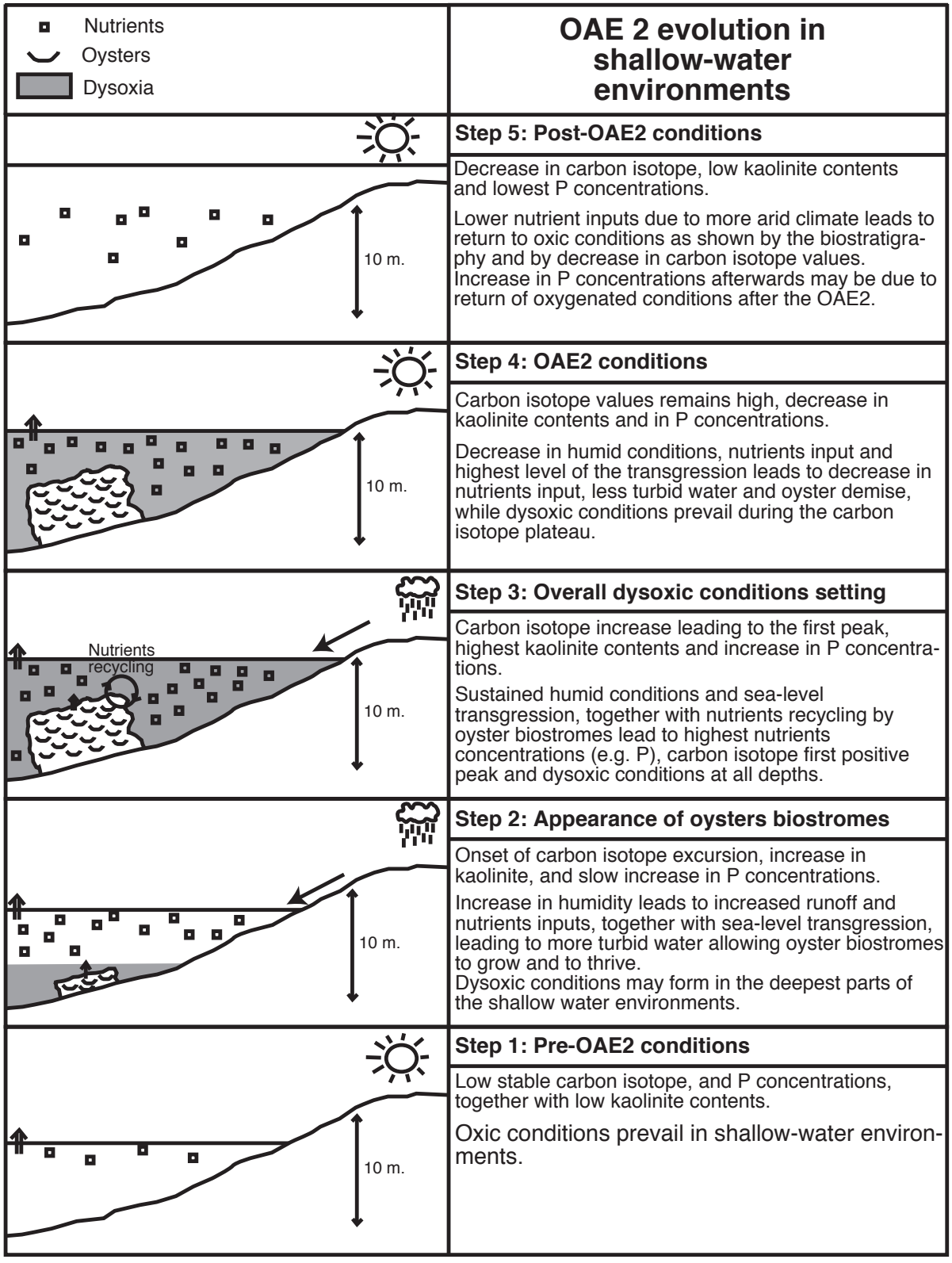

Figure 11: Model of the OAE2 in shallow water environments of the Azazoul sections.

and the high OI of some samples, suggesting that dysoxia in these environments was not strong enough to allow organic matter preservation.

Highest P concentrations are reached between the two oyster-rich limestone beds and after the last oyster-rich limestone bed (Fig. 9) when carbon isotope data are rising to the first peak. Decrease in P concentrations occurs during the carbon isotope excursion and lowest P concentrations are reached at the end of the carbon excursion, which agrees with Mort et al. (in press), although the separation between total phosphorus concentrations and δ13C peaks indicating a decoupling of P and C cycle is not evident at Azazoul. This could be explained by oyster deposits, which, perhaps, are not able to record P concentrations in the same way as limestone or shale.

The model of a decoupling of P and C cycle during OAE 2 postulated by Mort et al. (in press) is based on P concentrations, δ13C and TOC recorded in several sections from different paleodepths from the basin to shallow-water environments (e.g. Manilva, Furlo: basin; Pueblo, Eastbourne: 150-300 m.). Based on this model, P accumulates preferentially in sediments under oxic oceanic conditions. High concentrations of P may be due to a sea-level transgression and/or more humid climate. This in turn would lead to maximum P concentrations prior to the carbon isotope excursion, when oceanic conditions are still relatively oxic and permit the accumulation of P in the sediments.

At Azazoul, peak P concentrations are observed just prior to the first δ13C peak, consistent with the observations in deep-sea sections of Mort et al. (in press). However, comparison is limited at Azazoul by the absence of data in the 4 m thick oyster bed below this peak, which prevents conclusions as to the nature of this P increase. In addition, there is also the possibility of post-depositional diagenesis affecting P concentrations. For example, P could have been accumulated as a single peak, due to its high mobility in the sediment or due to diagenesis in the case of shallow-water sections. Further work will be necessary to explain the behavior of P in sediments that may have been affected by diagenesis.

A.P.4.8. General model for the OAE2 in shallow-water environments

The evolution of the late Cenomanian OAE2 can be explained by a model of feedbacks between the roles of oysters, δ13C peak, organic matter origin, climate and sea-level changes in shallow-water environments (Fig. 11).

(1) In pre-OAE2 conditions, climate is arid and seasonal with low continental runoff, low P concentrations and low δ13C values in oxic conditions.

(2) The appearance of oyster biostromes marks the onset of OAE2 with a gradual increase in δ13C and kaolinite contents leading to more humid conditions. The consequences of this climate change are increased continental runoff and nutrients input into the ocean. In shallow water/coastal environments, this leads to more turbid, brackish, nutrient-rich and dysoxic waters conducive to growth of oyster biostromes, and to thriving high stress foraminifera and nannofossil species.

(3) Overall dysoxic conditions in shallow-water/coastal environments are characterized by δ13C increase, high kaolinite contents and increased P concentrations. The development of dysoxic conditions in the whole water column is caused by sustained runoff, nutrient recycling by oyster biostromes and continued sea-level transgression.

(4) OAE 2 conditions are characterized by the δ13C plateau, decrease in kaolinite contents and P concentrations. Decreased humidity and continental runoff lead to decreased nutrient input and less turbid waters, which in turn cause the demise of oyster biostromes. Consequently, δ13C values stabilize, but remain at high values for some time, because of the sustained productivity due to dysoxic conditions (Mort et al., in press).

(5) Post-OAE 2 conditions are marked by a decrease in δ13C values and similar conditions than pre-OAE 2 conditions.

A.P.5. Conclusion

Inner shelf/coastal sequences have been rarely used to understand the OAE 2 during the late Cenomanian. This is in part due to the lack of biostratigraphic control and possible hiatuses. However, multi-disciplinary studies of such sequences can significantly improve knowledge of OAE2 in shallow water environments, such as Azazoul in northeastern Morocco. The following conclusions can be drawn for the OAE2 in this shallow water sequence:

(1) The δ13C excursion that characterizes the OAE2 is recorded in very shallow water sequences comparable trends to the GSSP section at Pueblo, Colorado.

(2) Age control can be achieved based on the integration of microfossil (nannofossils and planktic foraminifera), macrofossil (ammonites), and carbon isotope stratigraphies.

Presence of high stress benthic and planktic foraminifera, nannofossil species and oyster biostromes during the OAE2 confirms that dysoxic conditions prevailed in very shallow waters.

Oyster biostromes, which are present in several sub-tropical areas (Morocco, Egypt, Israel), played an important role in nutrient recycling, which may have triggered sustained and/or increased nutrients levels in shallow-water environments at the onset of OAE2.

Mineralogical results suggest that a humid climate and increased terrigenous runoff, and probably higher sea level, increased the nutrient supply and lead to the δ13C excursion and dysoxic conditions in shallow nearshore marine environments.

References

Abed, A.M., and Sadaqah, R. (1998). “Role of upper Cretaceous oyster bioherms in the deposition and accumulation of high-grade phosphorites in central Jordan”. Journal of Sedimentary Research 68, no 68: 1009-1020.

Adatte, T., Stinnesbeck, W., Keller, G. (1996). "Lithostratigraphic and mineralogic correlations of near K/T boundary sediments northeastern Mexico: Implications for origin and nature of deposition." The Cretaceous-Tertiary Event and Other Catastrophes in Earth History, Boulder, Colorado, v. Geological Society of America Special Paper 307: 211-226.

Arthur, M. A., W. E. Dean, et al. (1988). "Geochemical And Climatic Effects Of Increased Marine Organic-Carbon Burial At The Cenomanian Turonian Boundary." Nature 335(6192): 714-717.

Bauer, J., Marzouk, A.M., Steuber, T., and Kuss, J. (2001). “ Lithostratigraphy and biostratigraphyof the Cenomanian-Santonian strata of Sinai, Egypt”. Cretaceous Research 22: 497-526.

Behar, F., Beaumont, V., De B. Penteado, H.L. (2001). "Rock-Eval 6 technology:performances and developments." Oil & Gas Science and Technology: 111-134.

Bodin, S., Godet, A., Follmi, K.B., Vermeulen, J., Arnaud, H., Strasser, A., Fiet, N., Adatte, T., 2006. “The late Hauterivian Faraoni ocenic event in the western Tethys: Evidence from phosphorus burial rates.” Paleogeography, Paleoclimatology, Paleoecology 235(1-3): 245-264.

Bralower, T.J., 1988. Calcareous nannofossil biostratigraphy and assemblages of the Cenomanian-Turonian boundary interval: implications for the origin and timing of oceanic anoxia. Palaeoceanography 3, 275-316.

Bralower, T.J., Leckie, R.M., Sliter, W.V., Thierstein, H.R., 1995. An integrated Cretaceous microfossil biostratigraphy. SEPM Spec. Publ. 54, 65–79.

Buonocunto, F.P., Sprovieri, M., Bellanca, A., D’Argenio, B., Ferreri, V., Neri, R., Ferruzza, G. (2002). “Cyclostratigraphy and high-frequency carbon isotope fluctuations in Upper Cretaceous shallow-water carbonates, southern Italy”. Sedimentology 49: 1321-1337.

Burnett, J.A., l996. Nannofossils and Upper Cretaceous (sub-) stage boundaries – state of the art. Journal of Nannoplankton Research 18, 23-32. Burnett, J. A. 1998. Upper Cretaceous. In Calcareous nannofossil biostratigraphy (ed. Bown, P. R.), pp. 132–199 (Chapman & Hall, London).

Caron, M., S. Dall'Agnolo, et al. (2006). "High-resolution stratigraphy of the Cenomanian-Turonian boundary interval at Pueblo (USA) and wadi Bahloul (Tunisia) stable isotope and bio-events correlation." Geobios 39(2): 171-200.

Chamley, H. (1989). Clay sedimentology.

Clarke, L. J. and H. C. Jenkyns (1999). "New oxygen isotope evidence for long-term Cretaceous climatic change in the Southern Hemisphere." Geology 27(8): 699-702.

Coccioni, R., Galeotti, S. (2003).”The mid-Cenomanian Event: prelude to OAE2.” Paleogeography, Palaeoclimatology, Palaeoecology 190: 427-443.

Courtillot, V. E. and P. R. Renne (2003). "On the ages of flood basalt events." Comptes Rendus Geoscience 335(1): 113-140.

Davey, S.D., and Jenkyns, H.C. (1999). “Carbon-isotope stratigrfaphy of shallow-water limestones and implications for the timing of Late Cretaceoussea-level rise and anoxic events (Cenomanian-Turonian of the peri-Adriatic carbonate platform, Croatia)”. Eclogae geol. Helv. 92: 163-170.

Drzewiecky, P.A., and Simo, J.A. (1997). “Carbonate platform frowning and oceanic anoxic events on a

mid-Cretaceous carbonate platform, south-central Pyrenees, Spain". Journal of Sedimentary Research 67, No 4: 698-714.

Erba, E. and F. Tremolada (2004). "Nannofossil carbonate fluxes during the Early Cretaceous: Phytoplankton response to nutrification episodes, atmospheric CO2, and anoxia." Paleoceanography 19(1).

Erbacher, J., J. Thurow, et al. (1996). "Evolution patterns of radiolaria and organic matter variations: A new approach to identify sea-level changes in mid-Cretaceous pelagic environments." Geology 24(6): 499-502.

Espitalié, J., Deroo, G., Marquis, F. (1985). "La pyrolyse Rock-Eval et ses applications." Revue de l'Institut Français du Pétrole 40: 563-579.

Ettachfini, E.M., Souhel, A., Andreu B. and Caron, M. (2005). "The Cenomanian-Turonian boundary in the Central High Atlas, Morocco". Geobios 38: 57-68.

Froelich, P.N., Klinkhammer, G.P., Bender, M.L., Luedtke, N.A, Heath, G.R., Cullen, D., Dauphin, P., Hammond, D., Hartman, B., Maynard, V. (1979). "Early oxidation of organic matter in pelagic sediments of the eastern equatorial Atlantic: suboxic diagenesis". Geochemica et Cosmochimica Acta 43: 1075-1090.

Gale, A.S., Smith, A.B., Monks, N.E.A., Young, J.A., Howard, A., Wray, D.S., Huggett, J.M. (2000). " Marine biodiversity through the Late Cenomanian-Early Turonian: palaeoceanographic controls an d sequence stratigraphic biases." Journal of the Geological Society 157: 745-757.

Gertsch, B., Keller, G., Adatte, T., Berner, Z., Stueben, D., Tantawy, A.A.A.M., El-Sabbagh, A.M., and Mort, H.P. (in prep). "Cenomanian-Turonian transition in shallow water sequences of the Sinai, Egypt".

Glenn, C.R., and Arthur, M.A. (1990). "Anatomy and origin of a Cretaceous phosphorite-green sand giant, Egypt". Sedimentology 37:123-148.

Godet, A., Bodin, S., Adatte, T. and Foellmi, K.B. (in press). "Clay mineral assemblages along the Northern Tethyan margin during the Late Hauterivian - Early Aptian: Interactions beween climate change and carbonate platform evolution."

Grotsch, J., Billing, I., and Vahrenkamp V. (1998). "Carbon-isotope stratigraphy in shallow-water carbonates: implications for Cretaceous black-shale deposition". Sedimentology 45: 623-634.

Gustafsson, M., A. Holbourn, et al. (2003). "Changes in Northeast Atlantic temperature and carbon flux during the Cenomanian/Turonian paleoceanographic event: the Goban Spur stable isotope record." Palaeogeography Palaeoclimatology Palaeoecology 201(1-2): 51-66.

Hallam, A. (1992). "Phanerozoic sea level changes." Columbia press, New York.

Haq, B. U., J. Hardenbol, et al. (1987). "Chronology Of Fluctuating Sea Levels Since The Triassic." Science 235(4793): 1156-1167.

Hart, M. B. and P. N. Leary (1989). "The Stratigraphic And Paleogeographic Setting Of The Late Cenomanian Anoxic Event." Journal Of The Geological Society 146: 305-310.

Huber, B. T., D. A. Hodell, et al. (1995). "Middle-Late Cretaceous Climate Of The Southern High-Latitudes - Stable Isotopic Evidence For Minimal Equator-To-Pole Thermal-Gradients." Geological Society Of America Bulletin 107(10): 1164-1191.

Huber, B. T., R. D. Norris, et al. (2002). "Deep-sea paleotemperature record of extreme warmth during the Cretaceous." Geology 30(2): 123-126.

Jenkyns, H. C. (1980). "Cretaceous Anoxic Events - From Continents To Oceans." Journal Of The Geological Society 137(MAR): 171-188.

Jenkyns, H.C. (1991). "Impact of Cretaceous Sea Level Rise and Anoxic Events on the Mesozoic Carbonate Platform of Yugoslavia". The American Association of Petroleum Geologists Bulletin 75, n.6: 1007-1017.

Jenkyns, H.C., Gale, A.S., Corfield, R.M. (1994). "Carbon- and oxygen-isotope stratigraphy of the English Chalk and Italian Scaglia and its palaeoclimatic significance." Geological Magazine 131: p. 1-34.

Keller, G., Z. Berner, et al. (2004). "Cenomanian-Turonian and delta C-13, and delta O-18, sea level and salinity variations at Pueblo, Colorado." Palaeogeography Palaeoclimatology Palaeoecology 211(1-2): 19-43.

Keller, G., Q. Han, et al. (2001). "Palaeoenvironment of the Cenomanian-Turonian transition at Eastbourne, England." Cretaceous Research 22(4): 391-422.

Keller, G. and A. Pardo (2004). "Age and paleoenvironment of the Cenornanian-Turonian global stratotype section and point at Pueblo, Colorado." Marine Micropaleontology 51(1-2): 95-128.

Keller, G., Tantatawy, A.A., Berner, Z., Adatte, T., Chellai, E.H., Stueben, D. (in press). "Oceanic Events and Biotic Effects of the Cenomanian-Turonian Anoxic Event, Tarfaya Basin, Morocco."

Kennedy, W.J., Gale A.S., Lees, J.A., Caron M. (2006). "The Global Boundary Stratotype Section and Point (GSSP) for the base of the Cenomanian Stage, Mont Risou, Hautes-Alpes, France." Episodes 27(1): 21-30.

Kolonic, S., T. Wagner, et al. (2005). "Black shale deposition on the northwest African Shelf during the Cenomanian/Turonian oceanic anoxic event: Climate coupling and global organic carbon burial." Paleoceanography 20(1).

Kuhnt, W., F. Luderer, et al. (2005). "Orbital-scale record of the late Cenomanian-Turonian oceanic anoxic event (OAE-2) in the Tarfaya Basin (Morocco)." International Journal Of Earth Sciences 94(1): 147-159.

Kuhnt, W., A. Nederbragt, et al. (1997). "Cyclicity of Cenomanian-Turonian organic-carbon-rich sediments in the Tarfaya Atlantic Coastal Basin (Morocco)." Cretaceous Research 18(4): 587-601.

Kuypers, M. M. M., R. D. Pancost, et al. (2002). "Enhanced productivity led to increased organic carbon burial in the euxinic North Atlantic basin during the late Cenomanian oceanic anoxic event." Paleoceanography 17(4).

Kübler, B. (1983). "Dosage quantitatif des minéraux majeurs des roches sédimentaires par diffraction X." Cahiers de l'Institut de Géologie Series AX n°1.1 and 1.2: 1-13.

Kübler, B. (1987). "Cristallinité de l'illite: méthode normalisées de préparation de mesure, méthode automatique normalisées de mesure." Cahiers de l'Institut de Géologie.

Kübler, B., Jaboyedoff, M. (2000). "Illite Cristallinity." C.R. Ac. Sc. Paris, Sciences de la terre et des planès / Earth & Planetary Sciences 331 331: 75-89.

Lamolda, M. A., Gorostidi, A. and Paul, C. R. C., 1994. "Quantitative estimates of calcareous nannofossil changes across the Plenus Marls (latest Cenomanian), Dover, England; implication for the generation of the Cenomanian-Turonian boundary event." Cretaceous Research 15 (2), 143-164.

Larson, R. L. (1991). "Latest Pulse Of Earth - Evidence For A Midcretaceous Superplume." Geology 19(6): 547-550.

Larson, R. L. and E. Erba (1999). "Onset of the mid-Cretaceous greenhouse in the Barremian-Aptian: Igneous events and the biological, sedimentary, and geochemical responses." Paleoceanography 14(6): 663-678.

Leckie, R. M., T. J. Bralower, et al. (2002). "Oceanic anoxic events and plankton evolution: Biotic response to tectonic forcing during the mid-Cretaceous." Paleoceanography 17(3).

Lees, J.A., 2002. "Calcareous nannofossil biostratigraphy illustrates palaeoclimate change in the Late Cretaceous Indian Ocean." Cretaceous Research 23, 537-634.

Libes, S.M. (1992). "An Introduction to Marine Biogeochemistry". John Wiley and Sons, New York.

Luciani, V., and Cobianchi, M., l999. "The Bonarelli level and other black shales in the Cenomanian-Turonian of the northeastern Dolomites (Italy): calcareous nannofossil and foraminiferal data." Cretaceous Research 20, 135-167.

Luning, S., S. Kolonic, et al. (2004). "Integrated depositional model for the Cenomanian-Turonian organic-rich strata in North Africa." Earth-Science Reviews 64(1-2): 51-117.

Marshall, J.D. (1992). "Climatic and oceanographic isotopic signals from the carbonate rock record and their preservation". Geological Magazine 129(2): 143-160.

Mort, H. P., Adatte, T., Foellmi, K.B., Keller, G., Steinmann, P., Matera, V., Berner, Z., Stueben, D. (in press). "Phosphorus and the roles of productivity and nutrient recycling during Oceanic Event 2."

Norris, R. D., K. L. Bice, et al. (2002). "Jiggling the tropical thermostat in the Cretaceous hothouse." Geology 30(4): 299-302.

Pardo, A., Adatte, T., Keller, G., Oberhansli, H. (1999). " Paleoenvironmental changes across the Cretaceous-Tertiary boundary at Koshak, Kazakhstan, based on planktic foraminifera and clay mineralogy". Paleogeography, Paleoclimatology, Paleoecology 154: 247-273.

Paul, C.R.C., Lamolda, M.A., Mitchell, S.F., Vaziri, M.R., Gorostidi, A. and Marshall, J.D., l999. "The Cenomanian-turonian boundary at Eastbourne (Sussex, UK): a proposed European reference section." Paleogeography, Paleoclimatology, Paleoecology 150, 83-121.

Paul, C.R.C., Mitchell, S.F., Lamolda, M.A., and Gorostidi, A., 1994. "The Cenomanian-Turonian boundary event in northern Spain." Geol. Mag. 131(6), 801-817.

Paul, C. R. C., M. A. Lamolda, et al. (1999). "The cenomanian-turonian boundary at Eastbourne (Sussex, UK): a proposed European reference section." Palaeogeography Palaeoclimatology Palaeoecology 150(1-2): 83-121.

Perch-Nielsen, K., 1985. Cenozoic calcareous nannofossils. In Plankton stratigraphy (Bolli, H.M., Saunders, J.B., & Perch-Nielsen, K.): 422-454 (Cambridge University Press, Cambridge.

Premoli Silva, I., Erba, E., Salvini, G., Verga, D., Locatelli, C., 1999. "Biotic changes in Cretaceous anoxic events." J. Foraminiferal Res. 29, 352-370.

Pufahl, P.K., James, N.P. (2006). "Monospecific Pliocene oyster buildups, Murray Basin, South Australia: Brackish water end member of the reef spectrum". Paleogeography, Paleoclimatology, Paleoecology 233: 11-33.

Robaszynski, F., Caron, M., Dupuis, C., Amédro, F., Gonzalez Donoso, J. M., Linares, D., Hardenbol, J., Gartner, S., Calandra, F. and Deloffre, R., 1990. "A tentative integrated stratigraphy in the Turonian of central Tunisia: formations, zones and sequential stratigraphy in the Kalaat Senan area." Bulletin des Centres de Recherches Exploration-Production Elf Aquitaine 14, 213-384.

Rodriguez-Lazaro, J., A. Pascual, et al. (1998). "Cenomanian events in the deep western Basque Basin: the Leioa section." Cretaceous Research 19(6): 673-700.

Roth, P. H. and Krumbach, K. R., 1986. "Middle Cretaceous calcareous nannofossil biogeography and preservation in the Atlantic and Indian oceans: implications for palaeoceanography." Marine Micropaleontology 10, 235-266.

Sageman, B.B., Meyers, S.R., Arthur, M.A. (2006). "Orbital timescale and new C-isotope record for Cenomanian-Turonian boundary stratotype". Geology, 34 (2): 125-128.

Schrag, D.P., DePaolo, D.J., Richter, F.M. (1995). "Reconstructing past sea surface temperatures: Correcting for diagenesis of bulk marine carbonate". Geochemica et Cosmochimica Acta 59 (11): 2265-2278.

Shafik, S., 1990. "Late Cretaceous nannofossil biostratigraphy and biogeography of the Australian western margin." Australian Bureau of Mineral Resources, Geology and Geophysics, Report 295, 164 pp.

Sissingh, W., 1977. "Biostratigraphy of Cretaceous calcareous nannoplankton." Geologie en Mijnbouw 56, 37-65.

Tantawy, A.A., In review. "Calcareous Nannofossil Biostratigraphy and Paleoecology of the Cenomanian – Turonian Transition at Tazra, Tarfaya Basin, Southern Morocco." Cretaceous Research.

Tantawy, A. (2003). "Calcareous nannofossil biostratigraphy and paleoecology of the Cretaceous-Tertiary transition in the central Eastern Desert of Egypt." Marine Micropaleontology 47(3-4): 323-356.

Thiry, M. (2000). "Palaeoclimatic interpretation of clay minerals in marine deposits: an outlook from the continental origin." Earth-Science Reviews 49(1-4): 201-221.

Tsikos, H., H. C. Jenkyns, et al. (2004). "Carbon-isotope stratigraphy recorded by the Cenomanian-Turonian Oceanic Anoxic Event: correlation and implications based on three key localities." Journal Of The Geological Society 161: 711-719.

Ulicny, D., J. Hladikova, et al. (1993). "Record Of Sea-Level Changes, Oxygen Depletion And The Delta-C-13 Anomaly Across The Cenomanian-Turonian Boundary, Bohemian Cretaceous Basin." Cretaceous Research 14(2): 211-234.

Watkins, D.K., Wise, S.W., Pospichal, J.J. and Crux, J., 1996. "Upper Cretaceous calcareous nannofossil biostratigraphy and paleoceanography of the Southern Ocean." In Microfossils and oceanic environments (eds Moguilevsky, A. and Whatley, R.), pp. 355–381 (University of Wales, Aberystwyth Press, Aberystwyth).

Wiedmann, J., Butt, A., Einsele, G. (1978). "Vergleich von marokkanischen Kreide-Kusteaufschlussen und Tiefseebohrungen (DSDP): Stratigraphie, Palaoenvironment und Subsidenz and einem passiven Kontinentalrand." Geol. Rundsch. 67:

Cenomanian-Turonian transition in shallow water sequences of the Sinai, Egypt

This paper is in draft form. It is anticipated that it will be ready for publication next spring

Cenomanian-Turonian transition in shallow water sequences of the Sinai, Egypt

B. Gertsch[1], G. Keller[1], T. Adatte[2], Z. Berner[3], A.A.A.M. Tantawy[4], A.M. El-Sabbagh[4], H.P. Mort[2] and D. Stueben3

[1]*Department of Geosciences, Princeton University, Princeton NJ 08544, USA*

[2]*Geological Institute, University of Neuchatel, Neuchatel, CH-2007, Switzerland*

[3]*Institute for Mineralogy & Geochemistry, University of Karlsruhe, 76128 Karlsruhe, Germany*

[4]*Alexandria University, Faculty of Science, Department of Geology, Alexandria 21526, Egypt*

[5]*Department of Geology, Faculty of Science, South Valley University, Aswan 81528, Egypt*

A.Pb.1. Introduction

The late Cenomanian-early Turonian experienced major climatic and paleoceanographic changes, including greenhouse warming (Huber et al., 2002; Norris et al., 2002), a sea level transgression (Haq et al., 1987; Hallam, 1992), global oceanic anoxia known as OAE2 (Arthur et al., 1988; Kolonic et al., 2005) and faunal turnover (Erbacher et al., 1996; Leckie et al., 2002; Erba and Tremolda, 2002; Keller and Pardo, 2004). Deposition of organic-rich black shale is the most evident expression of OAE2, particularly in deeper waters, upwelling areas and basin settings of the low latitude Tethys ocean, but not in shallow marine platform and coastal areas. Organic-rich sediment deposition was not uniform across the Tethys continental shelf, but reached maximum accumulation rates in deep basins (e.g. Italy, Tunisia, Morocco), which have been studied extensively (e.g., Nederbragt & Fiorentino, l999; Kuhnt et al., l997, 2004; Kolonic et al., 2002, 2005; Mort et al., in press). The OAE2 is characterized by a positive 2‰ δ13C excursion consisting of two peaks separated by a trough (Jarvis et al., l988; Hart and Leary, 1989; Paul et al., l999; Keller et al., 2004; Tsikos et al., 2004). Less well known are the biotic and environmental effects of the oceanic anoxic events in shallow continental platform and coastal areas. The eastern Tethys, particularly Egypt (Sinai), presents an ideal area to investigate the nature of OAE2 in coastal and inner shelf settings.

During the Late Cretaceous, Egypt was part of a broad Tethyan Seaway with open marine circulation to the Indo-Pacific in the east and the Atlantic-Caribbean-Pacific in the west. Shallow seas covered continental regions in North Africa, Europe, the Middle East and the Ural region, and a warm climate, high marine productivity and rapid burial of organic matter created most of the currently known oil and gas resources in these regions. As sea levels fluctuated with global climate changes during the late Cretaceous, phosphorites were deposited in shallow environments throughout North Africa and the Middle East and their current mining provides major economic resources for Egypt and this region in general.

During the Cenomanian-Turonian (C-T), shallow inland seas in Egypt, Israel and Morocco deposited limestones, marls, sands and oyster beds, which are exposed today in hills of central and southern Sinai. Most studies of the Cenomanian-Turonian (C-T) sequences of Egypt have concentrated on biostratigraphy and faunal turnovers based on macrofossils (ammonites) and microfossils (foraminifera, nannofossils) and very few dealt with the paleoclimatic, environmental and paleoceanographic changes (Kora et al. 1987; Cherief et al., 1989; Orabi 1992; Kassab, 1994; Kora et al., 1994; Kassab, 1996; Kassab, 1999; Bauer et al., 2001; Kassab and Obaidalla 2001).

This study investigates the environmental effects of OAE2 upon a shallow water coastal

sequence in the Wadi El Ghaib of the Sinai, Egypt, and correlates these with shallow and deep-water sequences in Morocco. The investigation is based on: 1) biostratigraphy to obtain age control and evaluate the biotic effects; 2) stable carbon isotopes to evaluate changes in productivity and the extend of the OAE2 δ13C excursion in marine-coastal areas; 3) sedimentology to identify facies and sea level changes; 4) clay and bulk-rock mineralogy to evaluate the paleoclimatic evolution and depositional environment; and 5) total phosphorus quantification to test the hypothesis of decoupled C and P cycles during the C-T transition.

A.Pb.1.2. Geologic Setting and Location

The Whadi El Ghaib section is situated in the south central Sinai, Egypt (34°29°E and 28°48°N), with similar sections located to the east (Sheik Atiya) and along the Gulf of Suez (Wadi Feiran, Gabal Nezzazat, Fig. 1). The Cenomanian-Turonian strata consist of shallow marine carbonates and siliciclastics, which change to coastal and terrestrial facies in the south of Egypt (Luning et al., 1998, 2004).

In the southern Sinai, the lithostratigraphy in these Cenomanian-Turonian sections comprises three formations: the Raha (middle-late Cenomanian), the Abu Qada (late Cenomanian-early Turonian) and the Wata Formations (early Turonian) (Fig. 2). The Raha Formation (Ghorab, 1961) consists of poorly fossiliferous calcareous sandstones with few bioturbated horizons rich in small oysters and trigonid bivalves in it upper part. The lower and middle parts of the formation are generally fossiliferous. The Abu Qada Formation (Ghorab, 1961) is composed by marls, nodular marls, marly limestones, shales and oyster-rich limestone beds. The fauna consists of ammonites, gastropods, bivalves, echinoids, corals, and ichnofossils. The Wata Formation (Ghorab, 1961) consists of marls, marly limestone and nodular limestones with abundant ammonites of Turonian age.

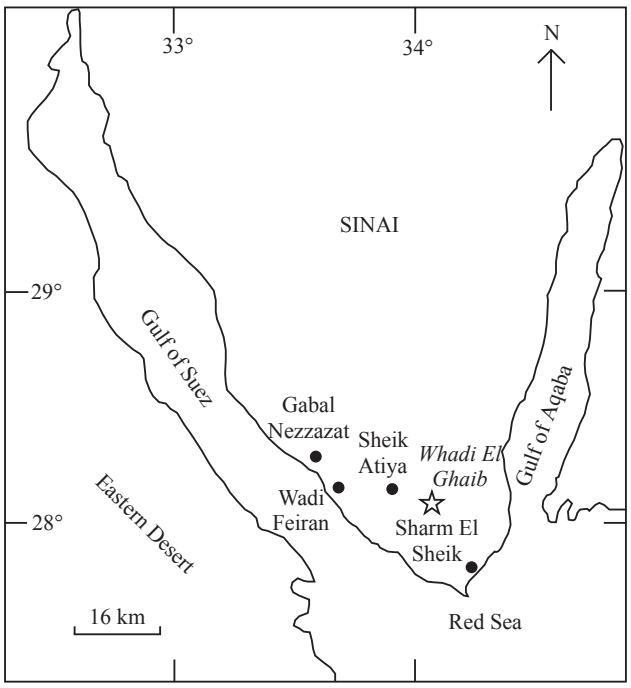

Figure 1: Location of the measured section, Whadi El Ghaib, Sinai, Egypt.

A.Pb.1.3. Lithology

The late Cenomanian to early Turonian Whadi El Ghaib sequence (Fig. 2) outcrops on hills to the north of Sharm El Sheik. The basal 3 m consist of bioturbated calcareous sandstones containing glauconite. Above this interval are alternating oyster-rich limestone beds and silty-sandy shale levels (3-17 m), which are topped by a limestone bed. Rare fossils are present, including the ammonite Neobilites vibrayeanus (sample WG 24, Figs. 2, 3). Marls containing nodules, gastropods and echinoids (18-26 m) overlie this interval, followed by a marly limestone bed (26-27 m). Above this sequence are marls with nodules, echinoids, gastropods and ammonites (27-31.5 m), which are followed by a marly limestone bed with echinoids, nodules, glauconite and ammonites (31.5-33 m). Laminated shales containing glauconite at the base and a 5 cm thick bentonite layer in the middle (33-35 m) overlie this interval, followed by laminated shale and marls (35-38 m). The top of the section consists of a marly limestone bed (38-38.5 m).

A.Pb.2. Methods

In the field, the sections were examined for lithological changes, burrows, macrofossils, and carefully described and measured. A total

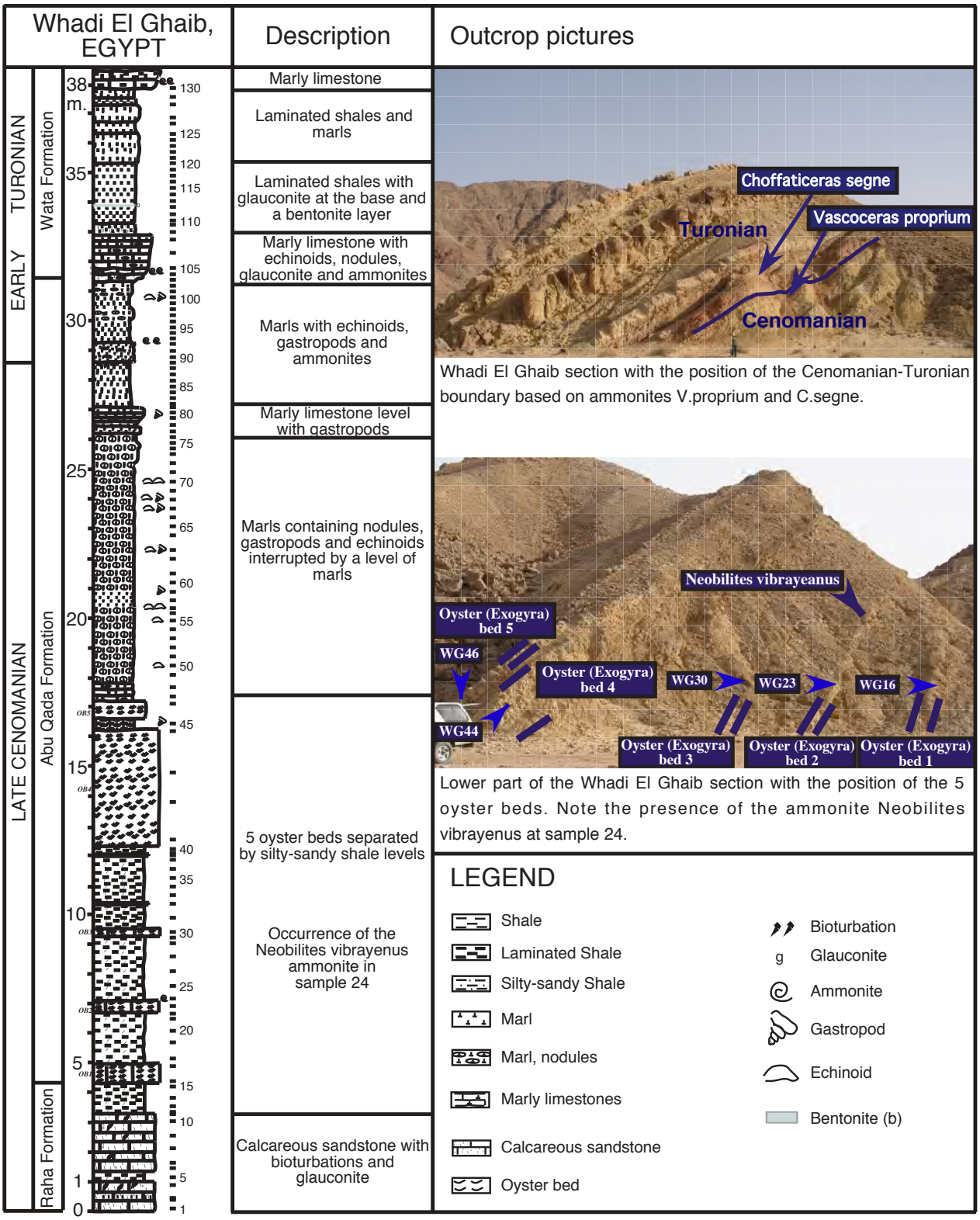

Figure 2: Lithological description of the Whadi El Ghaib section keyed with pictures.

of 130 samples were collected at an average of 25 cm intervals for the Whadi El Ghaib section. In the laboratory, samples were processed for foraminiferal analysis using standard methods (Keller et al., 2001). Species from each sample residue were picked and identified. Planktic foraminifera are generally rare. Wherever present, at least 100 foraminifera were counted.

Samples were processed for nannofossil analysis using methods described in Tantawy et al. (2003) and Perch-Nielsen (1985). Smear slides were examined using a light photomicroscope with 1000-2000X magnification.

Carbon isotopes were carried out on powdered bulk rock samples at the stable isotope laboratory at the University of Karlsruhe, Germany, using an Optima (Micromass, UK) ratio mass spectrometer equipped with an online carbonate preparation line (Multi Carb) with separate vials for each sample. The results were calibrated to the PDB scale with standard errors of 0.05 ‰ for $\delta^{13}C$ and of 0.1‰ for $\delta^{18}O$.

Mineralogical and total phosphorus quantification analyses were carried out at the Geological Institute of the University of Neuchâtel, Switzerland. Bulk rock and clay mineral assemblages were analyzed by X-ray diffraction (Scintag XRD 2000 Diffractometer) based on procedures described by Kubler (1983) and Adatte et al. (1996). This method permits the semi-quantification of whole-rock mineralogy, obtained by XRD patterns of random powder samples by using external standards with an error varying between 5 and 10% for the phyllosilicates and 5% for grain minerals.

Clay mineralogical analysis is based on methods developed by Kubler (1987) and Adatte et al. (1996). The intensities of the identified minerals are measured for a semi-quantitative estimate of the proportion of clay minerals, which is therefore given in relative percent without correction factors.

Total phosphorus quantification analysis was performed on bulk rock samples, following the procedure described in Bodin et al. (2006). The concentration of PO4 in mg/l is obtained by calibration with known standards solutions, using a photospectrometer (Perkin Elmer UV/Vis Photospectrometer Lambda 10).

A.Pb.3. Results

A.Pb.3.1. Biostratigraphy

The stratigraphy and fauna of the Cenomanian-Turonian succession of the Sinai have been widely discussed (Kora et al., 1987; Cherief et al., 1989; Orabi, 1992; Kassab, 1994; Kora et al., 1994; Kassab, 1996; Kassab, 1999; Kassab and Obaidalla 2001). Four ammonite biozones defined by Kassab and Obaidalla (2001) are recognized throughout Egypt:

Zone C1 - Vascoceras cauvini Interval Zone: This zone is defined by the first appearance (FA) of the index species at the base and the FAs of Vascoceras proprium and V. obessum at the top. At Wadi El Ghaib, the index species first appears in the middle of the Abu Qada Fm. However, based on the occurrence of this species in other sequences, the first appearance is in the upper Raha Formation. Vascoceratid ammonites and exogyrine oysters are the main faunal components (Exogyra olisiphonensis, Ceratostreum flabellum, Paranamites polymorpheum).

Zone T1 - Vascoceras proprium/ Pseudaspidoceras flexuosum Total Range Zone: This zone is defined by the total range of the two index species. At Wadi El Ghaib, the zone spans the upper part of the Abu Qada Formation (28.5-31.5 m, Fig. 3). Other taxa present include Vascoceras obessium, Mamites nodosoides, Fagesia catinus and Hymatogyra pseudafricana.

Zone T2 - Choffaticeras segne Total Range Zone: This zone is defined by the total range of Choffaticeras segne, a species that is synonymous with C. luciae, C. pavillieri, C. schweinfurthi, and C. securiforme (Kassab, 1985, 1994).

Zone T3 - Coilopoceras requienianum Zone: This zone is defined by the total range of the index species and was not observed at Wadi El Ghaib.

Thus, ammonites in the Whadi El Ghaib section provide age control. The Raha Formation is characterized by the occurrence of Hymatogyra africana. The lower part of the Abu Qada Formation is marked by the presence of Exogyra olisiponensis. Exogyra olisiponensis, Ceratostreon flabellum and the biomarkers of the V. cauvini (C1) biozone, Vascoceras cauvini and Paramites polymorpheum, are present in the deeper facies of the upper part of the Abu Qada Formation. First occurrence of Turonian biomarkers of the T1 zone, Vascoceras proprium and Pseudaspidoceras

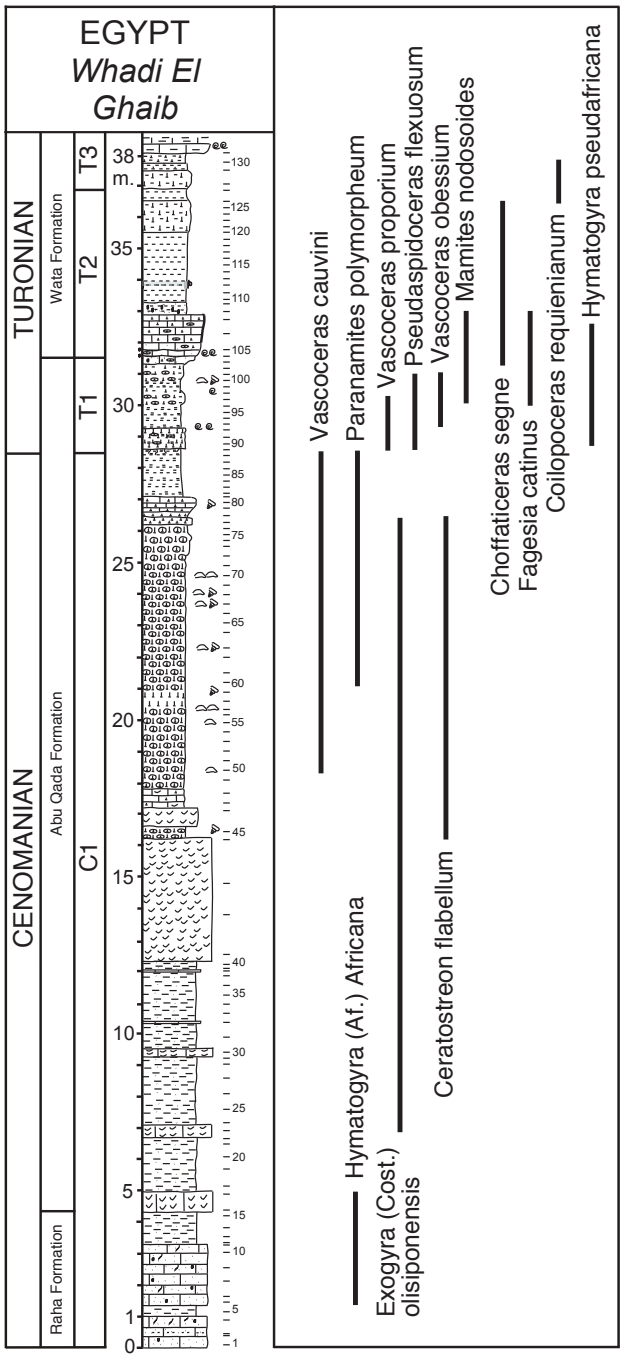

Figure 3: Ammonite biostratigraphy of the Whadi El Ghaib section.

flexuosum, identify the Cenomanian-Turonian boundary at the top of the V.cauvini zone (C1). Vascoceras obessium, Mamites nodosoides, Fagesia catinus and Hymatogyra pseudafricana are also present in the T1 zone. The base of the Wata Formation is marked by the first appearance of the biomarker of the T2 zone, Choffaticeras segne. The boundary between the T2 and T3 zones is marked by the last appearance of Choffaticeras segne and the first appearance of biomarker of the T3 zone, Coilopoceras requienianum (37 m).

A.Pb.3.2.Bulk rock

Calcite, quartz and phyllosilicates are the dominant minerals (Fig. 4). A three-point average curve shows the overall trends of each mineral. Phyllosilicates and unquantified show the same trends, leading to the conclusion that most of the unquantified may be phyllosilicates. The basal part of the section (0-12 m) below the 5 m-thick oyster-rich limestone bed is dominated by quartz (20-60%), phyllosilicates (20%) and plagioclases (5%). Calcite is almost absent, except in the oyster-rich limestone beds. Calcite is the dominant mineral (70-90%) from the large oyster bed to the marly limestone bed near the top of the Abu Qada Formation (12-27 m). In the same interval, quartz and plagioclase disappear and phyllosilicates decrease. From the marls marking the top of the Abu Qada formation to the top of the section, alternations of calcite-dominant intervals and quartz/phyllosilicates-dominant levels occur.

The detrital index (C/D=Calcite/(Quartz+Phyllosilicates+K-Feldspars+Na-Plagioclases)) shows highest values between 12 and 25 m and between 32 and 33 m, whereas low values indicate high detritus level in the rest of the section.

A.Pb.3.3. Clay mineralogy

Clay assemblages of the Whadi El Ghaib section are composed of kaolinite, chlorite, smectite, illite, palygorskite and I-S mixed layer (Fig. 5). A three-point average curve shows the overall trend of each type of clay. Kaolinite (60-80%) is the main clay of the basal 20 m, whereas smectite content remains low (10-40%). An abrupt decrease in kaolinite (<5%), together with a rapid increase in smectite (90%) occurs at 21 m. Smectite (50-90%) is the dominant clay mineral from this level to the top of the Abu Qada Formation with a gradual decrease from 25 m. Kaolinite and chlorite show three peaks in the top 5 m of the Abu Qada Formation. Above this interval, the basal part of

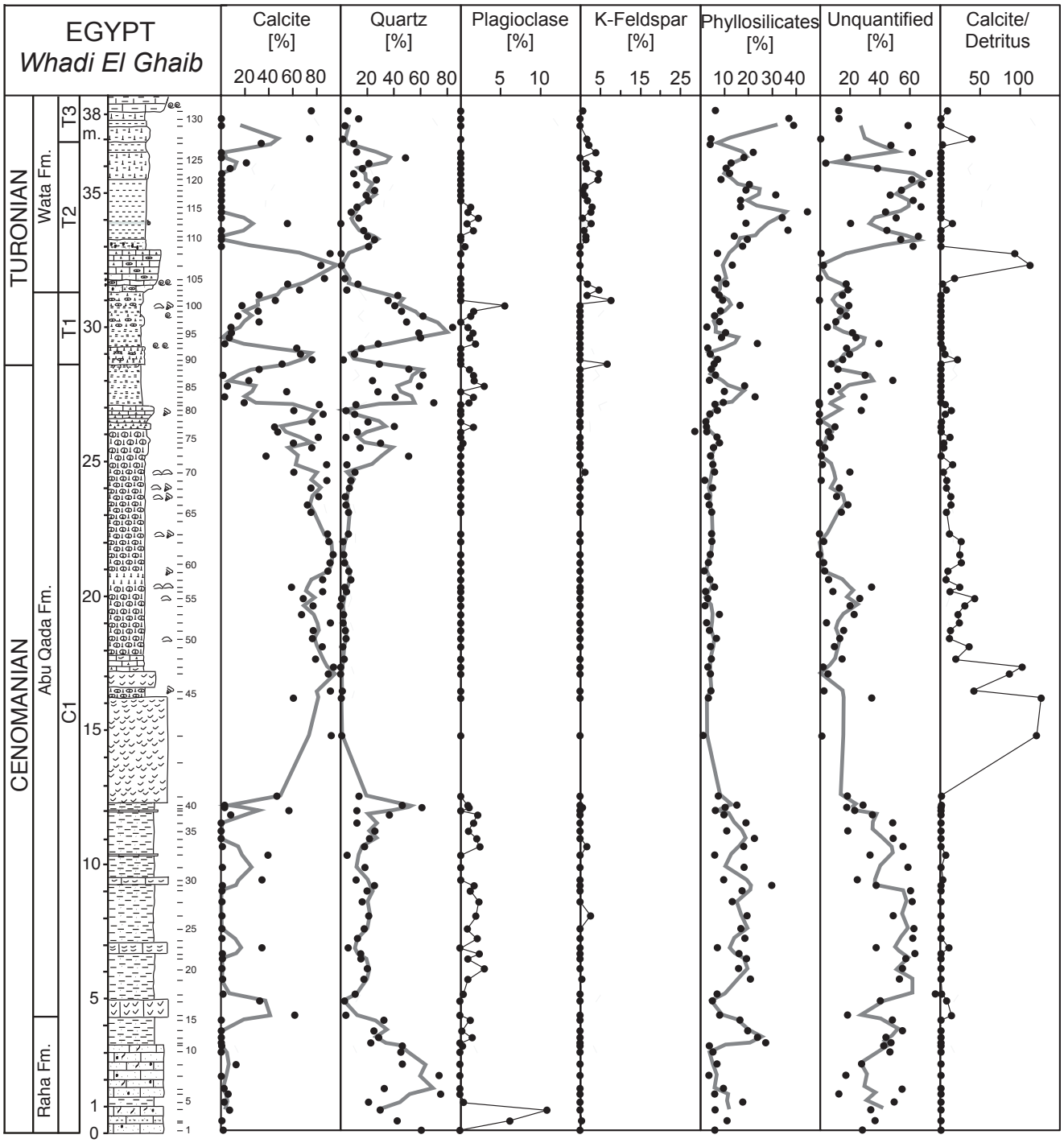

Figure 4: Bulk rock results. Grey lines for calcite, quartz, phyllosilicates and unquantified correspond to a three-points moving average.

the limestone/shale interval of the Wata Formation (31.5-35 m) is marked by the alternating dominance of illite (80-90%) and palygorskite (60-80%), and the absence of kaolinite and smectite. The upper part of the section is characterized by a return to a high smectite contents (40-80%).

A.Pb.3.4. Oxygen and carbon isotopes

The reliability of oxygen and carbon isotopes of bulk rock sediments is largely dependent upon the degree of diagenesis in the sediments. Oxygen and carbon isotopes do not react similarly to diagenetic effects. While carbon isotopes are little affected by diagenesis, except in case of influence organogenic carbon (Marshall, 1992), oxygen isotope are more

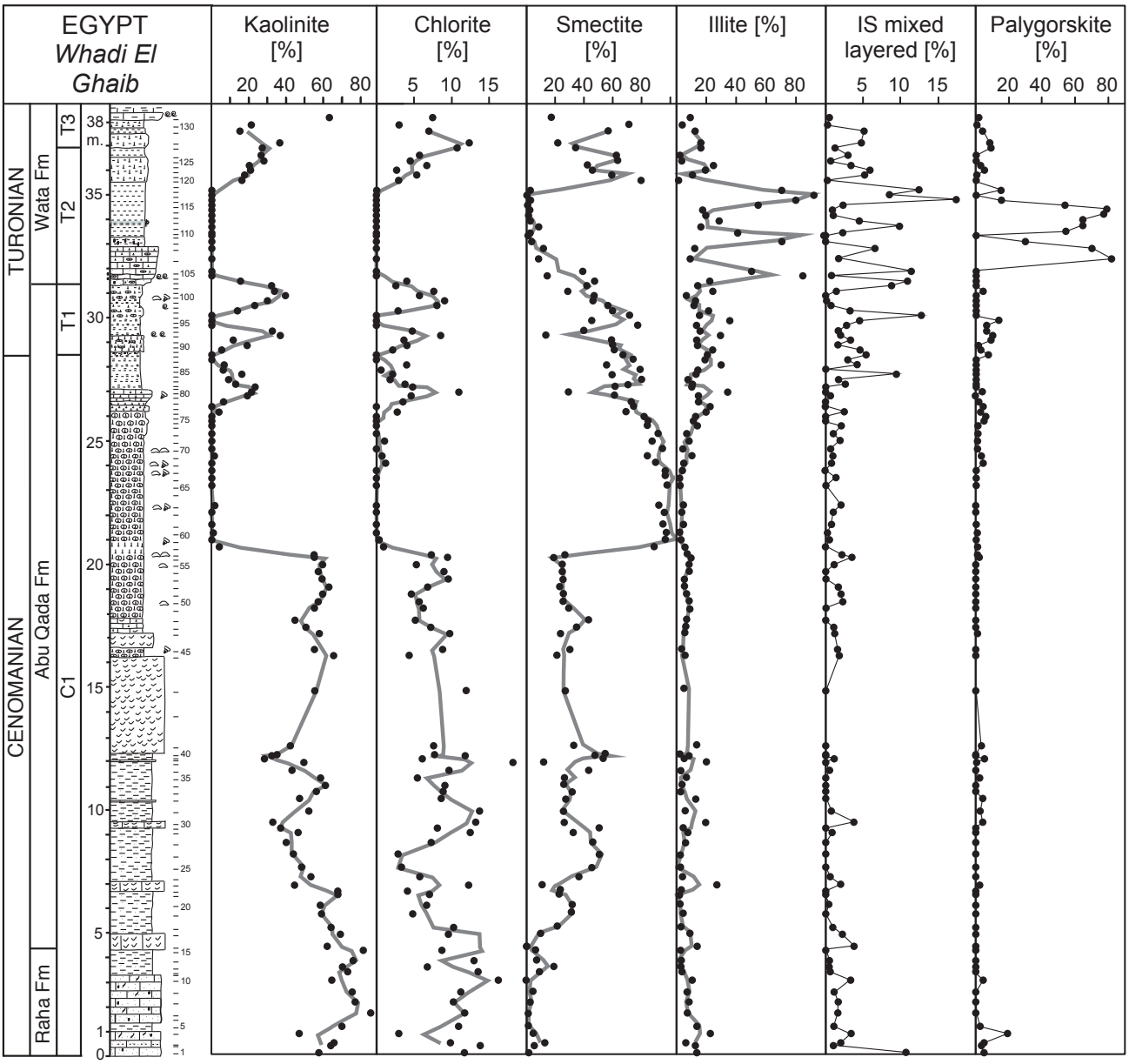

Figure 5: Clay mineralogical results. Grey lines for kaolinite, chlorite, smectite and illite correspond to a three-points moving average.

sensitive (Schrag et al., 1995). Pore waters and/or recrystalization present very negative δ18O ratio leading to a significant lowering of oxygen isotope ratios of the sediment.

A cross-plot of carbon- and oxygen-isotope data shows no significant correlation for the Whadi El Ghaib section (Fig. 6). δ18O values range from -9 to -2‰ and δ13C values range between -1 and 6‰. The relatively low oxygen isotope ratios imply a considerable diagenetic overprint due to the high capacity of oxygen exchange with interstitial fluids. These data are therefore considered unreliable to interpret climatic trends and will not be discussed further. This diagenetic effect does not affect carbon isotopes due to the scarcity of carbon in pore waters.

The carbon isotope curve shows relatively low values (-1-1‰) in the lower part of the section (4-12 m, Fig. 7). In the 5 m thick oyster-rich limestone bed, δ13C values suddenly increase and reach 4‰. A further increase to 5‰ occurs above the oyster-rich limestone in the nodular marl (17-19 m). Above it, δ13C values drop to 4‰ (18.5-19.5 m). A rapid increase to 6‰ at 20 m marks the second δ13C excursion with high values remaining steady between 5-6‰ up to 24 m. Above the second δ13C

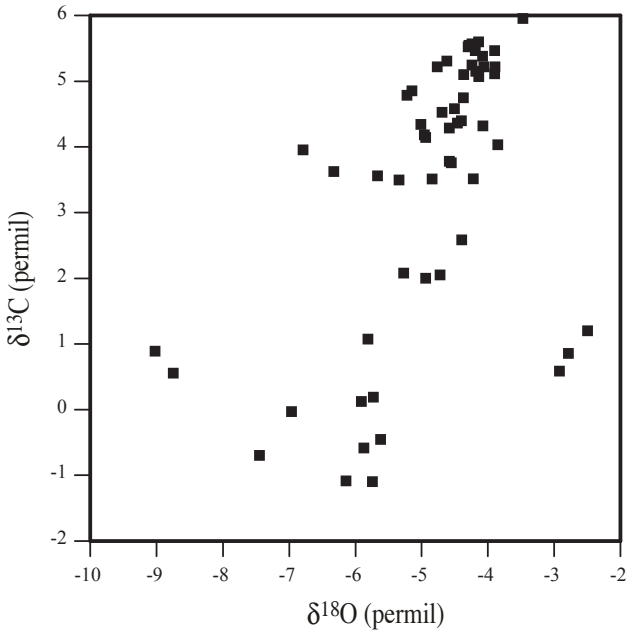

Figure 6: Cross-plot of oxygen versus carbon isotopes.

excursion, values gradually decrease to -1‰ by the top of the Abu Qada Formation.

A.Pb.3.5. Total phosphorus quantification

Total phosphorus contents range from 100 to 2000 ppm (Fig. 7). High values (200-1000 ppm with a peak at 2000 ppm) are reached in the basal 3 m of the Raha Formation. Phosphorus contents stabilize at 200-400 ppm (4-9 m), increase to a maximum of 1500 ppm between 9-10 m and gradually decrease to low values (10-12.5 m). The base of the 5 m thick oyster-rich limestone bed up to the Cenomanian-Turonian boundary (12.5-28.5 m) is low in phosphorus contents (~300 ppm). Gradual increase occurs in the T1 ammonite biozone, reaching a maximum (1500 ppm) at the boundary between the Abu Qada and Wata Formations. The upper part of the section (33-38 m) shows 3 smaller peaks reaching 1000 ppm, 600 ppm and 700 ppm.

A.Pb.4. Preliminary Interpretations

A.Pb.4.1. Paleoenvironment

A.Pb.4.1.2. Oyster ecology

A key feature of the shallow water Whadi El Ghaib section is the presence of oyster-rich limestone beds during the middle and late Cenomanian, as also observed in the late Cenomanian of Morocco (Gertsch et al. in prep) and Israel (Bauer et al., 2003). By analogy with Neogene to recent oyster beds, these deposits yield environmental information that can shed light on the depositional environment during the late Cenomanian to early Turonian in shallow coastal areas of the Sinai and elsewhere.

A recent study of Pliocene oyster buildups in Australia identifies 3 different types oyster deposits (e.g., bioherms, biostromes and subaqueous dunes), which correspond to shallow subtidal environments (Pufahl et al., 2006). Oyster bioherms are composed of disarticulated and articulated oysters. They usually show a gradational base expressed by the upward increase in oyster size and density, and contains other type of macrofossils (e.g., gastropods). Lateral extent of oyster bioherms ranges from a few hundreds of meters up to 4 km (Abed and Sadaqh, 1998). Biostromes corresponds to laterally extensive tabular beds of oysters. Subaqueous dunes are trough cross-stratified oyster rudstone comprising stacked co-sets of oyster shells and intercalated quartzose sand lenses.

At the Whadi El Ghaib section, 5 oyster-rich limestone beds are present and show no stratification. According to the above definitions, they correspond to meter-thick tabular oyster biostromes indicative of shallow subtidal environments. These environments can be interpreted based on the Pliocene oyster dominated environments.

In the Pliocene, the oyster biostromes consist of wave-resistant structures that formed in high-energy, shallow, faunally restricted environments. This implies brackish conditions similar to modern oyster communities, which are extremely efficient filters and tolerate a wide range of environmental conditions. The ecological success of oyster buildups is likely due to high oyster fecundity, which enables these r-strategists to thrive by responding quickly to environmental perturbations (Pufahl et al., 2006). Factors promoting oyster buildups include low salinity, mesotrophic nutrient level, a turbid water column and a high spatial homogeneity of oyster communities. In these aspects, oysters are opportunistic species, similar to the planktic

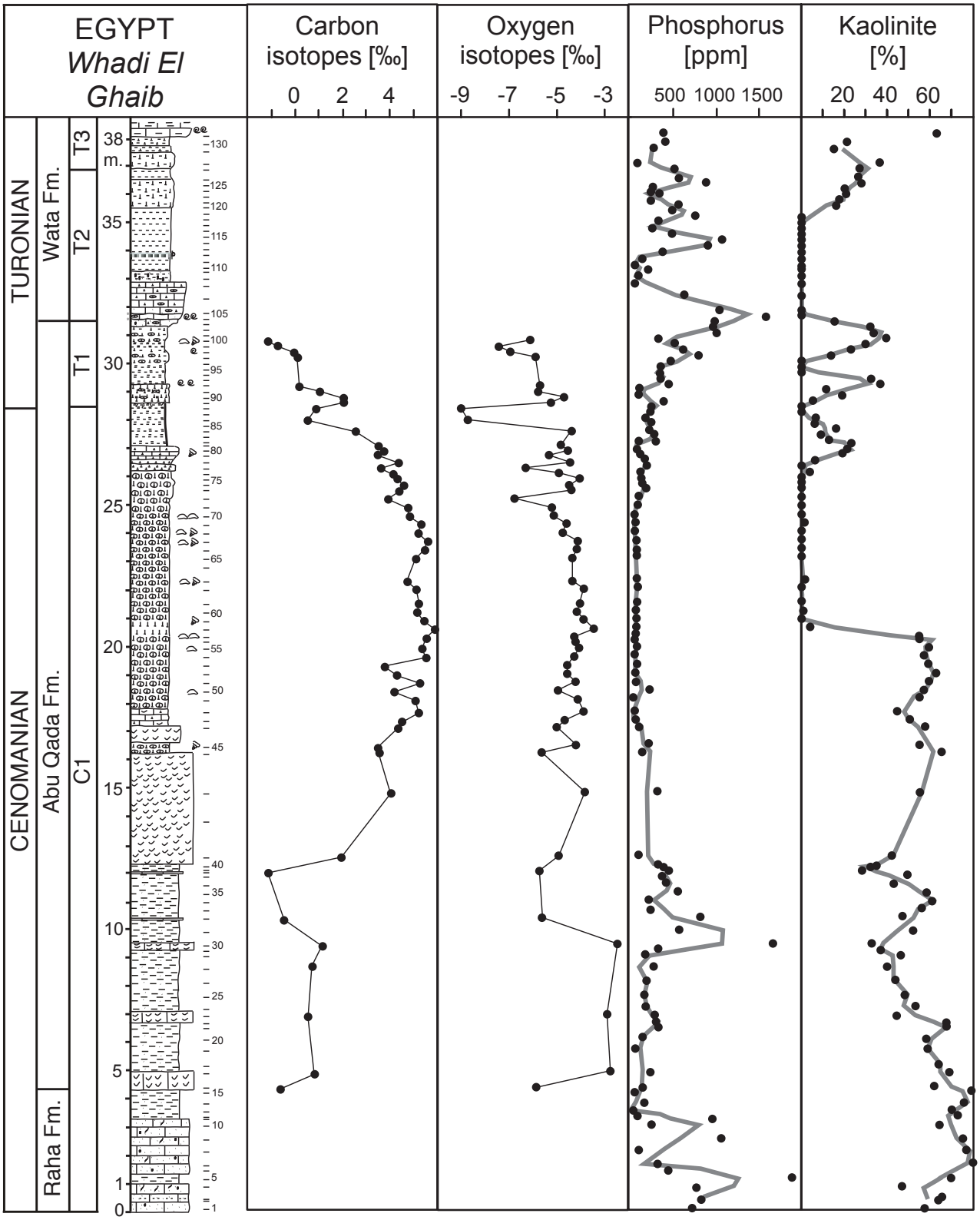

Figure 7: Summary figures with carbon and oxygen isotopes, phosphorus concentrations and kaolinite.

foraminifera Guembelitria (a disaster opportunist that thrives in nutrient-rich surface waters) and Heterohelix (low oxygen tolerant, Keller and Pardo, 2004). In the case of the Whadi El Ghaib section, variations of these factors may have triggered the thickness changes of these oyster biostromes, as well as lithological changes.

Oyster communities play an important role in nutrient recycling. Oyster buildups tend to amplify secondary benthic production, which is recorded by the establishment of extensive sea grass beds around oyster bioherms and biostromes (Pufahl et al., 2006). They enhance nutrient export through prolific feces production stimulated by filter feeding of large quantities of phytoplankton from the water column. Degradation of these organic-rich sediments under aerobic and dysaerobic microbial pathways (Froelich et al., 1979) allows the return of nitrogen (N) and phosphorus (P) to the water column (Libes, 1992). Thus, oyster buildups thrive under mesotrophic conditions and facilitate nutrient cycling exogenically outside of the community, within the environment. They are conduits through which N and P are changed into bio-available forms for other organism within coastal ecosystems (Pufahl et al., 2006).

A.Pb.4.1.3. Paleoenvironment based on gastropods, echinoids and ammonites

The most common fossils present in the Whadi El Ghaib section are gastropods, echinoids and ammonites. Gastropods are found in the intertidal flats and in shallow subtidal environments (Nield and Tucker, 1985). Turritella, Cerithium, Tylostoma and Nerinea inhabited warm water normal marine inner to middle neritc conditions (Nield and Tucker, 1985).

Echinoderms inhabited littoral to sublittoral environments, and the neritic zone commonly associated with reefs (Nield and Tucker, 1985).

Ammonites were living in both shallow and deep marine environments, but predominated in normal marine to middle neritic environments at water depths up to 300 m (Kassab, 1985; 1994).

A.Pb.4.1.4. Paleoenvironment inferred from mineralogy

Bulk-rock mineralogy shows generally low Calcite/Detritus ratios (C/D<5) for the Whadi El Ghaib section, suggesting that humid conditions and high continental runoff prevailed through the early late Cenomanian. The basal part of the section up to the base of the 5 m thick oyster-rich limestone bed, shows C/D ratios near zero, except in oyster-rich limestone beds. Highest C/D ratios (50-125) are reached in the 5 m thick oyster-rich limestone bed and in the following oyster-rich limestone bed, which could be interpreted as low continental runoff. However, these high C/D ratios cannot be explained in terms of low continental runoff because oyster growth is dependent on high nutrient waters and the nutrients in shallow shore environments largely come from continental runoff. Based on this consideration, that high terrigenous runoff occurs when oyster biostromes were built. Relatively high C/D ratios above the last oyster-rich limestone (17-24 m) indicate weaker continental runoff. Above this interval, low C/D ratios correspond to higher continental runoff (24-31.5 m). The marly limestone bed at the base of the Wata Formation (31.5-33 m) presents high C/D ratios suggesting low continental runoff. Very low C/D ratios prevail for the top of the section, marking a return to higher continental runoff.

Clay minerals, which form in terrestrial soils, are eroded and transported to the oceans. Climate changes and type of source rocks are the primary factors influencing their formation. The main clay minerals of clay assemblages are kaolinite and smectite. Kaolinite forms under humid conditions in equatorial soils, whereas smectite forms in tropical soils under dry, seasonal climate, or from the alteration of basalts (Chamley, 1989). Distribution of clay minerals in the sediments can be influenced by authigenesis (Chamley, 1989; Kubler, 2000) and differential settling of kaolinite versus smectite in the water column (Godet et al, in press). Diagenetic transformations due to burial (e.g. authigenesis) generally occur at sediment depths >2 km (Chamley, 1989). Thus, authigenesis is not a significant influence of the clay assemblages of the Whadi El Gaib section, which was buried in

less than 100 m of sediments. Differential settling cannot be evaluated on one single sequence and requires correlation with deeper sections, which are not available to date. Based on the paleoenvironmental reconstructions for the late Cenomanian-early Turonian in the Sinai (Luning et al., 1998), it seems reasonable to assume that no significant carbonate platform occurred, which lead to the conclusion that no differential settling occurs. Neverthless, oyster biostromes may have contributed to differential settling of kaolinite contents in the lower half of the section. However, high kaolinite values in this interval suggest that the primary cause of high contents is due to climate, with differential settling as a secondary influence. Therefore, it is most likely that clay assemblages reflect climatic conditions.

Within these constraints, the basal kaolinite dominated 21 m of the Whadi El Ghaib section suggests deposition under humid climate conditions. The upper part of the section (21-31.5 m) is dominated by smectite interpreted as a return to a dry, seasonally well-contrasted climate. Local high palygorskite and illite contents can reflect local pulses of wind-transported clay formed under dry conditions (e.g. palygorskite), such as deserts, together with high runoff (e.g. illite).

Bulk-rock and clay mineralogy interpretations lead to similar conclusions. The basal part of the section up to the last oyster-rich limestone bed is characterized by more humid conditions and higher continental runoff. Abrupt return to dry and seasonal conditions (high smectite contents) are marked by a carbonate-dominated sedimentation until the Cenomanian-Turonian boundary. The basal Turonian (T1 ammonite zone) corresponds to dry and seasonal conditions with high continental runoff. The basal T2 ammonite zone corresponds to low terrigenous influx by runoff, but high wind-driven detritus due to the high contents in palygorskite. The upper part of the section corresponds to a period with high detritus input due the high illite and playgorskite contents and low C/D ratios. The T3 Ammonite is marked by a return to dry and seasonal climate.

A.Pb.5. Geochemistry

A.Pb.5.1. Carbon isotope

The late Cenomanian OAE2 is characterized by a worldwide positive excursion of the δ13C (Arthur et al., 1988; Jenkyns et al., 1994; Tsikos et al., 2004). The typical shape of the late Cenomanian δ13C excursion, as for the GSSP section at Pueblo (Keller et al., 2004), comprises the following features: a rapid increase in δ13C to reach the first peak at 2‰, a short decrease of 0.6‰ forming a trough, a 1‰ increase forming the second peak, and prolonged high δ13C values forming a plateau.

The Whadi El Ghaib carbon isotope record shows similar trend, although few data are available in the lower part of the section due to the low calcite content. These results agree well with the carbon isotope curve of Pueblo, Colorado, GSSP section for the late Cenomanian OAE2, leading to the conclusion that shallow water sequences record the same carbon isotope record as deep-water sequences. Similar conclusions were drawn by Davey and Jenkyns (1999) and Gertsch et al. (in prep) in shallow-water/coastal environments.

A.Pb.5.2. Phosphorus

Total phosphorus quantification analyses were performed to test the hypothesis of Mort et al. (in press), showing that phosphorus mass accumulation rates reach a maximum, which predates the onset of the δ13C positive plateau in different Cenomanian-Turonian sequences. Interpretation of these trends involves the decoupling of phosphorus (P) and carbon (C) cycles during OAE2. Maximum in phosphorus concentrations occurs prior to and after the positive δ13C excursion, whereas the carbon isotope excursion corresponds to very low phosphorus contents. At Whadi El Ghaib section, these results agree with those of Mort et al. (in press). Highest P concentrations are reached prior to and after the δ13C excursion.

Redox-influenced phosphorus accumulation in sediments, as postulated by Mort et al. (in press), suggests that P accumulates preferentially under

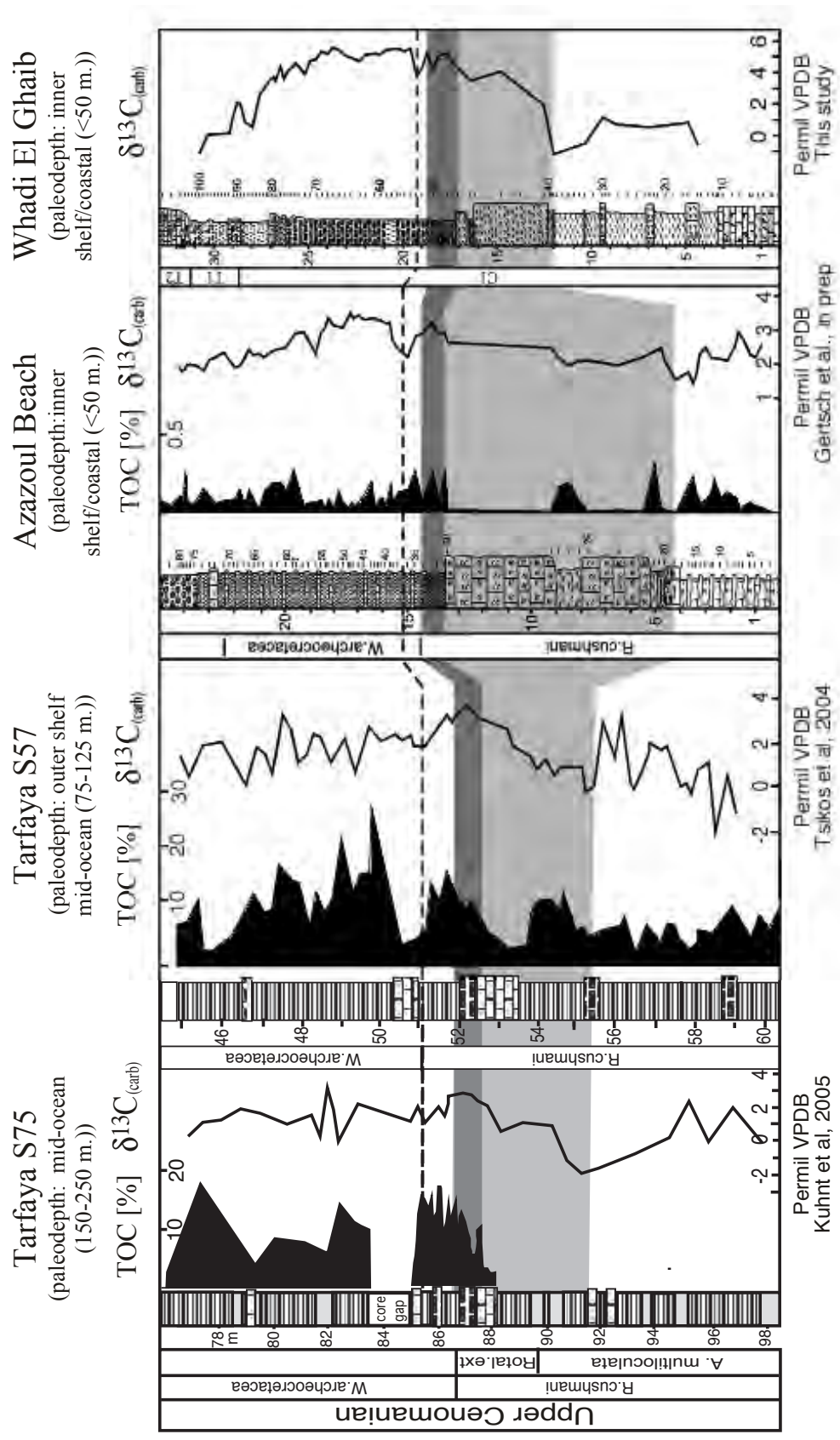

Figure 8: Correlation of the carbon isotope curve of the Whadi El Ghaib section with deep-water sections (Tarfaya, Morocco) and a shallow-water sequence (Azazoul Beach, Morocco). Light gray area corresponds to the carbon isotope increase and dark gray area corresponds to the first carbon isotope peak.

oxic conditions, explaining low P contents occurred during the carbon isotope excursion. Based on this assumption, phosphorus concentrations should be high before the carbon isotope excursion, and should not present a single peak. The latter raises the possibility of diagenetic influence of P concentrations or other driving processes of P accumulation in the sediment. Results of a similar shallow-water section in Morocco (Gertsch et al., in prep), show a possible diagenetically influenced P concentrations, confirming that further work are needed to understand P behavior.

A.Pb.6. Correlation between Azazoul Beach and Whadi El Ghaib section

Azazoul Beach, Morocco, (Gertsch et al., in prep) and the Whadi El Ghaib, Egypt, sections show many similarities and permit comparison and correlation of two geographically widely separated shallow environments at the time of OAE2. Both environments supported oyster biostromes during the late Cenomanian. The transgression during the C-T transition ended their reign depositing deeper facies as evident by the presence of benthic foraminiferal assemblages in the lower part of the sections, followed by the appearance of planktic foraminifera at Azazoul and ammonite at Whadi El Ghaib.

δ13C records of these two sections can be correlated and compared with deeper water sequences of the Tarfaya basin in southern Morocco (Fig. 8). In the shallow water sequences, the onset of the δ13C excursion is well marked at the base of the thickest oyster-rich limestone beds. The main excursion is well defined for both sections and occurs in the alternating thin shale/limestone layers at Azazoul and in the nodular marls at Wadi El Ghaib. Dysoxic conditions are indicated in these two sequences during the carbon isotope excursion by poor foraminiferal assemblages dominated by low-oxygen tolerant benthics and oyster biostromes.

The phosphorus concentration records show different trends. The P maximum extends over the entire range of increasing δ13C values at the Azazoul beach section, but is only present at the onset of the excursion at the Whadi El Ghaib section. The difference may be due to the low sample resolution in the oyster-rich beds. Alternatively, the difference may be due to post-depositional diagenesis influencing the P concentrations in the sediments.

Mineralogical assemblages are similar in both sections, with the oyster-rich beds dominated by kaolinite due to the humid climate. The disappearance of the oyster-rich limestone beds is associated with dominant smectite, which indicates dry and seasonal climatic conditions. The transition between these two climate regimes is different in the two sections. At Azazoul, the decrease in kaolinite is slow and constant, whereas at Whadi El Ghaib it is abrupt, possibly due to a hiatus or a more rapid climate change. No sedimentologic evidence for a hiatus was detected.

References

Abed, A.M., and Sadaqah, R. (1998). "Role of upper Cretaceous oyster bioherms in the deposition and accumulation of high-grade phosphorites in central Jordan". Journal of Sedimentary Research 68, no 68: 1009-1020.

Adatte, T., Stinnesbeck, W., Keller, G. (1996). "Lithostratigraphic and mineralogic correlations of near K/T boundary sediments northeastern Mexico: Implications for origin and nature of deposition." The Cretaceous-Tertiary Event and Other Catastrophes in Earth History, Boulder, Colorado, v. Geological Society of America Special Paper 307: 211-226.

Arthur, M. A., W. E. Dean, et al. (1988). "Geochemical And Climatic Effects Of Increased Marine Organic-Carbon Burial At The Cenomanian Turonian Boundary." Nature 335(6192): 714-717.

Bauer, J., Kuss, J., Steuber, T. (2003). "Sequence architecture and carbonate platform configuration (Late Cenomanian-Santonian), Sinai, Egypt." Sedimentology 50: 387-414.

Bauer, J., Marzouk, A.M., Steuber, T., and Kuss, J. (2001). " Lithostratigraphy and biostratigraphy of the Cenomanian-Santonian strata of Sinai, Egypt". Cretaceous Research 22: 497-526.

Bodin, S., Godet, A., Follmi, K.B., Vermeulen, J., Arnaud, H., Strasser, A., Fiet, N., Adatte, T., 2006. "The late Hauterivian Faraoni ocenic event in the western Tethys: Evidence from phosphorus burial rates." Paleogeography, Paleoclimatology, Paleoecology 235(1-3): 245-264.

Chamley, H. (1989). Clay sedimentology.

Cherief, O. H., Al Rifaiy, I.A., Al Afify, F.I. & Orabi, O.H. (1989). "Foraminiferal biostartigraphy and paleoecology of some Cenomanian-Turonian exposures in west central Sinai (Egypt)." Revue de Micropaléontologie 31: 243-262.

Davey, S.D., and Jenkyns, H.C. (1999). "Carbon-isotope stratigrfaphy of shallow-water limestones and implications for the timing of Late Cretaceoussea-level rise and anoxic events (Cenomanian-Turonian of the peri-Adriatic carbonate platform, Croatia)". Eclogae geol. Helv. 92: 163-170.

Erba, E. and F. Tremolada (2004). "Nannofossil carbonate fluxes during the Early Cretaceous: Phytoplankton response to nutrification episodes, atmospheric CO2, and anoxia." Paleoceanography 19(1).

Erbacher, J., J. Thurow, et al. (1996). "Evolution patterns of radiolaria and organic matter variations: A new approach to identify sea-level changes in mid-Cretaceous pelagic environments." Geology 24(6): 499-502.

Froelich, P.N., Klinkhammer, G.P., Bender, M.L., Luedtke, N.A, Heath, G.R., Cullen, D., Dauphin, P., Hammond, D., Hartman, B., Maynard, V. (1979). "Early oxidation of organic matter in pelagic sediments of the eastern equatorial Atlantic: suboxic diagenesis". Geochemica et Cosmochimica Acta 43: 1075-1090.

Gertsch, B., Keller, G., Adatte, T., Berner, Z., Stueben, D., Tantawy, A.A.A.M., El-Sabbagh, A.M., and Mort, H.P. (in prep). "Middle and Late Cenomanian Anoxia in the shallow shelf environment in NW Morocco".

Ghorab, M. A. (1961). "Abnormal stratigraphic features in Ras Gharib Oilfield, Egypt." Proceedings of the Third Arab Petroleum Congress, Alexandria, Egypt: 1-10.

Godet, A., Bodin, S., Adatte, T. and Foellmi, K.B. (in press). "Clay mineral assemblages along the Northern Tethyan margin during the Late Hauterivian - Early Aptian: Interactions beween climate change and carbonate platform evolution."

Hallam, A. (1992). "Phanerozoic sea level changes." Columbia press, New York.

Haq, B. U., J. Hardenbol, et al. (1987). "Chronology Of Fluctuating Sea Levels Since The Triassic." Science 235(4793): 1156-1167.

Hart, M. B. and P. N. Leary (1989). "The Stratigraphic And Paleogeographic Setting Of The Late Cenomanian Anoxic Event." Journal Of The Geological Society 146: 305-310.

Huber, B. T., R. D. Norris, et al. (2002). "Deep-sea paleotemperature record of extreme warmth during the Cretaceous." Geology 30(2): 123-126.

Jarvis, I., Carson, G. A., Cooper, M. K. E., Hart, M. B., Leary, P. N., Tocher, B. A., Horne, D. and Rosenfeld, A. (1988). Microfossil assemblages and the Cenomanian-Turonian (late Cretaceous) oceanic anoxic event. Cretaceous Research 9, 3-103.

Jenkyns, H.C., Gale, A.S., Corfield, R.M. (1994). "Carbon- and oxygen-isotope stratigraphy of the English Chalk and Italian Scaglia and its palaeoclimatic significance." Geological Magazine 131: p. 1-34.

Kassab, A. S. and N. A. Obaidalla (2001). "Integrated biostratigraphy and inter-regional correlation of the Cenomanian-Turonian deposits of Wadi Feiran, Sinai, Egypt." Cretaceous Research 22(1): 105-114.

Kassab, A. (1999). "Cenomanian-Turonian boundary in the Gulf of Suez region, Egypt: towards an inter-regional correlation, based on ammonites." Geological Society of Egypt, Special Publication 2: 61-98

Kassab, A. I., M.M. (1996). "Biostratigraphy of the Upper Cretaceous sequence of the Gebel Musabaa Salama area, south-west Sinai, Egypt." Arabian Gulf Journal of Scientific Research 14: 63-78.

Kassab, A. I., M.M. (1994). "Upper Cretaceous invertebrate fossils from the area northeast of Abu Zeneima, Sinai, Egypt." Neues Jahrbuch für Geologie und Paläontologie, Abhandlungen 191: 221-249.

Kassab, A. S. (1985). Palaeontological and stratigraphical studies of Cretaceous sections in Wadi Tarfa and Wadi Qena, Eastern Desert, Egypt. Ph D., thesis, Assiut University, Assiut, 221 pp.

Keller, G., Z. Berner, et al. (2004). "Cenomanian-Turonian and delta C-13, and delta O-18, sea level and salinity variations at Pueblo, Colorado." Palaeogeography Palaeoclimatology Palaeoecology 211(1-2): 19-43.

Keller, G., Q. Han, et al. (2001). "Palaeoenvironment of the Cenomanian-Turonian transition at Eastbourne, England." Cretaceous Research 22(4): 391-422.

Keller, G. and A. Pardo (2004). "Age and paleoenvironment of the Cenornanian-Turonian global stratotype section and point at Pueblo, Colorado." Marine Micropaleontology 51(1-2): 95-128.

Kolonic, S., Damste, J.S.S., Bottcher, M.E., Kuypers, M.M.M., Kuhnt, W., Beckmann, B., Scheeder, G., Wagner, T, (2002). "Geochemical characterization of Cenomanian/Turonian black shales from the Tarfaya Basin (SW Morocco) - Relationships between palaeoenvironmental conditions and early sulphurization of sedimentary organic matter." Journal of Petroleum Geology 25, 325-350.

Kolonic, S., T. Wagner, et al. (2005). "Black shale deposition on the northwest African Shelf during the Cenomanian/Turonian oceanic anoxic event: Climate coupling and global organic carbon burial." Paleoceanography 20(1).

Kora, M., Shahin, A. & Semiet, A. (1994). "Biostratigraphy and paleoecology of some Cenomanian successions in the west-central Sinai, Egypt." Neues Jahrbuch für Geologie und Paläontologie, Monatshefte 1994: 597-617.

Kora, M., Hamama, H.H. (1987). "Biostratigraphy of the Cenomanian-Turonian successionsof Gebel Gunna, southeastern Sinai, Egypt." Mansoura Faculty of Science, Bulletin 14: 289-301.

Kuhnt, W., Nederbragt, A., Leine, L. (1997). "Cyclicity of Cenomanian-Turonian organic-carbon-rich sediments in the Tarfaya Atlantic Coastal Basin (Morocco)." Cretaceous Research 18, 587-601.

Kuhnt, W., F. Luderer, F., Nederbragt, S., Thurow, J., Wagner, T. (2004). "Orbital-scale record of the late Cenomanian-Turonian oceanic anoxic event (OAE-2) in the Tarfaya Basin (Morocco)." International Journal Of Earth Sciences 94(1): 147-159.

Kübler, B. (1983). "Dosage quantitatif des minéraux majeurs des roches sédimentaires par diffraction X." Cahiers de l'Institut de Géologie Series AX n°1.1 and 1.2: 1-13.

Kübler, B. (1987). "Cristallinité de l'illite: méthode normalisées de préparation de mesure, méthode automatique normalisées de mesure." Cahiers de l'Institut de Géologie.

Kübler, B., Jaboyedoff, M. (2000). "Illite Cristallinity." C.R. Ac. Sc. Paris, Sciences de la terre et des planès / Earth & Planetary Sciences 331 331: 75-89.

Leckie, R. M., T. J. Bralower, et al. (2002). "Oceanic anoxic events and plankton evolution: Biotic response to tectonic forcing during the mid-Cretaceous." Paleoceanography 17(3).

Libes, S.M. (1992). "An Introduction to Marine Biogeochemistry". John Wiley and Sons, New York.

Luning, S., S. Kolonic, et al. (2004). "Integrated depositional

model for the Cenomanian-Turonian organic-rich strata in North Africa." Earth-Science Reviews 64(1-2): 51-117.

Luning, S., Marzouk, A.M., Morsi, A.M., Kuss, J. (1998). "Sequence stratigraphy of the Upper Cretaceous of central-east Sinai, Egypt." Cretaceous Research 19: 153-196.

Marshall, J.D. (1992). "Climatic and oceanographic isotopic signals from the carbonate rock record and their preservation". Geological Magazine 129(2): 143-160.

Mort, H. P., Adatte, T., Foellmi, K.B., Keller, G., Steinmann, P., Matera, V., Berner, Z., Stueben, D. (in press). "Phosphorus and the roles of productivity and nutrient recycling during Oceanic Event 2."

Nederbragt, A. & Fiorentino, A. (l999). "Stratigraphy and paleoceanography of the Cenomanian-Turonian boundary event in Oued Mellegue, northwestern Tunisia." Cretaceous Research 20, 47-62.

Nield, E.W. and Tucker, V.C.T. (1985). "Paleontology, An Introduction". Pergamon Press: 178 p.

Norris, R. D., K. L. Bice, et al. (2002). "Jiggling the tropical thermostat in the Cretaceous hothouse." Geology 30(4): 299-302.

Orabi, H. O. (1992). "Cenomanian-Turonian boundary in Whadi Watir, southeastern Sinai, Gulgf of Aqaba, Egypt." Journal of African Earth Sciences 15: 281-291.

Paul, C.R. C., Lamolda, M. A., Mitchell, S. F., Vaziri, M. R., Gorostidi, A. & Marshall, J. D. (l999). The Cenomanian-Turonian boundary at Eastbourne (Sussex, UK): a proposed European reference section. Paleogeography, Paleoclimatology, Paleoecology 150, 83-121.

Perch-Nielsen, K., 1985. Cenozoic calcareous nannofossils. In Plankton stratigraphy (Bolli, H.M., Saunders, J.B., & Perch-Nielsen, K.): 422-454 (Cambridge University Press, Cambridge.

Pufahl, P.K., James, N.P. (2006). "Monospecific Pliocene oyster buildups, Murray Basin, South Australia: Brackish water end member of the reef spectrum". Paleogeography, Paleoclimatology, Paleoecology 233: 11-33.

Schrag, D.P., DePaolo, D.J., Richter, F.M. (1995). "Reconstructing past sea surface temperatures: Correcting for diagenesis of bulk marine carbonate". Geochemica et Cosmochimica Acta 59 (11): 2265-2278.

Tantawy, A. (2003). "Calcareous nannofossil biostratigraphy and paleoecology of the Cretaceous-Tertiary transition in the central Eastern Desert of Egypt." Marine Micropaleontology 47(3-4): 323-356.

Tsikos, H., H. C. Jenkyns, et al. (2004). "Carbon-isotope stratigraphy recorded by the Cenomanian-Turonian Oceanic Anoxic Event: correlation and implications based on three key localities." Journal Of The Geological Society 161: 711-719.

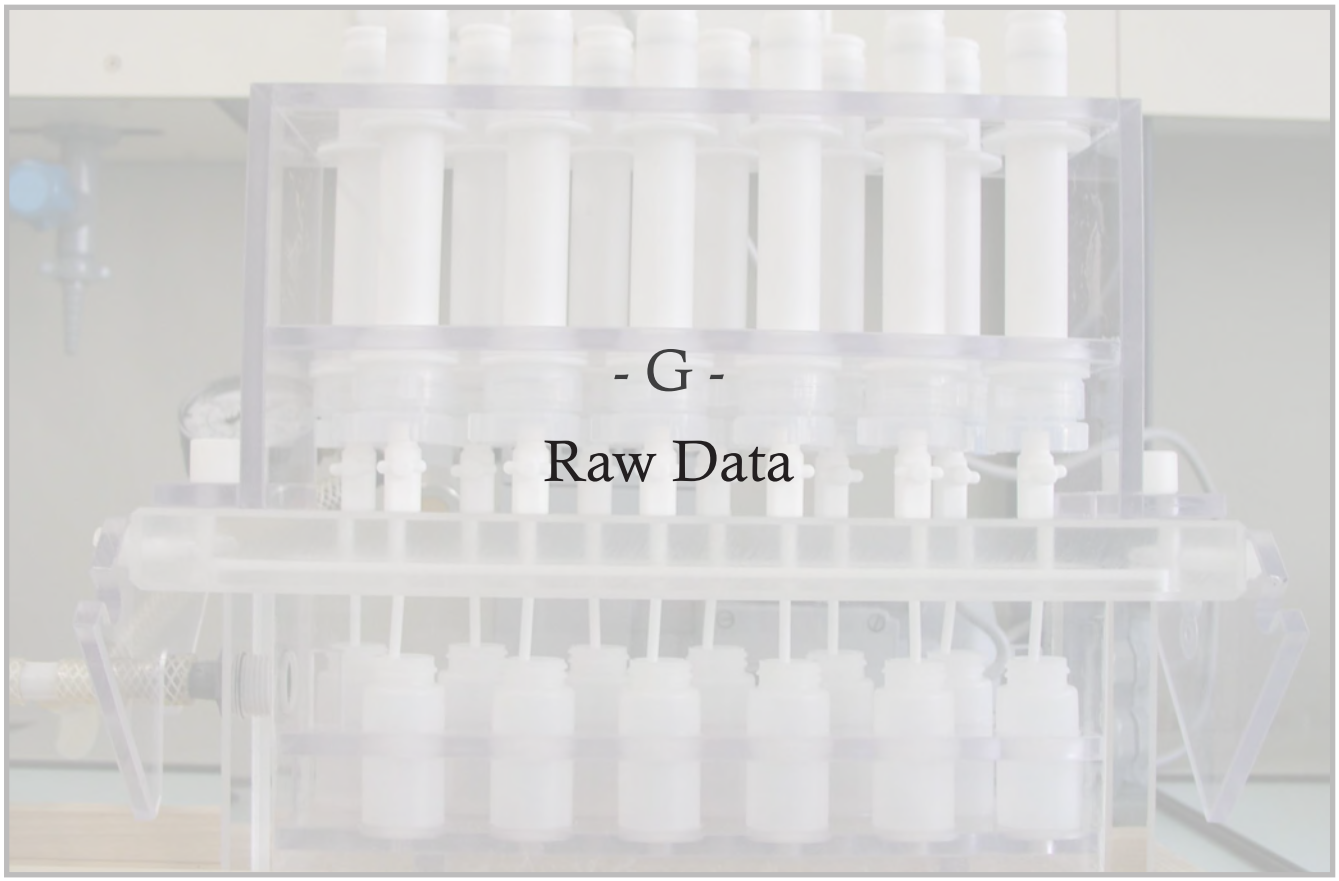

- G -

Raw Data

G.1. Phosphorus Speciation Data

Mohammed Plage, Morocco

Pueblo, USA

Eastbourne, UK

Furlo, Italy

Manilva, Spain

G.1.0.1. Mohammed Plage, Morocco: Authigenic-P

Depth (m)	No. GEA	No. Client	Wt. (mg)	Abs	[P] (mM)	dilution correction	[P] ug/L	P mg/L er mg sample		[P] mg/g	[P] ppm
17.75	24488	MB 82	100.4	0.673	32.48	32.48	1005.78	1.01	0.00	0.10	100.18
18.2	26037	MB 85	101.5	0.353	16.86	16.86	522.21	0.52	0.00	0.05	51.45
18.45	26039	MB 87	100.2	0.558	26.86	26.86	832.00	0.83	0.00	0.08	83.03
18.65	26040	MB 88	101.7	0.247	11.69	11.69	362.03	0.36	0.00	0.04	35.60
19.1	26042	MB 90	102	0.295	14.03	14.03	434.57	0.43	0.00	0.04	42.60
19.3	26043	MB 91	101.9	0.723	34.92	34.92	1081.34	1.08	0.00	0.11	106.12
19.45	26044	MB 92	103.7	0.359	17.15	17.15	531.28	0.53	0.00	0.05	51.23
19.6	26045	MB 93	100.8	0.599	28.87	28.87	893.96	0.89	0.00	0.09	88.69
19.75	26046	MB 94	100.9	0.577	27.79	27.79	860.71	0.86	0.00	0.09	85.30
19.95	26047	MB 95	103.7	0.654	31.55	31.55	977.07	0.98	0.00	0.09	94.22
20.15	26048	MB 96	101.2	0.785	37.94	37.94	1175.03	1.18	0.00	0.12	116.11
20.3	26049	MB 97	105.7	0.703	33.94	33.94	1051.12	1.05	0.00	0.10	99.44
20.5	26050	MB 98	100.2	0.581	27.99	27.99	866.76	0.87	0.00	0.09	86.50
20.7	26051	MB 99	99.4	0.691	33.35	33.35	1032.98	1.03	0.00	0.10	103.92
20.85	26052	MB 100	101	0.672	32.43	32.43	1004.27	1.00	0.00	0.10	99.43
21	26053	MB 101	100.3	0.314	14.96	14.96	463.28	0.46	0.00	0.05	46.19
21.1	26054	MB 102	101.6	0.406	19.45	19.45	602.31	0.60	0.00	0.06	59.28
21.2	26055	MB 103	102.7	0.28	13.30	13.30	411.90	0.41	0.00	0.04	40.11
21.3	26056	MB 104	100.8	0.118	5.40	5.40	167.09	0.17	0.00	0.02	16.58
21.4	26057	MB 105	100.6	0.452	21.69	21.69	671.82	0.67	0.00	0.07	66.78
21.55	26058	MB 106	104.1	0.5	24.03	24.03	744.35	0.74	0.00	0.07	71.50
21.75	26059	MB 107	101.2	0.429	20.57	20.57	637.06	0.64	0.00	0.06	62.95
21.95	26060	MB 108	104	0.33	15.74	15.74	487.46	0.49	0.00	0.05	46.87
22.1	26061	MB 109	103.7	0.366	17.50	17.50	541.86	0.54	0.00	0.05	52.25
22.3	26062	MB 110	102.2	0.375	17.94	17.94	555.46	0.56	0.00	0.05	54.35
22.45	26063	MB 111	97.8	0.764	36.92	36.92	1143.30	1.14	0.00	0.12	116.90
22.7	26064	MB 112	104	0.503	24.18	24.18	748.89	0.75	0.00	0.07	72.01
23.15	26066	MB 114	101.9	0.442	21.20	21.20	656.71	0.66	0.00	0.06	64.45
23.25	26067	MB 115	103.2	0.702	33.89	33.89	1049.60	1.05	0.00	0.10	101.71
23.4	26068	MB 116	106.1	0.39	18.67	18.67	578.13	0.58	0.00	0.05	54.49
23.55	26069	MB 117	104.7	0.265	12.57	12.57	389.23	0.39	0.00	0.04	37.18
23.7	26070	MB 118	101.2	0.397	19.01	19.01	588.70	0.59	0.00	0.06	58.17
23.85	26071	MB 119	98.1	0.413	19.79	19.79	612.88	0.61	0.00	0.06	62.48
24.05	26072	MB 120	102	1.488	72.24	72.24	2237.37	2.24	0.00	0.22	219.35

G.1.0.2. Mohammed Plage, Morocco: Detrital-P

Depth (m)	No. GEA	No. Client	Wt. (mg)	Abs	[P] (mM)	dilution correction	[P] ug/L	P mg/L er mg sample		[P] mg/g	[P] ppm
17.75	24488	MB 82	100.4	0.28	12.0	120.15	3721	3.72	0.00037	0.371	371
18.2	26037	MB 85	101.5	0.027	1.2	12.28	380	0.38	0.00004	0.037	37
18.45	26039	MB 87	100.2	0.122	5.3	52.79	1635	1.63	0.00016	0.163	163
18.65	26040	MB 88	101.7	0.121	5.2	52.36	1622	1.62	0.00016	0.159	159
19.1	26042	MB 90	102.0	0.114	4.9	49.38	1529	1.53	0.00015	0.150	150
19.3	26043	MB 91	101.9	0.742	31.7	317.11	9821	9.82	0.00096	0.964	964
19.45	26044	MB 92	103.7	0.098	4.3	42.55	1318	1.32	0.00013	0.127	127
19.6	26045	MB 93	100.8	0.241	10.4	103.52	3206	3.21	0.00032	0.318	318
19.75	26046	MB 94	100.9	0.241	10.4	103.52	3206	3.21	0.00032	0.318	318
19.95	26047	MB 95	103.7	0.628	26.9	268.51	8316	8.32	0.00080	0.802	802
20.15	26048	MB 96	101.2	0.352	15.1	150.84	4672	4.67	0.00046	0.462	462
20.3	26049	MB 97	105.7	0.017	0.8	8.02	248	0.25	0.00002	0.024	24
20.5	26050	MB 98	100.2	0.019	0.9	8.87	275	0.27	0.00003	0.027	27
20.7	26051	MB 99	99.4	0.326	14.0	139.76	4328	4.33	0.00044	0.435	435
20.85	26052	MB 100	101.0	0.607	26.0	259.56	8039	8.04	0.00080	0.796	796
21	26053	MB 101	100.3	0.12	5.2	51.93	1608	1.61	0.00016	0.160	160
21.1	26054	MB 102	101.6	0.125	5.4	54.07	1674	1.67	0.00016	0.165	165
21.2	26055	MB 103	102.7	0.044	2.0	19.53	605	0.60	0.00006	0.059	59
21.3	26056	MB 104	100.8	0.053	2.3	23.37	724	0.72	0.00007	0.072	72
21.4	26057	MB 105	100.6	0.058	2.6	25.50	790	0.79	0.00008	0.079	79
21.55	26058	MB 106	104.1	0.013	0.6	6.32	196	0.20	0.00002	0.019	19
21.75	26059	MB 107	101.2	0.01	0.5	5.04	156	0.16	0.00002	0.015	15
21.95	26060	MB 108	104.0	0.032	1.4	14.42	446	0.45	0.00004	0.043	43
22.1	26061	MB 109	103.7	0.018	0.8	8.45	262	0.26	0.00003	0.025	25
22.3	26062	MB 110	102.2	0.149	6.4	64.30	1991	1.99	0.00019	0.195	195
22.45	26063	MB 111	97.8	0.022	1.0	10.15	314	0.31	0.00003	0.032	32
22.7	26064	MB 112	104.0	0.019	0.9	8.87	275	0.27	0.00003	0.026	26
23.15	26066	MB 114	101.9	0.009	0.5	4.61	143	0.14	0.00001	0.014	14
23.25	26067	MB 115	103.2	0.011	0.5	5.46	169	0.17	0.00002	0.016	16
23.4	26068	MB 116	106.1	0.041	1.8	18.25	565	0.57	0.00005	0.053	53
23.55	26069	MB 117	104.7	0.029	1.3	13.14	407	0.41	0.00004	0.039	39
23.7	26070	MB 118	101.2	0.035	1.6	15.70	486	0.49	0.00005	0.048	48
23.85	26071	MB 119	98.1	0.028	1.3	12.71	394	0.39	0.00004	0.040	40
24.05	26072	MB 120	102.0	0.013	0.6	6.32	196	0.20	0.00002	0.019	19

G.1.0.3. Mohammed Plage, Morocco: Organic-P

Depth (m)	No. GEA	No. Client	Wt. (mg)	Abs	[P] (mM)	dilution correction	[P] ug/L	P mg/L er mg sample		[P] mg/g	[P] ppm
17.75	24488	MB 82	100.4	0.015	0.640	6.402	198	0.198	0.000	0.020	20
18.2	26037	MB 85	101.5	0.009	0.384	3.841	119	0.119	0.000	0.012	12
18.45	26039	MB 87	100.2	0.014	0.598	5.975	185	0.185	0.000	0.018	18
18.65	26040	MB 88	101.7	0.011	0.469	4.695	145	0.145	0.000	0.014	14
19.1	26041	MB 89	100	0.452	19.291	385.830	11949	11.949	0.001	1.195	1195
19.3	26043	MB 91	101.9	0.043	1.835	18.353	568	0.568	0.000	0.056	56
19.45	26044	MB 92	103.7	0.013	0.555	5.548	172	0.172	0.000	0.017	17
19.6	26045	MB 93	100.8	0.027	1.152	11.524	357	0.357	0.000	0.035	35
19.75	26046	MB 94	100.9	0.02	0.854	8.536	264	0.264	0.000	0.026	26
19.95	26047	MB 95	103.7	0.034	1.451	14.511	449	0.449	0.000	0.043	43
20.15	26048	MB 96	101.2	0.038	1.622	16.219	502	0.502	0.000	0.050	50
20.3	26049	MB 97	105.7	0.019	0.811	8.109	251	0.251	0.000	0.024	24
20.5	26050	MB 98	100.2	0.011	0.469	4.695	145	0.145	0.000	0.015	15
20.7	26051	MB 99	99.4	0.017	0.726	7.256	225	0.225	0.000	0.023	23
20.85	26052	MB 100	101	0.094	4.012	40.119	1243	1.243	0.000	0.123	123
21	26053	MB 101	100.3	0.016	0.683	6.829	211	0.211	0.000	0.021	21
21.1	26054	MB 102	101.6	0.015	0.640	6.402	198	0.198	0.000	0.020	20
21.2	26055	MB 103	102.7	0.011	0.469	4.695	145	0.145	0.000	0.014	14
21.3	26056	MB 104	100.8	0.009	0.384	3.841	119	0.119	0.000	0.012	12
21.4	26057	MB 105	100.6	0.009	0.384	3.841	119	0.119	0.000	0.012	12
21.55	26058	MB 106	104.1	0.004	0.171	1.707	53	0.053	0.000	0.012	12
21.75	26059	MB 107	101.2	0.001	0.043	0.427	13	0.013	0.000	0.015	15
21.95	26060	MB 108	104	0	0.000	0.000	0	0.000	0.000	0.017	17
22.1	26061	MB 109	103.7	0.006	0.256	2.561	79	0.079	0.000	0.021	21
22.3	26062	MB 110	102.2	0.032	1.366	13.658	423	0.423	0.000	0.026	26
22.45	26063	MB 111	97.8	0.002	0.085	0.854	26	0.026	0.000	0.015	15
22.7	26064	MB 112	104	0.005	0.213	2.134	66	0.066	0.000	0.026	26
23.15	26066	MB 114	101.9	0.005	0.213	2.134	66	0.066	0.000	0.014	14
23.25	26067	MB 115	103.2	0.005	0.213	2.134	66	0.066	0.000	0.015	15
23.4	26068	MB 116	106.1	0.001	0.043	0.427	13	0.013	0.000	0.023	23
23.55	26069	MB 117	104.7	0.013	0.555	5.548	172	0.172	0.000	0.022	22
23.7	26070	MB 118	101.2	0.001	0.043	0.427	13	0.013	0.000	0.014	14
23.85	26071	MB 119	98.1	0.01	0.427	4.268	132	0.132	0.000	0.017	17
24.05	26072	MB 120	102	0.008	0.341	3.414	106	0.106	0.000	0.014	14

G.1.0.4. Pueblo GSSP, USA: Iron-bound-P

Depth (m)	No. Client	Wt. (mg)	P mg/L	- blank	[P] mg/g	[P] ppm
8.85	PC-45	100.4	0.418	0.304	0.030	30
9.7	PC-48	100.1	0.361	0.247	0.025	25
10.12	PC-50	101.1	0.434	0.320	0.032	32
10.4	PC-51	100.3	0.417	0.303	0.030	30
10.7	PC-52	98	0.476	0.362	0.037	37
11.22	PC-54	100.7	0.483	0.369	0.037	37
11.35	PC-55	100.6	0.535	0.421	0.042	42
11.75	PC-58	100.7	0.51	0.396	0.039	39
11.85	PC-60	100.2	0.483	0.369	0.037	37
12.02	PC-62	99.6	0.44	0.326	0.033	33
12.1	PC-63	99.9	0.425	0.311	0.031	31
12.22	PC-64	101.1	0.445	0.331	0.033	33
12.27	PC-65	99.4	0.304	0.190	0.019	19
12.4	PC-66	99.8	0.492	0.378	0.038	38
12.4	PC-66	100.4	0.385	0.271	0.027	27
12.57	PC-67	100	0.231	0.117	0.012	12
12.7	PC-68	99.9	0.219	0.105	0.011	11
12.95	PC-70	99.6	0.215	0.101	0.010	10
13.08	PC-71	99.6	0.216	0.102	0.010	10
13.27	PC-74	100.7	0.172	0.058	0.006	6
13.77	PC-77	100.6	0.313	0.199	0.020	20

G.1.0.5. Pueblo GSSP, USA: Authigenic-P

Depth (m)	No. GEA	No. Client	Wt. (mg)	Abs	[P] (mM)	dilution correction	[P] ug/L	P mg/L	- blank	[P] mg/g	[P] ppm
8.85	13408	PC-45	100.4	0.421	7.6	75.95	2352	2.35	0.00023	0.234	23.43
9.7	13411	PC-48	100.1	0.226	3.9	39.04	1209	1.21	0.00012	0.121	12.08
10.12	13413	PC-50	101.1	0.515	9.4	93.75	2903	2.90	0.00029	0.287	28.72
10.4	13414	PC-51	100.3	0.457	8.3	82.77	2563	2.56	0.00026	0.256	25.56
10.7	13415	PC-52	9.8	0.256	4.5	44.72	1385	1.38	0.00141	1.413	141.31
11.22	13417	PC-54	100.7	0.564	10.3	103.03	3191	3.19	0.00032	0.317	31.69
11.35	13418	PC-55	100.6	0.845	15.6	156.23	4838	4.84	0.00048	0.481	48.10
11.62	13419	PC-56	100.5	0.923	17.1	171.00	5296	5.30	0.00053	0.527	52.69
11.75	13421	PC-58	100.7	1.052	19.5	195.42	6052	6.05	0.00060	0.601	60.10
11.85	13423	PC-60	100.2	0.793	14.6	146.38	4534	4.53	0.00045	0.452	45.24
12.02	13425	PC-62	99.6	2.38	44.7	446.84	13839	13.84	0.00139	1.389	138.94
12.1	13426	PC-63	99.9	0.604	11.1	110.60	3425	3.43	0.00034	0.343	34.29
12.22	13427	PC-64	101.1	0.497	9.0	90.34	2798	2.80	0.00028	0.277	27.67
12.27	13428	PC-65	99.4	0.593	10.9	108.52	3361	3.36	0.00034	0.338	33.81
12.4	13429	**PC-66**	99.8	0.068	0.9	9.12	283	0.28	0.00003	0.028	2.83
12.57	13430	PC-67	100	0.261	4.6	45.66	1414	1.41	0.00014	0.141	14.14
12.7	13431	PC-68	99.9	2.275	42.7	426.96	13223	13.22	0.00132	1.324	132.36
12.95	13433	PC-70	99.6	0.68	12.5	124.99	3871	3.87	0.00039	0.389	38.86
13.08	13434	PC-71	99.6	1.835	34.4	343.66	10643	10.64	0.00107	1.069	106.86
13.27	13437	PC-74	100.7	0.649	11.9	119.12	3689	3.69	0.00037	0.366	36.64
13.77	13440	**PC-77**	100.6	0.371	6.6	66.49	2059	2.06	0.00020	0.205	20.47
13.77	13440	PC-77 (dupli)	100.3	0.359	6.4	64.22	1989	1.99	0.00020	0.198	19.83

G.1.0.6. Pueblo GSSP, USA: Detrital-P

Depth (m)	No. GEA	No. Client	Wt. (mg)	Abs	[P] (mM)	dilution correction	[P] ug/L	P mg/L - blank		[P] mg/g	[P] ppm
8.85	13408	PC-45	100.4	0.440	6.83	68	100400	2114.22684	2.114	0.2106	21.06
9.7	13411	PC-48	100.1	0.211	3.04	30	100100	940.99077	0.941	0.0940	9.40
10.12	13413	PC-50	101.1	0.147	1.98	20	101100	612.07480	0.612	0.0605	6.05
10.4	13414	PC-51	100.3	0.195	2.77	28	100300	858.50561	0.859	0.0856	8.56
11.22	13417	PC-54	100.7	0.295	4.42	44	100700	1370.32345	1.370	0.1361	13.61
11.35	13418	PC-55	100.6	0.192	2.72	27	100600	842.62338	0.843	0.0838	8.38
11.75	13421	PC-58	100.7	0.239	3.50	35	100700	1083.41856	1.083	0.1076	10.76
11.85	13423	PC-60	100.2	0.475	7.40	74	100200	2292.51774	2.293	0.2288	22.88
12.02	13425	PC-62	99.6	0.054	0.44	4	99600	135.60775	0.136	0.0136	1.36
12.1	13426	PC-63	99.9	0.245	3.59	36	99900	1111.59671	1.112	0.1113	11.13
12.22	13427	PC-64	101.1	0.240	3.52	35	101100	1090.59118	1.091	0.1079	10.79
12.27	13428	PC-65	99.4	0.522	8.18	82	99400	2533.31292	2.533	0.2549	25.49
12.4	13429	PC-66	99.8	0.059	0.52	5	99800	161.22426	0.161	0.0162	1.62
12.4	13429	**PC-66 (dupli)**	100.4	0.048	0.34	3	100400	104.86794	0.105	0.0104	1.04
12.57	13430	PC-67	100	0.247	3.63	36	100000	1124.40497	1.124	0.1124	11.24
12.7	13431	PC-68	99.9	0.097	1.15	11	99900	355.90972	0.356	0.0356	3.56
13.08	13434	PC-71	99.6	0.070	0.70	7	99600	217.58058	0.218	0.0218	2.18
13.27	13437	PC-74	100.7	0.237	3.47	35	100700	1073.17195	1.073	0.1066	10.66
13.77	13440	PC-77	100.6	0.197	2.80	28	100600	868.23989	0.868	0.0863	8.63
13.77	13440	**PC-77 (dupli)**	100.3	0.168	2.32	23	100300	719.66414	0.720	0.0718	7.18

G.1.0.7. Pueblo GSSP, USA: Organic-P

Depth (m)	No. GEA	No. Client	Wt. (mg)	Abs	[P] (mM)	dilution correction	[P] ug/L	P mg/L - blank		[P] mg/g	[P] ppm
8.85	13408	PC-45	100.4	0.12	1.98	19.836	614	0.6143	0.000061	0.061	6.119
9.7	13411	PC-48	100.1	0.10	1.62	16.157	500	0.5004	0.000050	0.050	4.999
10.12	13413	PC-50	101.1	0.09	1.49	14.877	461	0.4607	0.000046	0.046	4.557
10.4	13414	PC-51	100.3	0.08	1.31	13.117	406	0.4062	0.000041	0.041	4.050
10.7	13415	PC-52	98.0	0.09	1.50	15.037	466	0.4657	0.000048	0.048	4.752
11.22	13417	PC-54	100.7	0.04	0.62	6.239	193	0.1932	0.000019	0.019	1.919
11.35	13418	PC-55	100.6	0.03	0.43	4.319	134	0.1338	0.000013	0.013	1.330
11.75	13421	PC-58	100.7	0.04	0.59	5.919	183	0.1833	0.000018	0.018	1.820
11.85	13423	PC-60	100.2	0.09	1.38	13.757	426	0.4261	0.000043	0.043	4.252
12.02	13425	PC-62	99.6	0.02	0.38	3.839	119	0.1189	0.000012	0.012	1.194
12.1	13426	PC-63	99.9	0.07	1.09	10.878	337	0.3369	0.000034	0.034	3.372
12.22	13427	PC-64	101.1	0.04	0.59	5.919	183	0.1833	0.000018	0.018	1.813
12.27	13428	PC-65	99.4	0.07	1.04	10.398	322	0.3220	0.000032	0.032	3.240
12.4	13429	PC-66	99.8	0.02	0.35	3.519	109	0.1090	0.000011	0.011	1.092
12.4	13429	**PC-66 (dupli)**	100.4	0.03	0.43	4.319	134	0.1338	0.000013	0.013	1.332
12.57	13430	PC-67	100.0	0.07	1.14	11.358	352	0.3517	0.000035	0.035	3.517
12.7	13431	PC-68	99.9	0.01	0.22	2.240	69	0.0694	0.000007	0.007	0.694
12.95	13433	PC-70	99.6	0.09	1.39	13.917	431	0.4310	0.000043	0.043	4.327
13.08	13434	PC-71	99.6	0.02	0.34	3.359	104	0.1040	0.000010	0.010	1.045
13.27	13437	PC-74	100.7	0.04	0.58	5.759	178	0.1783	0.000018	0.018	1.771
13.77	13440	PC-77	100.6	0.082	1.31	13.117	406	0.40624026	0.000040	0.040	4.038
13.77	13440	PC-77 (dupli)	100.3	0.079	1.26	12.637	391	0.39137781	0.000039	0.039	3.902

G.1.0.8. Eastbourne, UK: Iron-bound-P

Depth (m)	No. Client	Wt. (mg)	P mg/L - blank		[P] mg/g	[P] ppm
0.35	EB 1	99.4	0.361	0.361	0.036	36.32
0.50	EB 2	101.8	0.359	0.359	0.035	35.27
0.65	EB 3	100.9	0.254	0.254	0.025	25.17
0.75	EB 4	100.3	0.236	0.236	0.024	23.53
0.95	EB 5	99.4	0.237	0.237	0.024	23.84
1.10	EB 6	101	0.188	0.188	0.019	18.61
1.25	EB 7	99.8	0.11	0.11	0.011	11.02
1.40	EB 8	100.6	0.429	0.429	0.043	42.64
1.55	EB 9	100.1	0.279	0.279	0.028	27.87
1.70	EB 10	100.3	0.196	0.196	0.020	19.54
1.80	EB 11	100.6	0.256	0.256	0.025	25.45
1.85	EB 12	99	0.228	0.228	0.023	23.03
1.90	EB 13	103.2	0.151	0.151	0.015	14.63
1.92	EB 14	102.2	0.113	0.113	0.011	11.06
2.15	EB 15	100	0.000	0.000	0.000	0.00
2.25	EB 16	99.3	0.000	0.000	0.000	0.00
2.60	EB 17	100.3	0.107	0.107	0.011	10.67
2.90	EB 18	101.3	0.106	0.106	0.010	10.46
3.25	EB 19	99.7	0.000	0.000	0.000	0.00
3.65	EB 20	101.8	0.000	0.000	0.000	0.00
3.85	EB 21	100.5	0.000	0.000	0.000	0.00
4.00	EB 22	100.4	0.000	0.000	0.000	0.00

G.1.0.9. Eastbourne, UK: Authigenic-P

Depth (m)	No. GEA	No. Client	Wt. (mg)	Abs	[P] (mM)	dilution correction	[P] ug/L	P mg/L	[P] mg/g	[P] ppm
0.35	-	EB 1	99.40	0.63	26.149	261	8098	8.098	0.815	815
0.50	-	EB 2	101.80	0.56	23.189	232	7182	7.182	0.705	705
0.65	-	EB 3	100.90	0.50	20.968	210	6494	6.494	0.644	644
0.75	-	EB 4	100.30	0.77	32.070	321	9932	9.932	0.990	990
0.95	-	EB 5	99.40	0.68	28.287	283	8761	8.761	0.881	881
1.10	-	EB 6	101.00	0.65	27.012	270	8366	8.366	0.828	828
1.25	-	EB 7	99.80	0.59	24.587	246	7614	7.614	0.763	763
1.40	-	EB 8	100.60	0.67	27.917	279	8646	8.646	0.859	859
1.55	-	EB 9	100.10	0.94	38.854	389	12033	12.033	1.202	1202
1.70	-	EB 10	100.30	0.93	38.648	386	11969	11.969	1.193	1193
1.80	-	EB 11	100.60	0.68	28.328	283	8773	8.773	0.872	872
1.85	-	EB 12	99.00	0.65	27.177	272	8417	8.417	0.850	850
1.90	-	EB 13	103.20	0.95	39.512	395	12237	12.237	1.186	1186
1.92	-	EB 14	102.20	0.72	29.849	298	9244	9.244	0.905	905
2.15	-	EB 15	100.00	0.57	23.764	238	7360	7.360	0.736	736
2.25	-	EB 16	99.30	0.59	24.669	247	7640	7.640	0.769	769
2.60	-	EB 17	100.30	0.56	23.353	234	7232	7.232	0.721	721
2.90	-	EB 18	101.30	0.52	21.791	218	6749	6.749	0.666	666
3.25	-	EB 19	99.70	0.62	25.820	258	7996	7.996	0.802	802
3.65	-	EB 20	101.80	0.57	23.764	238	7360	7.360	0.723	723
3.85	-	EB 21	100.5	0.68	28.205	282	8735	8.735	0.869	869
4.00	-	EB 22	100.4	0.50	20.968	210	6494	6.494	0.647	647

G.1.1.0. Eastbourne, UK: Detrital-P

Depth (m)	No. GEA	No. Client	Wt. (mg)	Abs	[P] (mM)	dilution correction	[P] ug/L	P mg/L	[P] mg/g	[P] ppm
0.35	-	EB 1	99.40	0.017	0.723	7.23	224	0.224	0.023	2.25
0.50	-	EB 2	101.80	0.009	0.383	3.83	119	0.119	0.012	1.16
0.65	-	EB 3	100.90	0.017	0.723	7.23	224	0.224	0.022	2.22
0.75	-	EB 4	100.30	0.038	1.617	16.17	501	0.501	0.050	4.99
0.95	-	EB 5	99.40	0.011	0.468	4.68	145	0.145	0.015	1.46
1.10	-	EB 6	101.00	0.044	1.872	18.72	580	0.580	0.057	5.74
1.25	-	EB 7	99.80	0.014	0.596	5.96	184	0.184	0.018	1.85
1.40	-	EB 8	100.60	0.010	0.425	4.25	132	0.132	0.013	1.31
1.55	-	EB 9	100.10	0.149	6.339	63.39	1963	1.963	0.196	19.61
1.70	-	EB 10	100.30	0.108	4.594	45.94	1423	1.423	0.142	14.19
1.80	-	EB 11	100.60	0.158	6.721	67.21	2082	2.082	0.207	20.69
1.85	-	EB 12	99.00	0.140	5.956	59.56	1844	1.844	0.186	18.63
1.90	-	EB 13	103.20	0.151	6.424	64.24	1989	1.989	0.193	19.28
1.92	-	EB 14	102.20	0.055	2.340	23.40	725	0.725	0.071	7.09
2.15	-	EB 15	100.00	0.037	1.574	15.74	487	0.487	0.049	4.87
2.25	-	EB 16	99.30	0.017	0.723	7.23	224	0.224	0.023	2.26
2.60	-	EB 17	100.30	0.025	1.064	10.64	329	0.329	0.033	3.28
2.90	-	EB 18	101.30	0.029	1.234	12.34	382	0.382	0.038	3.77
3.25	-	EB 19	99.70	0.049	2.085	20.85	646	0.646	0.065	6.48
3.65	-	EB 20	101.80	0.037	1.574	15.74	487	0.487	0.048	4.79
3.85	-	EB 21	100.50	0.007	0.298	2.98	92	0.092	0.009	0.92
4.00	-	EB 22	100.40	0.017	0.723	7.23	224	0.224	0.022	2.23

G.1.1.1. Eastbourne, UK: Organic-P

Depth (m)	No. GEA	No. Client	Wt. (mg)	Abs	[P] (mM)	dilution correction	[P] ug/L	P mg/L	[P] mg/g	[P] ppm
0.35	-	EB 1	99.4	0.002	0.086	0.86	27	0.027	0.003	0.27
0.50	-	EB 2	101.8	0.005	0.216	2.16	67	0.067	0.007	0.66
0.65	-	EB 3	100.9	0.003	0.129	1.29	40	0.040	0.004	0.40
0.75	-	EB 4	100.3	0.005	0.216	2.16	67	0.067	0.007	0.67
0.95	-	EB 5	99.4	0.003	0.129	1.29	40	0.040	0.004	0.40
1.10	-	EB 6	101.0	0.005	0.216	2.16	67	0.067	0.007	0.66
1.25	-	EB 7	99.8	0.002	0.086	0.86	27	0.027	0.003	0.27
1.40	-	EB 8	100.6	0.004	0.173	1.73	53	0.053	0.005	0.53
1.55	-	EB 9	100.1	0.014	0.604	6.04	187	0.187	0.019	1.87
1.70	-	EB 10	100.3	0.013	0.561	5.61	174	0.174	0.017	1.73
1.80	-	EB 11	100.6	0.017	0.733	7.33	227	0.227	0.023	2.26
1.85	-	EB 12	99.0	0.016	0.690	6.90	214	0.214	0.022	2.16
1.90	-	EB 13	103.2	0.012	0.518	5.18	160	0.160	0.016	1.55
1.92	-	EB 14	102.2	0.011	0.474	4.74	147	0.147	0.014	1.44
2.15	-	EB 15	100.0	0.012	0.518	5.18	160	0.160	0.016	1.60
2.25	-	EB 16	99.3	0.011	0.474	4.74	147	0.147	0.015	1.48
2.60	-	EB 17	100.3	0.007	0.302	3.02	93	0.093	0.009	0.93
2.90	-	EB 18	101.3	0.010	0.431	4.31	134	0.134	0.013	1.32
3.25	-	EB 19	99.7	0.005	0.216	2.16	67	0.067	0.007	0.67
3.65	-	EB 20	101.8	0.012	0.518	5.18	160	0.160	0.016	1.57
3.85	-	EB 21	100.5	0.011	0.474	4.74	147	0.147	0.015	1.46
4.00	-	EB 22	100.4	0.009	0.388	3.88	120	0.120	0.012	1.20

G.1.1.2. Furlo, Italy: Iron-bound-P

Depth (m)	No. Client	Wt. (mg)	P mg/L	- blank	[P] mg/g	[P] ppm
8.2	Fu-7	100	0.1	0.00	0.000	0.000
8.49	Fu-10	100.3	0.118	0.00	0.000	0.000
8.69	Fu-12	100.1	0.434	0.23	0.023	2.318
8.79	Fu-13	100.3	0.417	0.22	0.021	2.144
8.81	Fu-14	99.7	0.476	0.27	0.027	2.748
8.85	Fu-16	100	0.483	0.28	0.028	2.810
8.9	Fu-17	100	0.535	0.33	0.033	3.330
8.95	Fu-18	100	0.51	0.31	0.031	3.080
9.06	Fu-20	99.7	0.483	0.28	0.028	2.818
9.15	Fu-22	100.6	0.44	0.24	0.024	2.366
9.3	Fu-24	99.9	0.425	0.22	0.022	2.232
9.47	Fu-27	100.1	0.445	0.24	0.024	2.428
9.6	Fu-28	100.7	0.304	0.10	0.010	1.013
9.72	**Fu-30 (dupli)**	99.8	0.313	0.11	0.011	1.112
9.99	Fu-33	100.4	0.385	0.18	0.018	1.823
10.07	Fu-36	100.7	0.231	0.03	0.003	0.288
10.19	Fu-38	100.1	0.219	0.02	0.002	0.170
10.3	Fu-41	100	0.215	0.00	0.000	0.000
10.51	Fu-43	100.4	0.1	0.00	0.000	0.000
10.7	Fu-46	100.3	0.203	0.00	0.000	0.000
10.88	Fu-49	100.1	0.275	0.07	0.007	0.729

G.1.1.3. Furlo, Italy: Authigenic-P

Depth (m)	No. GEA	No. Client	Wt. (mg)	Abs	[P] (µM)	dilution correction	[P] ug/L	P mg/L	[P] mg/g	[P] ppm
8.20	-	Fu-7	100.0	-1.060	3.93	39.29	1217	1.217	0.122	122
8.49	-	Fu-10	100.3	-1.032	6.52	65.17	2018	2.018	0.201	201
8.69	-	Fu-12	100.1	-1.034	6.33	63.32	1961	1.961	0.196	196
8.79	-	Fu-13	100.3	-0.975	11.78	58.92	1825	1.825	0.182	182
8.81	-	Fu-14	99.7	-0.945	14.56	72.78	2254	2.254	0.226	226
8.85	-	Fu-16	100.0	-0.984	10.95	54.76	1696	1.696	0.170	170
8.90	-	Fu-17	100.0	-0.975	11.78	58.92	1825	1.825	0.182	182
8.95	-	Fu-18	100.0	-0.943	14.74	73.70	2283	2.283	0.228	228
9.06	-	Fu-20	99.7	-0.964	12.80	64.00	1982	1.982	0.199	199
9.15	-	Fu-22	100.6	-1.097	0.51	0.51	16	0.016	0.002	2
9.30	-	Fu-24	99.9	-1.069	3.10	3.10	96	0.096	0.010	10
9.47	-	Fu-27	100.1	-1.098	0.42	0.42	13	0.013	0.001	1
9.60	-	Fu-28	100.7	-0.707	36.55	36.55	1132	1.132	0.112	112
9.72	-	Fu-30	99.8	-0.813	26.75	26.75	829	0.829	0.083	83
9.72	-	**Fu-30 (dupli)**	99.8	-1.032	6.52	32.58	1009	1.009	0.101	101
9.99	-	Fu-33	100.4	-0.556	50.50	50.50	1564	1.564	0.156	156
10.07	-	Fu-36	100.7	-0.991	10.31	51.53	1596	1.596	0.158	158
10.19	-	Fu-38	100.1	-1.017	7.90	39.51	1224	1.224	0.122	122
10.30	-	Fu-41	100.0	-0.922	16.68	83.41	2583	2.583	0.258	258
10.51	-	Fu-43	100.4	-0.892	19.45	19.45	602	0.602	0.060	60
10.70	-	Fu-46	100.3	-0.991	10.31	10.31	319	0.319	0.032	32
10.88	-	Fu-49	100.1	-1.028	6.89	34.43	1066	1.066	0.107	107

G.1.1.4. Furlo, Italy: Detrital-P

Depth (m)	No. GEA	No. Client	Wt. (mg)	Abs	[P] (µM)	dilution correction	[P] ug/L	P mg/L	[P] mg/g	[P] ppm
8.20	-	Fu-7	100.0	0.018	0.25	2.48	77	0.077	0.008	7.67
8.49	-	Fu-10	100.3	0.034	0.51	5.12	159	0.159	0.016	15.81
8.69	-	Fu-12	100.1	0.028	0.41	4.13	128	0.128	0.013	12.77
8.79	-	Fu-13	100.3	0.915	15.07	301.47	9336	9.336	0.931	930.86
8.81	-	Fu-14	99.7	0.388	6.36	63.63	1971	1.971	0.198	197.66
8.85	-	Fu-16	100.0	0.416	6.83	68.26	2114	2.114	0.211	211.40
8.90	-	Fu-17	100.0	0.226	3.69	36.85	1141	1.141	0.114	114.14
8.95	-	Fu-18	100.0	0.589	9.69	96.85	3000	3.000	0.300	299.95
9.06	-	Fu-20	99.7	0.980	16.15	161.48	5001	5.001	0.502	501.60
9.15	-	Fu-22	100.6	0.090	1.44	14.38	445	0.445	0.044	44.26
9.30	-	Fu-24	99.9	0.033	0.50	4.96	153	0.153	0.015	15.36
9.47	-	Fu-27	100.1	0.078	1.24	12.39	384	0.384	0.038	38.34
9.60	-	Fu-28	100.7	0.019	0.26	2.64	82	0.082	0.008	8.12
9.72	-	Fu-30	99.8	0.044	0.68	6.77	210	0.210	0.021	21.02
9.72	-	**Fu-30 (dupli)**	99.8	0.060	0.94	9.42	292	0.292	0.029	29.23
9.99	-	Fu-33	100.4	0.023	0.33	3.30	102	0.102	0.010	10.19
10.07	-	Fu-36	100.7	0.033	0.50	4.96	153	0.153	0.015	15.24
10.19	-	Fu-38	100.1	0.026	0.38	3.80	118	0.118	0.012	11.75
10.30	-	Fu-41	100.0	0.014	0.18	1.81	56	0.056	0.006	5.62
10.51	-	Fu-43	100.4	0.024	0.35	3.47	107	0.107	0.011	10.70
10.70	-	Fu-46	100.3	0.022	0.31	3.14	97	0.097	0.010	9.69
10.88	-	Fu-49	100.1	0.015	0.20	1.98	61	0.061	0.006	6.13

G.1.1.5. Furlo, Italy: Organic-P

Depth (m)	No. GEA	No. Client	Wt. (mg)	Abs	[P] (µM)	dilution correction	[P] ug/L	P mg/L	[P] mg/g	[P] ppm
8.20	-	Fu-7	100.0	0.004	0.064	0.64	20	0.020	0.002	1.97
8.49	-	Fu-10	100.3	0.007	0.111	1.11	34	0.034	0.003	3.43
8.69	-	Fu-12	100.1	0.011	0.175	1.75	54	0.054	0.005	5.40
8.79	-	Fu-13	100.3	0.087	1.382	13.82	428	0.428	0.043	42.66
8.81	-	Fu-14	99.7	0.028	0.445	4.45	138	0.138	0.014	13.81
8.85	-	Fu-16	100.0	0.030	0.476	4.76	148	0.148	0.015	14.75
8.90	-	Fu-17	100.0	0.027	0.429	4.29	133	0.133	0.013	13.28
8.95	-	Fu-18	100.0	0.036	0.572	5.72	177	0.177	0.018	17.71
9.06	-	Fu-20	99.7	0.052	0.826	8.26	256	0.256	0.026	25.65
9.15	-	Fu-22	100.6	0.044	0.699	6.99	216	0.216	0.022	21.51
9.30	-	Fu-24	99.9	0.041	0.651	6.51	202	0.202	0.020	20.18
9.47	-	Fu-27	100.1	0.024	0.381	3.81	118	0.118	0.012	11.79
9.60	-	Fu-28	100.7	0.018	0.286	2.86	89	0.089	0.009	8.79
9.72	-	Fu-30	99.8	0.014	0.222	2.22	69	0.069	0.007	6.90
9.99	-	Fu-33	100.4	0.029	0.461	4.61	143	0.143	0.014	14.21
10.07	-	Fu-36	100.7	0.032	0.508	5.08	157	0.157	0.016	15.63
10.19	-	Fu-38	100.1	0.032	0.508	5.08	157	0.157	0.016	15.72
10.30	-	Fu-41	100.0	0.019	0.302	3.02	93	0.093	0.009	9.34
10.51	-	Fu-43	100.4	0.027	0.429	4.29	133	0.133	0.013	13.23
10.70	-	Fu-46	100.3	0.018	0.286	2.86	89	0.089	0.009	8.83
10.88	-	Fu-49	100.1	0.021	0.333	3.33	103	0.103	0.010	10.32

G.1.1.6. Manilva, Spain: Iron-bound-P

Depth (m)	No. Client	Wt. (mg)	P mg/L - blank		[P] mg/g	[P] ppm
2.82	MA-25	101.5	0.000	0.00	0.000	0.000
3.05	MA-28	99.7	0.760	0.76	0.076	76.229
3.17	MA-31	100.2	2.330	2.33	0.233	232.535
3.3	MA-33	101	0.877	0.88	0.087	86.832
3.35	MA-34	100	0.824	0.82	0.082	82.400
3.38	MA-35	101.2	2.510	2.51	0.248	248.024
3.45	MA-36	99.2	0.420	0.42	0.042	42.339
3.5	MA-37	103.2	1.120	1.12	0.109	108.527
3.54	MA-39	99.3	0.520	0.52	0.052	52.367
3.57	MA-38	99.1	5.490	5.49	0.554	553.986
3.6	MA-40	99.7	0.883	0.88	0.089	88.566
3.66	MA-41	100.3	4.730	4.73	0.472	471.585
3.79	MA-44	99.3	0.000	0.00	0.000	0.000
3.85	MA-45	101.6	4.640	4.64	0.457	456.693
3.92	MA-46	100.4	0.000	0.00	0.000	0.000
4	MA-47	102.4	1.320	1.32	0.129	128.906
4.05	MA-48	99.8	2.390	2.39	0.239	239.479
4.1	MA-49	101.3	4.990	4.99	0.493	492.596
4.14	MA-50	101.2	1.350	1.35	0.133	133.399
4.2	MA-51	100.8	0.894	0.89	0.089	88.690
4.24	MA-52	100.9	5.230	5.23	0.518	518.335
4.6	MA-64	100.2	0.915	0.915	0.091	91.317

G.1.1.7. Manilva, Spain: Authigenic-P

Depth (m)	No. GEA	No. Client	Wt. (mg)	Abs	[P] (µM)	dilution correction	[P] ug/L	P mg/L	[P] mg/g	[P] ppm
2.82	14289	MA-25	101.5	0.629	29.12	29.12	902	0.902	0.089	89
3.05	14292	MA-28	99.7	0.258	11.21	56.07	1737	1.737	0.174	174
3.17	14295	MA-31	100.2	0.248	10.73	53.66	1662	1.662	0.166	166
3.30	14297	MA-33	101.0	0.158	6.39	31.94	989	0.989	0.098	98
3.35	14298	MA-34	100.0	0.432	19.61	19.61	607	0.607	0.061	61
3.38	14299	MA-35	101.2	0.195	8.17	8.17	253	0.253	0.025	25
3.45	14300	MA-36	99.2	0.199	8.37	41.83	1296	1.296	0.131	131
3.50	14301	MA-37	103.2	0.312	13.82	13.82	428	0.428	0.041	41
3.54	14303	MA-38	99.3	0.213	9.04	9.04	280	0.280	0.028	28
3.57	14302	MA-39	99.1	0.253	10.97	54.87	1699	1.699	0.171	171
3.66	14305	MA-41	100.3	0.253	10.97	54.87	1699	1.699	0.169	169
3.79	14308	MA-44	99.3	0.256	11.12	11.12	344	0.344	0.035	35
3.85	14309	MA-45	101.6	0.145	5.76	5.76	178	0.178	0.018	18
3.92	14310	MA-46	100.4	0.213	9.04	9.04	280	0.280	0.028	28
4.00	14311	**MA-47**	102.4	0.147	5.86	5.86	181	0.181	0.018	18
4.05	14312	MA-48	99.8	0.102	3.68	3.68	114	0.114	0.011	11
4.10	14313	MA-49	101.3	0.211	8.95	8.95	277	0.277	0.027	27
4.14	14314	MA-50	101.2	0.146	5.81	5.81	180	0.180	0.018	18
4.20	14315	MA-51	100.8	0.061	1.71	1.71	53	0.053	0.005	5
4.24	14316	MA-52	100.9	0.253	10.97	10.97	340	0.340	0.034	34
4.60	14300	MA-64	100.2	0.326	14.50	14.50	449	0.449	0.045	45

G.1.1.8. Manilva, Spain: Detrital-P

Depth (m)	No. GEA	No. Client	Wt. (mg)	Abs	[P] (µM)	dilution correction	[P] ug/L	P mg/L	[P] mg/g	[P] ppm
2.82	14289	MA-25	101.5	0.018	0.58	5.76	178	0.18	0.02	18
3.05	14292	MA-28	99.7	0.171	7.11	355.73	11017	11.02	1.11	1105
3.17	14295	MA-31	100.2	0.417	17.63	176.28	5459	5.46	0.54	545
3.30	14297	MA-33	101.0	0.126	5.19	51.91	1608	1.61	0.16	159
3.35	14298	MA-34	100.0	0.042	1.60	16.01	496	0.50	0.05	50
3.38	14299	MA-35	101.2	0.152	6.30	315.13	9759	9.76	0.96	964
3.45	14300	MA-36	99.2	0.516	21.86	218.59	6770	6.77	0.68	682
3.50	14301	MA-37	103.2	0.079	3.18	31.83	986	0.99	0.10	96
3.54	14302	MA-39	99.3	0.363	15.32	153.20	4745	4.74	0.48	478
3.57	14303	MA-38	99.1	0.039	1.47	14.73	456	0.46	0.05	46
3.66	14305	MA-41	100.3	0.478	20.24	202.35	6267	6.27	0.62	625
3.79	14308	MA-44	99.3	0.086	3.48	34.82	1078	1.08	0.11	109
3.85	14309	MA-45	101.6	0.020	0.66	6.61	205	0.20	0.02	20
3.92	14310	MA-46	100.4	0.022	0.75	7.47	231	0.23	0.02	23
4.00	14311	MA-47	102.4	0.011	0.28	2.77	86	0.09	0.01	8
4.05	14312	MA-48	99.8	0.023	0.79	7.89	244	0.24	0.02	24
4.10	14313	MA-49	101.3	0.052	2.03	20.29	628	0.63	0.06	62
4.14	14314	MA-50	101.2	0.023	0.79	7.89	244	0.24	0.02	24
4.20	14315	MA-51	100.8	0.018	0.58	5.76	178	0.18	0.02	18
4.24	14316	MA-52	100.9	0.090	3.65	36.53	1131	1.13	0.11	112
4.60	14300	MA-64	100.2	0.065	2.58	25.84	800	0.80	0.08	80

G.1.1.9. Manilva, Spain: Organic-P

Depth (m)	No. GEA	No. Client	Wt. (mg)	Abs	[P] (µM)	dilution correction	[P] ug/L	P mg/L	[P] mg/g	[P] ppm
2.82	14289	MA-25	101.5	0.006	0.03	0.34	10	0.01	0.00	1
3.05	14292	MA-28	99.7	0.130	5.29	52.87	1637	1.64	0.16	164
3.17	14295	MA-31	100.2	0.052	1.98	19.82	614	0.61	0.06	61
3.30	14297	MA-33	101.0	0.032	1.14	11.35	352	0.35	0.03	35
3.35	14298	MA-34	100.0	0.012	0.29	2.88	89	0.09	0.01	9
3.38	14299	MA-35	101.2	0.072	2.83	28.30	876	0.88	0.09	87
3.45	14300	MA-36	99.2	0.017	0.50	5.00	155	0.15	0.02	16
3.50	14301	MA-37	103.2	0.027	0.92	9.23	286	0.29	0.03	28
3.54	14302	MA-39	99.3	0.294	12.24	122.35	3789	3.79	0.38	382
3.57	14303	MA-38	99.1	0.030	1.05	10.50	325	0.33	0.03	33
3.60	14304	MA-40	99.7	0.425	17.79	177.86	5508	5.51	0.55	552
3.66	14305	MA-41	100.3	0.091	3.63	36.35	1126	1.13	0.11	112
3.79	14308	MA-44	99.3	0.603	25.33	253.27	7844	7.84	0.79	790
3.85	14309	MA-45	101.6	0.062	2.41	24.06	745	0.75	0.07	73
3.92	14310	MA-46	100.4	0.061	2.36	23.64	732	0.73	0.07	73
4.00	14311	MA-47	102.4	0.410	17.15	171.50	5311	5.31	0.52	519
4.05	14312	MA-48	99.8	0.030	1.05	10.50	325	0.33	0.03	33
4.10	14313	MA-49	101.3	0.061	2.36	23.64	732	0.73	0.07	72
4.14	14314	MA-50	101.2	0.016	0.46	4.57	142	0.14	0.01	14
4.20	14315	MA-51	100.8	0.032	1.14	11.35	352	0.35	0.03	35
4.24	14316	MA-52	100.9	0.155	6.35	63.46	1965	1.97	0.19	195
4.6	14300	MA-64	100.2	0.03	1.05	10.50	325	0.33	0.03	32

G.2. Bulk Rock (including Detrital Indicies) and Clay Analysis

Mohammed Plage, Morocco
Pueblo, USA
Eastbourne, UK
Furlo, Italy
Manilva, Spain

G.2.0.1. Mohammed Plage, Bulk Rock XRD

Depth	Samples	Phyllosilicates	Quartz	Feldspath-K	Plagioclase-Na	Calcite	Gypse	Ankerite	Indicies	Detrial Index
0.4	20936	12.75	25.21	1.69	0.00	18.66	1.61	0.38	39.70	2.12
0.6	20935	20.13	22.53	1.94	0.00	19.34	1.18	8.48	26.40	2.31
0.75	20934	12.12	45.34	7.35	2.03	21.85	0.00	2.28	9.03	3.06
0.9	20933	9.81	25.50	0.00	0.00	15.64	0.92	1.72	46.41	2.26
1.02	20932	12.58	15.82	18.27	0.00	9.59	1.44	0.56	41.74	4.87
1.25	20931	12.59	14.78	0.00	0.00	18.89	0.00	0.45	53.29	1.45
1.35	20930	11.82	0.00	0.00	0.00	86.44	0.00	0.00	1.74	0.14
1.5	20929	11.89	18.90	5.41	0.00	62.41	0.00	0.00	1.39	0.58
2.2	20919	7.31	16.22	0.00	0.00	65.23	0.00	0.00	11.24	0.36
2.34	20920	10.31	28.58	0.00	1.07	19.97	0.00	0.00	40.08	2.00
2.5	20921	15.53	22.57	0.00	0.00	61.23	0.00	0.00	0.67	0.62
2.62	20922	12.36	21.55	18.58	0.00	10.41	1.07	0.77	35.26	5.04
2.84	20924	15.06	25.92	12.89	0.00	12.61	1.08	0.71	31.73	4.27
2.95	20925	8.57	42.60	0.00	0.00	34.08	1.34	0.48	12.93	1.50
3.12	20926	9.01	44.77	0.00	0.00	46.01	0.00	0.00	0.21	1.17
3.3	20927	8.07	26.76	2.99	0.00	51.20	1.64	1.54	7.80	0.74
3.5	20882	8.78	54.53	0.00	3.51	30.71	0.00	1.67	0.81	2.18
3.78	20883	11.23	1.73	0.00	0.00	82.99	0.00	0.94	3.10	0.16
3.88	20884	4.35	18.02	0.00	0.00	77.54	0.00	0.00	0.09	0.29
4.05	20885	7.81	5.90	0.00	0.00	59.23	0.00	0.00	27.06	0.23
4.18	20886	8.48	20.70	0.00	0.00	52.14	0.00	0.89	17.79	0.56
4.36	20887	10.13	28.22	0.00	0.00	46.30	0.00	2.31	13.03	0.83
4.55	20888	13.24	19.04	5.05	0.00	59.04	0.00	2.38	1.25	0.63
4.7	20889	5.03	12.34	0.00	3.52	76.32	0.00	2.08	0.71	0.27
4.8	20890	13.39	6.33	0.00	3.10	61.37	0.00	1.79	14.02	0.37
4.9	20891	8.97	27.23	15.14	0.00	37.23	1.66	0.69	9.09	1.38
5.08	20892	13.77	23.75	5.06	0.00	50.92	0.00	1.32	5.18	0.84
5.18	20893	9.60	8.96	8.93	0.00	56.26	0.00	0.00	16.25	0.49
5.24	20894	10.24	16.16	5.76	0.00	64.72	0.00	2.16	0.97	0.50
5.4	20895	10.21	5.85	0.00	0.00	70.12	0.00	0.94	12.88	0.23
5.66	20896	1.96	57.56	9.67	0.00	25.23	2.50	0.92	2.16	2.74
5.75	20897	10.03	30.04	6.06	0.00	47.29	0.00	1.17	5.41	0.98
5.92	20898	9.82	22.67	4.68	0.00	41.45	0.00	1.00	20.37	0.90
6.07	20899	7.33	17.99	14.11	0.00	56.91	0.00	2.22	1.44	0.69
6.4	20900	5.65	12.57	4.36	0.00	59.63	0.00	0.00	17.79	0.38
6.62	20901	4.35	34.59	9.09	0.00	51.55	0.00	0.00	0.42	0.93
6.5	20902	7.49	19.91	7.77	0.00	55.49	0.00	1.58	7.76	0.63
6.85	20903	7.29	8.39	14.22	0.00	64.67	0.00	0.00	5.43	0.46
7.03	20904	7.08	8.16	7.37	0.00	74.89	0.00	0.00	2.50	0.30

G.2.0.2. continued...

Depth	Samples	Phyllosilicates	Quartz	Feldspath-K	Plagioclase-Na	Calcite	Gypse	Ankerite	Indicies	Detrial Index
7.15	20905	4.77	2.01	0.00	0.00	67.87	0.00	0.00	25.35	0.10
7.28	20906	7.18	12.13	9.79	0.00	46.72	2.04	0.89	21.25	0.62
7.38	20907	6.59	14.29	6.54	0.00	69.54	0.00	0.00	3.04	0.39
7.55	20908	3.53	3.99	12.85	0.00	78.15	0.00	0.00	1.47	0.26
7.78	20909	7.05	0.00	0.00	0.00	91.23	0.00	0.00	1.72	0.08
7.95	20910	9.27	4.89	0.00	0.00	61.17	0.00	0.00	24.67	0.23
8.17	20911	14.36	13.56	4.72	0.00	62.78	0.00	0.00	4.58	0.52
8.36	20912	4.59	5.54	13.90	0.00	73.04	0.00	0.71	2.22	0.33
8.59	20913	6.46	4.63	12.39	0.00	66.39	0.00	0.00	10.12	0.35
8.79	20914	11.71	7.91	10.51	0.00	67.45	0.00	0.70	1.72	0.45
8.97	20915	7.23	8.38	0.00	0.00	54.98	0.00	0.00	29.41	0.28
9.12	24441	17.59	18.80	0.00	0.00	42.38	0.00	0.00	21.23	0.86
9.35	24443	10.69	15.81	0.00	0.00	55.84	0.00	0.00	17.66	0.47
9.56	24444	9.88	16.63	0.00	0.00	65.31	0.00	0.69	7.48	0.41
10.1	24446	6.74	7.11	0.00	0.00	77.89	0.00	1.67	6.59	0.18
10.18	24447	10.38	13.13	0.00	0.00	64.69	0.00	0.45	11.35	0.36
10.7	24450	4.87	23.24	0.00	0.00	66.74	0.00	0.00	5.16	0.42
10.9	24452	8.64	5.67	0.00	0.00	58.09	0.00	0.00	27.60	0.25
11.15	24453	6.52	8.22	0.00	0.00	61.29	0.00	0.00	23.97	0.24
11.45	24455	10.99	14.11	0.00	0.00	61.33	0.00	1.04	12.53	0.41
12.85	24463	5.91	5.40	0.00	0.00	73.64	0.00	0.00	15.05	0.15
13.25	24465	8.16	7.42	0.00	0.00	82.54	0.00	0.00	1.89	0.19
13.6	24466	9.60	8.64	0.00	0.00	71.23	0.00	0.80	9.73	0.26
14	24467	6.97	5.36	0.00	0.00	69.68	0.00	0.00	17.99	0.18
14.15	24468	0.87	10.61	0.00	0.00	76.28	0.00	0.00	12.24	0.15
14.3	24469	4.53	4.89	0.00	0.00	65.23	0.00	0.00	25.35	0.14
14.5	24470	5.46	5.79	0.00	0.00	69.74	0.00	0.00	19.01	0.16
14.65	24471	7.23	14.87	0.00	0.00	55.92	0.00	0.51	21.47	0.40
15.15	24474	8.56	7.43	0.00	0.00	65.24	0.00	0.00	18.77	0.25
15.3	24475	9.34	8.39	0.00	0.00	50.94	0.00	0.87	30.46	0.35
15.5	24476	9.40	12.60	0.00	0.00	68.60	0.00	0.32	9.08	0.32
16	24479	6.74	3.08	0.00	0.00	74.71	0.00	0.00	15.47	0.13
16.25	24480	12.16	9.14	0.00	0.00	61.23	0.00	0.65	16.82	0.35
16.6	24482	13.12	15.83	0.00	0.00	48.31	0.00	1.02	21.71	0.60
17.05	24484	8.03	9.27	0.00	0.00	53.12	0.00	0.00	29.58	0.33
17.3	24485	7.44	5.21	0.00	0.00	63.45	0.00	0.00	23.90	0.20
17.4	24486	7.88	12.27	0.00	0.00	56.93	0.00	0.00	22.91	0.35
17.5	24487	10.98	17.41	0.00	0.00	57.27	0.00	0.00	14.34	0.50
17.75	24488	12.28	18.21	0.00	0.00	59.99	0.00	0.00	9.52	0.51

G.2.0.3. continued...

Depth	Samples	Phyllosilicates	Quartz	Feldspath-K	Plagioclase-Na	Calcite	Gypse	Ankerite	Indicies	Detrial Index
17.9	24489	4.79	3.00	0.00	0.00	79.74	0.00	0.00	12.47	0.10
18.1	26036	2.76	5.33	0.00	0.00	67.34	0.00	0.00	24.57	0.12
18.2	26037	4.73	7.69	0.00	0.00	71.19	0.00	0.00	16.39	0.17
18.3	26038	5.93	2.71	0.00	0.00	88.03	0.00	0.00	3.33	0.10
18.45	26039	6.75	10.11	4.17	0.00	58.97	0.00	0.00	20.00	0.36
18.65	26040	8.12	10.02	0.00	0.00	75.04	0.00	0.83	6.00	0.24
18.8	26041	6.67	6.57	3.44	0.00	61.77	0.00	0.00	21.54	0.27
19.1	26042	3.87	3.60	0.00	0.00	63.78	0.00	0.00	28.75	0.12
19.3	26043	4.55	7.36	0.00	0.00	76.18	0.00	0.00	11.91	0.16
19.45	26044	6.81	4.97	2.18	0.00	75.19	0.00	0.59	10.26	0.19
19.6	26045	7.14	6.50	0.00	0.00	69.66	0.00	0.00	16.70	0.20
19.75	26046	10.71	3.02	0.00	0.00	76.30	0.00	1.20	8.77	0.18
19.95	26047	5.86	10.97	2.68	0.00	72.26	0.00	0.00	8.23	0.27
20.15	26048	6.27	5.04	0.00	0.00	73.58	0.00	0.00	15.11	0.15
20.3	26049	5.77	4.86	0.00	0.00	68.34	0.00	0.00	21.03	0.16
20.5	26050	4.04	4.20	0.00	5.60	77.18	0.00	0.00	8.98	0.18
20.7	26051	4.75	2.03	0.00	0.00	70.51	0.00	0.00	22.71	0.10
20.85	26052	15.32	17.56	5.75	0.00	60.44	0.00	0.00	0.93	0.64
21	26053	7.21	4.42	2.31	0.00	59.90	0.00	0.00	26.16	0.23
21.1	26054	2.65	2.47	14.21	0.00	73.91	0.00	0.00	6.76	0.26
21.2	26055	3.68	5.70	0.00	0.00	81.15	0.00	0.00	9.47	0.12
21.3	26056	3.05	1.09	4.34	0.00	85.73	0.00	0.00	5.79	0.10
21.4	26057	6.31	4.73	0.00	0.00	69.33	0.00	0.00	19.63	0.16
21.55	26058	4.51	2.95	0.00	0.00	72.13	0.00	0.00	20.41	0.10
21.75	26059	3.87	2.25	0.00	0.00	75.66	3.33	0.00	14.89	0.08
21.95	26060	4.40	2.31	0.00	0.00	74.89	0.00	0.00	18.40	0.09
22.1	26061	3.63	1.29	0.00	0.00	74.50	0.00	0.00	20.58	0.07
22.3	26062	4.76	1.54	2.79	0.00	72.87	3.78	0.00	14.26	0.12
22.45	26063	4.29	3.31	0.00	0.00	70.40	0.00	0.00	22.00	0.11
22.7	26064	3.78	3.75	0.00	6.10	68.81	0.00	0.00	17.56	0.20
22.9	26065	4.18	3.95	0.00	0.00	76.90	2.14	0.00	12.83	0.11
23.15	26066	3.91	1.94	0.00	0.00	68.57	0.00	0.00	25.58	0.09
23.25	26067	4.09	33.40	0.00	0.00	44.27	5.24	0.00	13.01	0.85
23.4	26068	5.62	2.57	0.00	0.00	70.04	0.00	0.00	21.78	0.12
23.55	26069	1.25	11.48	0.00	0.00	67.37	1.84	1.25	16.81	0.19
23.7	26070	3.07	2.83	0.00	0.00	80.02	0.00	0.00	14.08	0.07
23.85	26071	2.49	1.96	0.00	0.00	80.91	3.60	0.76	10.28	0.05
24.05	26072	1.43	1.54	0.00	0.00	94.67	0.00	1.26	1.10	0.03

G.2.1.1. Pueblo, Bulk Rock XRD

Depth	Samples	Phyllosilicates	Quartz	Feldspath-K	Plagioclase-Na	Calcite	Gypse	Ankerite	Indicies	Detrial Index
0.01	PC-1	18.00	25.26	0.52	0.58	28.16	0.00	-	27.47	1.58
0.3	PC-3	14.86	10.95	0.00	0.00	72.19	0.00	-	1.99	0.36
0.45	PC-4	14.33	20.65	0.00	0.52	55.69	0.00	-	8.81	0.64
0.65	PC-5	4.78	18.14	0.00	0.54	76.52	0.00	-	0.03	0.31
0.89	PC-7	20.54	13.60	0.57	0.48	26.85	0.00	-	37.96	1.31
1.1	PC-8	13.27	22.28	0.40	0.77	56.32	0.00	-	6.96	0.65
1.3	PC-9	24.07	18.70	0.00	0.48	31.84	0.00	-	24.92	1.36
1.5	PC-10	19.44	23.89	0.00	0.66	26.07	0.00	-	29.94	1.69
1.7	PC-11	15.40	15.76	0.26	0.39	34.00	0.00	-	34.19	0.94
1.9	PC-12	10.83	12.78	0.00	0.37	39.19	0.00	-	36.83	0.61
1.97	PC-13	20.92	27.23	0.24	0.58	21.94	0.00	-	29.10	2.23
2.1	PC-16	12.71	30.38	0.35	0.26	56.07	0.00	-	0.23	0.78
2.27	PC-17	0.00	6.20	0.00	0.34	93.38	0.00	-	0.08	0.07
2.35	PC-18	16.49	14.46	0.00	0.30	40.94	0.00	-	27.82	0.76
2.45	PC-19	21.62	9.63	0.00	0.00	16.25	21.10	-	31.41	1.92
2.48	PC-20	12.16	12.11	0.50	0.55	36.09	0.00	-	38.59	0.70
2.53	PC-21	17.49	7.78	0.00	0.49	27.09	2.15	-	45.01	0.95
2.6	PC-22	12.14	14.59	0.00	0.43	39.41	2.57	-	30.86	0.69
3	PC-24	12.15	14.85	0.00	0.00	69.45	0.00	-	3.55	0.39
3.3	PC-25	9.33	9.46	0.00	0.00	81.04	0.00	-	0.17	0.23
3.6	PC-26	17.10	19.55	0.58	1.22	32.39	0.00	-	29.16	1.19
3.9	PC-27	16.39	18.51	0.00	1.03	29.50	0.00	-	34.57	1.22
4.2	PC-28	15.38	20.44	0.00	0.83	41.26	0.00	-	22.08	0.89
4.5	PC-29	44.28	3.10	0.00	0.22	14.68	37.36	-	0.35	3.24
4.6	PC-30	15.30	20.67	0.00	0.77	43.55	0.00	-	19.72	0.84
4.95	PC-31	13.56	15.47	0.00	0.53	17.51	4.17	-	48.76	1.69
5.25	PC-32	7.71	8.24	0.00	0.00	49.30	0.00	-	34.75	0.32
5.6	PC-33	16.12	17.10	0.00	0.00	28.40	0.00	-	38.37	1.17
5.95	PC-34	26.07	15.74	0.00	0.00	32.86	0.93	-	24.40	1.27

G.2.1.2. cont...

Depth	Samples	Phyllosilicates	Quartz	Feldspath-K	Plagioclase-Na	Calcite	Gypse	Ankerite	Indicies	Detrial Index
6.23	PC-35	13.89	7.94	0.00	0.00	31.27	0.00	-	46.90	0.87
6.58	PC-36	13.82	16.70	0.00	0.49	47.88	8.83	-	12.29	0.82
6.85	PC-37	15.54	16.26	0.00	0.79	29.58	1.19	-	36.64	0.79
7.08	PC-38	12.18	15.58	0.00	0.53	45.05	1.52	-	25.15	0.60
7.3	PC-39	0.00	5.09	0.00	0.00	77.13	3.94	-	13.84	0.42
7.65	PC-40	5.84	8.92	0.00	0.00	25.53	12.64	-	47.08	0.39
7.95	PC-41	17.70	16.07	0.00	0.36	64.10	0.98	-	0.79	0.59
8.53	PC-43	17.88	18.85	0.00	0.28	55.57	0.00	-	7.43	0.46
8.75	PC-44	7.09	8.61	0.00	0.36	83.65	0.00	-	0.29	0.59
8.85	PC-45	8.71	8.60	0.00	0.35	19.22	33.49	-	29.63	0.56
9.7	PC-48	21.28	15.23	0.37	0.75	38.59	0.00	-	23.79	0.68
9.85	PC-49	9.52	17.05	0.45	0.00	72.08	0.00	-	0.89	0.76
10.12	PC-50	17.40	14.57	0.00	0.00	34.05	0.00	-	33.98	0.63
10.4	PC-51	21.36	14.75	0.71	0.00	62.71	0.00	-	0.48	0.70
10.7	PC-52	10.42	12.44	0.00	0.26	40.85	0.00	-	36.03	0.63
11	PC-53	15.51	14.48	0.37	0.48	41.41	0.00	-	27.74	0.52
11.22	PC-54	10.14	8.05	0.00	1.81	79.25	0.00	-	0.75	0.38
11.35	PC-55	4.47	6.48	0.00	0.77	87.63	0.00	-	0.63	0.17
11.62	PC-56	4.12	7.93	0.00	0.00	87.32	0.00	-	0.63	0.19
11.69	PC-57	11.98	10.50	0.00	0.76	76.75	0.00	-	0.01	0.19
11.75	PC-58	0.00	10.51	0.00	0.00	88.83	0.00	-	0.66	0.34
11.8	PC-59	16.02	11.46	0.00	0.54	47.54	0.00	-	24.44	0.42
11.85	PC-60	18.93	11.62	0.00	0.34	56.91	0.00	-	12.20	0.44
12.02	PC-62	4.96	8.44	0.00	0.00	70.23	0.00	-	16.37	0.40
12.1	PC-63	6.83	3.75	0.00	0.00	23.36	0.00	-	66.07	1.35
12.22	PC-64	26.98	5.22	0.00	0.00	9.44	0.00	-	58.36	1.54
12.27	PC-65	21.35	4.76	0.00	0.00	34.12	0.00	-	39.77	1.60
12.57	PC-67	19.62	11.18	0.00	0.56	49.44	0.00	-	19.19	0.52
12.7	PC-68	7.04	6.54	0.00	0.00	86.11	0.00	-	0.30	0.49
12.77	PC-69	18.60	6.58	0.00	0.48	37.21	0.00	-	37.14	0.56
12.95	PC-70	16.73	20.76	0.00	0.38	45.31	0.00	-	16.82	0.54
13.08	PC-71	4.57	2.84	0.00	0.00	79.83	0.00	-	12.76	1.37

G.2.1.3. cont...

Depth	Samples	Phyllosilicates	Quartz	Feldspath-K	Plagioclase-Na	Calcite	Gypse	Ankerite	Indicies	Detrial Index
13.18	PC-72	42.60	2.14	0.47	0.38	14.36	0.93	-	39.11	3.17
13.22	PC-73	7.77	3.69	0.00	0.00	84.86	0.00	-	3.67	0.14
13.27	PC-74	15.28	6.59	0.00	0.98	76.28	0.00	-	0.88	0.30
13.4	PC-75	10.67	15.57	0.00	0.00	73.23	0.00	-	0.53	0.36
13.5	PC-76	7.92	15.82	0.00	0.00	56.05	1.50	-	18.73	0.42
13.77	PC-77	2.93	7.05	0.00	0.00	20.66	22.35	-	47.01	0.48
13.67	PC-77A	3.65	5.37	0.00	0.00	60.43	0.00	-	30.55	0.15
13.87	PC-78	18.99	16.24	0.00	0.84	33.54	0.00	-	30.39	1.08
14.33	PC-80	11.55	2.99	0.00	0.68	66.86	0.00	-	17.92	0.23
14.67	PC-81	8.93	7.30	0.00	0.26	71.98	9.44	-	2.08	0.23
14.5	PC-81A	4.40	16.44	0.00	0.00	58.49	0.00	-	20.66	0.36
14.9	PC-82	8.39	4.77	0.00	0.00	75.84	0.00	-	11.01	0.17
15.25	PC-83	11.69	5.76	0.00	0.46	64.38	0.00	-	17.71	0.28
15.1	PC-83A	7.29	5.69	0.00	0.00	60.30	0.00	-	26.73	0.22
15.5	PC-84	7.15	1.18	0.00	0.32	84.47	0.00	-	6.88	0.10
15.75	PC-85	8.70	4.32	0.00	0.00	86.56	0.00	-	0.42	0.15
16	PC-86	10.61	5.86	0.00	0.75	82.36	0.00	-	0.42	0.21
15.9	PC-86A	8.74	10.16	0.00	0.37	62.78	0.00	-	17.95	0.31
16.25	PC-87	9.54	10.85	0.00	0.79	75.97	0.00	-	2.86	0.28
16.2	PC-87A	3.97	6.05	0.00	0.00	63.37	0.00	-	26.61	0.16
16.4	PC-88	13.99	12.86	0.00	2.64	71.05	0.00	-	-0.55	0.42
16.56	PC-89	12.47	6.04	0.00	0.00	81.14	0.00	-	0.35	0.23
17	PC-91	7.70	5.92	0.00	0.75	56.45	0.00	-	29.17	0.25
17.05	PC-92	4.93	6.02	0.00	0.84	55.57	0.00	-	32.63	0.21
17.15	PC-93	12.37	4.43	0.00	0.80	33.50	0.00	-	48.90	0.53
17.27	PC-94	10.74	7.25	0.00	0.00	62.51	0.00	-	19.51	0.29
17.5	PC-95	7.20	2.18	0.00	0.00	90.30	0.00	-	0.32	0.10
17.7	PC-96	16.72	5.68	0.00	0.47	41.71	0.00	-	35.43	0.55
17.85	PC-97	10.35	7.08	0.00	1.00	81.00	0.00	-	0.58	0.23
17.95	PC-98	8.77	3.50	0.00	0.70	48.30	0.00	-	38.73	0.27
18.05	PC-99	4.19	5.26	0.00	0.59	76.18	0.00	-	13.77	0.13
18.17	PC-100	4.39	2.94	0.00	0.64	42.04	0.00	-	49.98	0.19

G.2.2.1. Eastbourne, Bulk Rock XRD

Depth	Samples	Phyllosilicates	Quartz	Feldspath-K	Plagioclase-Na	Calcite	Gypse	Ankerite	Indicies	Detrial Index
0.35	EB1	4.86	1.21	0.00	0.00	93.94	-	-	-	0.06
0.50	EB2	4.22	1.23	0.00	0.00	94.55	-	-	-	0.06
0.65	EB3	4.27	1.10	0.00	0.00	94.74	-	-	-	0.06
0.75	EB4	10.02	3.65	0.00	0.00	86.33	-	-	-	0.16
0.95	EB5	9.81	2.61	0.00	0.00	87.57	-	-	-	0.14
1.10	EB6	6.15	2.53	0.00	0.00	91.31	-	-	-	0.10
1.20	EB14	14.71	6.84	0.00	0.56	94.18	-	-	-	0.23
1.25	EB7	3.90	1.92	0.00	0.00	91.73	-	-	-	0.06
1.40	EB8	6.21	2.05	0.00	0.00	90.24	-	-	-	0.09
1.55	EB9	7.41	2.34	0.00	0.00	89.75	-	-	-	0.11
1.70	EB10	8.27	1.98	0.00	0.00	77.47	-	-	-	0.13
1.80	EB11	17.74	4.79	0.00	0.00	77.24	-	-	-	0.29
1.85	EB12	16.37	6.39	0.00	0.00	81.16	-	-	-	0.28
1.90	EB13	15.08	3.76	0.00	0.00	77.88	-	-	-	0.24
2.15	EB15	13.40	4.08	0.00	0.00	82.53	-	-	-	0.21
2.25	EB16	10.34	2.59	0.00	0.00	87.07	-	-	-	0.15
2.60	EB17	13.64	2.89	0.00	0.00	83.48	-	-	-	0.20
2.90	EB18	15.00	4.05	0.00	0.60	80.34	-	-	-	0.24
3.25	EB19	17.13	4.63	0.00	0.00	78.24	-	-	-	0.28
3.65	EB20	10.78	4.12	0.00	0.40	84.70	-	-	-	0.18
3.85	EB21	10.00	3.67	0.43	0.41	85.50	-	-	-	0.17
4.00	EB22	11.17	3.68	0.00	0.00	85.15	-	-	-	0.17
4.15	EB23	9.64	3.16	0.00	0.00	87.21	-	-	-	0.15
4.25	EB24	7.89	3.91	0.00	0.00	88.20	-	-	-	0.13
4.40	EB25	7.60	2.59	0.00	0.00	89.81	-	-	-	0.11
4.60	EB26	9.93	3.28	0.00	0.00	86.78	-	-	-	0.15
4.75	EB27	8.96	2.83	0.00	0.00	88.22	-	-	-	0.13
4.90	EB28	12.01	3.74	0.00	0.00	84.25	-	-	-	0.19
5.15	EB29	12.95	4.29	0.00	0.00	82.76	-	-	-	0.21

G.2.2.2. cont...

Depth	Samples	Phyllosilicates	Quartz	Feldspath-K	Plagioclase-Na	Calcite	Gypse	Ankerite	Indicies	Detrial Index
5.40	EB30	13.61	5.63	0.00	0.00	80.76	-	-	-	0.24
5.65	EB31	12.19	5.61	0.73	0.00	81.47	-	-	-	0.23
5.82	EB32	11.93	5.76	0.79	0.00	81.51	-	-	-	0.23
6.00	EB33	11.25	3.84	0.00	0.00	84.91	-	-	-	0.18
6.20	EB33'	10.65	3.44	0.00	0.00	85.91	-	-	-	0.16
6.40	EB34	10.17	3.42	0.00	0.00	86.41	-	-	-	0.16
6.60	EB35	6.28	1.91	0.00	0.00	91.80	-	-	-	0.09
6.70	EB36	11.00	2.40	0.00	0.00	86.61	-	-	-	0.15
6.80	EB37	13.46	2.67	0.00	0.00	83.86	-	-	-	0.19
6.85	EB38	22.66	2.59	0.00	0.00	74.75	-	-	-	0.34
6.90	EB39	21.85	3.31	0.00	0.00	74.84	-	-	-	0.34
6.97	EB40	6.66	1.01	0.00	0.00	92.32	-	-	-	0.08
7.15	EB41	8.62	1.35	0.00	0.00	90.03	-	-	-	0.11
7.42	EB42	6.04	1.18	0.00	0.00	92.78	-	-	-	0.08
7.65	EB43	5.93	1.30	0.00	0.00	92.77	-	-	-	0.08
7.70	EB44	14.14	3.67	0.00	0.00	82.19	-	-	-	0.22
7.85	EB45	4.72	1.35	0.00	0.00	93.93	-	-	-	0.06
8.10	EB46	3.52	1.03	0.00	0.00	95.45	-	-	-	0.05
8.25	EB47	5.05	0.73	0.00	0.00	94.22	-	-	-	0.06
8.50	EB48	4.68	1.16	0.00	0.00	94.16	-	-	-	0.06
8.70	EB49	5.12	1.27	0.00	0.00	93.61	-	-	-	0.07
8.90	EB50	3.93	0.38	0.00	0.00	95.70	-	-	-	0.04
9.10	EB51	3.77	0.92	0.00	0.00	95.31	-	-	-	0.05
9.20	EB52	8.36	1.79	0.00	0.00	89.86	-	-	-	0.11
9.45	EB53	5.14	0.98	0.00	0.00	93.87	-	-	-	0.07
9.60	EB54	12.83	2.71	0.00	0.00	84.46	-	-	-	0.18
9.78	EB-12	7.44	1.33	0.00	0.00	91.22	-	-	-	0.10
9.85	EB-11	4.20	0.12	0.00	0.00	95.68	-	-	-	0.05
10.05	EB-10	5.53	1.30	0.00	0.00	93.18	-	-	-	0.07

G.2.2.3. cont...

Depth	Samples	Phyllosilicates	Quartz	Feldspath-K	Plagioclase-Na	Calcite	Gypse	Ankerite	Indicies	Detrial Index
10.20	EB-9	3.74	0.91	0.00	0.00	95.35	-	-	-	0.05
10.40	EB-8	6.38	0.80	0.00	0.00	92.82	-	-	-	0.08
10.65	EB-7	3.14	0.75	0.00	0.00	96.12	-	-	-	0.04
10.95	EB-6	6.83	1.48	0.00	0.00	91.69	-	-	-	0.09
11.20	EB-5	5.33	1.31	0.00	0.00	93.36	-	-	-	0.07
11.35	EB-4	16.08	3.70	0.00	0.00	80.22	-	-	-	0.25
11.40	EB-3	4.95	1.38	0.00	0.00	93.68	-	-	-	0.07
11.55	EB-2	4.18	1.18	0.00	0.00	94.64	-	-	-	0.06
11.70	EB-1	3.88	0.74	0.00	0.00	95.38	-	-	-	0.05
11.75	EB 0	13.29	3.06	0.50	0.00	83.16	-	-	-	0.20
11.80	EB55	5.38	1.53	0.00	0.00	93.09	-	-	-	0.07
12.00	EB56	5.12	1.08	0.00	0.00	93.80	-	-	-	0.07
12.25	EB57	4.74	1.13	0.00	0.00	94.13	-	-	-	0.06
12.50	EB58	3.12	0.97	0.00	0.00	95.90	-	-	-	0.04
12.75	EB59	4.21	1.19	0.00	0.00	94.59	-	-	-	0.06

G.2.3.1. Furlo, Bulk Rock XRD

Depth	Samples	Phyllosilicates	Quartz	Feldspath-K	Plagioclase-Na	Calcite	Gypse	Ankerite	Indicies	Detrial Index
7.60	Fu-1	5.69	3.16	0.00	0.00	70.72	0.00	-	20.43	0.13
7.70	Fu-2	1.93	2.37	0.00	0.00	81.16	0.00	-	14.53	0.05
7.75	Fu-3	4.18	2.30	0.00	0.00	58.59	0.00	-	34.93	0.11
7.90	Fu-4	1.42	3.62	0.00	0.00	68.73	0.00	-	26.22	0.07
7.95	Fu-5	25.80	1.56	0.00	0.00	57.15	0.00	-	15.49	0.48
8.10	Fu-6	1.78	2.05	0.00	0.00	39.03	0.00	-	57.14	0.10
8.20	Fu-7	3.47	2.73	0.00	0.00	65.48	0.00	-	28.31	0.09
8.33	Fu-8	0.00	0.00	0.00	0.00	0.00	0.00	-	0.00	0.00
8.45	Fu-9	4.83	5.67	0.00	0.00	60.82	0.00	-	28.67	0.17
8.49	Fu-10	4.77	9.47	0.00	0.00	60.15	0.00	-	25.61	0.24
8.59	Fu-11	2.29	9.02	0.00	0.00	61.20	0.00	-	27.50	0.18
8.69	Fu-12	3.69	10.34	0.00	0.00	61.90	0.00	-	24.07	0.23
8.79	Fu-13	2.44	16.98	0.00	0.00	41.02	0.00	-	39.56	0.47
8.81	Fu-14	6.91	21.83	0.00	0.00	17.44	0.00	-	53.82	1.65
8.82	Fu-15	9.78	27.38	0.00	0.00	20.95	1.21	-	40.68	1.77
8.85	Fu-16	4.89	30.51	0.00	0.00	7.05	0.00	-	57.55	5.02
8.90	Fu-17	8.23	35.95	0.00	0.00	2.68	1.23	-	51.92	16.51
8.95	Fu-18	5.44	39.38	0.00	0.00	0.48	0.82	-	53.88	92.63
9.03	Fu-19	10.70	31.22	0.00	0.00	0.00	0.00	-	58.08	41916
9.06	Fu-20	7.21	35.01	0.00	0.00	0.00	0.00	-	57.78	42221
9.11	Fu-21	6.00	35.67	0.00	0.00	0.00	0.00	-	58.33	41672
9.15	Fu-22	8.21	27.23	0.00	0.00	0.00	2.22	-	62.34	35443
9.21	Fu-23	7.70	37.84	0.00	0.00	0.00	1.28	-	53.18	45542
9.27	Fu-24	15.30	23.38	2.08	0.00	0.00	0.00	-	59.24	40763
9.30	Fu-24a	24.39	23.04	1.58	0.98	0.00	1.06	-	48.95	49992
9.42	Fu-25	14.18	24.00	0.00	0.00	0.00	0.71	-	61.11	38182
9.47	Fu-26	8.21	22.64	1.03	0.00	1.17	3.26	-	63.70	27.26
9.52	Fu-27	5.57	40.20	0.00	0.00	0.00	0.75	-	53.48	45769
9.62	Fu-28	7.29	40.67	0.00	0.00	0.00	0.00	-	52.04	47965
										dissolution

G.2.3.2. cont...

Depth	Samples	Phyllosilicates	Quartz	Feldspath-K	Plagioclase-Na	Calcite	Gypse	Ankerite	Indicies	Detrial Index
9.99	Fu-29	5.19	37.40	0.00	0.00	0.00	0.63	-	56.78	42588
10.02	Fu-30	5.78	42.22	0.00	0.00	47.09	0.00	-	4.91	1.02
10.05	Fu-31	14.21	32.84	0.00	0.00	0.00	0.00	-	52.95	47047
10.09	Fu-32	10.21	37.90	0.00	0.00	0.56	0.00	-	51.33	85.34
10.14	Fu-33	7.13	30.86	0.00	0.00	0.00	0.77	-	61.25	37985
10.19	Fu-34	6.30	35.75	0.00	0.00	0.00	0.00	-	57.95	42047
10.24	Fu-35	5.95	35.41	0.96	0.00	0.00	0.78	-	56.90	42317
10.27	Fu-36	10.98	29.75	0.00	0.00	0.00	0.00	-	59.27	40728
10.42	Fu-37	6.56	31.80	0.84	0.00	2.86	0.00	-	57.94	13.73
10.47	Fu-38	4.26	21.88	0.00	0.00	27.36	0.00	-	46.49	0.96
10.51	Fu-39	11.00	41.82	0.79	0.00	3.96	0.00	-	42.43	13.52
10.585	Fu-40	8.27	19.95	0.00	0.00	38.38	0.00	-	33.40	0.74
10.66	Fu-41	5.06	14.45	0.00	0.00	59.99	0.00	-	20.50	0.33
10.67	Fu-42	25.86	20.99	0.93	0.75	0.00	0.00	-	51.48	48524
10.67	Fu-43	6.02	14.26	0.00	0.00	34.56	0.00	-	45.17	0.59
10.77	Fu-44	5.51	15.31	0.00	0.00	75.83	0.00	-	3.35	0.27
10.78	Fu-45	21.70	15.85	1.27	0.00	17.28	0.00	-	43.90	2.25
10.88	Fu-45a	4.88	14.43	0.00	0.00	66.43	0.00	-	14.26	0.29
10.9	Fu-46	6.69	15.53	0.00	0.00	66.95	0.00	-	10.82	0.33
11.3	Fu-47	21.97	13.31	0.00	0.00	50.60	0.00	-	14.12	0.70
11.4	Fu-48	2.01	8.68	0.00	0.00	61.06	0.00	-	28.25	0.18
11.5	Fu-49	7.31	26.09	0.00	0.00	52.01	0.00	-	14.59	0.64
11.8	Fu-50	2.66	11.11	0.00	0.00	69.45	0.00	-	16.78	0.20
11.95	Fu-51	6.09	41.99	0.00	0.00	27.19	0.00	-	24.73	1.77
12.05	Fu-52	5.14	12.30	0.00	0.00	75.06	0.00	-	7.50	0.23
12.15	Fu-53	7.30	25.21	0.00	0.00	44.65	0.00	-	22.83	0.73
12.25	Fu-54	3.18	19.12	0.00	0.00	75.81	0.00	-	1.88	0.29
12.35	Fu-55	6.77	6.37	0.00	0.00	58.48	0.00	-	28.38	0.22
12.45	Fu-56	2.83	9.31	0.00	0.00	77.87	0.00	-	9.99	0.16
12.55	Fu-57	5.27	26.98	0.00	0.00	46.56	0.00	-	21.19	0.69
12.66	Fu-58	1.92	36.98	0.00	0.00	27.10	0.00	-	34.00	1.44
12.72	Fu-59	5.02	8.63	0.00	0.00	85.46	0.00	-	0.90	0.16
12.83	Fu-60	5.34	4.47	0.00	0.00	81.56	0.00	-	8.63	0.12
										dissolution

G.2.4.1. Manilva, Bulk Rock XRD

Depth	Samples	Phyllosilicates	Quartz	Feldspath-K	Plagioclase-	Calcite	Gypse	Ankerite	Indicies	Detrial Index
2.70	MA-24	5.41	1.56	0.00	0.00	93.24	0.00	0	-0.21	0.07
2.93	MA-26	2.11	2.42	0.00	0.00	62.65	0.00	0	32.82	0.07
3.00	MA-27	4.13	20.98	0.00	0.00	28.40	0.00	0	46.49	0.88
3.05	MA-28	21.32	13.03	0.00	0.00	0.00	0.00	0	65.65	34349
3.10	MA-29	12.97	22.84	0.00	0.00	0.00	0.00	0	64.19	35812
3.15	MA-30	6.38	32.87	0.00	0.00	0.00	0.00	0	60.75	39246
3.17	MA-31	12.00	28.17	0.00	0.00	0.00	0.00	0	59.83	40169
3.30	MA-33	12.04	33.54	0.00	0.00	0.00	0.00	0	54.43	45574
3.35	MA-34	5.53	30.94	0.00	0.00	0.00	0.00	0	63.52	36477
3.38	MA-35	10.29	32.99	0.00	0.00	0.00	0.00	0	56.71	43286
3.57	MA-39	14.59	21.15	0.00	0.00	3.47	0.00	0	60.79	10.30
3.60	MA-40	0.00	37.07	0.00	0.00	1.55	0.00	0	61.38	23.96
3.66	MA-41	11.63	28.97	0.00	0.00	0.00	0.00	0	59.39	40608
3.70	MA-42	17.59	33.02	0.00	0.00	0.00	0.00	0	49.39	50611
3.75	MA-43	15.88	20.98	0.00	0.00	0.00	0.00	0	63.14	36857
3.79	MA-44	25.58	12.83	0.00	0.00	0.00	7.17	0	51.42	38410
3.85	MA-45	8.23	27.01	0.00	0.00	2.88	7.97	0	53.91	12.23
3.92	MA-46	27.00	23.49	0.00	0.00	1.72	5.26	0	42.53	29.35
4.00	MA-47	16.94	19.37	0.00	0.00	3.86	6.62	0	53.21	9.41
4.05	MA-48	7.87	28.71	0.00	0.00	0.00	0.00	0	63.42	36582
4.10	MA-49	18.54	29.25	0.00	0.83	0.00	0.00	0	51.39	48614
4.14	MA-50	4.62	28.28	0.00	0.00	0.00	0.00	0	67.10	32897
4.20	MA-51	2.26	29.11	0.00	0.00	2.11	0.00	0	66.52	14.87
4.24	MA-52	31.91	21.04	0.00	0.00	0.84	1.11	0	45.11	63.29
4.27	MA-53	18.66	1.87	0.00	0.00	0.93	4.45	0	74.09	22.01
4.30	MA-54	0.00	27.71	0.00	0.00	0.00	0.00	0	72.29	27705.26
4.36	MA-56	8.73	5.47	0.00	0.00	3.46	2.21	0	79.53	4.11
4.43	MA-58	15.37	19.97	0.00	0.00	6.00	16.57	0	41.12	5.89
4.46	MA-59	3.13	19.68	0.00	0.00	2.23	2.64	0	72.32	10.22
										dissolution

G.2.4.2. cont...

Depth	Samples	Phyllosilicates	Quartz	Feldspath-K	Plagioclase-Na	Calcite	Gypse	Ankerite	Indicies	Detrial Index
4.52	MA-61	11.79	37.95	0.00	0.00	0.00	0.00	0.00	50.26	49740
4.55	MA-62	25.15	19.38	0.00	0.00	0.00	0.00	0.00	55.47	44528
4.57	MA-63	16.16	29.54	0.00	0.00	0.00	0.00	0.00	54.29	45707
4.60	MA-64	7.92	29.22	0.00	0.00	0.00	0.63	0.00	62.22	37149
4.63	MA-65	21.15	10.46	0.00	0.91	0.00	0.00	0.00	67.48	32516
4.69	MA-66	1.59	14.46	0.00	0.00	17.44	0.00	0.00	66.51	0.92
4.82	MA-69	3.41	8.84	0.00	0.00	41.99	0.00	0.00	45.77	0.29
4.88	MA-70	7.12	7.70	0.00	0.00	52.94	0.00	0.00	32.24	0.28
4.93	MA-71	5.02	12.49	0.00	0.00	41.16	0.00	0.00	41.33	0.43
5.05	MA-72	3.36	16.46	0.00	0.00	53.66	0.00	0.00	26.51	0.37
5.10	MA-73	4.04	5.99	0.00	0.00	39.71	0.00	0.00	50.27	0.25
5.16	MA-74	6.16	7.51	0.00	0.00	41.77	0.00	0.00	44.55	0.33
5.20	MA-75	9.34	4.48	0.00	0.00	38.82	0.00	0.00	47.36	0.36
5.25	MA-76	0.00	13.10	0.00	0.00	29.42	0.00	0.00	57.48	0.45
5.30	MA-77	2.33	3.97	0.00	0.00	36.09	0.00	0.00	57.61	0.17
5.37	MA-78	4.07	5.62	0.00	0.00	53.30	0.00	0.00	37.00	0.18
5.40	MA-79	6.52	6.37	0.00	0.00	68.15	0.00	0.00	18.97	0.19
5.52	MA-80	5.65	4.94	0.00	0.00	75.41	0.00	0.00	14.00	0.14
5.90	MA-82	7.99	3.63	0.00	0.00	74.34	0.00	0.00	14.04	0.16
6.02	MA-83	1.79	1.83	0.00	0.00	38.10	0.00	0.00	58.27	0.10
										dissolution

G.3. Stable Carbon Isotope Data

G.3.1. Mohammed Plage, $\delta^{13}C$

Mohammed Plage			Mohammed Plage Cont..		
Depth (m)	**$\delta^{13}C$ (VPDB)**	**N° sample**	**Depth (m)**	**$\delta^{13}C$ (VPDB)**	**N° sample**
0.6	-27.77	-7	11.45	-27.80	49
0.75	-27.79	-6	11.7	-28.16	50
0.9	-27.91	-5	11.9	-27.66	51
1.02	-28.28	-4	12.1	-27.76	52
1.25	-28.29	-3	12.25	-27.84	53
1.35	-28.27	-2	12.4	-27.25	54
1.5	-27.55	-1	12.6	-27.68	55
2.2	-27.29	/4	12.7	-27.97	56
2.34	-27.80	/5	12.85	-27.30	57
2.5	-27.41	/6	13	-28.16	58
2.62	-28.56	/7	13.25	-27.82	59
2.95	-27.61	/10	14	-27.51	61
3.12	-27.26	/11	14.3	-27.95	63
3.3	-27.88	/12	14.5	-27.67	64
3.5	-28.07	1	14.65	-27.30	65
3.78	-28.09	2	14.8	-27.91	66
3.88	-28.52	3	14.95	-28.11	67
4.18	-28.55	5	15.15	-27.94	68
4.36	-28.08	6	15.3	-27.70	69
4.55	-28.70	7	15.5	-27.85	70
4.7	-28.18	8	15.6	-27.99	71
4.8	-28.24	9	15.8	-27.76	72
4.9	-28.21	10	16	-27.50	73
5.08	-27.73	11	16.25	-28.14	74
5.18	-28.39	12	16.4	-27.63	75
5.24	-28.17	13	16.6	-27.63	76
5.4	-28.07	14	16.75	-27.98	77
5.66	-27.65	15	17.05	-27.59	78
5.75	-27.72	16	18.45	-27.92	87
5.92	-28.45	17	18.65	-28.25	88
6.07	-26.41	18	18.8	-27.39	89
6.4	-27.58	19	19.1	-27.89	90
6.62	-28.13	20	19.3	-27.66	91
6.5	-28.22	21	19.45	-28.31	92
6.85	-27.46	22	19.6	-28.36	93
7.03	-27.45	23	19.75	-28.42	94
7.15	-28.42	24	19.95	-28.08	95
7.28	-28.04	25	20.15	-28.13	96
7.38	-28.80	26	20.3	-28.17	97
7.55	-28.61	27	20.5	-27.28	98
7.78	-28.79	28	20.7	-27.60	99
7.95	-28.79	29	20.85	-27.51	100
8.17	-28.82	30	21	-24.73	101
8.36	-28.17	31	21.1	-24.59	102
8.59	-28.52	32	21.2	-24.64	103
8.79	-28.51	33	21.3	-24.72	104
8.97	-28.32	34	21.55	-25.72	106
9.2	-27.57	36	21.95	-25.55	108
9.35	-27.70	37	22.1	-24.81	109
9.56	-27.62	38	22.3	-24.90	110
9.85	-27.09	39	22.7	-25.21	112
10.1	-27.55	40	23.15	-25.42	114
10.18	-27.79	41	23.25	-26.34	115
10.3	-28.31	42	23.4	-24.72	116
10.8	-27.24	45	23.55	-24.85	117
11.3	-27.58	48	23.85	-25.17	119

G.3.2. Eastbourne and Pueblo $\delta^{13}C$

Eastbourne			Pueblo		
Depth	**$\delta^{13}C$ (VPDB)**	**N° sample**	**Depth (m)**	**$\delta^{13}C$ (VPDB)**	**N° sample**
0.35	2.83	EB1	0.00	0.25	PC1
0.5	2.83	EB2	0.30	-0.16	PC4
0.65	2.83	EB3	0.85	0.04	PC7
0.75	2.75	EB4	0.85	-0.02	PC7
0.95	2.75	EB5	1.10	-0.07	PC8
1.1	2.81	EB6	1.45	-0.57	PC10
1.25	2.83	EB7	1.65	-0.23	PC11
1.4	2.88	EB8	1.95	-0.22	PC13
1.55	2.75	EB9	2.15	0.07	PC16
1.7	2.81	EB10	2.45	0.53	PC19
1.8	2.68	EB11	2.60	0.69	PC22
1.85	2.91	EB12	3.00	0.47	PC24
1.9	3.07	EB13	3.55	0.12	PC26
1.92	3.24	EB14	3.95	0.36	PC27
2.15	3.29	EB15	4.35	0.24	PC29
2.25	3.38	EB16	4.50	-0.10	PC30
2.6	3.92	EB17	5.40	0.11	PC32
2.9	4.11	EB18	5.70	-0.24	PC33
3.25	4.16	EB19	6.25	0.45	PC35
3.65	4.36	EB20	6.85	-0.06	PC37
3.85	3.98	EB21	7.15	0.22	PC38
4	4.44	EB22	7.40	0.73	PC39
4.15	4.47	EB23	7.95	0.33	PC41
4.25	4.45	EB24	8.25	0.22	PC42
4.4	4.54	EB25	8.55	1.35	PC43
4.6	4.5	EB26	8.75	0.70	PC44
4.9	4.4	EB28	8.85	0.75	PC45
5.15	4.28	EB29	8.95	0.21	PC46
5.4	4.18	EB30	9.30	0.81	PC47
5.65	4.15	EB31	9.75	0.13	PC48
6	4.19	EB33	9.85	1.02	PC49
6.4	4.31	EB34	10.20	-0.29	PC50
6.6	4.44	EB35	10.50	0.80	PC51
6.7	4.35	EB36	10.75	0.64	PC52
6.8	4.43	EB37	11.00	0.92	PC53
6.85	4.57	EB38	11.25	1.44	PC54
6.9	4.52	EB39	11.75	2.07	PC57
6.97	4.76	EB40	11.80	2.19	PC59
7.15	4.9	EB41	11.85	1.64	PC60
7.42	4.94	EB42	11.90	1.62	PC61
7.65	5.03	EB43	12.10	2.01	PC63
7.7	5.03	EB44	12.25	2.52	PC64
7.85	4.83	EB45	12.30	1.60	PC65
8.1	4.82	EB46	12.60	2.20	PC67
8.25	4.93	EB47	12.80	2.07	PC69
8.5	4.69	EB48	12.95	1.60	PC70
8.7	4.81	EB49	13.20	1.91	PC72
8.9	5.01	EB50	13.35	1.70	PC74
9.1	4.63	EB51	13.35	1.83	PC74
9.2	4.77	EB52	13.55	2.11	PC76
9.45	4.59	EB53	13.75	2.11	PC77
9.6	4.61	EB54	14.00	1.63	PC78
9.78	5.00	EB-12	14.25	2.13	PC79
9.85	4.88	EB-11	14.45	2.35	PC80
10.05	4.88	EB-10	14.45	2.41	PC80
10.2	4.81	EB-9	14.75	1.86	PC81
10.4	4.71	EB-8	14.75	1.78	PC81
10.65	4.81	EB-7	15.30	1.67	PC83
10.95	4.68	EB-6	15.55	1.96	PC84
11.2	4.56	EB-5	16.00	1.82	PC86
11.35	4.67	EB-4	16.45	1.81	PC88
11.4	4.75	EB-3	16.65	1.66	PC89
11.55	4.6	EB-2	16.80	1.61	PC90
11.7	4.62	EB-1	16.80	1.32	PC90
11.75	4.98	EB 0	17.35	0.94	PC94
11.8	4.97	EB55	17.75	1.18	PC96
12	4.79	EB56	18.00	1.29	PC98
12.25	4.58	EB57			
12.5	4.45	EB58			
12.75	4.61	EB59			

G.3.2. Furlo and Manilva $\delta^{13}C$

Furlo		
Depth (m)	**$\delta^{13}C$ (VPDB)**	**N° sample**
8.9	-25.93	FU17
8.95	-25.58	FU18
9.03	-26.24	FU19
9.06	-25.98	FU20
9.11	-25.97	FU21
9.15	-25.22	FU22
9.21	-24.73	FU23
9.27	-23.91	FU24
9.3	-24.06	FU24A
9.36	-23.39	FU25
9.39	-23.35	FU26
9.47	-23.73	FU27
9.52	-24.10	FU28
9.62	-23.55	FU29
9.72		FU30
9.82	-23.27	FU31
9.9	-23.55	FU32
9.99	-23.43	FU33
10.01	-23.51	FU34
10.05	-24.00	FU35
10.1	-26.48	FU36
10.14	-26.10	FU37
10.24	-25.61	FU39
10.47	-26.29	FU42

Manilva		
Depth (m)	**$\delta^{13}C$ (VPDB)**	**N° sample**
3.05	-23.99	MA-28
3.1	-25.37	MA-29
3.12	-25.76	MA-30
3.17	-25.28	MA-31
3.3	-26.15	MA-33
3.35	-26.08	MA-34
3.38	-25.97	MA-35
3.6	-25.56	MA-40
3.66	-23.27	MA-41
3.7	-23.25	MA-42
3.74	-26.05	MA-43
3.79	-23.36	MA-44
3.85	-23.28	MA-45
3.92	-22.83	MA-46
4.05	-23.65	MA-48
4.1	-23.56	MA-49
4.14	-23.26	MA-50
4.2	-24.05	MA-51
4.24	-23.42	MA-52
4.26	-22.64	MA-53
4.3	-22.36	MA-54
4.36	-22.13	MA-56
4.46	-22.74	MA-59
4.52	-22.78	MA-61
4.55	-23.52	MA-62
4.57	-23.08	MA-63
4.6	-26.05	MA-64
4.63	-24.41	MA-65

excursion in the global seawater d13C record. Sedimentary sections at Rock Creek Canyon (Pueblo, CO), ODP Site 1138 (Kerguelen Plateau), Bass River (NJ), Totuma well (Venezuela) and Baranca el Canyon (Mexico) were chosen to examine potential trace metal patterns and gradients around the proposed source of hydrothermal inputs - the Caribbean Plateau, whose initial volcanic activity has been dated at 93-89 Ma. ICP-AES and ICP-MS elemental abundances from whole rock samples are normalized to Zr to remove the effect of terrestrial inputs. We find prominent trace metal "spikes" (up to 50 times background) for elements known to be concentrated in volatile degassing of magmas and in hydrothermal plumes resulting from seawater-rock reactions. These anomalies begin at the onset and continue well into the d13C excusion at all five sites. Furthermore, the magnitude of the anomalies decreases with distance from the Caribbean region, and the pattern of elements shifts from a wide range of metals near-source to predominantly long residence time metals far "downstream".

PP42C-07 1525h INVITED

Last ODP Legs Expand Black Shale Legacy of Scientific Ocean Drilling

Philip A Meyers[1] (734-764-0597; pameyers@umich.edu)

Scientific Party Leg 207[2]

Scientific Party Leg 210[2]

[1]Department of Geological Sciences, The University of Michigan, 425 East University Avenue, Ann Arbor, MI 48109-1063, United States

[2]Ocean Drilling Program, Texas A&M University, College Station, TX 77845, United States

Scientific ocean drilling has been central to our basic knowledge about Cretaceous black shales and to our growing understanding of the paleoceanographic and paleoclimatic processes that participated in their deposition. Spot-coring during early DSDP legs charted the geographical and temporal occurrence of black shales in the ocean basins. The concept of Oceanic Anoxic Events (OAE) is a product of this legacy. Subsequent [illegible] that have [illegible] sequences and have encouraged reconstructions of the paleoceanographic histories recorded by these differences. Sequences recovered by the last few ODP Legs have expanded this legacy and have opened new opportunities for improved understandings about black shales. Leg 198 recovered a classic section of TOC-rich (35 percent) early Aptian black shale from the Shatsky Rise that corresponds to OAE1a. Leg 207 recovered Cenomanian-Turonian (OAE2) and Coniacian-Santonian (OAE3) black shales, some containing nearly 30 percent TOC, from five sites on the Demerara Rise. Leg 210 recovered TOC-rich (4 percent) laminated black shales from the deep Newfoundland Margin that correspond to OAE1d and OAE2. The Demerara Rise sequences are particularly impressive in ranging in thickness from 56m to 93m and in having well-developed laminations and shale-limestone cycles. The five sites constitute a 1km paleodepth transect and record both high surface productivity and enhanced organic matter preservation under an intensified oxygen-minimum layer impinging on the Demerara Rise.

PP42D MCC: 3004 Thursday 1600h

Nature and Causes of Cyclicity in Triassic Through Miocene Paleoclimate Records II *(joint with OS)*

Presiding: K L Bice, Woods Hole Oceanographic Institution; T Wagner, University Bremen

PP42D-01 1600h INVITED

Milankovitch Forcing in Equatorial, Late Triassic Pangea: (Deep River; Dan River, and Richmond Basins, Southeastern USA)

Paul E Olsen[1] (845-365-8491; polsen@ldeo.columbia.edu)

Dennis V Kent[1,2] (845-365-8544; dvk@ldeo.columbia.edu)

Peter M LeTourneau[1] (845-365-8621; letour@ldeo.columbia.edu)

[1]Lamont-Doherty Earth Observatory, 61 Route 9W, Palisades, NY 10964, United States

[2]Dept. of Geological Sciences, Rutgers University, Piscataway, NJ 08854, United States

The Milankovitch character of lake level fluctuations in the tropics of central Pangea has been well established since the pioneering work of Van Houten in the 1960's (1) that laid the foundation for quantitative analysis of core and outcrops in the 1990's (2,3). In the region from about 3° to 10° N latitude giant rift lakes fluctuated to the classic Milankovitch frequencies of precessional forcing of 20, 96, 128, and 404 ky, as well as the less well known 1.75 and 3.5 m.y. cycles. The latter are the Triassic values for the periods of g4-g3 of eccentricity related precessional forcing and the secular resonance, theta (2(g4- g3) - (s4-s3)), of precessional and obliquity related forcing. We attribute the forcing of lake depth largely to modulation of the strength of tropical convergence. Late Triassic rifts located from 0° to 3° N latitude show similar patterns, except with a strong tendency towards a doubling of the climatic precessional frequency and a lack of evaporites as previously reported from the Dan River basin (4,5,6). Here we report on new analyses of coal-bearing cores and drill holes from the Deep River, Dan River, and Richmond basin of older Late Triassic lacustrine strata that reinforce this pattern but show that the doubling of the precessional frequency is not ubiquitous at the equator and also show that very strong climatic transitions appear related to the 1.75 and 3.5 m.y. cycles juxtaposing coals and caliches in vertical sequence and sometimes coinciding with major faunal and floral transitions. (1) Van Houten FB. 1964. Kansas Geol. Surv. Bull. 169:497. (2) Olsen PE & Kent DV. 1996. Palaeogeo. Palaeoclim. Palaeoecol. 122;1-26. (3) Olsen PE & Kent DV. 1999. Phil. Trans. Roy. Soc. Lond. (A) 357:1761-1787. (4) Olsen PE & Kent DV.1996. Eos, Trans., AGU 77(46), Suppl.:301. (5) Olsen PE. 1997. Ann. Rev. Earth Planet. Sci. 25:337-401. (6) Olsen PE & Kent DV. 2000. in Bachmann G. and Lerche I. (eds.), Epicontinental Triassic, Vol. 3, Zent. Geol. Palaont. VIII:1475-1496.

PP42D-02 1620h INVITED

Organic Carbon Cyclicity in the Kimmeridge Clay (Dorset, UK)

Richard V Tyson[1] (44-191-222-6605; r.v.tyson@ncl.ac.uk)

Graham Weedon[2] (graham.weedon@luton.ac.uk)

[1]School of Civil Engineering and Geosciences, University of Newcastle, Newcastle NE17RU, United Kingdom

[2]Centre for Environmental Change, University of Luton, Luton LU13JU, United Kingdom

The type section of the Late Jurassic Kimmeridge Clay Formation (KCF) of Dorset (UK) has recently been completely cored and studied during the NERC RGGE project. The middle 250m of the formation is characterized by conspicuous metre-scale Milankovitch cyclicity, expressed primarily by marine total organic carbon (MTOC) content, and thought to record 38ka obliquity and 19ka precession cycles. The cyclicity is clearest where mean compacted sedimentation rates are <80m/Ma, the low dilution amplifying the effect of productivity and redox cycles on MTOC content. Overall the dominant first MTOC mode varies symmetrically from 0.5% at the top and base of the KCF, to 4-5% in the central endoxus-wheatleyensis interval, reflecting the long term relative sea level trend and its effects on clastic dilution and bottom water oxygenation. Superimposed third order cycles also influence the cyclicity. Algorithms relating sedimentation rate, carbon delivery flux, bottom water oxygen, burial efficiency and TOC in modern marine sediments yield low to moderate mean paleoproductivity estimates of 40-150 gC/m2/a. Given low dilution and good preservation high absolute paleoproductivity is not required to explain typical MTOC values, but MTOC variation is influenced by the interaction of input, preservation and dilution (IPD) factors in a complex multivariate fashion. In this distal facies phytoclast and palynomorph concentration data (No. per mg rock) are primarily controlled by inorganic sediment dilution, not organic matter supply, which forces positive correlations between genetically unrelated particles; the concentration of refractory phytoclasts may thus provide an intra-cycle proxy for relative mineral dilution. Using this approach, comparison of different cycles suggests that the MTOC is also influenced by dilution at this scale, but changes in all the IPD variables are probably important. Excess organic-walled plankton concentrations are sometimes correlated with heavier d13Com values, suggestive of short-term productivity spikes (calculated palaeoproductivities of up to 400 gC/m2/a), while other d13Com anomalies are apparently associated with higher contents of isotopically heavy sulphurised organic matter.

PP42D-03 1640h

Orbital Cycles, Climate, and Diagenesis Mimic Methane Releases: Results from a High Resolution Study of OAE2, New Jersey Coastal Plain

James D Wright[1] (732 445-5722; jdwright@rci.rutgers.edu)

Benjamin S Cramer[2] (022-217-6625; benjamin@dges.tohoku.ac.jp)

Kenneth G Miller[1] (732 445-3622; kgmt@rci.rutgers.edu)

Miriam E Katz[1] (732 445-3445; mimikatz@rci.rutgers.edu)

[1]Rutgers University, Dept of Geological Sciences 610 Taylor Road, Piscataway, NJ 08854, United States

[2]Tohoku University, Aoba, Aramaki, Institute of Geology and Paleontology, Sendai, NJ 980-8578, Japan

The Cenomanian-Turonian (Upper Cretaceous) section from Bass River State Park, New Jersey contains a 15 m thick interval representing Ocean Anoxic Event (OAE2). Our high resolution (5cm) bulk sediment inorganic stable isotope record, can be used to define OAE2 at Bass River. The down-hole gamma log shows well-developed cycles throughout the OAE2 interval that we interpret as short eccentricity cycles, providing a chronology for the OAE2 event. Assuming a 95 kyr eccentricity cycle and that OAE2 at Bass River is defined the interval of high $\delta^{13}C$ values, the duration of this event was ~700±100 kyr. The dominant eccentricity forcing in the Bass River OAE2 record suggests that a monsoonal circulation controlled the regional and global carbon cycles as evidenced by sedimentary organic carbon and $\delta^{13}C_i$ respectively. Our results show a series of negative $\delta^{13}C$ excursions, that are typically on the order of 3 to 5 per mil, but in two instances the excursions were >20 per mil. We initially interpreted these excursions as reflecting methane releases from gas hydrates. Closer examination shows that the $\delta^{13}C$ excursions were produced by seafloor diagenesis in the presence of elevated organic carbon levels. [illegible] are characterized by: 1) the [illegible] carbon $\delta^{13}C$ [illegible] 3) increased %$CaCO_3$. The $\delta^{13}C$ value of the authigenic $CaCO_3$ is ~-25 per mil, indicating that reducing organic-rich sediments supplied much of the CO_2. We argue that increases in organic carbon flux raised alkalinity (through sulfate reduction) and resulted in authigenic precipitation of $CaCO_3$ at Bass River. In our model, negative $\delta^{13}C$ excursions are the result of seafloor diagenesis that is forced by climate rather than from the dissociation of methane hydrate.

PP42D-04 1700h INVITED

African climate variability and organic carbon accumulation in the Coniacian-Satonian eastern tropical Atlantic: Insights how insolation-cycles in the Cretaceous were transformed to marine black shales

Peter Hofmann[1] (49-221-470-4008; adg03@uni-koeln.de)

Thomas Wagner[2] (49-421-218-8950; twagner@uni-bremen.de)

Britta Beckmann[2] (49-421-218-8938; bbeckman@uni-bremen.de)

Sascha Floegel[3] (49-431-600-2836; sfloegel@geomar.de)

[1]University of Cologne, Department of Geology, Zuelpicher Str. 49a, Cologne 50674, Germany

[2]University Bremen, Geosciences, PO Box 330440, Bremen 28334, Germany

[3]GEOMAR Research Centre, Wischofstr. 1-3, Kiel 24148, Germany

There is increasing evidence from marine proxy records that tropical regions during the late Cretaceous were hotter than previously reported and were by far exceeding modern average temperatures. Tropical sea surface temperatures in the range of 32-36°C apparently lasted from the latest Cenomanian to the early Campanian. A fundamental consequence of superheated Cretaceous tropics is a vigorous hydrological cycle operating in equatorial regions. Geological evidence supporting such an enhanced hydrological cycle and a direct link to the formation of marine black shale cycles was recently reported for ODP Site 959 from the Deep Ivorian Basin (DIB) off equatorial West-Africa. Millennial-scale marine and terrigenous proxy records from that site provide a unique opportunity to investigate short-term variability of the ocean-climate system, to discuss the role of orbital forcing and to

Cite abstracts as: *Eos. Trans. AGU, 84*(46), Fall Meet. Suppl., Abstract #####-##, 2003.

Appendix 2 - Selected Conference Abstracts

A Multi-site Phosphorus Speciation Across the Cenomanian-Turonian Boundary: Implications for the processes leading to Red Bed Formation.

H. Mort, T. Adatte, P. Steinmann, V. Matera, G. Keller, D. Stueben and Z. Berner

Abstract

The availability of oxygen at the sediment-water interface is the dominant limiting factor in the burial efficiency of many redox sensitive metals. The formation of Cretaceous Oceanic Red Beds (CORBs) is therefore likely to been largely regulated by the abundance (or lack) of oxygen in the world's oceans.

We present a testable model for the formation of CORBs by linking them to the formation of Cretaceous Oceanic Anoxic Events (OAEs) via results obtained from measuring the accumulation of various types of phosphorus (P) across the C/T boundary in different parts of the world.

An initial increase in P mass accumulation rates (P MARs) is observed prior to positive $\delta^{13}C$ within the upper Rotalipora cushmani zone, followed by a sharp decrease. P accumulation is, like Fe, affected by both oxygen availability and productivity. We suggest that the initial increase in P is a result of elevated productivity, whereas the decrease is an artifact of reduced oxygen availability and thus P retention ability of the sediment. The scenario may have also occurred with iron; although it's different redox sensitivity may cause these changes to be diachronous with P, especially if dysoxia developed on the scale of ka's.

A gradual reintroduction of oxygenated bottom waters to the different basins of the world's oceans may cause the enlarged global dissolved inorganic Fe (and P) budget to start fluxing back into sediments, creating the characteristic CORBs.

Workshop on cretaceous oceanic red beds: Paleoclimate and paleoclimatology, Beijing, China.

Palaeoenvironmental impacts on changes in bottom water oxygen availability at the Cenomanian-Turonian Anoxic Event. in EGU general assembly 2006.

Haydon P. Mort, Thierry Adatte, Karl B. Föllmi, Gerta Keller, Philipp Steinmann, Virginie Matera, Zsolt Berner, Doris Stüben

Abstract

Phosphorus (P) accumulation rates provide evidence of nutrient regeneration during the late Cenomanian oceanic anoxic event (OAE 2) in four geographic localities whose sediments were deposited under paleoenvironmental regimes (Pueblo, Colorado, USA; Eastbourne, UK; Furlo, Italy, Manilva, Spain). At each locality, accumulation rates of phosphorus bound to iron oxyhydroxides, authigenic apatite and organic matter increase during the positive □13C excursion and return to pre-excursion values shortly after the first isotope peak. Subsequent to this, total organic carbon (TOC) and Hydrogen Index (HI) data display a positively correlated increase in values, suggesting that in the later stages of OAE 2, organic carbon accumulation was strongly linked to preservation under increasingly dysoxic conditions. Both the reduction in P MARs and the clear relationship between TOC and HI values, suggest that lower oxygen availability lead to a decrease in P burial efficiency (PBE). □13C values remain at a relatively high plateau. Large positive increases in the Corg/Preactive molar ratios at the onset of high organic matter accumulation and drops in P MARs both suggest the presence of O2 depleted bottom waters, which facilitated the processes of nutrient regeneration, which in turn sustained elevated primary productivity and the $\delta^{13}C$ plateau.

EGU, Vienna, Austria, 2006

Palaeoenvironmental Impacts on Changes in Bottom Water Oxygen Availability at the Cenomanian-Turonian Anoxic Event

Haydon Mort, Thierry Adatte, Karl Föllmi, Gerta Keller, Philippe Steinmann, Virginie Matera, Zoltz Berner, Doris Stuben

Abstract

The accumulation rate of phosphorus bound to its inorganic phases is, amongst other things, dependant on the abundance of free O2 at the sediment-water interface. Studying the behavior of phosphorus in its different phases is therefore fundamentally important assessing the true extent of dysoxia/anoxia during a 'oceanic anoxic event' (OAE). Equally as important is the understanding of what caused the reduction in O2 availability, evident at the major OAEs. This study focuses on OAE 2 close, to the Cenomanian-Turonian boundary (~93.5 Ma).

To assess changes in O2 availability and its causes and consequences, we present phosphorus (P) speciations corrected for sedimentation rate (P MARs), from 5 localities possessing different depositional histories from shallow water, deep pelagic to an upwelling zone (Pueblo, Colorado; Eastbourne, UK; Furlo, Italy; Manilva, Spain; Mohammad Beach, Morocco). We also present d13C isotopes, carbon/phosphorus molar ratios and Rock-Eval data for each of these sections in order to try and better understand the environmental processes that caused the variations in O2 availability (as inferred from P MARs).

Our results indicate that OAE 2 started with a burst in productivity that increased the sedimentation rate in bottom waters in a variety of palaeoenvironments. We see the increased accumulation rate of chemically precipitated Pauthigenic, indicating that whilst productivity was high, a considerable amount of free oxygen was still available. During what we assume to be a purely productivity driven positive d13C isotope excursion, P MARs decrease in both organic and inorganic phases. This points to a drop in the initial intense productivity allowing organic matter to break down faster than it was arriving, whilst condition were becoming increasingly dysoxic thereby preventing the effective precipitation of Pauthigenic or PFe. A molar ration between Corg and Preactive (total phosphorus content) increase at the point P MARs decrease, reflecting the sediments inability to retain phosphorus. This phosphorus may have been recycled back into the photic zone where it would may have sustained productivity. After this time there is a good postive correlation between total organic carbon content (TOC %) and hydrogen indices (HI) (R2=0.5-0.7). As this correlation is only apparent after the spike in Corg/Preative ratios, this indicates that the ocean system was entering a more advanced stage of dysoxia where the abundance of organic matter was not dictated by productivity, but rather the increased preservation potential associated sediments overlain by O2 depleted waters.

Inherent in this scenario is an increase in atmospheric O2 content as a nutrient recycling positive feedback sustained primary productivity. The gradual consumption of nutrients, reduction in continental nutrient influx and the increase in the pO2(atmosphere) may have both been factors in bring about an end to OAE 2.

In Fourteenth Metting of the Swiss Sedimentologists, Fribourg, Switzerland.

Evidence for Nutrient Recycling During OAE 2: Implications From a Multisite Phosphorus Speciation

Mort Haydon, Adatte Thierry, Föllmi Karl B, Föllmi, Keller Gerta, Steinmann Phillippe, Matera Virginie,

Abstract

Understanding how the Earth's biosphere reacts to global temperature and sea level fluctuations is of central importance when trying to understand what we observe today and what we may expect in the future. The oceanic anoxic events that punctuate much of the lower to mid Cretaceous provide us with the opportunity to study various biogeochemical pathways and feedbacks that may

develop under a greenhouse climate and elevated ocean primary productivity.

Whilst being a crucial element involved in limiting primary productivity, the accumulation of phosphorus in marine sediments is not mediated exclusively by productivity. For example phosphorus can be delivered directly from continental run-off to ocean sediments without being incorporated into organic matter first. The reduction of organic matter by bacteria also causes phosphate to be released back into the water column to enhance productivity or to be precipitated as authigenic phosphates.

We present data from four sections with different paleogeographies and environments. The GSSP for the Cenomanian-Turonian boundary in Pueblo, Colorado, Eastbourne (UK), Furlo (Italy) and Manilva (Spain). Remarkably, all sections display a similar trend in total-P values. A maximum in phosphorus mass accumulation rates (P MARs) predates the 1st peak in d13C by 10's of ka. P MARs in all sediments return to pre-excursion values before or immediately after the d13C peak, remaining low during the characteristic isotope plateau. We hypothesis that the accumulation of phosphorus was inhibited once the environment became too dysoxic. To substantiate this we carried out a phosphorus speciation on the four sections paying particular attention to authigenic-P whose accumulation is strongly regulated by the availability of oxygen. Authigenic-P MARs also appear to peak before or during the d13C excursion peak. This suggests that the enhanced productivity and biopump initially lead to the phosphorus liberated via bacterial respiration to be oxidised into authigenic-P. However, as the environment became more and more dysoxic a threshold was probably crossed preventing the formation of authigenic-P. With less phosphate being buried, a larger proportion of the total-P could have been recycled sustaining primary productivity in a positive feedback. There are also clear discrepancies in the P MAR curves. However these differences are telling. In the deeper sections (Furlo and Manilva) accumulation rates of authigenic-P are consistently an order of magnitude less than in Pueblo and Eastbourne, probably a simple reflection of the attenuation of dissolved oxygen with depth. However a more interesting dissimilarity is that when correlated in time, the deeper sections display their peak in authigenic-P before the shallower section. This suggests that the threshold at which dysoxia prevented authigenic-P formation was not coeval on continental shelves by several thousand years. This observation is consistent with the stepwise extinction of planktonic foraminifera from deeper to shallower paleodepths, reflecting the gradual expansion in the oxygen minimum zone in a well-stratified water column.

7th International Syposium on the Cretaceous, Neuchâtel, Switzerland.

Biogeochemical Changes During OAE 2: A Multisite Phosphorus Speciation

Haydon Mort, Thierry Adatte, Karl Follmi, Phillippe Steinmann, Virginie Matera & Gerta Keller

Abstract

Understanding the sources and behaviour of productivity limiting nutrients, such as phosphorus, is critical in our understanding the triggers and development of past climate changes. We present results from a sequential extraction of phosphorus from four sections that differ in their paleoenvironmental situation during oceanic anoxic event 2, (93.5 Ma). The sections are Pueblo (Colorado), Furlo (Italy), Manilva (Spain) and Eastbourne (UK). Mass accumulation rate corrections have been applied in all cases is give P MARs. We also integrate kaolinite and rock-eval data, collected from Pueblo, into our disussion.

We observe a significant peak in all P MARs. The must abundant of these is authigenic in origin. However the first d13C peak is offset from the P MAR peaks by some tens of thousands of years. P MARs tend to rise, initially in step with d13C values but then decrease to pre-excursion values at or just after the first isotope peak. This behaviour is indicative of phosphorus recycling under increasingly anoxic conditions. The regeneration of phosphorus may have

sustained productivity beyond that which would have been possible by continental nutrient influx alone. Kaolinite clearly spikes at the base of the isotope excursion in Pueblo, suggesting a brief period of humidity preceded isotope excursion. Rock-eval shows a rapid sea-level transgression at the d13C excursion, which could have reworked the kaolinite and/or remobilised nutrients. The abundance of shallow seas during this period make it possible that one or both of these factors was responsible for supplying the initial nutrient levels to boost productivity. However if productivity was responsible for the characteristic isotope plateaux during OAE 2, then it is unlikely that nutrients alone were directly responsible. The decline in P MAR, as an expression of recycling under anoxia, is an appealing explanation for sustained productivity.

These results give valuable insights into the causal mechanism of OAE 2 and offer new avenues of investigation into the other OAEs that occurred periodically during the mid-late Cretaceous.

Aptian-Turonian events during the 120-190 Ma supermagnetochron: geological, biological, geodynamic and geochemical record. Grenoble, France 2005

Preservation and Productivity: Considerations during the Cretaceous Anoxic Events

Haydon Mort, Thierry Adatte, Karl Follmi, Phillippe Steinmann, Virginie Matera & Gerta Keller

Abstract

The enigmatic Cretaceous Oceanic Anoxic Events (OAE's) have been of considerable interest to geologists over the past 30 years. We present new mass accumulation rates of total phosphorous (P MAR) at four Cenomanian-Turonian boundary localities, each with differing paleoenvironmental settings. MAR's were also calculated for total organic carbon (TOC). ä13C and biostratigraphic correlations were used to calculate both P and TOC MAR's. A consistent feature emerges from this data which causes us to reassess the mechanisms involved behind the Cenomanian-Turonian event (OAE 2). Phosphorous MAR (unspeciated) is seen to increase prior to TOC MAR and the positive ä13C excursion. Our most accurate accumulation rates are from Pueblo, Colorado and Eastbourne, UK. The calculated time lag, based in these accumulation rates ranges from 30-70 ka. We argue that despite potentially longer residence times during the Cretaceous oceans, this lag is too long to be easily explained via conventional models related to increased continental weathering and oceanic nutrient input. Uncertainty remains as to the phase(s) from which the phosphorous derives (e.g. detrital, Fe-bound, Mn-bound or authigenic) as a speciation has not yet been completed. However the results have allowed us to construct a simple, testable model that treats OAE's and red beds as facets of the same processes, essentially combining parts of the phosphorous and iron cycles. The model also offers a potential reconciliation in the productivity vs. preservation debate surrounding the OAE's.

32nd International Geological Congress. Florance, Italy, 2004.

New Insights into OAEs and Red Beds: The Behavior of Phosphorus during OAE 2

Haydon Mort, Thierry Adatte, Karl Follmi, Phillippe Steinmann, Virginie Matera & Gerta Keller

Abstract

The ensuing debate following the discovery of widespread and coeval black shale deposits during the Cretaceous period, 30 years ago, has produced more questions than answers. Termed oceanic anoxic events (OAE's), these periods of carbon burial and positive □13C excursions have lead to two broad trains of thought relating to their formation. One model requires enhanced

productivity to stimulate anoxic conditions and organic carbon preservation. The alternative model does not require productivity, and instead relies on a source (probably volcanic) of CO2 to produce sufficiently anoxic conditions that would also result in enhanced preservation. We present new phosphorous (unspeciated) mass accumulation rate (MAR) data collected from four Cenomanian-Turonian localities, each deposited under differing paleoenvironmental circumstances. These sites are Pueblo, Colorado; Eastbourne, UK; Manilva, Spain and Furlo, Italy. This data is combined with TOC (MAR corrected) and $\delta^{13}C$ measurements also taken at each of the localities. Dates, derived from foraminiferal stratigraphy, isotope correlation and 40Ar/39Ar from bentonites (present in Pueblo) enabled a robust accumulation rate framework to be constructed for each of the sites.

We find a pronounced peak in P MAR close to the top of the R. cushmani zone. Intriguingly at each site, the P MAR peak consistently precedes both TOC MAR and the positive $\delta^{13}C$ excursion peaks (FAD W. archeocretacea). The cause of this is by no means obvious. The best time control on our accumulation rates are found at Pueblo and Eastbourne where the distance in time between the peaks is 36 ka and 70 ka respectively. Although phosphorous residence times in the late Cretaceous oceans were possibly longer than today's estimates (1 ka), we argue this lag is too long to be easily explained via conventional models related to increased continental weathering and oceanic nutrient input. Phosphorous speciation (soon to be carried out) would help identify the source of this P MAR peak, separating it from it's various phases (detrital, Fe-bound, Mn-bound and authigenic).

The observation that this phenomena is found in four widely separated sites under three very different depositional settings is solid evidence for this to be a hemispherical or global feature, although more sites are needed to confirm this. We consider the implications to published ideas. In addition, the results have allowed us to construct a simple, testable model that treats OAE's and red beds as facets of the same processes, essentially combining parts of the phosphorous and iron cycles. The model also offers the potential of a reconciliation in the productivity vs. preservation debate surrounding the OAE's.

Twelfth Meeting of Swiss Sedimentologists. Fribourg, Switzerland. Oral Presentation

Productivity and Continental weathering in the Western Interior During Oceanic Anoxic Event 2: An Example from the Pueblo Stratotype, Colorado

Haydon Mort, Thierry Adatte, Karl Follmi, Phillippe Steinmann, Virginie Matera & Gerta Keller

Abstract

We present a multidisciplinary study in which the palaeoenvironment of the Pueblo Section, Colorado is studied. Small surface dwelling planktic foraminifera Hedbergella planispira register a +2.0 to 2.5‰ $\delta^{13}C$ excursion across the Harland Shale and the Bridge Creek Limestone members (late Cenomanian-early Turonian in age respectively). Coincident with this positive shift is the progressive extinction of 5 surface planktic species (Rotalipora deekei, R. greenhornensis, R. cushmani, P. inornata, G. bentonensis) which are replaced by foraminifera with high depth and low O2 tolerances. $\delta^{18}O$ values also increase from around -11‰ to -7‰, indicating that although a marine transgression certainly occurred, a large fresh water influence still remained. The sediments of the Greenhorn Formation are clearly post-depositionally altered, however it is deemed that such negative $\delta^{18}O$ values cannot be explained by diagenetic overprint alone. XRD mineralogy and Rock-Eval analysis reveals increases in calcite, a decline in phyllosilicates and a switch in dominance from OI to HI (continental to marine derived organic matter), indicating generally higher sea levels and enhanced preservation. Phosphate (PO4) and Aluminum (Al) accumulation data show a close correlation with each other. Although considerable scattering is displayed, a clear drift towards lower values is seen to occur with the

onset of the □13C excursion, fostering the notion of less terrestrial input and high sea levels and low productivity. Biogenic Barium (Ba(biogenic)) accumulation displays a short increase during the primary phase of the □13C excursion but drops abruptly (by around 200 ppm) with the last occurrence datum (LAD) of the 5 surface planktic species (approximately the first peak of the □13C excursion). This may indicate that although there may have been no net biodiversity loss (introduction of deeper species) there may well have been a drop in marine surface productivity resulting from the extinction and anoxia. Aside from the main focus of this study, the mid-Cenomanian event was possibly identified lower in the section with a short lived positive □13C shift and negative □18O shift. Interestingly PO4 accumulation shows a sharp spike in concentrations, more than doubling to over 1000 ppm. It is also at this point that OI values begin to exceed the HI suggesting a possible sea level regression and an enhanced continentally derived organic matter influx.

Réunion spécialisée de la Société de la géologique de France. Mesozoic Paleoceanography. Paris 2003. Oral Presentation

Paleoenvironmental Constraints on Productivity at the Cenomanian-Turonian Boundary: An example from the Pueblo Stratotype, Colorado

Haydon Mort, Thierry Adatte, Karl Follmi, Phillippe Steinmann, Virginie Matera & Gerta Keller, Alfonso Pardo

Abstract

Surface dwelling planktic foraminifera, H. planispira, register a +2.0 to 2.5‰ δ13C excursion straddling the Harland Shale and Bridge Creek Limestone member (latest Cenomanian) at the Pueblo Stratotype, Colorado. Post-excursion, the δ13C values remain at approximately 2.0‰ dipping only slightly in the early Turonian (H. helvetica zone). During the initial phases of the δ13C excursion, 5 planktic species consecutively become extinct (Rotalipora deekei, R. greenhornensis, R. cushmani, P. inornata, G. bentonensis). These are subsequently replaced in the latter stages of the excursions by 5 new species with high depth tolerances, resulting in no net diversity loss. The extinction is therefore likely to have been as a direct result from the increased water mass stratification. A temporary decrease in bottom water productivity is also suggested by oxygenated bottom waters (presence of Cibidicoides) and a minimum of low O2 tolerant species (hetrohelicids). Elevated HI/OH indexes, an increases in calcite and a decline in phyllosilicates all indicate generally higher sea levels and enhanced preservation. Throughout the whole section, δ18O ratios exhibit a wide range of values, from –12.0 to –6.5‰. Such light isotopic values are only conceivable in a system with a substantial fresh water influence. The basal 2.5 m of the Harland Shales appears to contain a relative sea level transgression with positive shifts in δ13C (1.2‰) and δ18O (3.5‰), that correlate well with HI/OI index increases. Values in the mid-section (2.5-10 m) of the Harland Shales remain lower than average. However, large positive spikes of up to 4.0‰ were also recorded here. These are coincident with increases in calcite, indicating a relatively low fluctuating sea level with periodic marine incursions. Frequent benthonite layers across the boundary provide a good temporal framework in which to generate more accurate models for both carbon and phosphorous accumulation rates. This phosphate analysis also sheds light on the productivity versus preservation relationships in operation at the time of the various depositional phases.

European Union of Geosciences Joint Assembly, Nice, France. Poster Presentation

Complete List
Reverse Chronological Order

Mort H. P., Smart C. W., and Price G. P. (2002) Dissolution and productivity at the Paleocene-Eocene thermal maximum. In Carbon burial, climate change and ocean chemistry (Mesozoic-Paleogene).

Mort H. P. (2002) Paleoceanography, paleoproductivity and the application of novel inorganic geochemical proxies during the Paleocene-Eocene Thermal Maximum, University of Plymouth.

Adatte T., Steinmann P., **Mort H. P.,** Affolter S., Jaquat O., Paratte G. D., and Ducommun P. (2002) The Cenomanian-Turonian Anoxic Event in Northern Italy (Southern Alps and Central Appenines): Correlation with the Penibetic Zone (South Spain). In Carbon burial, climate change and ocean chemistry (Mesozoic-Paleogene).

Mort H. P., Adatte T., Steinmann P., Matera V., Keller G., Stueben D., and Berner Z. (2003a) Productivity and Continental Weathering in the Western Interior During Oceanic Anoxic Event 2: An example from the Pueblo Stratotype, Colorado. In Réunion spécialisée de la Société de la géologique de France. Mesozoic Paleoceanography.

Mort H. P., Adatte T., Steinmann P., Keller G., Stueben D., Berner Z., and Pardo A. (2003b) Palaeoenvironmental constraints on productivity at the Cenomanian-Turonian Boundary: An example From The Pueblo Stratotype, Colorado. In European Union of Geosciences Joint Assembly.

Mort H. P., Adatte T., Steinmann P., Föllmi K. B., Matera V., Keller G., Stuben D., and Berner Z. (2003c) Productivity and Continental Weathering in the Western Interior During Oceanic Anoxic Event 2: An Example From the Pueblo Stratotype, Colorado. In Réunion spécialisée de la Société de la géologique de France. Mesozoic Paleoceanography.

Adatte T., **Mort H. P.**, Keller G., Berner Z., Stuben D., and Rais P. (2003) The Cenomanian-Turonian global events: a review. In Eleventh Meeting of the Swiss Sedimentologists.

Mort H. P. and Adatte T. (2003) The Paleocene-Eocene boundary: early Tertiary climate optimum: possible clatherate feedback mechanisms, extinction events and geochemical fluctuations. In Joint presentation for the Deptartment of Geological Sciences of Bern, Neuchâtel and Fribourg (BeNeFri): Geochemical appraoch to the system Earth.

Mort H. P., Smart C. W., and Price G. P. (2003d) Dissolution and productivity at the Paleocene-Eocene thermal maximum. In Eleventh Meeting of the Swiss Sedimentologists.

Mort H. P., Adatte T., Steinmann P., Matera V., Keller G., Stuben D., Berner Z., and Follmi K. (2004a) New insights into OAE's and Red Bed: The behavior of Phosphorous during OAE 2. In Twelfth Meeting of Swiss Sedimentologists, pp. 39.

Mort H. P., Adatte T., Föllmi K. B., Steinmann P., Matera V., Keller G., Stuben D., and Berner Z. (2004b) Preservation and productivity: Considerations during the Cretaceous Anoxic Events. In 32nd International geological Congress.

Mort H. P., Adatte T., Föllmi K. B., Steinmann P., Matera V., and Keller G. (2005a) Biogeochemical changes during OAE 2: A multisite phosphorus speciation. In Aptian-Turonian events during the 120-190 Ma supermagnetochron: geological, biological, geodynamic and geochemical record.

Mort H. P., Adatte T., Föllmi K. B., Steinmann P., Jaquat O., Matera V., and Keller G. (2005b) Multi-site Phosphorus Speciation for Oceanic Anoxic Event 2. In Thirteenth Meeting of the Swiss Sedimentologists, Vol. 13.

Mort H. P., Adatte T., Föllmi K. B., Keller G., Steinmann P., and Matera V. (2005c) Evidence for nutrient recycling during OAE 2: Implications from a multisite phosphorus speciation. In 7th International Syposium on the Cretaceous., Vol. 7 (ed. A. Godet, H. P. Mort, P. Linder, and S. Bodin), pp. 149.

Mort H. P., Adatte T., Föllmi K. B., Keller G., Steinmann P., Matera V., Berner Z., and Stueben D. (2006a) Palaeoenvironmental impacts on changes in bottom oxygen availability at the Cenomanian-Turonian Anoxic Event. In Fourteenth Metting of the Swiss Sedimentologists.

Mort H. P., Adatte T., Föllmi K. B., Keller G., Steinmann P., Matera V., Berner Z., and Stuben D. (2006b) Palaeoenvironmental impacts on changes in bottom water oxygen availability at the Cenomanian-Turonian Anoxic Event. In EGU General Assembly 2006.

Mort H. P., Adatte T., Steinmann P., Matera V., Keller G., and Berner Z. (2006c) A muit-site phosphorus speciation across the Cenomanian-Turonian Boundary: Implicatiosn for the processes leading to Red Bed formation. In Workshop on cretaceous oceanic red beds: Paleoclimate and paleoclimatology.

Mort H. P., Jaquat O., Adatte T., Steinmann P., Follmi K., Matera V., Berner Z., and Stuben D. (in press) The Cenomanian-Turonian anoxic event in Italy and Spain: enhanced productivity and/or better preservation. Cretaceous Research.

Mort H. P., Jaquat O., Adatte T., Steinmann P., Follmi K., Matera V., Berner Z., and Stuben D. (submitted-a) Phosphorus and the roles of productiviity and nutrient recycling during Oceanic Anoxic Event 2. Geology.

Mort H. P., Adatte T., Keller G., Bartel D., Föllmi K. B., Steinmann P., and Berner Z. (submitted-b) Organic carbon deposition and phosphorus accumulation during Oceanic Anoxic Event 2 in Tarfaya, Morocco. Cretaceous Research.